

University of Alberta

**Bisphosphonate-Modified Nanoparticles as Drug Delivery Systems for
Bone Diseases**

by

Guilin Wang

A thesis submitted to the Faculty of Graduate Studies and Research
in partial fulfillment of the requirements for the degree of

Doctor of Philosophy

in

Chemical Engineering

Department of Chemical & Materials Engineering

©Guilin Wang
Spring 2011
Edmonton, Alberta

Permission is hereby granted to the University of Alberta Libraries to reproduce single copies of this thesis and to lend or sell such copies for private, scholarly or scientific research purposes only. Where the thesis is converted to, or otherwise made available in digital form, the University of Alberta will advise potential users of the thesis of these terms.

The author reserves all other publication and other rights in association with the copyright in the thesis and, except as herein before provided, neither the thesis nor any substantial portion thereof may be printed or otherwise reproduced in any material form whatsoever without the author's prior written permission.

Examining Committee

Dr. Hasan Uludağ, Department of Chemical & Materials Engineering

Dr. Larry Unsworth, Department of Chemical & Materials Engineering

Dr. Raimar Löbenberg, Faculty of Pharmacy & Pharmaceutical Sciences

Dr. Phillip Choi, Department of Chemical & Materials Engineering

Dr. Hicham Fenniri, Department of Chemistry

Dr. Janet Elliott (chair), Department of Chemical & Materials Engineering

Dr. Dong Wang, Department of Pharmaceutical Sciences, University of Nebraska

Medical Center

ABSTRACT

The objective of this thesis is to design nanoparticle (NP)-based drug delivery systems suitable for treatment of bone diseases. Two types of nanocarriers, (1) polymer coated bovine serum albumin (BSA) NPs and (2) lipid based NPs (micelles and liposomes) were investigated.

The BSA NPs were prepared by a coacervation method and stabilized with a polymer coating approach. For bone-specific delivery of bone morphogenetic protein-2 (BMP-2), a copolymer polyethyleneimine-graft-poly(ethylene glycol) conjugated with 2-(3-mercaptopropylsulfanyl)-ethyl-1,1-bisphosphonic acid (PEI-PEG-thiolBP) was synthesized and used for coating the BSA NPs. The particle size and ζ -potential of the NPs could be effectively modulated by the processing parameters. All the NPs showed no or low cytotoxicity (except for a high concentration of PEI), and the NP encapsulated BMP-2 displayed full retention of its bioactivity. By encapsulating ^{125}I -labeled BMP-2, the polymer-coated NPs were assessed for hydroxyapatite (HA) affinity; all NP-encapsulated BMP-2 showed significant affinity to HA as compared with free BMP-2 *in vitro*, and the PEI-PEG-thiolBP coated NPs improved the *in vivo* retention of BMP-2 compared with uncoated NPs. However, the biodistribution of NPs after intravenous injection in a rat model indicated no beneficial effects of thiolBP-coated NPs for bone targeting.

Alternatively, micelles and liposomes were prepared with a conjugate of

distearoylphosphoethanolamine-polyethyleneglycol with thiolBP (DSPE-PEG-thiolBP) to create mineral-binding nanocarriers. The thiolBP-decorated liposomes also displayed a stronger binding affinity to HA and a collagen/HA (Col/HA) scaffold and gave increased retention in the scaffold in a subcutaneous implant model in rats. Taking advantage of the high HA affinity of the BP-liposomes, a sustainable release system was developed by sequestering the liposomal drugs in the Col/HA scaffolds. Three different model drugs, carboxyfluorescein, doxorubicin and lysozyme, were used to evaluate the drug release profiles from the liposome-loaded scaffolds, and all showed a slowing effect of the BP on the release of the liposome-encapsulated drugs from the Col/HA scaffolds. This liposome-scaffold combination will provide a platform for the application of various therapeutic agents for bone regeneration.

In conclusion, the BP-modified NPs showed strong mineral-binding affinity. Although the systemic bone targeting was limited by physiological barriers, these NPs are promising in local delivery and controlled release of bioactive molecules for treatment of bone diseases.

ACKNOWLEDGEMENTS

This project was financially supported by an operating grant from Canadian Institutes of Health Research (CIHR) and Alberta Advanced Education & Technology. I was personally funded by a studentship from the China Scholarship Council (CSC) and a Trainee Award from CIHR-Skeletal Regenerative Medicine Team grant.

I would like to express my greatest gratitude to my supervisor, Dr. Hasan Uludağ, for his efficient and endless guidance throughout this research work, for his encouragement from the beginning and generous support to the end of my study. I also thank my supervisory committee members, Drs. Larry Unsworth and Raimar Löbenberg, for their guidance and advice.

I am grateful to Ms. Xiaoyue Lin and Mr. Cezary Kucharski for the technical support in cell culture and animal studies, Dr. Hamid Montazeri for help with the IV injections and Dr. Charles Doillon (Laval University, Quebec City, Canada) for initial help with the purification protocol for collagen. I also thank my colleagues in Dr. Uludağ's laboratory for their help and advice in this study. My thanks also go to Dr. Walter Sebald (University of Würzburg, Germany) for kindly providing the BMP-2, and Mr. Matthias Rebmann (Lipoid GmbH, Germany) for providing the DSPC and DSPE-PEG.

Finally, I am forever indebted to my parents for their understanding, endless patience and unequivocal support over the years.

TABLE OF CONTENTS

Chapter 1. Recent Developments in Nanoparticle-Based Drug Delivery and Targeting Systems with Emphasis on Protein-Based Nanoparticles	1
1.1 Overview of Nanoparticulate Drug Carriers	2
1.2 Principal Preparation Methods for Nanoparticles	4
1.2.1 Emulsion/Solvent Extraction Process	5
1.2.2 Coacervation Process	7
1.2.3 Polyelectrolyte Complexation (Complex Coacervation)	10
1.2.4 Salt Precipitation	13
1.3 Surface Modification of Nanoparticles with PEG	14
1.4 Nanoparticle Properties Critical for Drug Delivery	16
1.4.1 Particle Size and Circulation Time	17
1.4.2 Nanoparticle Opsonization and Phagocytosis	18
1.4.3 Factors Controlling Drug Release	21
1.5 Designing Nanoparticles for Targeting to Specific Tissues	22
1.5.1 Brain Targeting	23
1.5.2 Tumor Targeting	24
1.5.3 Bone Targeting	25
1.6 Conclusions	27
References	35
Chapter 2. Scope of Dissertation	52
Chapter 3. Preparation of BMP-2 Containing Bovine Serum Albumin (BSA) Nanoparticles Stabilized by Polymer Coating	58
3.1 Introduction	59
3.2 Materials and Methods	62
3.3 Results and Discussion	70
3.4 Conclusions	86
References	98

Chapter 4. Bisphosphonate-Coated BSA Nanoparticles Lack Bone Targeting after Systemic Administration	103
4.1 Introduction	104
4.2 Materials and methods	107
4.3 Results	118
4.4 Discussion	127
4.5 Conclusions	135
References	148
Chapter 5. Bisphosphonate-Decorated Nanoparticles Designed as Drug Carriers for Bone Diseases	153
5.1 Introduction	154
5.2 Materials and Methods	156
5.3 Results and Discussion	165
5.4 Conclusions	174
References	184
Chapter 6. Bisphosphonate-Derivatized Liposomes to Control Drug Release from Collagen/ Hydroxyapatite Scaffolds.....	187
6.1 Introduction	188
6.2 Materials and Methods	191
6.3 Results and Discussion	197
6.4 Conclusions	210
References	217
Chapter 7. General Discussion, Conclusions and Future Directions	223
7.1 General Discussion.....	224
7.2 Conclusions	232
7.3 Future Directions.....	234
References	239
Appendix. Bioistribution of Micelles and Liposomes after Intravenous	

Injection	242
I) Introduction.....	242
II) Methods.....	243
III) Results and Discussion	244

LIST OF TABLES

Table 1-1. A representative summary of biomaterials used for preparation of nanoparticulate delivery systems and drugs used for delivery	29
Table 1-2. A summary of ligands used for NP derivatization for targeting NPs to specific tissues	30
Table 3-1. Experimental control factors and their levels for the statistical experiment testing	87
Table 3-2. Orthogonal array and results of the statistical experiment testing.....	87
Table 3-3. Data analysis of the statistical experiment testing	88
Table 5-1. Particle size and polydispersity index of micelles and liposomes and encapsulation efficiency (EE%) of DOX and LYZ in different formulations	175

LIST OF FIGURES

Figure 1-1. Typical size (nm) ranges of polyester, protein and chitosan NPs reported in the literature.....	31
Figure 1-2. Commonly used methods to prepare nanoparticles: double emulsion, coacervation (and salt precipitation), and polyelectrolyte complexation.	33
Figure 1-3. Influence of pH on the size and polydispersity index of BSA NPs	34
Figure 3-1. Influence of BSA concentration, pH value of coacervation solution and ethanol:water ratio on particle size and polydispersity of BSA NPs.	89
Figure 3-2. Dependence of particle size and polydispersity on: BSA concentration, ethanol:water ratio, pH value and stirring rate.....	90
Figure 3-3. Comparison of the size of BSA NPs prepared by using ethanol and acetone as the non-solvent	91
Figure 3-4. Size distribution of the NPs prepared by using acetone and ethanol as non-solvent.....	92
Figure 3-5. The amount of polymer adsorbed onto NPs, mean particle diameter and zeta potential of NPs coated with different concentrations of PLL and PEI.....	93
Figure 3-6. AFM of uncoated BSA NPs obtained right after the coacervation process and BSA NPs coated with 50 µg/mL PLL and PEI	94
Figure 3-7. MTT assay of the PEI and PLL coated NPs in the human BMSCs and rat BMSCs.....	95
Figure 3-8. ALP activity of BMP-2 encapsulated in uncoated and coated NPs in human BMSCs and rat BMSCs	96
Figure 3-9. Calcification of rat BMSCs at day 14	97
Figure 4-1. ¹ H-NMR spectrum of PEI-PEG and PEI-PEG-thiolBP in D ₂ O	138
Figure 4-2. ThiolBP conjugation efficiency as a function of PEG/PEI molar ratio and the influence of PEG substitution and thiolBP conjugation on HA affinity.....	139

Figure 4-3. ζ -potential of BSA NPs coated by different concentrations of PEI, PEI-PEG and PEI-PEG-thiolBP (0-12 μ M) and the effect of thiolBP substitution on PEI-PEG-thiolBP on ζ -potential of the NPs.....	140
Figure 4-4. Particle size analysis and size distributions of uncoated BSA NPs and PEI-PEG-thiolBP coated NPs	141
Figure 4-5. Effect of the coating concentration on particle size of polymer-coated BSA NPs	142
Figure 4-6. AFM images of BSA NPs in acetone/water and PEI-PEG-thiolBP coated BSA NPs prepared by using evaporation method for coating	143
Figure 4-7. Cytotoxicity of polymer conjugates on C2C12 cells, and rat BMSCs, and polymer coated BSA NPs on C2C12 cells, and rat BMSCs	144
Figure 4-8. ALP activity of NP-encapsulated BMP-2 on C2C12 cells and rat BMSCs.....	145
Figure 4-9. <i>In vitro</i> HA affinity and <i>in vivo</i> implant retention of 125 I-labeled BMP-2 in different NP formulations	146
Figure 4-10. The biodistribution of 125 I-labeled BMP-2 encapsulated in different BSA NPs	147
Figure 5-1. Chemical structure of DSPE-PEG-MAL and DSPE-PEG-thiolBP and schematic for the preparation of the bisphosphonate-decorated micelles and liposomes	176
Figure 5-2. 1 HNMR spectra of DSPE-PEG-MAL and DSPE-PEG-thiolBP	177
Figure 5-3. Visualization for HA binding of BP-micelles and liposomes	178
Figure 5-4. Effect of BP content on the HA binding of micelles and liposomes and the HA affinity of encapsulated DOX and LYZ in micelles and liposomes	179
Figure 5-5. The binding of liposomes to HA in PBS and serum-containing PBS	180
Figure 5-6. <i>In vitro</i> and <i>in vivo</i> affinity of liposomes to Col/HA scaffold.....	181
Figure 5-7. Cytotoxicity of micelles and liposomes on C2C12 cells	182
Figure 5-8. ALP activity of the BMP-2 encapsulated in the liposomes on human C2C12 cells and rat BMSCs	183

Figure 6-1. Appearance of the Col/HA scaffold and its pore structure observed under SEM	211
Figure 6-2. Standard curves for determination of CF, DOX and LYZ concentrations	212
Figure 6-3. Release of CF, DOX and FITC-labeled LYZ from PEG- and BP-liposomes by dialysis method	213
Figure 6-4. Binding affinity of the liposomes to collagen and Col/HA scaffolds in PBS and different concentrations of phosphate buffer	214
Figure 6-5. Release of liposomes from the Col/HA scaffolds in PBS and the effect of phosphate concentration on the liposome release.....	215
Figure 6-6. Release profiles of CF, DOX and LYZ from the liposome-loaded collagen and Col/HA scaffolds	216
Figure A-1. The biodistribution of DiI-labeled micelles and liposomes in rats after IV injection	247

LIST OF ABBREVIATIONS

AFM	atomic force microscope
ALP	alkaline phosphatase
AZT	azidothymidine
BBB	brain-blood-barrier
bFGF	basic fibroblast growth factor
BMP	bone morphogenetic protein
BMP-2	bone morphogenetic protein-2
BMSC	bone marrow stromal cell
BP	bisphosphonate
BPA	4- <i>N</i> -(3,5-ditetradecyloxybenzoyl)-aminobutane-1-hydroxy-1,1-bisphosphonic acid
BSA	bovine serum albumin
CF	carboxyfluorescein
CH	cholesterol
CH-TOE-BP	cholesteryl-trisoxoethylene-bisphosphonic acid
Col/HA	collagen/hydroxyapatite
DiI:	1,1'-dioctadecyl-3,3',3'-tetramethylindocarbocyanine iodide
DMEM:	dulbecco's modified Eagle's medium
DMSO:	dimethyl sulfoxide
<i>dof</i>	degree of freedom
DOX	doxorubicin
DSPC	distearoylphosphatidylcholine
DSPE	distearoylphosphoethanolamine
DSPE-PEG	distearoylphosphoethanolamine- <i>N</i> -poly(ethylene glycol)
EE	encapsulation efficiency
FBS:	fetal bovine serum
FITC	fluorescein isothiocyanate
GA	glutaraldehyde

GM	glutamax-1
HA	hydroxyapatite
hBMSC	human bone marrow stromal cell
HBSS	Hank's buffered salt solution
HER2	human epidermal growth factor receptor 2
hGH	human growth hormone
HPMA	N-(2-hydroxypropyl)methacrylamide
HSA	human serum albumin
IFN- γ	interferon- γ
IGF:	insulin-like growth factor
IgG	immunoglobulin G
IV	intravenous(ly)
LFH	lipid film hydration
LYZ	lysozyme
MTT	3-(4,5-dimethylthiazol-2-yl)-2,5-diphenyltetrazolium bromide
MW	molecular weight
MWCO	molecular weight cut off
NHS-PEG-MAL	succinimidyl-([N-maleimidopropionamido]- polyethyleneglycol)ester
NP	nanoparticle
PAA	poly(amidoamine)
PBS	phosphate buffered saline
PCL	poly(ϵ -caprolactone)
PCS	photon correlation spectroscopy
PDI	polydispersity index
PE ⁺	cationic polyelectrolyte
PE ⁻	anionic polyelectrolyte
PEG	poly(ethylene glycol)
PEI	polyethylenimine
PEO	poly(ethylene oxide)

PGA	poly(glycolic acid)
pI	isoelectric point
PLA	poly(lactic acid)
PLGA	poly(lactic-co-glycolic acid)
PLL	poly- <i>L</i> -lysine
p-NPP	p-nitrophenyl phosphate
PSMA	prostate specific membrane antigen
PTAAC	poly(thioetheramidoacid)
PTX	paclitaxel
PVA	poly(vinyl alcohol)
rBMSC	rat bone marrow stromal cell
RES	reticuloendothelial system
REV	reverse-phase evaporated vesicle
SD	standard deviation
SLN	solid lipid nanoparticles
SEM	scanning electronic microscope
SMCC	<i>N</i> -succinimidyl 4-[<i>N</i> -maleimidomethyl]cyclohexane-1-carboxylate
thiolBP	2-(3-mercaptopropylsulfanyl)-ethyl-1,1-bisphosphonic acid
TM	Taguchi method
TNBS	2,4,6-trinitrobenzene sulfonic acid (also called picrylsulfonic acid)

Chapter 1

Recent Developments in Nanoparticle-Based Drug Delivery and Targeting Systems with Emphasis on Protein-Based Nanoparticles¹

¹A version of this chapter has been published in: Wang G, Uludag H. *Expert Opinion on Drug Delivery*. 2008; 5: 499-515.

1.1 Overview of Nanoparticulate Drug Carriers

Injectable colloidal systems (hereon referred as nanoparticles, NPs) hold promise for systemic administration of different therapeutic agents, including conventional pharmacological agents, disease modifying bioactive factors (e.g., interleukins), protein growth factors, as well as nucleic-acid based agents intended for gene-based therapies. Nanoparticulate drug delivery systems, in the form of solid spheres, micellar emulsions, and liposomes, have been used in the past two decades as injectable formulations for systemic and tissue-specific delivery of drugs. Several types of biodegradable macromolecules have served as the foundation of drug carriers (**Table 1-1**). Conventional synthetic polyesters, whose prototypical examples include poly(lactic acid) (PLA) and poly(lactic-co-glycolic acid) (PLGA), have been extensively employed; (i) their long history of clinical use brings comfort to their tolerability in body, (ii) their well-understood degradation pattern allows better engineering of drug release kinetics, and; (iii) established processing methodologies enable a relatively ‘homogenous’ product whose performance is better predicted and controlled.

Proteins, primarily members of the albumin family, have served as an alternative biomaterial for carriers, facilitated by the obvious compatibility of this material in physiological systems. Administration of albumin in body should not

raise any adverse effects, as long as the source of the protein is free of transmissible diseases. Two albumin-based particulate formulations, AlbunexTM as an ultrasound contrast agent and AbraxaneTM as a carrier of anticancer drug paclitaxel [1], have been accepted for use in humans. Some plant proteins, such as legumin and gliadin, have also been attempted in the development of nanoparticle-based drug delivery systems. Due to unique structure of proteins with multifunctional moieties and/or domains, it might be possible to tailor unique carrier-drug combinations when proteins are employed as carriers. For example, albumin with its hydrophobic core displays a high affinity for hydrophobic drugs, and such combinations may form exceptionally slow-release formulations under physiological situations. As the primary structure of proteins contains $-NH_2$, $-COOH$, $-SH$ and other functional groups, protein NPs can offer various possibilities for covalent as well as non-covalent (electrostatic) modification of particulate surfaces. The latter is critical for the design of tissue-specific carriers, or when physiological responses to carriers need to be controlled. This is an advantage over polymeric biomaterials, which are rather homogenous and typically provide only a single functional group for modifications. Multifunctional polymers from copolymerization strategies might need to be alternatively utilized to accommodate various modifications for improved drug delivery.

In addition to protein and polyesters, other macromolecules used to

formulate NP carriers include polysaccharides, synthetic degradable acrylates (e.g., polycyanoacrylate), and natural/synthetic polyelectrolytes (e.g., chitosan and polyethylenimine, PEI). The biological fate of the latter macromolecules is less understood, and may pose a challenge for their clinical development. Another attractive idea to achieve controlled drug delivery and release is the use of solid lipid nanoparticles (SLN), which are primarily derived from middle chain triglycerides (e.g., trimyristin) or partial glycerides (e.g., Invitor[®] 900 and Compritol[®] 888 ATO) as lipid phase, with other ingredients including emulsifier and water [2].

This review summarizes the recent developments in nanoparticle-based drug delivery systems promising for systemic administration of therapeutic agents, with emphasis on the NPs fabricated from PLA (or PLGA) and albumin, which are two most widely used family of macromolecules. The methods to formulate nanoparticle carriers, the surface modification of the NPs, and the physicochemical properties in the design of drug delivery systems have been evaluated, and finally the functionalization of specific tissue-targeting delivery has been discussed in detail.

1.2 Principal Preparation Methods for Nanoparticles

Several distinct methods developed for preparation of NPs include

emulsification-solvent extraction, ‘salting-out’ or precipitation, spray-drying, solvent displacement, and coacervation and complex formation. Significant overlap exists among some of these methods and it is common to combine more than one process to obtain NPs tailored for specific applications. Each method usually needs to be optimized for entrapment of a drug of interest at high efficiency and retention of the desired pharmacological activity (especially important for protein therapeutics). An additional requirement for process success is the control over final NP size, usually diameter. A survey of the literature indicated that most reported NPs are between 100 and 1000 nm. **Figure 1-1** summarizes typical sizes reported for NPs prepared from polyesters, proteins and chitosan, respectively, as representative biomaterials. Although some processes are able to yield sub-100 nm sizes, this is rare. Three of more promising methods are emulsion/solvent evaporation, coacervation or desolvation, and polyelectrolyte complexation. **Figure 1-2** schematically outlines the principles behind these methods.

1.2.1 Emulsion/Solvent Extraction Process

The emulsification and solvent extraction process is widely used method for polymeric NPs. It is possible to adopt this technique for protein NPs, although particle sizes are generally larger as compared to the coacervation process described below [3]. In its simplest form, a polymer solution (in organic solvent,

O) or protein solution (in aqueous buffer, W) is dispersed in an appropriate non-solvent to form O/W or W/O emulsions, after which the solvents/non-solvents are removed to form the NPs (**Figure 1-2A**). Use of certain organic solvents, such as ethylacetate and chloroform, and surface-active agents, such as poly(vinyl alcohol) (PVA) and polysorbate-80, is not desirable since they may alter bioactivity of protein therapeutics [4,5]. They may additionally elicit undesired reactions against NPs and need to be reduced to insignificant levels. Surfactants are critical to control particle size; surfactants such as PluronicTM stabilized formation of smaller fluid particles in emulsions that lead to smaller solid particles [6]. Such a stabilization results from interaction of surfactants with the NP matrix. Surfactants are likely to influence drug-matrix interactions and possibly release rate of drugs in the physiological milieu [6]. It was possible to prepare PLGA NPs without surfactants [7]. The W/O method was recently employed to prepare surface-functionalized NPs after addition of desired molecules into the aqueous phase [8]. The W/O/W double-emulsion method can be specially used for encapsulation of proteins and hydrophilic drugs [9]; the primary W/O emulsion is introduced into a second water phase to form a double emulsion by using a surfactant for emulsion stabilization. The organic solvent is then removed, and the NPs are finally retained in the aqueous medium.

For PLGA NPs, polymer concentration and solvent composition were the

primary factors affecting size [10]. Encapsulation of conventional drugs (e.g., doxorubicin) could be optimized by controlling the ionization state of the drugs[11]. Proteins can be also encapsulated in PLGA NPs with high efficiency (e.g., >50% [12] or 30-50% [13]). For protein NPs, protein concentration and relative volume of solvent:non-solvent during emulsification were the critical parameters [3]. Bovine serum albumin (BSA) NPs with sizes in 100-800 nm range were reported in a W/O method, depending on BSA concentration and relative W:O volume ratio [14]. Excellent encapsulation efficiency (>80%) could be obtained with model macromolecular compounds (e.g., fluorescein isothiocyanide (FITC)-dextran), partly due to minimal solubility of the compound in the non-aqueous phase. Encapsulation efficiency of conventional drugs is usually lower, for example 10-60% for tamoxifen [6]. The bone inducing morphogen, BMP-2, was formulated with PLGA/heparin NPs [15], but protein loading was performed by adsorption post-fabrication, even though prior evidence suggests compatibility of the emulsion process with growth factors such as BMPs[16] and IGFs [17].

1.2.2 Coacervation Process

Coacervation or desolvation process under mild conditions is preferable for preparation of protein-based NPs and encapsulation of protein drugs. A colloidal system is formed when the solvent used for dissolving NP matrix is

extracted into a non-solvent phase, forming a phase with a colloidal component, or coacervate, and a second phase with a solvent/non-solvent mixture (**Figure 1-2B**). The particle formation initially proceeds with an increase in size until a stable size is reached, after which the number of particles gradually increase with increasing desolvation [18]. Lin et al. [19] described a pH-controlled coacervation method to prepare ~100 nm human serum albumin (HSA) NPs. The particles were prepared by acetone addition to an aqueous HSA solution at pH 7-9, and followed by stabilization of the particles by glutaraldehyde (GA) crosslinking. Langer et al. [18,20] prepared HSA NPs via desolvation with ethanol; process parameters such as HSA concentration, rate of non-solvent (ethanol) addition, pH of coacervation phase, and purification conditions were evaluated, and optimized for particle sizes between 100 and 300 nm. The pH prior to desolvation procedure was identified as the main factor affecting the size, high pH values leading to smaller particles [20]. This was independently confirmed in our hands, using ethanol as the non-solvent and BSA as the matrix (**Figure 1-3**). The pH and, to a lesser degree, osmolarity was important in maintaining the stability (size) of the particles, since conditions leading to net-zero surface charge were more conducive to particle aggregation [20]. Replacing BSA with the smaller β -lactoglobulin (a similar isoelectric point, pI, to BSA) led to a reduction in particle sizes (from 170 to 130 nm, with acetone as non-solvent), presumably due to lower hydrophobicity of the β -lactoglobulin [21]. Denaturation of

β -lactoglobulin by heat treatment further reduced the NP sizes to ~ 60 nm, and the authors attributed this result to reduced hydrophobic interactions among the extended proteins [21]. Chemically modified proteins may be additionally used as the NP matrix (e.g., polyethylene glycol-modified BSA, PEG-BSA), but use of modified proteins may require changes in the choice of solvents and non-solvents[22].

BSA NPs can achieve very high encapsulation efficiencies for protein drugs. Encapsulation efficiencies in excess of 95% were reported for interferon- γ (IFN- γ) [23] and we observed high entrapment efficiencies ($\sim 90\%$) for BMP-2 in BSA NPs [24]. It was interesting that high entrapment was obtained even with simple absorption of IFN- γ onto NPs, suggesting a favorable interaction between the NP matrix (BSA) and IFN- γ . This effect is expected to be drug dependent and, in the case of ganciclovir, entrapment during NP formation was more beneficial than simple adsorption [25].

Despite its known carcinogenicity and, hence, the need for its complete removal before human use, GA has been traditionally used as a crosslinker to stabilize albumin NPs after coacervation. As expected [18], Segura et al. [23,26] observed GA crosslinking to reduce the extent of $-\text{NH}_2$ groups at the particle surfaces, affecting biodegradability and drug release from the NPs. GA may crosslink the protein amines to BSA matrix, which was also noted for the

encapsulation of recombinant IFN- γ , leading to complete abrogation of its bioactivity, while IFN- γ adsorbed on GA-crosslinked NPs retained its bioactivity[23,26]. The GA crosslinking may also be problematic for small molecular drugs, such as doxorubicin [27] or adriamycin [28]. An independent study did not indicate any adverse effect of GA on doxorubicin loaded HSA NPs, although drug release was not assessed in this study [29]. GA crosslinking did not also appear to affect the integrity of an antisense oligonucleotide entrapped in HSA NPs [30], suggesting that GA reaction can be controlled to minimize any adverse effects. An alternative approach is to use high temperature/low moisture crosslinking [18,31], but this may be problematic due to drug deactivation or protein denaturation at high temperature. Macromolecular crosslinkers, such as oxidized dextran, could be alternatively used to replace GA [32], since they are less likely to freely diffuse into NP matrix and react with the functional groups on the NP surface. A different approach for NP stabilization is non-covalent coating of NP surfaces; BSA NPs could be coated with cationic polymers in aqueous buffers to create a coating that not only improves particle stability but also controls the release rate of a protein. The feasibility of this approach was demonstrated with BMP-2 entrapped in BSA NPs and coated with PEI [24].

1.2.3 Polyelectrolyte Complexation (Complex Coacervation)

Macromolecular interactions under aqueous conditions due to electrostatic

forces can lead to coacervation complexes (**Figure 1-2C**). Formation of insoluble complexes between proteins and oppositely-charged polymers will strongly depend on medium pH; use of polyanions for NP formation will require a pH lower than the protein pI, and vice-versa for polycations [33]. Cationic polymers such as poly-*L*-lysine (PLL) and PEI are commonly used for condensing long, string-like DNA molecules into NPs by complexation with anionic Os in the phosphodiester backbone of DNA [34]. The driving force for this type of interactions is usually entropic, due to release of the small counterions, rather than enthalpic [35]. Comb-type polyelectrolytes were proposed to be particularly suitable for preparation of water-soluble complexes [35,36], since hydrophilic segments facilitate aqueous solubility that is essential for systemic application[35]. Serefoglou et al. [37] described preparation of soluble NPs with hydrodynamic radii between 65-83 nm through coulombic interaction of BSA with anionic copolymers at a pH lower than the pI of BSA (~4.5). These NPs contained, on the average, 13-14 BSA molecules held together by two polymeric molecules. They were proposed to bear a hydrophobic core of BSA/anionic polymer moieties (~20 nm in diameter) and a polymeric corona. In addition to electrostatic interactions, H-bonding or hydrophobic interactions can also drive albumin/polymer complexation [38], the balance between the polymer-polymer and polymer-protein interactions dictating the number of proteins/polymer in a complex. The size of intermolecular complexes was dependent on the number of

protein/polymer bound, but its dependence was variable for individual polymers (and possibly interaction mechanisms within the complexes). Rhaese et al. [39] prepared HSA-PEI-DNA NPs using complex coacervation induced by charge neutralization, as a delivery system for gene therapy. These NPs were much larger in size (300-1000 nm) as compared to BSA particles formed at low pH. Smaller particles with a much broader distribution (30-300 nm) were reported by using a combination of protamine, oligonucleotides and albumin; incorporating albumin into such particles were achieved by electrostatic assembly and seemed to significantly influence intracellular distribution of the internalized oligonucleotides [40].

Polyelectrolyte complexation can be additionally employed for coating of protein aggregates by layer-by-layer assembly (**Figure 1-2C**, [41,42]). This process may provide exquisite control over the structure of NPs formed, but reported results indicated primary aggregates of 100-300 nm in size (similar to BSA NPs) that was further assembled to form microscopic structures as a result of coating. Prevention of larger aggregates in a reproducible way, for example with sonication [42], is paramount to obtain uniform nano-sized particles. It was possible to control the release rate of proteins from such NPs by controlling the coating layer (i.e., nature of the polymer and the order of coating), providing a convenient method for controlled release [41]. Distinguishing the underlying

release mechanism, i.e., protein diffusion vs. NP disintegration in a destabilizing environment, will be important for any therapeutic effect obtained.

NP formation by complexation is particularly suited for naturally-occurring polymers such as alginate and chitosan. Chitosan offers a unique biological matrix since it is mucoadhesive and acts as a good substrate for cellular binding. In addition to water-soluble, deacetylated chitosan, successful NPs were prepared with N-trimethylated (200-400 nm, [43]) and N-(2-hydroxy)-propyl-3-trimethylated chitosan (110-180 nm, [44]), using tripolyphosphate as the counter polyion. Model proteins (albumin and ovalbumin) were encapsulated with upto 80-100% efficiency under optimized conditions. As much as 50% of NPs could be made with the protein fraction, indicating the possibility of obtaining protein NPs as a result of polyelectrolyte-mediated aggregation.

1.2.4 Salt Precipitation

A simple approach to prepare protein NPs is simply ‘salting out’ a protein solution to form protein coacervates. The simplicity of this approach is attractive, provided that the precipitation process does not change the bioactivity or conformational structure of the protein. Insulin particles, for example, were prepared in this way by exposing the protein solution to high NaCl concentration

(>0.5 M) at low pH (<2.0) [42]. The particle sizes were 100-1000 nm depending on the pH, and appeared to display a large heterogeneity compared to other NP fabrication methods. Coating of such particles with polyelectrolytes can be easily achieved, and this helps to stabilize the NPs, as well as to facilitate control under certain conditions [42]. The latter will depend on the pI of encapsulated proteins, and the net charge of coating polyelectrolyte(s).

1.3 Surface Modification of Nanoparticles with PEG

Much effort has been spent to obtain “stealth” NPs with reduced reticuloendothelial system (RES) uptake and prolonged circulation time. One widely used method is surface adsorption or grafting with PEG to create a hydrophilic barrier [45-47], which can block electrostatic and hydrophobic interactions responsible for opsonization. PEG-functionalized PLGA NPs were prepared from PLA-PEG and PLGA-PEG copolymers [48-51]. By using di-block PEG-PLA, PEG-PLGA, and PEG-PCL polymers, the influence of PEG MW and content on the plasma protein adsorption and phagocytosis was investigated [52]. The sterically-stabilized PEG surface was found to reduce protein adsorption, but not eliminate it. The PEG MW critical for significant reduction of protein adsorption varied between 1.5 to 5 kDa [52,53], and it appeared that the critical MW to prevent protein adsorption might depend on the specific protein, individual proteins requiring a different length of PEG chain for prevention of

adsorption. Methoxy-PEG (mPEG)-PLGA block copolymers with different sizes of mPEG block (M_n 550, 750 and 2000) were used for the hydrophilic layer on PLGA NPs [54]. The average particle size was slightly increased with increasing mPEG MW due to extended PEG corona extending into aqueous medium.

Surface coating by adsorption is especially attractive for NP modification since the process can be separately controlled from the fabrication process. Based on a comb polymer of PLL-g-PEG designed for modification of metal oxide surfaces for protein resistance [55-57], PLL-g-PEG were used to coat PLGA microspheres through electrostatic interactions between cationic PLL backbone and anionic PLGA surface [58]. A drastic decrease in protein adsorption (by two orders of magnitude) was the result. Similarly, protein (HSA) NPs were stabilized with oxidized dextran-PEG conjugate, ultimately leading to surface grafting of PEG chains [32].

As an alternative to coating or grafting, it is possible to obtain surface-modified NPs by using derivatized proteins in the fabrication process. Lin et al. [32] were the first to report HSA NPs prepared from HSA modified with methoxy-PEG (HSA-mPEG), poly(amidoamine)-PEG (HSA-PAA-PEG) and poly(thioetheramidoacid)-PEG (HSA-PTAAC-PEG) [22,59]. The existence of a hydrated barrier surrounding the NPs was confirmed and the surface-modified particles showed a reduced plasma protein adsorption. The PEG MW was again

important for prevention of protein adsorption, where a 2 kDa (but not 5 kDa) PEG was most effective. The particles made from PEG-BSA displayed increased stability upon salt/pH challenge [22]. The fact that a reduction in protein adsorption was not always proportional to PEG size or extent of engraftment indicated the possibility of unique interactions with the matrix of the albumin NPs. Affecting the release rate of entrapped drugs as a result of surface modification is always a concern, but it was possible to achieve NP modification with PEG without affecting the release pattern of drugs [14].

1.4 Nanoparticle Properties Critical for Drug Delivery

Delivery of pharmacological agents formulated in NPs can be broadly classified into two categories, those intended for local vs. systemic administration. In the case of local administration, the NP formulation is expected to act as a 'depot', where a local concentration of the drug is maintained while preserving the agent in active form usually in a hostile environment. The NP may additionally act as a controlled release formulation, where NP properties precisely control the drug release rate. In the case of systemic administration, the NP formulation is expected to circumvent the initial clearance mechanisms in circulation, and preferably localize at the site of action of the drug. The NP formulation, once successfully localized to a desired site, becomes a local depot formulation. Understanding relationships among the physicochemical properties

of NPs and their physiological performance is paramount for successful delivery. Towards this end, a summary of pertinent literature is provided below, specifically focusing on NP properties critical for systemic and local delivery.

1.4.1 Particle Size and Circulation Time

Long-circulating carriers have a better chance of reaching their target and leading to a therapeutic benefit. Larger NPs are more likely to sediment in circulation or filtered in capillary beds and it is generally accepted that the NPs should not exceed 200 nm for this reason [60]. Despite several reports with exquisite control over NP size, the effect of size on circulation time is under-studied. Using relatively small BSA NPs (110-125 nm), PEG-functionalization of NPs was shown to improve the circulation time (systemic mean retention time increased by ~1.5-fold) as well as localization in some tissues, in particular brain [14]. Harashima et al. [61] reported the size-dependence of opsonization (see below for more details on opsonization process) for liposomes, and suggested that smaller carriers led to a reduced adsorption of proteins and opsonins and accordingly reduced uptake by phagocytic cells. The extent of opsonization decreased with a reduction in size from 800 to 200 nm, and no enhancement of phagocytic uptake was recorded below 200 nm. Besides systemic clearance, biodistribution of the NPs is also affected by their size. Porter et al. [62], using PEG-decorated NPs in rabbits,

showed that particles of <150 nm exhibited an increased localization in bone marrow, while ~250 nm particles were mostly sequestered in the spleen and liver, presumably by selective filtration in these organs [60]. In the bone marrow, a membrane of lining cells functions as a marrow-blood barrier, and not all NP localized to bone are actually accessible to bone-resident cells [63]. It is suggested that the vasculature in bone have pores of 80-100 nm [54,64] and NPs need to have a hydrodynamic sizes of <80 nm to extravasate into bone tissue. However, particles <100 nm may also pass through fenestrated hepatic sinusoidal endothelium [65], and may get entrapped in the liver, ultimately reducing their availability to the bone-resident cells.

For some applications, it is desirable to engineer NPs especially taken up by the phagocytic cells. Immuno-stimulation of macrophages against microbial infections, or immuno-suppression of macrophages in auto-inflammatory diseases, may be achieved with large NPs of 200-300 nm [23]. Gelatin NPs containing the cytotoxic drug clodronate, a bisphosphonate drug usually formulated with liposomes [66], were successfully employed for elimination of macrophages [67].

1.4.2 Nanoparticle Opsonization and Phagocytosis

A major obstacle for particulate drug carriers is the opsonization and clearance by the RES. The opsonization process is the adsorption and/or

activation of proteins capable of interacting with specific receptors on monocytes and various subsets of tissue macrophages, thus promoting particle recognition and uptake [65]. As much as 95% foreign particles may undergo opsonization and clearance by the RES [45]. Opsonization typically takes place in the blood circulation and can take anywhere from a few seconds to many days to complete[68]. The exact mechanism through which this process is activated is not yet fully understood. The small size of the NPs is no impediment for cellular uptake, and sizes and surface characteristics have been repeatedly emphasized as important factors affecting clearance behavior and tissue distribution of particulate carriers [65]. Neutral and hydrophilic particles have a much lower opsonization rate than the charged and hydrophobic particles [69]. The core properties of the NPs, although generally considered shielded from the physiological contact, may also affect the extent and nature of protein adsorption[52]. PEGylation is the standard approach to reduce protein adsorption to NPs (see below), but some degree of protein adsorption might be beneficial to prevent NP aggregation if the surface properties alone is not sufficient (e.g., low PEG density) to prevent aggregation [32]. Recent studies with poly(isobutylcyanoacrylate) NPs indicated the particle size (100-300 nm) not influencing the extent of complement activation [70]. But surface chemistry, specifically the choice of polysaccharide coating, was important, chitosan coating giving relatively low complement activation that could be reduced to background

levels with high MW chitosans. Whereas the size of naked poly(cyanoacrylate-co-*N*-hexadecyl cyanoacrylate) NPs did not influence protein adsorption, PEGylation of such NPs resulted in lower protein adsorption and phagocytic uptake *in vitro* with decreasing particle size [71]. The ideal PEG MW for effective reduction of opsonization, however, was variable in different NP preparations, and this was likely to reflect the exact configuration of the PEG on NP surfaces [72].

With BSA NPs, the negative ζ -potential (-15 to -30 mV) was considered a significant advantage since it can reduce non-specific interaction with cellular surfaces. Despite an anionic surface, however, ~200 nm HSA NPs were readily internalized by primary human macrophages [20]. Cationic gelatin NPs (300-500 nm) were also internalized by the rat macrophage-like cells [67]. The effect of particle size on internalization was not systematically investigated for protein NPs, but having highly anionic and cationic surfaces was equally detrimental for uptake in macrophage-like U937 cells and mouse macrophages [69]. Internalization of cationic NPs was not surprising but anionic NPs were presumably opsonized for such a stimulated uptake [69]. Unlike *in vitro* results, *in vivo* uptake into the major clearance organ (liver) was not affected by the ζ -potential of these particular NPs (size: ~500 nm) [69].

1.4.3 Factors Controlling Drug Release

Mechanism(s) controlling drug release from NPs may include (i) dissolution of drugs from a solid state, (ii) displacement of adsorbed drugs from NP matrix, (iii) diffusion through NP matrix or surface coating (if any), and (iv) degradation of NP matrix or surface coating [46]. For drugs strongly interacting with a NP matrix [6], displacement with buffer components (*in vitro*) or endogenous solutes (*in vivo*) may be a critical factor. With conventional drugs of high diffusivity, such as ganciclovir [25] and clodronate [67], release patterns indicated two types of drug fractions, a weakly and a strongly bound fraction. The former fraction is released upon changes in medium composition where the drug solubility is enhanced or displacing moieties appear in the new medium. A rapid release could be observed without a distinctive ‘burst’ vs. ‘sustained release’ pattern [14] and the extent of the initial release is likely to depend on the loading method [25]. NPs prepared from synthetic polyesters, as compared to proteins, might be better engineered for a smaller burst release [73,74], and longer duration of release [12,75,76] by controlling the MW and/or composition of polymers used for NP fabrication [74,75]. Although sustained release is usually desired, a ‘burst’ release might be sufficient for some indications; IFN- γ released within a 24-hour period was sufficient for a lasting immuno-stimulatory activity [23].

Enzymatic degradation is an important mechanism for protein and

polyester NPs. It is usually a surface-restricted [6], and may cause accelerated NP degradation due to large surface area:volume ratio. Little work has been performed in assessing the degradation of NPs under physiological conditions. Wartlick et al. [77] showed a correlation between the extent of GA crosslinking and rate of enzymatic degradation of HSA NPs *in vitro*. This was also the case after NP internalization, where HSA particles remained intact when NPs were excessively crosslinked, but the NP cargo was dispersed in cytoplasm for under-crosslinked particles [77]. Since these studies relied on fluorescently-labeled molecules, and the integrity of the label was not explored, these results need to be considered with caution. BSA and β -lactoglobulin particles also displayed a relatively rapid ($t_{1/2} \sim 8$ -15 hours) enzymatic degradation *in vitro* [21]. The effect of degradation on pharmacological activity needs to be probed for individual indications, as well as the correlation between the drug release rate and enzymatic degradation.

1.5 Designing Nanoparticles for Targeting to Specific Tissues

An exciting possibility for NPs could be realized if they can be made 'Tissue-seeking'. Although particle size and surface characteristics may alter biodistribution *in vivo*, tissue-specificity can only arise if NPs display a preferential affinity to a target tissue. To accomplish this goal, NPs are functionalized with tissue-specific molecular ligands. These ligands usually

display an affinity to tissue-specific cell surface molecules, and they improve retention of NPs due to enhanced local affinity and slowing of NP loss from the tissues. Alternatively, substrates for tissue-specific transporters have been used for NPs to improve cellular uptake (i.e., cells responsible for barrier functions, such as brain-blood-barrier) into the desired tissues. While natural ligands have been preferred, synthetic ligands with no biological function have been also utilized for this purpose. The impetus for the latter ligands is the superior affinity of the ligands to target tissues (e.g., bisphosphonates for bone) or an ability to tailor target affinity and specificity via chemical engineering (e.g., aptamers). A summary of current efforts for tissue-targeting NPs is provided in **Table 1-2** and a select set of applications are discussed below.

1.5.1 Brain Targeting

Targeting NPs to brain have relied on ligands that display facilitated transport at the blood-brain barrier (BBB). Transferrin is one such ligand and Mishra et al. [14] described modification of BSA NPs with maleimide-PEG-*N*-hydroxysuccinimide (MAL-PEG-NHS) so as to functionalize the NP surfaces with transferrin. Only a small fraction of surface PEG groups were coupled to transferrin (3-4%), so that an effective PEG coating for improved biodistribution could be achieved by this method. Delivering azidothymidine (AZT) to brain in transferrin-PEG-HSA NPs was 2-3 fold more effective than the

PEG-HSA NPs, which was more effective as compared to free AZT or AZT entrapped in unmodified NPs [14]. Liver uptake was also enhanced for transferrin-functionalized NP, and these two organs, at times, accounted for ~50% of the administered dose [14]. NPs functionalized with apolipoprotein E were also prepared for brain-targeting by direct coupling with MAL-PEG-NHS linker[78,79] or indirect coupling via avidin/biotin bridge [79]. A desired pharmacological effect was observed only when the drug of interest, loperamide which is impermeable to BBB, was formulated in apolipoprotein E-decorated NPs [78,79]. The extent of NP targeting as a result of apolipoprotein E coupling remains to be quantified. By using a variety of isoforms, the mechanism of NP transport appeared to be specific for apolipoprotein E and it relied on transcytosis pathway undertaken by lipoprotein particles.

1.5.2 Tumor Targeting

Surface modification of BSA [80,81], gelatin [81], PLA [82] and PLGA NPs [76] with anti-human epidermal growth factor receptor 2 (HER2) antibodies was attempted for targeting NPs to breast cancers. The uptake of antibody-coupled NPs was facilitated by HER2-expressing tumor cell lines *in vitro*. On prolonged incubation, however, even non-specific NPs (e.g., PEG-HSA) were internalized [80]. This was unexpected since (i) the NPs displayed a ζ -potential of approximately -40 mV (repulsive to anionic cell surfaces), and (ii)

PEG molecules should have reduced non-specific cell-surface interactions. Sedimentation might be one mechanism to deposit NPs on cell surface, but how this translates to *in vivo* situation remains to be seen. PLA NPs functionalized with a control (non-internalizing) antibody gave little uptake as compared to HER2-mediated uptake [82], suggesting that the internalization was specific and not due to chemical derivatization on the surface. *In vivo* studies on these NPs remain to be reported. PLGA NPs functionalized with aptamers against prostate specific membrane antigen, on the other hand, yielded ~4-fold improved targeting of the carriers in a xenograft prostate graft model [83], and significantly improved the survival in a xenograft model as compared to non-targeted chemotherapeutic delivery [84].

1.5.3 Bone Targeting

The structural qualities of bone, especially the presence of hydroxyapatite, and specific affinity of certain molecules to this mineral, provide a unique opportunity to target drugs to bone tissue. Molecules with diverse structural features were reported with bone affinity [85,86]. Unlike natural molecules used for targeting to other tissues, bone-targeting ligands are generally synthetic entities, among which bisphosphonates (BP) play a prominent role. BPs are a class of synthetic compounds structurally related to pyrophosphates, but feature a geminal diphosphonate (P-C-P) instead of hydrolyzable P-O-P bond of

pyrophosphate. BPs are highly water-soluble, acidic compounds at the physiological pH, and remain bound to bone mineral after systemic administration. BPs have been traditionally conjugated to therapeutic molecules for bone targeting but utilizing NPs functionalized with BPs might be a superior alternative; bone targeting can be achieved without modifying the pharmacological agent *per se*, an important consideration particularly for bioactive protein therapeutics.

The design of bone-seeking PLGA NPs (micelles) was reported by using a PLGA polymer grafted with alendronate [54]. The NPs were 40-60 nm in size (a suitable size for vascular penetration at bones), and were able to entrap and release a hydrophobic drug (estrogen) from its PLGA core. Although the alendronate-incorporated NPs displayed hydroxyapatite (HA) affinity, it was not clear whether the binding was due to alendronate *per se*, since binding of unfunctionalized NPs were not reported. BPs were also incorporated into liposomes by using a lipophilic BP derivative, cholesteryl-trisoxoethylene-bisphosphonic acid (CHOL-TOE-BP) [87]. Such liposomes were 100-135 nm in size, and displayed an *in vitro* HA affinity that was dependent on the extent of BP incorporated in liposomes. The pharmacokinetics and tissue distribution of the BP-conjugated NPs and liposomes remains to be probed to explore their full potential to act as bone-seeking NPs.

Future studies in bone-targeting efforts are likely to be accelerated since

basic foundation of this approach is being steadily established in independent labs. Synthetic polymers with BP moieties have been synthesized and their superior bone affinity was demonstrated [64]. Such polymers can be easily fabricated into bone-seeking NP formulations. Our extensive experience on protein derivatization with BPs could yield bone-seeking protein NPs if the derivatized proteins can be fabricated into NPs. Cationic polymers, such as PLL and PEI, were recently reported to display a hydroxyapatite affinity that was equivalent to BP-mediated affinity [88]. Such polymers can be used in coating NPs for bone targeting.

1.6 Conclusions

Pharmacological agents entrapped in NPs are attracting increasing attention to overcome delivery challenges posed *in vivo*. Well-established approaches to fabricate NPs are continually optimized to improve the encapsulation efficiency while preserving the bioactivity of therapeutic agents. New methods to formulate NPs are being proposed, and molecular assembly along with precise control of biomaterial structures are leading the way in this effort. While the size of NPs from several fabrication processes is now routinely controlled, understanding the impact of size on various facets of drug delivery, such as phagocytosis, circulation time and drug release kinetics, remains understudied. Several avenues have been taken to functionalize the surface of NPs with desired ligands. These include NP fabrication from modified biomaterials,

coating NPs with designed polymers, surface-grafting post-fabrication, and using non-covalent ‘affinity’ bridges to place ligands on NP surfaces. These efforts are establishing the foundation of tissue-specific drug delivery by NPs. Therapeutic applications of tissue targeting are expected to broaden and more efforts will be needed to better understand *in situ* fate of NPs, as well as the relationship among NP degradation, drug release and observed therapeutic effects.

Table 1-1. A representative summary of biomaterials used for preparation of nanoparticulate delivery systems and drugs used for delivery.

Biomaterial	Drugs	Particle size (nm)	Author [Ref.]
<i>Polyester</i>			
Poly(lactic acid)	Protein C	200-250	Zambaux [75]
Poly(lactic-co-glycolic acid)	Estrogen	40-60	Choi [54]
Poly(ϵ -caprolactone)	Tamoxifen	250-300	Chawla [6]
<i>Protein</i>			
Human serum albumin	Doxorubicin	150-500	Dreis [29]
Bovine serum albumin	Interferon- γ	300-340	Segura [26]
β -Lactoglobulin	-	60-130	Ko [21]
Protamine	Oligonucleotides	80-200	Lochmann [89]
Gelatin	Clodronate	300-500	Li [67]
Gliadin	α -Tocopherol/ benzalkonium chloride/linalool and linalyl acetate	900-950	Duclairoir [90]
Legumin	-	250-300	Irache [91]
<i>Polysaccharide</i>			
Chitosan	Ovalbumin	350	Amidi [43]
<i>Polycyanoacrylate</i>			
Poly(isobutylcyanoacrylate), Poly(isohexylcyanoacrylate)	Oligonucleotides	N/A	Fattal [92]
Poly(butylcyanoacrylate)	Doxorubicin	178	Reddy [93]
Poly(hexadecylcyanoacrylate)	-	150	Peracchia [94]
<i>Lipids</i>			
Trimyristin	Paclitaxel	200-250	Lee [95]
Glycerol monostearin	Mifepristone	27	Yuan [96]
Glyceryl behenate	Vitamin A	300-500	Jenning [97]
<i>Polyelectrolyte</i>			
Polyethylenimine	Cyclosporine	100-300	Cheng [98]
Poly(styrene sulfonate)/ poly(allylamine.HCl)	Chymotrypsin	100-300	Balabushevitch [41]
Poly(L-maleic acid)/Chitosan	Insulin	100-250	Fan [42]

Table 1-2. A summary of ligands used for NP derivatization for targeting NPs to specific tissues

Ligand	NP Derivatized	Target cells/Tissue	Evaluation	Ref.
Folate	BSA	Cancerous Cells	In vitro	[125]
Folate	PLGA	Cancerous Cells	In vitro	[160]
Aptamer against PSMA	PLGA	Tumor	In vivo	[83,84]
Wheat germ agglutinin	PLGA	Tumor	In vivo	[161]
HER2	HSA	Cancerous Cells	In vitro	[80,81]
HER2	PLA or PLGA	Cancerous Cells	In vitro	[76,82]
GFdTGFLS-Glucose	PLGA	Brain	In vivo	[162]
Apolipoprotein E	HSA	Brain	In vivo	[78,79]
Synthetic opioid peptides	PLGA	Brain	In vivo	[163]
Transferrin	HSA	Brain	In vivo	[14]
Bisphosphonate	liposome	Bone	In vitro	[87]
Bisphosphonate	PLGA	Bone	In vitro	[54]
Cyclic-RGD	PLGA	Endothelial cells	In vitro	[164]
Linear-GRGDS	PLGA/PLGA-PEG /PCL-PEG	M cells	In vitro	[13]
Tetanus toxin C	PLGA-PEG	Neuronal cells	In vitro	[50]

BSA: Bovine serum albumin; HSA: Human serum albumin; NP: Nanoparticle; PCL: Poly(ϵ -caprolactone); PEG: Poly(ethylene glycol); PLA: Poly(lactic acid); PLGA: Poly(lactic-co-glycolic acid); PSMA: Prostate specific membrane antigen.

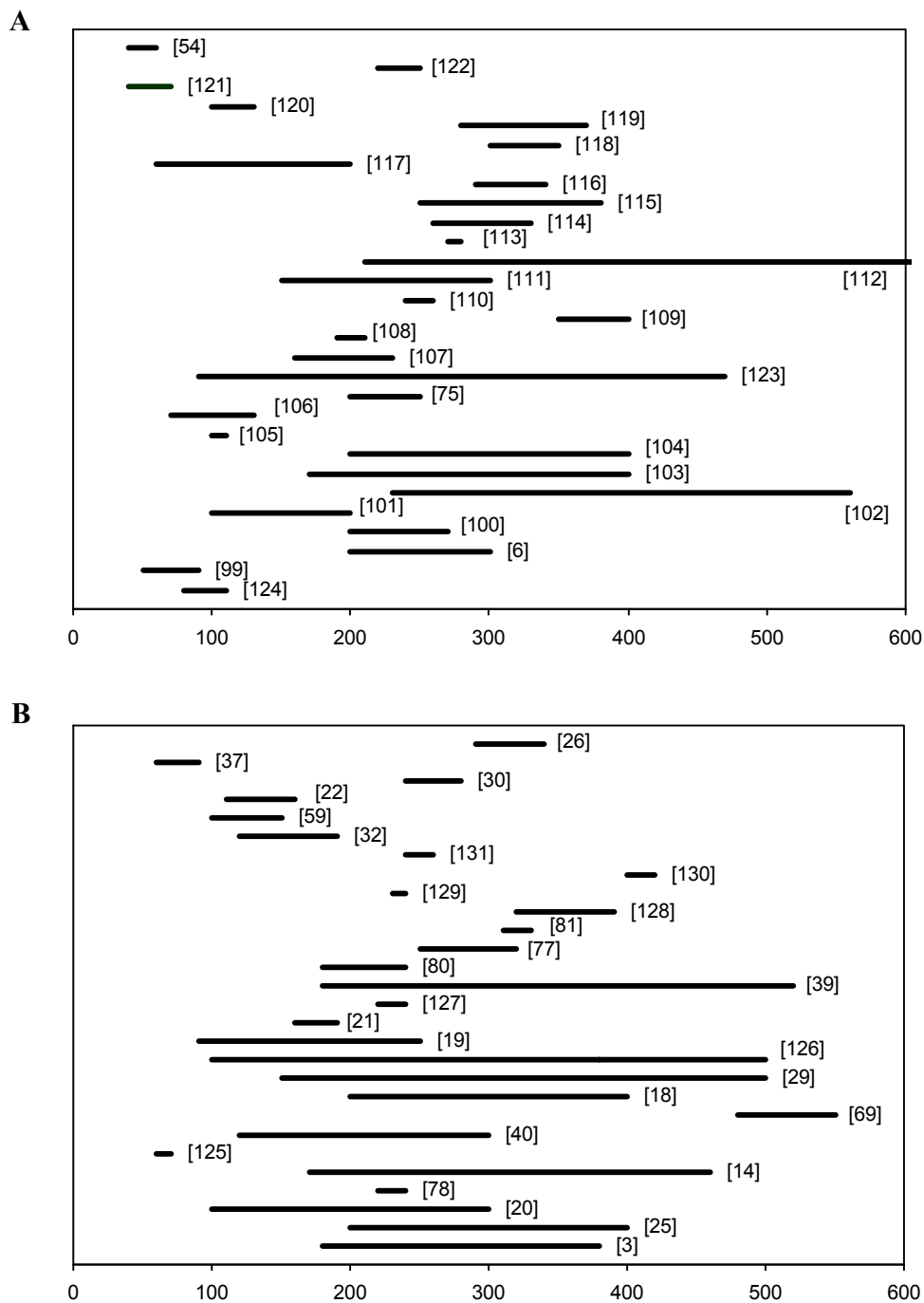


Figure 1-1 Typical size (nm) ranges of polyester (A), protein (B) and chitosan (C) NPs reported in the literature. Note that the chosen references were not intended to be exhaustive, but rather representative of common size ranges reported. Chitosan was chosen as a representative polyelectrolyte-based NP since it has recently received attention for a diverse range of biomedical applications.

C

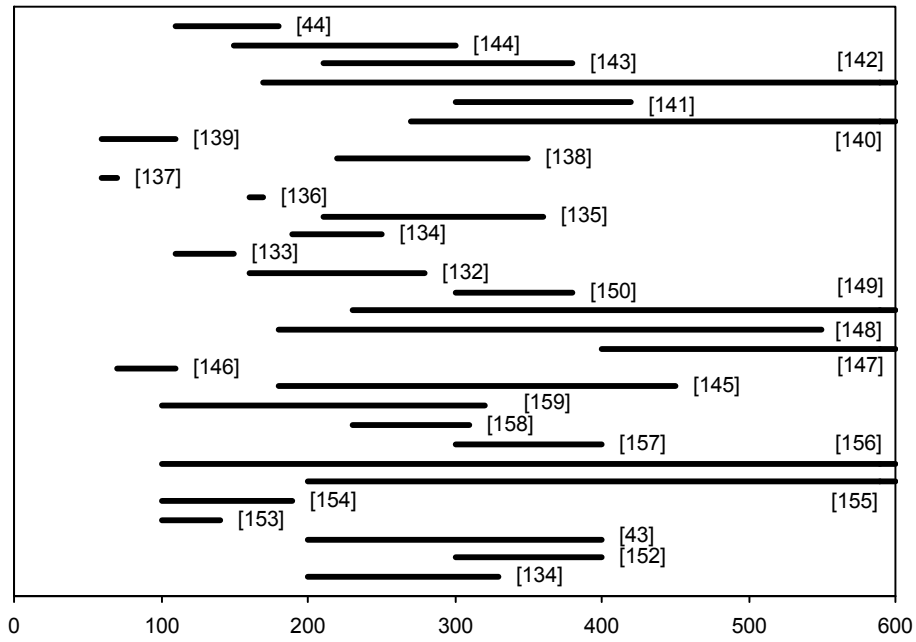


Figure 1-1 (Continued)

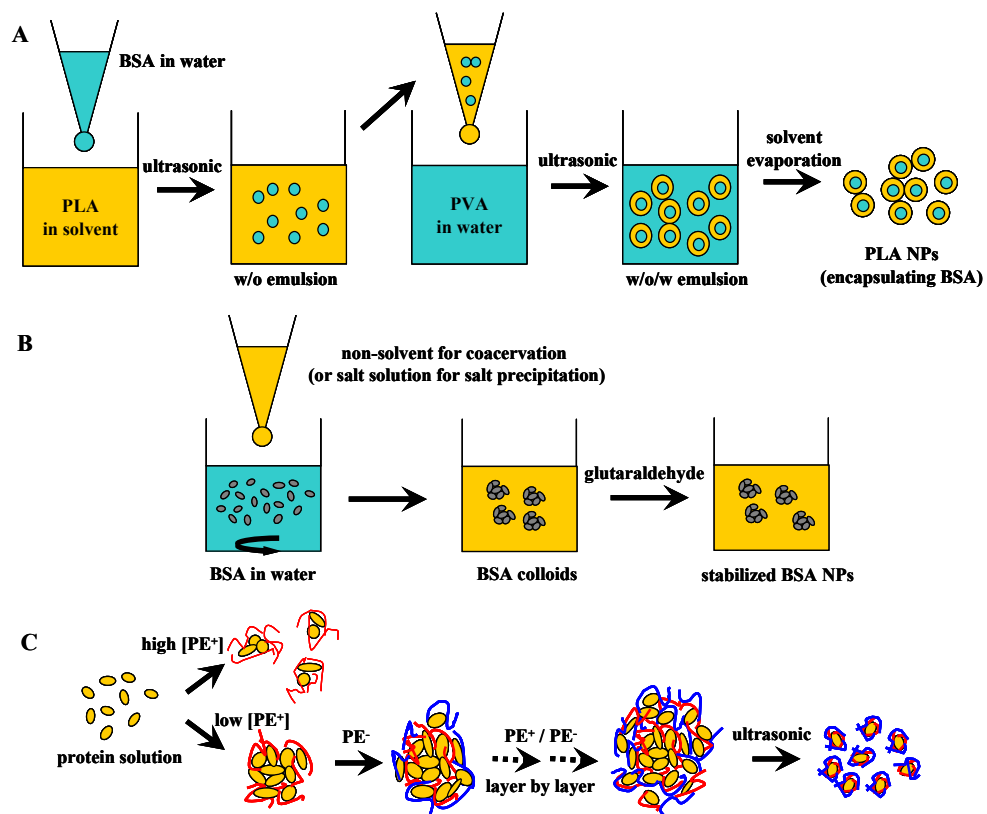


Figure 1-2 Commonly used methods to prepare nanoparticles: (A) double emulsion, (B) coacervation (and salt precipitation), and (C) polyelectrolyte complexation.

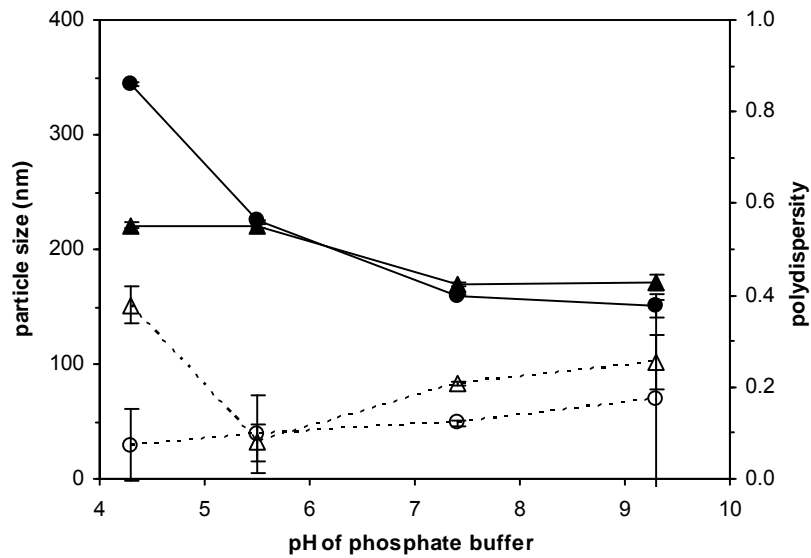


Figure 1-3 Influence of pH on the size (solid line) and polydispersity index (dashed line) of BSA NPs. NPs were prepared by dropwise addition of ethanol to a mixture of equal volumes of BSA solution (circle: 10 mg/mL, triangle: 30 mg/mL) and 10 mM phosphate buffer (pH of 4.3, 5.5, 7.4 and 9.3). Size (from dynamic light scattering) and polydispersity data are expressed as mean \pm S.D. (n = 3). Note the gradual reduction of particle size as the pH of the NP preparation solution is increased.

REFERENCES

- [1]. Socinski, M. Update on nanoparticle albumin-bound paclitaxel. *Clin Adv Hematol Oncol* **2006**, *4*, 745-746.
- [2]. Mehnert, W.; Mader, K. Solid lipid nanoparticles: Production, characterization and applications. *Adv Drug Deliv Rev* **2001**, *47*, 165-196.
- [3]. Muller, B. G.; Leuenberger, H.; Kissel, T. Albumin nanospheres as carriers for passive drug targeting: an optimized manufacturing technique. *Pharm Res* **1996**, *13*, 32-37.
- [4]. Raghuvanshi, R. S.; Goyal, S.; Singh, O.; Panda, A. K. Stabilization of dichloromethane-induced protein denaturation during microencapsulation. *Pharm Devel Technol* **1998**, *3*, 269-276.
- [5]. Sturesson, C.; Carlfors, J. Incorporation of protein in PLG-microspheres with retention of bioactivity. *J Control Rel* **2000**, *67*, 171-178.
- [6]. Chawla, J. S.; Amiji, M. M. Biodegradable poly(ϵ -caprolactone) nanoparticles for tumor-targeted delivery of tamoxifen. *Int J Pharm* **2002**, *249*, 127-138.
- [7]. Nehilla, B. J.; Bergkvist, M.; Popat, K. C.; Desai, T. A. Purified and surfactant-free coenzyme Q10-loaded biodegradable nanoparticles. *Int J Pharm* **2008**, *348*, 107-114.
- [8]. Sussman, E. M.; Clarke, M. B.; Shastri, V. P. Single-step process to produce surface-functionalized polymeric nanoparticles. *Langmuir* **2007**, *23*, 12275-12279.
- [9]. Zambaux, M. F.; Bonneaux, F.; Gref, R.; Maincent, P.; Dellacherie, E.; Alonso, M. J.; Labrude, P.; Vigneron, C. Influence of experimental parameters on the characteristics of poly(lactic acid) nanoparticles prepared by a double emulsion method. *J Control Rel* **1998**, *50*, 31-40.
- [10]. Song, X.; Zhao, Y.; Wu, W.; Bi, Y.; Cai, Z.; Chen, Q.; Li, Y.; Hou, S. PLGA nanoparticles simultaneously loaded with vincristine sulfate and verapamil hydrochloride: systematic study of particle size and drug entrapment efficiency. *Int J Pharm* **2008**, *350*, 320-329.
- [11]. Tewes, F.; Munnier, E.; Antoon, B.; Ngaboni Okassa, L.; Cohen-Jonathan,

- S.; Marchais, H.; Douziech-Eyrolles, L.; Souce, M.; Dubois, P.; Chourpa, I. Comparative study of doxorubicin-loaded poly(lactide-co-glycolide) nanoparticles prepared by single and double emulsion methods. *Euro J Pharm Biopharm* **2007**, *66*, 488-492.
- [12]. Li, Y. P.; Pei, Y. Y.; Zhang, X. Y.; Gu, Z. H.; Zhou, Z. H.; Yuan, W. F.; Zhou, J. J.; Zhu, J. H.; Gao, X. J. PEGylated PLGA nanoparticles as protein carriers: synthesis, preparation and biodistribution in rats. *J Control Rel* **2001**, *71*, 203-211.
- [13]. Garinot, M.; Fievez, V.; Pourcelle, V.; Stoffelbach, F.; des Rieux, A.; Plapied, L.; Theate, I.; Freichels, H.; Jerome, C.; Marchand-Brynaert, J.; Schneider, Y. J.; Preat, V. PEGylated PLGA-based nanoparticles targeting M cells for oral vaccination. *J Control Rel* **2007**, *120*, 195-204.
- [14]. Mishra, V.; Mahor, S.; Rawat, A.; Gupta, P. N.; Dubey, P.; Khatri, K.; Vyas, S. P. Targeted brain delivery of AZT via transferrin anchored pegylated albumin nanoparticles. *J Drug Target* **2006**, *14*, 45-53.
- [15]. Chung, Y. I.; Ahn, K. M.; Jeon, S. H.; Lee, S. Y.; Lee, J. H.; Tae, G. Enhanced bone regeneration with BMP-2 loaded functional nanoparticle-hydrogel complex. *J Control Rel* **2007**, *121*, 91-99.
- [16]. Isobe, M.; Yamazaki, Y.; Mori, M.; Ishihara, K.; Nakabayashi, N.; Amagasa, T. The role of recombinant human bone morphogenetic protein-2 in PLGA capsules at an extraskeletal site of the rat. *J Biomed Mater Res* **1999**, *45*, 36-41.
- [17]. Meinel, L.; Zoidis, E.; Zapf, J.; Hassa, P.; Hottiger, M. O.; Auer, J. A.; Schneider, R.; Gander, B.; Luginbuehl, V.; Bettschart-Wolfisberger, R.; Illi, O. E.; Merkle, H. P.; Rechenberg, B. v. Localized insulin-like growth factor I delivery to enhance new bone formation. *Bone* **2003**, *33*, 660-672.
- [18]. Weber, C.; Coester, C.; Kreuter, J.; Langer, K. Desolvation process and surface characterisation of protein nanoparticles. *Int J Pharm* **2000**, *194*, 91-102.
- [19]. Lin, W.; Coombes, A. G. A.; Davies, M. C.; Davis, S. S.; Illum, L. Preparation of sub-100 nm human serum albumin nanoparticles using a pH-coacervation method. *J Drug Target* **1993**, *1*, 237-243.
- [20]. Langer, K.; Balthasar, S.; Vogel, V.; Dinauer, N.; von Briesen, H.; Schubert, D. Optimization of the preparation process for human serum

- albumin (HSA) nanoparticles. *Int J Pharm* **2003**, *257*, 169-180.
- [21]. Ko, S.; Gunasekaran, S. Preparation of sub-100-nm β -lactoglobulin (BLG) nanoparticles. *J Microencapsul* **2006**, *23*, 887-898.
- [22]. Lin, W.; Garnett, M. C.; Schacht, E.; Davis, S. S.; Illum, L. Preparation and in vitro characterization of HSA-mPEG nanoparticles. *Int J Pharm* **1999**, *189*, 161-170.
- [23]. Segura, S.; Gamazo, C.; Irache, J. M.; Espuelas, S. Gamma interferon loaded onto albumin nanoparticles: in vitro and in vivo activities against *Brucella abortus*. *Antimicrob Agents Chemother.* **2007**, *51*, 1310-1314.
- [24]. Zhang, S.; Wang Guilin; Lin, X.; Jennissen, H.; Chadzinikolaidou, M.; Uludag, H. Polyethylenimine-coated albumin nanoparticles for BMP-2 delivery. *Biotechnol Prog* **2008**, *24*, 945-956.
- [25]. Merodio, M.; Arnedo, A.; Renedo, M. J.; Irache, J. M. Ganciclovir-loaded albumin nanoparticles: characterization and in vitro release properties. *Euro J Pharm Sci* **2001**, *12*, 251-259.
- [26]. Segura, S.; Espuelas, S.; Renedo, M. a. J. s.; Irache, J. M. Potential of albumin nanoparticles as carriers for interferon gamma. *Drug Devel Ind Pharm* **2005**, *31*, 271-280.
- [27]. Leo, E.; ngela Vandelli, M.; Cameroni, R.; Forni, F. Doxorubicin-loaded gelatin nanoparticles stabilized by glutaraldehyde: involvement of the drug in the cross-linking process. *Int J Pharm* **1997**, *155*, 75-82.
- [28]. Willmott, N.; Cummings, J.; Florence, A. T. In vitro release of adriamycin fro drug-loaded albumin and haemoglobin microspheres. *J Microencapsul* **1985**, *2*, 293-304.
- [29]. Dreis, S.; Rothweiler, F.; Michaelis, M.; Cinatl, J.; Kreuter, J.; Langer, K. Preparation, characterisation and maintenance of drug efficacy of doxorubicin-loaded human serum albumin (HSA) nanoparticles. *Int J Pharm* **2007**, *341*, 207-214.
- [30]. Arnedo, A.; Irache, J. M.; Merodio, M.; Espuelas Millan, M. S. Albumin nanoparticles improved the stability, nuclear accumulation and anticytomegaloviral activity of a phosphodiester oligonucleotide. *J Control Rel* **2004**, *94*, 217-227.
- [31]. Chen, C. Q.; Lin, W.; Coombes, A. G. A.; Davis, S. S.; Illum, L.

- Preparation of human serum albumin microspheres by a novel acetone-heat denaturation method. *J Microencapsul* **1994**, *11*, 395-407.
- [32]. Lin, W.; Coombes, A. G. A.; Garnett, M. C.; Davies, M. C.; Schacht, E.; Davis, S. S.; Illum, L. Preparation of sterically stabilized human serum albumin nanospheres using a novel dextranox-mPEG crosslinking agent. *Pharm Res* **1994**, *11*, 1588-1592.
- [33]. Wang, Y.; Gao, J. Y.; Dubin, P. L. Protein separation via polyelectrolyte coacervation: selectivity and efficiency. *Biotechnol Prog* **1996**, *12*, 356-362.
- [34]. Farrell, L. L.; Pepin, J.; Kucharski, C.; Lin, X.; Xu, Z.; Uludag, H. A comparison of the effectiveness of cationic polymers poly-L-lysine (PLL) and polyethylenimine (PEI) for non-viral delivery of plasmid DNA to bone marrow stromal cells (BMSC). *Euro J Pharm Biopharm* **2007**, *65*, 388-397.
- [35]. Nisha, C. K.; Manorama, S. V.; Ganguli, M.; Maiti, S.; Kizhakkedathu, J. N. Complexes of poly(ethylene glycol)-based cationic random copolymer and calf thymus DNA: a complete biophysical characterization. *Langmuir* **2004**, *20*, 2386-2396.
- [36]. Dautzenberg, H.; Zintchenko, A.; Konak, C.; Reschel, T.; Subr, V.; Ulbrich, K. Polycationic graft copolymers as carriers for oligonucleotide delivery. complexes of oligonucleotides with polycationic graft copolymers. *Langmuir* **2001**, *17*, 3096-3102.
- [37]. Serefoglou, E.; Oberdisse, J.; Staikos, G. Characterization of the soluble nanoparticles formed through coulombic interaction of bovine serum albumin with anionic graft copolymers at low pH. *Biomacromolecules* **2007**, *8*, 1195-1199.
- [38]. Matsudo, T.; Ogawa, K.; Kokufuta, E. Complex formation of protein with different water-soluble synthetic polymers. *Biomacromolecules* **2003**, *4*, 1794-1799.
- [39]. Rhaese, S.; von Briesen, H.; Rubsamen-Waigmann, H.; Kreuter, J.; Langer, K. Human serum albumin-polyethylenimine nanoparticles for gene delivery. *J Control Rel* **2003**, *92*, 199-208.
- [40]. Vogel, V.; Lochmann, D.; Weyermann, J.; Mayer, G.; Tziatzios, C.; van den Broek, J. A.; Haase, W.; Wouters, D.; Schubert, U. S.; Kreuter, J.;

- Zimmer, A.; Schubert, D. Oligonucleotide-protamine-albumin nanoparticles: preparation, physical properties, and intracellular distribution. *J Control Rel* **2005**, *103*, 99-111.
- [41]. Balabushevitch, N. G.; Sukhorukov, G. B.; Moroz, N. A.; Volodkin, D. V.; Larionova, N. I.; Donath, E.; Mohwald, H. Encapsulation of proteins by layer-by-layer adsorption of polyelectrolytes onto protein aggregates: factors regulating the protein release. *Biotechnol Bioeng* **2001**, *76*, 207-213.
- [42]. Fan, Y. F.; Wang, Y. N.; Fan, Y. G.; Ma, J. B. Preparation of insulin nanoparticles and their encapsulation with biodegradable polyelectrolytes via the layer-by-layer adsorption. *Int J Pharm* **2006**, *324*, 158-167.
- [43]. Amidi, M.; Romeijn, S. G.; Borchard, G.; Junginger, H. E.; Hennink, W. E.; Jiskoot, W. Preparation and characterization of protein-loaded N-trimethyl chitosan nanoparticles as nasal delivery system. *J Control Rel* **2006**, *111*, 107-116.
- [44]. Xu, Y.; Du, Y.; Huang, R.; Gao, L. Preparation and modification of N-(2-hydroxyl) propyl-3-trimethyl ammonium chitosan chloride nanoparticle as a protein carrier. *Biomaterials* **2003**, *24*, 5015-5022.
- [45]. Malafaya, P. B.; Silva, G. A.; Baran, E. T.; Reis, R. L. Drug delivery therapies I: General trends and its importance on bone tissue engineering applications. *Curr Opin Solid State Mater Sci* **2002**, *6*, 283-295.
- [46]. Soppimath, K. S.; Aminabhavi, T. M.; Kulkarni, A. R.; Rudzinski, W. E. Biodegradable polymeric nanoparticles as drug delivery devices. *J Control Rel* **2001**, *70*, 1-20.
- [47]. Lee, K. Y.; Yuk, S. H. Polymeric protein delivery systems. *Prog Polym Sci* **2007**, *32*, 669-697.
- [48]. Stolnik, S.; Dunn, S. E.; Garnett, M. C.; Davies, M. C.; Coombes, A. G. A.; Taylor, D. C.; Irving, M. P.; Purkiss, S. C.; Tadros, T. F.; Davis, S. S.; Illum, L. Surface modification of poly(lactide-co-glycolide) nanospheres by biodegradable poly(lactide)-poly(ethylene glycol) copolymers. *Pharm Res* **1994**, *11*, 1800-1808.
- [49]. Gref, R.; Minamitake, Y.; Peracchia, M. T.; Trubetskoy, V.; Torchilin, V.; Langer, R. Biodegradable long-circulating polymeric nanospheres. *Science* **1994**, *263*, 1600-1603.

- [50]. Townsend, S. A.; Evrony, G. D.; Gu, F. X.; Schulz, M. P.; Brown Jr, R. H.; Langer, R. Tetanus toxin C fragment-conjugated nanoparticles for targeted drug delivery to neurons. *Biomaterials* **2007**, *28*, 5176-5184.
- [51]. Gryparis, E. C.; Mattheolabakis, G.; Bikiaris, D.; Avgoustakis, K. Effect of conditions of preparation on the size and encapsulation properties of PLGA-mPEG nanoparticles of cisplatin. *Drug Deliv* **2007**, *14*, 371-380.
- [52]. Gref, R.; Luck, M.; Quellec, P.; Marchand, M.; Dellacherie, E.; Harnisch, S.; Blunk, T.; Muller, R. H. 'Stealth' corona-core nanoparticles surface modified by polyethylene glycol (PEG): influences of the corona (PEG chain length and surface density) and of the core composition on phagocytic uptake and plasma protein adsorption. *Colloids Surf B: Biointerfaces* **2000**, *18*, 301-313.
- [53]. Bergstrom, K.; Osterberg, E.; Holmberg, K.; Hoffman, A. S.; Schuman, T. P.; Kozlowski, A.; Harris, J. H. Effects of branching and molecular weight of surface-bound poly(ethylene oxide) on protein rejection. *J Biomater Sci Polym Ed* **1994**, *6*, 123-132.
- [54]. Choi, S. W.; Kim, J. H. Design of surface-modified poly(D,L-lactide-co-glycolide) nanoparticles for targeted drug delivery to bone. *J Control Rel* **2007**, *122*, 24-30.
- [55]. Kenausis, G. L.; Voros, J.; Elbert, D. L.; Huang, N.; Hofer, R.; Ruiz-Taylor, L.; Textor, M.; Hubbell, J. A.; Spencer, N. D. Poly(L-lysine)-g-poly(ethylene glycol) layers on metal oxide surfaces: attachment mechanism and effects of polymer architecture on resistance to protein adsorption. *J Phys Chem B* **2000**, *104*, 3298-3309.
- [56]. Huang, N. P.; Michel, R.; Voros, J.; Textor, M.; Hofer, R.; Rossi, A.; Elbert, D. L.; Hubbell, J. A.; Spencer, N. D. Poly(L-lysine)-g-poly(ethylene glycol) layers on metal oxide surfaces: surface-analytical characterization and resistance to serum and fibrinogen adsorption. *Langmuir* **2001**, *17*, 489-498.
- [57]. VandeVondele, S.; Voros, J.; Hubbell, J. A. RGD-grafted poly-L-lysine-graft-(polyethylene glycol) copolymers block non-specific protein adsorption while promoting cell adhesion. *Biotechnol Bioeng* **2003**, *82*, 784-790.
- [58]. Faraasen, S.; Voros, J.; Csucs, G.; Textor, M.; Merkle, H. P.; Walter, E. Ligand-specific targeting of microspheres to phagocytes by surface

- modification with poly(L-lysine)-grafted poly(ethylene glycol) conjugate. *Pharm Res* **2003**, *20*, 237-246.
- [59]. Lin, W.; Garnett, M. C.; Davies, M. C.; Bignotti, F.; Ferruti, P.; Davis, S. S.; Illum, L. Preparation of surface-modified albumin nanospheres. *Biomaterials* **1997**, *18*, 559-565.
- [60]. Moghimi, S. M.; Hedeman, H.; Muir, I. S.; Illum, L.; Davis, S. S. An investigation of the filtration capacity and the fate of large filtered sterically-stabilized microspheres in rat spleen. *Biochim Biophys Acta* **1993**, *1157*, 233-240.
- [61]. Harashima, H.; Sakata, K.; Funato, K.; Kiwada, H. Enhanced hepatic uptake of liposomes through complement activation depending on the size of liposomes. *Pharm Res* **1994**, *11*, 402-406.
- [62]. Porter, C. J. H.; Moghimi, S. M.; Illum, L.; Davis, S. S. The polyoxyethylene/polyoxypropylene block co-polymer Poloxamer-407 selectively redirects intravenously injected microspheres to sinusoidal endothelial cells of rabbit bone marrow. *FEBS Lett* **1992**, *305*, 62-66.
- [63]. Hirabayashi, H.; Fujisaki, J. Bone-specific drug delivery systems: approaches via chemical modification of bone-seeking agents. *Clin Pharm* **2003**, *42*, 1319-1330.
- [64]. Wang, D.; Miller, S.; Sima, M.; Kopeckova, P.; Kopecek, J. Synthesis and evaluation of water-soluble polymeric bone-targeted drug delivery systems. *Bioconjugate Chem* **2003**, *14*, 853-859.
- [65]. Moghimi, S. M.; Hunter, A. C.; Murray, J. C. Long-circulating and target-specific nanoparticles: theory to practice. *Pharmacol Rev* **2001**, *53*, 283-318.
- [66]. van Rooijen, N.; van Kesteren-Hendriks, E. Clodronate liposomes: perspectives in research and therapeutics. *J Liposome Res* **2002**, *12*, 81-94.
- [67]. Li, P.; Tan, Z.; Zhu, Y.; Chen, S.; Ding, S.; Zhuang, H. Targeting study of gelatin adsorbed clodronate in reticuloendothelial system and its potential application in immune thrombocytopenic purpura of rat model. *J Control Rel* **2006**, *114*, 202-208.
- [68]. Owens III, D. E.; Peppas, N. A. Opsonization, biodistribution, and pharmacokinetics of polymeric nanoparticles. *Int J Pharm* **2006**, *307*,

93-102.

- [69]. Roser, M.; Fischer, D.; Kissel, T. Surface-modified biodegradable albumin nano- and microspheres. II: effect of surface charges on in vitro phagocytosis and biodistribution in rats. *Euro J Pharm Biopharm* **1998**, *46*, 255-263.
- [70]. Bertholon, I.; Vauthier, C.; Labarre, D. Complement activation by core-shell poly(isobutylcyanoacrylate)-polysaccharide nanoparticles: influences of surface morphology, length, and type of polysaccharide. *Pharm Res* **2006**, *23*, 1313-1323.
- [71]. Fang, C.; Shi, B.; Pei, Y. Y.; Hong, M. H.; Wu, J.; Chen, H. Z. In vivo tumor targeting of tumor necrosis factor- α -loaded stealth nanoparticles: effect of MePEG molecular weight and particle size. *Euro J Pharm Sci* **2006**, *27*, 27-36.
- [72]. Zahr, A. S.; Davis, C. A.; Pishko, M. V. Macrophage Uptake of core-shell nanoparticles surface modified with poly(ethylene glycol). *Langmuir* **2006**, *22*, 8178-8185.
- [73]. Zambaux, M. F.; Bonneaux, F.; Gref, R.; Dellacherie, E.; Vigneron, C. Protein C-loaded monomethoxypoly (ethylene oxide)-poly(lactic acid) nanoparticles. *Int J Pharm* **2001**, *212*, 1-9.
- [74]. Mittal, G.; Sahana, D. K.; Bhardwaj, V.; Ravi Kumar, M. N. V. Estradiol loaded PLGA nanoparticles for oral administration: Effect of polymer molecular weight and copolymer composition on release behavior in vitro and in vivo. *J Control Rel* **2007**, *119*, 77-85.
- [75]. Zambaux, M. F.; Bonneaux, F.; Gref, R.; Dellacherie, E.; Vigneron, C. Preparation and characterization of protein C-loaded PLA nanoparticles. *J Control Rel* **1999**, *60*, 179-188.
- [76]. Sun, B.; Ranganathan, B.; Feng, S. S. Multifunctional poly(d,l-lactide-co-glycolide)/montmorillonite (PLGA/MMT) nanoparticles decorated by Trastuzumab for targeted chemotherapy of breast cancer. *Biomaterials* **2008**, *29*, 475-486.
- [77]. Wartlick, H.; Spankuch-Schmitt, B.; Strebhardt, K.; Kreuter, J.; Langer, K. Tumour cell delivery of antisense oligonucleotides by human serum albumin nanoparticles. *J Control Rel* **2004**, *96*, 483-495.

- [78]. Kreuter, J.; Hekmatara, T.; Dreis, S.; Vogel, T.; Gelperina, S.; Langer, K. Covalent attachment of apolipoprotein A-I and apolipoprotein B-100 to albumin nanoparticles enables drug transport into the brain. *J Control Rel* **2007**, *118*, 54-58.
- [79]. Michaelis, K.; Hoffmann, M. M.; Dreis, S.; Herbert, E.; Alyautdin, R. N.; Michaelis, M.; Kreuter, J.; Langer, K. Covalent linkage of apolipoprotein E to albumin nanoparticles strongly enhances drug transport into the brain. *J Pharmacol Exp Ther* **2006**, *317*, 1246-1253.
- [80]. Steinhauser, I.; Spankuch, B.; Strebhardt, K.; Langer, K. Trastuzumab-modified nanoparticles: Optimisation of preparation and uptake in cancer cells. *Biomaterials* **2006**, *27*, 4975-4983.
- [81]. Wartlick, H.; Michaelis, K.; Balthasar, S.; Strebhardt, K.; Kreuter, J.; Langer, K. Highly specific HER2-mediated cellular uptake of antibody-modified nanoparticles in tumour cells. *J Drug Target* **2004**, *12*, 461-471.
- [82]. Nobs, L.; Buchegger, F.; Gurny, R.; Allemann, E. Biodegradable nanoparticles for direct or two-step tumor immunotargeting. *Bioconjugate Chem* **2006**, *17*, 139-145.
- [83]. Sun, B.; Ranganathan, B.; Feng, S. S. Multifunctional poly(d,l-lactide-co-glycolide)/montmorillonite (PLGA/MMT) nanoparticles decorated by trastuzumab for targeted chemotherapy of breast cancer. *Biomaterials* **2008**, *29*, 475-486.
- [84]. Farokhzad, O. C.; Cheng, J.; Teply, B. A.; Sherifi, I.; Jon, S.; Kantoff, P. W.; Richie, J. P.; Langer, R. Targeted nanoparticle-aptamer bioconjugates for cancer chemotherapy in vivo. *Proc Natl Acad Sci USA* **2006**, *103*, 6315-6320.
- [85]. Zhang, S.; Gangal, G. 'Magic bullets' for bone diseases: progress in rational design of bone-seeking medicinal agents. *Chem Soc Rev* **2007**, *36*, 507-531.
- [86]. Gittens, S. A.; Bansal, G.; Zernicke, R. F.; Uludag, H. Designing proteins for bone targeting. *Adv Drug Deliv Rev* **2005**, *57*, 1011-1036.
- [87]. Hengst, V.; Oussoren, C.; Kissel, T.; Storm, G. Bone targeting potential of bisphosphonate-targeted liposomes: Preparation, characterization and hydroxyapatite binding in vitro. *Int J Pharm* **2007**, *331*, 224-227.

- [88]. Zhang, S.; Wright, J. E. I.; Uludag, H.; Ozber, N. The interaction of cationic polymers and their bisphosphonate derivatives with hydroxyapatite. *Macromol Biosci* **2007**, *7*, 656-670.
- [89]. Lochmann, D.; Vogel, V.; Weyermann, J.; Dinauer, N.; von Briesen, H.; Kreuter, J.; Schubert, D.; Zimmer, A. Physicochemical characterization of protamine-phosphorothioate nanoparticles. *J Microencapsul* **2004**, *21*, 625-641.
- [90]. Duclairoir, C.; Orecchioni, A.-M.; Depraetere, P.; Osterstock, F.; Nakache, E. Evaluation of gliadins nanoparticles as drug delivery systems: a study of three different drugs. *Int J Pharm* **2003**, *253*, 133-144.
- [91]. Irache, J. M.; Bergougnoux, L.; Ezpeleta, I.; Gueguen, J.; Orecchioni, A. M. Optimization and in vitro stability of legumin nanoparticles obtained by a coacervation method. *Int J Pharm* **1995**, *126*, 103-109.
- [92]. Fattal, E.; Vauthier, C.; Aynie, I.; Nakada, Y.; Lambert, G.; Malvy, C.; Couvreur, P. Biodegradable polyalkylcyanoacrylate nanoparticles for the delivery of oligonucleotides. *J Control Rel* **1998**, *53*, 137-143.
- [93]. Reddy, L. H.; Sharma, R. K.; Murthy, R. S. R. Enhanced Tumour Uptake of Doxorubicin Loaded Poly(butyl cyanoacrylate) Nanoparticles in Mice Bearing Dalton's Lymphoma Tumour. *J Drug Target* **2004**, *12*, 443-451.
- [94]. Peracchia, M. T.; Fattal, E.; Desmaele, D.; Besnard, M.; Noel, J. P.; Gomis, J. M.; Appel, M.; d'Angelo, J.; Couvreur, P. Stealth(R) PEGylated polycyanoacrylate nanoparticles for intravenous administration and splenic targeting. *J Control Rel* **1999**, *60*, 121-128.
- [95]. Lee, M. K.; Lim, S. J.; Kim, C. K. Preparation, characterization and in vitro cytotoxicity of paclitaxel-loaded sterically stabilized solid lipid nanoparticles. *Biomaterials* **2007**, *28*, 2137-2146.
- [96]. Yuan, H.; Huang, L. F.; Du, Y. Z.; Ying, X. Y.; You, J.; Hu, F. Q.; Zeng, S. Solid lipid nanoparticles prepared by solvent diffusion method in a nanoreactor system. *Colloids Surf B: Biointerfaces* **2008**, *61*, 132-137.
- [97]. Jennings, V.; Schafer-Korting, M.; Gohla, S. Vitamin A-loaded solid lipid nanoparticles for topical use: drug release properties. *J Control Rel* **2000**, *66*, 115-126.
- [98]. Cheng, W. P.; Gray, A. I.; Tetley, L.; Hang, T. L. B.; Schatzlein, A. G.;

- Uchegbu, I. F. Polyelectrolyte nanoparticles with high drug loading enhance the oral uptake of hydrophobic compounds. *Biomacromolecules* **2006**, *7*, 1509-1520.
- [99]. Chen, J.; Tian, B.; Yin, X.; Zhang, Y.; Hu, D.; Hu, Z.; Liu, M.; Pan, Y.; Zhao, J.; Li, H.; Hou, C.; Wang, J.; Zhang, Y. Preparation, characterization and transfection efficiency of cationic PEGylated PLA nanoparticles as gene delivery systems. *J Biotechnol* **2007**, *130*, 107-113.
- [100]. Lemarchand, C.; Gref, R.; Lesieur, S.; Hommel, H.; Vacher, B.; Besheer, A.; Maeder, K.; Couvreur, P. Physico-chemical characterization of polysaccharide-coated nanoparticles. *J Control Rel* **2005**, *108*, 97-111.
- [101]. Rodrigues, J. S.; Santos-Magalhaes, N. S.; Coelho, L. C. B. B.; Couvreur, P.; Ponchel, G.; Gref, R. Novel core(polyester)-shell(polysaccharide) nanoparticles: protein loading and surface modification with lectins. *J Control Rel* **2003**, *92*, 103-112.
- [102]. Trimaille, T.; Pichot, C.; Elaissari, A.; Fessi, H.; Briancon; Delair Poly(D,L-lactic acid) nanoparticle preparation and colloidal characterization. *Colloid Polym Sci* **2003**, *281*, 1184-1190.
- [103]. Gao, H.; Yang, Y. w.; Fan, Y. g.; Ma, J. b. Conjugates of poly(DL-lactic acid) with ethylenediamino or diethylenetriamino bridged bis(β -cyclodextrin)s and their nanoparticles as protein delivery systems. *J Control Rel* **2006**, *112*, 301-311.
- [104]. Gao, H.; Wang, Y. N.; Fan, Y. G.; Ma, J. B. Conjugates of poly(D,L-lactide-co-glycolide) on amino cyclodextrins and their nanoparticles as protein delivery system. *J Biomed Mater Res A* **2007**, *80A*, 111-122.
- [105]. Lu, W.; Wan, J.; She, Z.; Jiang, X. Brain delivery property and accelerated blood clearance of cationic albumin conjugated pegylated nanoparticle. *J Control Rel* **2007**, *118*, 38-53.
- [106]. Lu, W.; Zhang, Y.; Tan, Y. Z.; Hu, K. L.; Jiang, X. G.; Fu, S. K. Cationic albumin-conjugated pegylated nanoparticles as novel drug carrier for brain delivery. *J Control Rel* **2005**, *107*, 428-448.
- [107]. Shenoy, D. B.; Amiji, M. M. Poly(ethylene oxide)-modified poly(ϵ -caprolactone) nanoparticles for targeted delivery of tamoxifen in breast cancer. *Int J Pharm* **2005**, *293*, 261-270.

- [108]. Akagi, T.; Kaneko, T.; Kida, T.; Akashi, M. Multifunctional conjugation of proteins on/into bio-nanoparticles prepared by amphiphilic poly(γ -glutamic acid). *J Biomater Sci Polym Ed* **2006**, *17*, 875-892.
- [109]. Hirsjarvi, S.; Peltonen, L.; Hirvonen, J. Layer-by-layer polyelectrolyte coating of low molecular weight poly(lactic acid) nanoparticles. *Colloids Surf B Biointerfaces* **2006**, *49*, 93-99.
- [110]. Farokhzad, O. C.; Jon, S.; Khademhosseini, A.; Tran, T. T.; laVan, D. A.; Langer, R. Nanoparticle-aptamer bioconjugates: a new approach for targeting prostate cancer cells. *Cancer Res* **2004**, *64*, 7668-7672.
- [111]. Perez, C.; Sanchez, A.; Putnam, D.; Ting, D.; Langer, R.; Alonso, M. J. Poly(lactic acid)-poly(ethylene glycol) nanoparticles as new carriers for the delivery of plasmid DNA. *J Control Rel* **2001**, *75*, 211-224.
- [112]. Kim, I. S.; Lee, S. K.; Park, Y. M.; Lee, Y. B.; Shin, S. C.; Lee, K. C.; Oh, I. J. Physicochemical characterization of poly(L-lactic acid) and poly(D,L-lactide-co-glycolide) nanoparticles with polyethylenimine as gene delivery carrier. *Int J Pharm* **2005**, *298*, 255-262.
- [113]. Trimaille, T.; Pichot, C.; Delair, T. Surface functionalization of poly(D,L-lactic acid) nanoparticles with poly(ethylenimine) and plasmid DNA by the layer-by-layer approach. *Colloids Surf A Physicochem Eng Aspects* **2003**, *221*, 39-48.
- [114]. Messai, I.; Munier, S.; taman-Onal, Y.; Verrier, B.; Delair, T. Elaboration of poly(ethylenimine) coated poly(D,L-lactic acid) particles. Effect of ionic strength on the surface properties and DNA binding capabilities. *Colloids Surf B Biointerfaces* **2003**, *32*, 293-305.
- [115]. Lee, S. H.; Zhang, Z.; Feng, S. S. Nanoparticles of poly(lactide)-tocopheryl polyethylene glycol succinate (PLA-TPGS) copolymers for protein drug delivery. *Biomaterials* **2007**, *28*, 2041-2050.
- [116]. Zhang, Z.; Feng, S. S. Nanoparticles of poly(lactide)/vitamin E TPGS copolymer for cancer chemotherapy: Synthesis, formulation, characterization and in vitro drug release. *Biomaterials* **2006**, *27*, 262-270.
- [117]. Song, C. X.; Labhasetwar, V.; Murphy, H.; Qu, X.; Humphrey, W. R.; Shebuski, R. J.; Levy, R. J. Formulation and characterization of biodegradable nanoparticles for intravascular local drug delivery. *J Control Rel* **1997**, *43*, 197-212.

- [118]. Cegnar, M.; Kos, J.; Kristl, J. Cystatin incorporated in poly(lactide-co-glycolide) nanoparticles: development and fundamental studies on preservation of its activity. *Euro J Pharm Sci* **2004**, *22*, 357-364.
- [119]. Davda, J.; Labhasetwar, V. Characterization of nanoparticle uptake by endothelial cells. *Int J Pharm* **2002**, *233*, 51-59.
- [120]. Desai, M. P.; Labhasetwar, V.; Amidon, G. L.; Levy, R. J. Gastrointestinal uptake of biodegradable microparticles: effect of particle size. *Pharm Res* **1996**, *13*, 1838-1845.
- [121]. Astete, C. E.; Kumar, C. S. S. R.; Sabliov, C. M. Size control of poly(D,L-lactide-co-glycolide) and poly(D,L-lactide-co-glycolide)-magnetite nanoparticles synthesized by emulsion evaporation technique. *Colloids Surf A Physicochem Eng Aspects* **2007**, *299*, 209-216.
- [122]. Lboutounne, H.; Guillaume, Y. C.; Michel, L.; Makki, S.; Humbert, Ph.; Millet, J. Study and development of encapsulated forms of 4, 5', 8-trimethylpsoralen for topical drug delivery. *Drug Dev Res* **2004**, *61*, 86-94.
- [123]. Sholes, P. D.; Coombes, A. G. A.; Illum, L.; Davis, S. S.; Vert, M.; Davies, M. C. The preparation of sub-200 nm poly(lactide-co-glycolide) microspheres for site-specific drug delivery. *J Control Rel* **1993**, *25*, 145-153.
- [124]. Dong, Y.; Feng, S. S. Methoxy poly(ethylene glycol)-poly(lactide) (MPEG-PLA) nanoparticles for controlled delivery of anticancer drugs. *Biomaterials* **2004**, *25*, 2843-2849.
- [125]. Zhang, L.; Hou, S.; Mao, S.; Wei, D.; Song, X.; Lu, Y. Uptake of folate-conjugated albumin nanoparticles to the SKOV3 cells. *Int J Pharm* **2004**, *287*, 155-162.
- [126]. Rahimnejad, M.; Jahanshahi, M.; Najafpour, G. D. Production of biological nanoparticles from bovine serum albumin for drug delivery. *African J Biotechnol* **2006**, *5*, 1918-1923.
- [127]. Arbos, P.; Campanero, M. A.; Arangoa, M. A.; Irache, J. M. Nanoparticles with specific bioadhesive properties to circumvent the pre-systemic degradation of fluorinated pyrimidines. *J Control Rel* **2004**, *96*, 55-65.

- [128]. Michaelis, M.; Langer, K.; Arnold, S.; Doerr, H. W.; Kreuter, J.; Cinatl, J. Pharmacological activity of DTPA linked to protein-based drug carrier systems. *Biochem Biophys Res Commun* **2004**, *323*, 1236-1240.
- [129]. Brzoska, M.; Langer, K.; Coester, C.; Loitsch, S.; Wagner, T. O. F.; Mallinckrodt, C. Incorporation of biodegradable nanoparticles into human airway epithelium cells--in vitro study of the suitability as a vehicle for drug or gene delivery in pulmonary diseases. *Biochem Biophys Res Commun* **2004**, *318*, 562-570.
- [130]. Langer, K.; Coester, C.; Weber, C.; von Briesen, H.; Kreuter, J. Preparation of avidin-labeled protein nanoparticles as carriers for biotinylated peptide nucleic acid. *Euro J Pharm Biopharm* **2000**, *49*, 303-307.
- [131]. Arnedo, A.; Espuelas, S.; Irache, J. M. Albumin nanoparticles as carriers for a phosphodiester oligonucleotide. *Int J Pharm* **2002**, *244*, 59-72.
- [132]. Huang, M.; Vitharana, S. N.; Peek, L. J.; Coop, T.; Berkland, C. Polyelectrolyte complexes stabilize and controllably release vascular endothelial growth factor. *Biomacromolecules* **2007**, *8*, 1607-1614.
- [133]. Lin, Y. H.; Mi, F. L.; Chen, C. T.; Chang, W. C.; Peng, S. F.; Liang, H. F.; Sung, H. W. Preparation and characterization of nanoparticles shelled with chitosan for oral insulin delivery. *Biomacromolecules* **2007**, *8*, 146-152.
- [134]. Prego, C.; Torres, D.; Fernandez-Megia, E.; Novoa-Carballal, R.; Quinoa, E.; Alonso, M. J. Chitosan-PEG nanocapsules as new carriers for oral peptide delivery: effect of chitosan pegylation degree. *J Control Rel* **2006**, *111*, 299-308.
- [135]. Bravo-Osuna, I.; Millotti, G.; Vauthier, C.; Ponchel, G. In vitro evaluation of calcium binding capacity of chitosan and thiolated chitosan poly(isobutyl cyanoacrylate) core-shell nanoparticles. *Int J Pharm* **2007**, *338*, 284-290.
- [136]. Mi, F. L.; Wu, Y. Y.; Chiu, Y. L.; Chen, M. C.; Sung, H. W.; Yu, S. H.; Shyu, S. S.; Huang, M. F. Synthesis of a novel glycoconjugated chitosan and preparation of its derived nanoparticles for targeting HepG2 cells. *Biomacromolecules* **2007**, *8*, 892-898.
- [137]. Tan, W. B.; Huang, N.; Zhang, Y. Ultrafine biocompatible chitosan nanoparticles encapsulating multi-coloured quantum dots for

bioapplications. *J Colloid Interface Sci* **2007**, *310*, 464-470.

- [138]. Chen, F.; Zhang, Z. R.; Huang, Y. Evaluation and modification of N-trimethyl chitosan chloride nanoparticles as protein carriers. *Int J Pharm* **2007**, *336*, 166-173.
- [139]. Bodnar, M.; Hartmann, J. F.; Borbely, J. Synthesis and Study of Cross-Linked Chitosan-N-Poly(ethylene glycol) Nanoparticles. *Biomacromolecules* **2006**, *7*, 3030-3036.
- [140]. Katas, H.; Alpar, H. O. Development and characterisation of chitosan nanoparticles for siRNA delivery. *J Control Rel* **2006**, *115*, 216-225.
- [141]. Cetin, M.; Aktas, Y.; Vural, I.; Capan, Y.; Dogan, L. A.; Duman, M.; Dalkara, T. Preparation and in vitro evaluation of bFGF-loaded chitosan nanoparticles. *Drug Deliv* **2007**, *14*, 525-529.
- [142]. Gan, Q.; Wang, T. Chitosan nanoparticle as protein delivery carrier--Systematic examination of fabrication conditions for efficient loading and release. *Colloids Surf B Biointerfaces* **2007**, *59*, 24-34.
- [143]. Zhu, S.; Qian, F.; Zhang, Y.; Tang, C.; Yin, C. Synthesis and characterization of PEG modified N-trimethylaminoethylmethacrylate chitosan nanoparticles. *Euro Polym J* **2007**, *43*, 2244-2253.
- [144]. Zhao, X.; Yu, S. B.; Wu, F. L.; Mao, Z. B.; Yu, C. L. Transfection of primary chondrocytes using chitosan-pEGFP nanoparticles. *J Control Rel* **2006**, *112*, 223-228.
- [145]. Cafaggi, S.; Russo, E.; Stefani, R.; Leardi, R.; Caviglioli, G.; Parodi, B.; Bignardi, G.; De Toter, D.; Aiello, C.; Viale, M. Preparation and evaluation of nanoparticles made of chitosan or N-trimethyl chitosan and a cisplatin-alginate complex. *J Control Rel* **2007**, *121*, 110-123.
- [146]. Loretz, B.; Thaler, M.; Bernkop-Schnurch, A. Role of sulfhydryl groups in transfection? A case study with chitosan-NAC nanoparticles. *Bioconjugate Chem* **2007**, *18*, 1028-1035.
- [147]. Diebold, Y.; Jarrin, M.; Saez, V.; Carvalho, E. L. S.; Orea, M.; Calonge, M.; Seijo, B.; Alonso, M. J. Ocular drug delivery by liposome-chitosan nanoparticle complexes (LCS-NP). *Biomaterials* **2007**, *28*, 1553-1564.
- [148]. Bravo-Osuna, I.; Teutonico, D.; Arpicco, S.; Vauthier, C.; Ponchel, G. Characterization of chitosan thiolation and application to thiol

quantification onto nanoparticle surface. *Int J Pharm* **2007**, *340*, 173-181.

- [149]. Krauland, A. H.; Alonso, M. J. Chitosan/cyclodextrin nanoparticles as macromolecular drug delivery system. *Int J Pharm* **2007**, *340*, 134-142.
- [150]. Grenha, A.; Grainger, C. I.; Dailey, L. A.; Seijo, B.; Martin, G. P.; Remunan-Lopez, C.; Forbes, B. Chitosan nanoparticles are compatible with respiratory epithelial cells in vitro. *Euro J Pharm Sci* **2007**, *31*, 73-84.
- [151]. Prego, C.; Fabre, M.; Torres, D.; Alonso, M. Efficacy and mechanism of action of chitosan nanocapsules for oral peptide delivery. *Pharm Res* **2006**, *23*, 549-556.
- [152]. Zheng, Y.; Wu, Y.; Yang, W.; Wang, C.; Fu, S.; Shen, X. Preparation, characterization, and drug release in vitro of chitosan-glycyrrhetic acid nanoparticles. *J Pharm Sci* **2007**, *95*, 181-191.
- [153]. Zhang, H.; Oh, M.; Allen, C.; Kumacheva, E. Monodisperse chitosan nanoparticles for mucosal drug delivery. *Biomacromolecules* **2004**, *5*, 2461-2468.
- [154]. Chen, L.; Subirade, M. Chitosan/ β -lactoglobulin core-shell nanoparticles as nutraceutical carriers. *Biomaterials* **2005**, *26*, 6041-6053.
- [155]. Calvo, P.; Remunan-Lopez, C.; Vila-Jato, J. L.; Alonso, M. J. Chitosan and chitosan/ethylene oxide-propylene oxide block copolymer nanoparticles as novel carriers for proteins and vaccines. *Pharm Res* **1997**, *14*, 1431-1436.
- [156]. Gan, Q.; Wang, T.; Cochrane, C.; McCarron, P. Modulation of surface charge, particle size and morphological properties of chitosan-TPP nanoparticles intended for gene delivery. *Colloids Surf B Biointerfaces* **2005**, *44*, 65-73.
- [157]. Sajeesh, S.; Sharma, C. P. Novel pH responsive polymethacrylic acid-chitosan-polyethylene glycol nanoparticles for oral peptide delivery. *J Biomed Mater Res B Appl Biomater* **2006**, *76*, 298-305.
- [158]. Park, K.; Kim, J. H.; Nam, Y. S.; Lee, S.; Nam, H. Y.; Kim, K.; Park, J. H.; Kim, I. S.; Choi, K.; Kim, S. Y.; Kwon, I. C. Effect of polymer molecular weight on the tumor targeting characteristics of self-assembled glycol chitosan nanoparticles. *J Control Rel* **2007**, *122*, 305-314.
- [159]. Jintapattanakit, A.; Junyaprasert, V. B.; Mao, S.; Sitterberg, J.; Bakowsky,

- U.; Kissel, T. Peroral delivery of insulin using chitosan derivatives: A comparative study of polyelectrolyte nanocomplexes and nanoparticles. *Int J Pharm* **2007**, *342*, 240-249.
- [160]. Kim, S. H.; Jeong, J. H.; Chun, K. W.; Park, T. G. Target-specific Cellular uptake of PLGA nanoparticles coated with poly(L-lysine)-poly(ethylene glycol)-folate conjugate. *Langmuir* **2005**, *21*, 8852-8857.
- [161]. Mo, Y.; Lim, L. Y. Paclitaxel-loaded PLGA nanoparticles: Potentiation of anticancer activity by surface conjugation with wheat germ agglutinin. *J Control Rel* **2005**, *108*, 244-262.
- [162]. Tosi, G.; Costantino, L.; Rivasi, F.; Ruozi, B.; Leo, E.; Vergoni, A. V.; Tacchi, R.; Bertolini, A.; Vandelli, M. A.; Forni, F. Targeting the central nervous system: In vivo experiments with peptide-derivatized nanoparticles loaded with Loperamide and Rhodamine-123. *J Control Rel* **2007**, *122*, 1-9.
- [163]. Costantino, L.; Gandolfi, F.; Tosi, G.; Rivasi, F.; Vandelli, M. A.; Forni, F. Peptide-derivatized biodegradable nanoparticles able to cross the blood-brain barrier. *J Control Rel* **2005**, *108*, 84-96.
- [164]. Zhang, N.; Chittasupho, C.; Duangrat, C.; Siahaan, T. J.; Berkland, C. PLGA nanoparticle-peptide conjugate effectively targets intercellular cell-adhesion molecule-1. *Bioconjugate Chem* **2008**, *19*, 145-152.

Chapter 2

Scope of Dissertation

Drug delivery systems with nm dimensions (nanoparticles, NPs) are attracting increasing attention since they can sequester drugs in systemic circulation, prevent non-specific biodistribution, and target to specific tissues. Several molecular targets have been identified based on a better understanding of the pathogenesis of various bone diseases. However, the application of drug delivery systems specific for bone is still very limited. Subject of this thesis is the design of NP based drug carriers suitable for treatment of bone diseases.

Chapter 1 reviewed the recent literature pertinent to nanoparticle-based drug delivery systems, primarily emphasizing NPs fabricated from proteins such as BSA. A summary of common NP fabrication techniques is provided along with the range of sizes and functional properties obtained. The NP properties critical for injectable drug carriers are discussed, as well as the attempts to design ‘tissue-specific’ NPs or so-called ‘targeted’ drug delivery. It has been possible to design NPs in the range of 10-1000 nm from different biomaterials, and further understanding of *in vivo* stability and interactions with physiological systems will lead to improved drug delivery systems.

The scope of the thesis is presented in **Chapter 2** (the present chapter).

Particle size and surface properties are important parameters that influence the fate of the NPs when applied *in vivo*, and these properties can be modulated

by the NP preparation process. The preparation of BSA NPs and optimization of the processing conditions were described in **Chapter 3**. The NPs were prepared by a coacervation method, and the effects of process parameters on NP size and polydispersity were examined. The NPs were stabilized by a polymer coating (PLL and PEI) and characterized with respect to the amount of adsorbed polymer, particle size and ζ -potential. The size of NPs could be controlled in the 50-400 nm range by process parameters including BSA concentration, non-solvent:solvent ratio and pH value. After coating with cationic polymers, the particle size and ζ -potential were significantly increased. Using human and rat bone marrow stromal cells (BMSC), biocompatibility of the NPs was investigated by the MTT Assay. BMP-2 was encapsulated into the BSA NPs during preparation, and the bioactivity of the encapsulated BMP-2 was investigated by alkaline phosphates (ALP) induction and calcification of BMSC.

In **Chapter 4**, a polymeric conjugate of polyethyleneimine-graft-poly(ethylene glycol) and 2-(3-mercaptopropylsulfanyl)-ethyl-1,1-bisphosphonic acid (PEI-PEG-thiolBP) was prepared and used for surface coating of BSA NPs designed for bone-specific delivery of BMP-2. The NP coating was achieved with a dialysis and an evaporation method, and the obtained NPs were characterized by particle size, ζ -potential, morphology, and cytotoxicity *in vitro*. The particle size and surface charge of the NPs could be effectively controlled by the PEG and

thiolBP substitution ratios of the conjugate, the coating method, and the polymer concentration used for coating. The effects of PEG and BP modification on the toxicity of PEI and the coated NPs were evaluated by MTT assay with human C2C12 cells and rat BMSC. ALP induction assay was carried out to assess the effects of the PEG and BP on the bioactivity of NP encapsulated BMP-2. By encapsulating ¹²⁵I-labeled BMP-2, the polymer-coated NPs were assessed for *in vitro* and *in vivo* hydroxyapatite (HA) affinity, and biodistribution in rats after intravenous injection.

As an alternative to BSA NPs, micelles and liposomes were designed by BP-modification for bone targeting, and this work is summarized in **Chapter 5**. A conjugate of distearoylphosphoethanolamine-polyethyleneglycol with 2-(3-mercaptopropylsulfanyl)-ethyl-1,1-bisphosphonic acid (DSPE-PEG-thiolBP) was synthesized and incorporated into micelles and liposomes to create mineral-binding nanocarriers for therapeutic agents. The micelles and liposomes were used to encapsulate the anti-cancer drug doxorubicin (DOX) and a model protein lysozyme (LYZ) by using lipid film hydration (LFH) and reverse-phase evaporation vesicle (REV) methods. The capability of the micelles and liposomes to encapsulate different drugs was discussed based on the encapsulation efficiency obtained from the two methods. The affinity of the micellar and liposomal formulations to hydroxyapatite (HA) was assessed *in vitro*, specifically to

determine if the thiolBP-decorated liposomes (i) displayed a stronger binding to a biomimetic collagen/HA composite scaffold and (ii) gave increased retention of drugs in the scaffolds in a subcutaneous implant model in rats. Similar to BSA NPs, the ability of the designed liposomes to entrap the bone morphogenetic protein-2 (BMP-2) in a bioactive form was evaluated.

Based on the high HA binding affinity of the BP-liposomes, sustainable drug release is expected from the liposomes in an HA containing matrix. **Chapter 6** studied the release profile of the liposomes and the liposomal drugs from liposome-loaded HA-embedded collagen scaffolds. The collagen/HA (Col/HA) composite scaffolds were prepared by freeze-drying method. Three model drugs, carboxyfluorescein (CF), DOX and LYZ were encapsulated into the PEG- and BP-liposomes, and then loaded into the scaffolds. The release profiles of the three drugs from the liposomes as well as liposome-loaded scaffolds were investigated respectively. Since the release pattern of drugs are expected to ultimately affect their pharmacological properties, these studies are expected to provide a fundamental insight into the mechanism of action of the NPs

Taken together, the work presented in this dissertation was explored based on the hypothesis that the bone-targeting delivery system can be designed by surface modification of the drug carriers with BP, a targeting moiety with strong affinity for bone mineral. In **Chapters 3-6**, we attempted two categories of

nanoparticles, BSA NPs and lipid based NPs (liposomes and micelles), for bone-specific drug delivery via the approach of BP modification. The last section, **Chapter 7**, is devoted to general discussion, overall conclusions and future directions, where numerous additional studies are suggested for developing better drug delivery and controlled release systems with potential application in bone tissue engineering.

Chapter 3

Preparation of BMP-2 Containing Bovine Serum Albumin (BSA) Nanoparticles Stabilized by Polymer Coating¹

¹A version of this chapter has been published in: Wang G, Siggers K, Zhang S, Jiang H, Xu Z, Zernicke RF, Matyas J, Uludag H. *Pharmaceutical Research* 2008; 25: 2896-2909.

3.1 INTRODUCTION

Several peptides and proteins are being currently developed as potential therapeutic agents for musculoskeletal diseases. However, fundamental shortcomings have hampered their extensive clinical utility, including a relatively short half-life after administration and lack of long-term stability in physiological milieu [1]. Nanoparticles (NPs) derived from biocompatible materials can serve as controlled delivery systems for therapeutic agents and help to alleviate the shortcomings of therapeutic delivery of these agents. By encapsulating a therapeutic agent, NPs isolate the agent from the physiological milieu, protect the peptide/protein drugs from enzymatic degradation, and provide a means for sustained release. A prolonged retention of biological activity is the expected outcome when therapeutic agents are delivered as a result of formulation in NPs.

The physicochemical properties of NPs are expected to be critical in controlling the release of therapeutic agents as well as the fate of the delivery systems in the body. Size and surface charge are two basic properties that can influence the biodistribution of NPs upon administration [2-5], especially after systemic injection. With respect to particle size, larger particles are more rapidly removed from the circulation by the reticuloendothelial system, and accumulate in liver and spleen at a higher extent than the smaller particles [5-7]. The particles are also expected to be small enough to escape from the vascular system via

fenestrations or cavities in the lining of the blood vessels [3]. It has been suggested that the size of a solid particle should not exceed 200 nm for long-circulation [5]. With respect to surface charge, small neutral particles have a longer circulation time than their anionic counterparts [8]. Particles with positive surface charge is considered beneficial for penetrating plasma membrane of cells[9]; however, it is a major disadvantage for systemic administration since cationic particles can nonspecifically bind to cell surfaces and activate the complement system [10]. These adverse effects for the use of cationic particles *in vivo* can be overcome by reducing particle size and lowering surface charge [4].

Bovine serum albumin (BSA) is a naturally-occurring biomaterial that has been used as a matrix in NP preparations. Due to its proteinous nature, BSA NPs are naturally biodegradable and non-toxic [11,12], since they can be metabolized with natural mechanisms into harmless end-products. BSA NPs can be easily prepared under mild conditions by simple coacervation, or desolvation process and their size distribution can be engineered by controlling the process parameters[2,13-15]. To obtain stable particles, glutaraldehyde (GA) was typically used to cross-link the NPs via the free amines after coacervation. However, the toxicity of GA is a concern for *in vivo* delivery [16,17]. GA might be also reactive with any amines of the encapsulated peptide/protein drugs [18,19], as well as small drugs such as doxorubicin [20], which could adversely affect their integrity and bioactivity. As an alternative to GA cross-linking, we recently proposed the

cationic polymers polyethylenimine (PEI) to stabilize BSA NPs. This method was used in our lab to encapsulate bone morphogenetic protein-2 (BMP-2) during BSA NP preparation by coacervation method [21]. A high loading efficiency (>90%) and controlled release of bioactive BMP-2 from the PEI-coated BSA NPs were achieved. However, the BSA NPs used in that study were prepared by using ethanol as the non-solvent, which led to relatively large NPs (230-400 nm) especially after PEI coating. The NPs coated with higher concentrations of PEI (> 0.1 mg/mL) also indicated some toxicity as compared to the uncoated NPs.

The present study was conducted to better understand the process parameters that control NP size. The effects of such process parameters as BSA concentration, pH value, non-solvent:water ratio and stirring rate on NP size and polydispersity were investigated. The feasibility of coating NPs with an additional cationic polymer, poly-*L*-Lysine (PLL), was explored at relatively low concentrations (<0.1 mg/mL). Our results identified several process parameters that significantly affected the NP size, and indicated PLL to be a suitable substitute for PEI. The final particle size obtained in this study typically ranged between 200-400 nm after polymer coating, and retained the bioactivity of BMP-2 with no obvious cytotoxicity to bone marrow stromal cells.

3.2 MATERIALS and METHODS

Materials

BSA, 3-(4,5-dimethylthiazol-2-yl)-2,5-diphenyl-tetrazolium bromide (MTT), *p*-nitrophenol phosphate (*p*-NPP), ascorbic acid, β -glycerolphosphate, PLL (M_w ~24 kDa) and branched PEI (M_w ~25 kDa) were obtained from Sigma-Aldrich (St. Louis, MO, USA). The non-solvents, ethanol and acetone, were reagent grade solvents from Fisher Scientific. Reagent-grade NaCl was from EMD Chemical Inc. (Darmstadt, Germany). Recombinant human bone morphogenetic protein-2 (BMP-2) was expressed in *E. coli* and purified as described before [22]. Fluorescein isothiocyanate (FITC) was obtained from Pierce (Rockford, IL, USA) and it was used to label the polymers PLL and PEI according to previously described methodology [23]. Dulbecco's Modified Eagle Medium (DMEM), Hank's Balanced Salt Solution (HBSS), GlutaMax-1 (GM), penicillin (10,000 U/mL) and streptomycin (10,000 μ g/mL) were from Invitrogen (Carlsbad, CA, USA). Fetal bovine serum (FBS) was from Atlanta Biologics (Atlanta, GA, USA). All tissue culture plasticware was from Corning (Corning, NY, USA). The Spectra/Por dialysis tubing with molecular weight cut-off (MWCO) of 12–14 kDa was acquired from Spectrum Laboratories (Rancho Dominguez, CA, USA) and used in all dialysis procedures. Distilled/deionized water (ddH₂O) used for buffer preparations were derived from a Millipore ELIX

purification system. The phosphate-buffered saline (PBS, pH 7.4) used in dialysis was diluted from the stock of 10× PBS (80 g/L NaCl, 2 g/L KCl, 14.4 g/L Na₂HPO₄ and 2.4 g/L KH₂PO₄). Phosphate buffers used to dissolve the reagents were diluted from the stock prepared by mixing 0.5 M Na₂HPO₄ and 0.5 M NaH₂PO₄·H₂O solutions to obtain the appropriate pH.

Preparation of BSA NPs

The BSA NPs were prepared by a coacervation method based on previously published literature [2,13], except cross-linking by GA was eliminated as described previously [21]. The non-solvents used were either ethanol or acetone. In a typical process, the non-solvents were added drop-wise to an aqueous BSA solution under constant stirring. Initially by using ethanol, the influences of BSA concentration, pH value of the aqueous solution, and ethanol:water ratio (the final volume ratio of ethanol added to the starting aqueous BSA solution) on particle size were examined independently. For this, the BSA solution at given concentration was mixed with equal volume of 10 mM NaCl or 10 mM phosphate buffers of pH 4.3, 5.5, 7.4 and 9.3, and coacervated with different volumes of ethanol under constant stirring (800 rpm). A systematic method, Taguchi Method (TM) with an orthogonal array design [24,25], was next applied to re-analyze the effects of the process parameters. The experimental control factors and their levels selected for the statistical testing are listed in **Table**

3-1. From the numbers of factors and levels, the total degree of freedom for this system was $3 \times (4-1) + (3-1) + 1 = 12$. This degree of freedom value led to the choice of an $L_{18}(4^3 \times 3)$ orthogonal array. The control factor levels for the testing were arranged in the orthogonal array as shown in **Table 3-2**. Then, ethanol was replaced by acetone as the non-solvent to investigate the dependence of the particle size on the non-solvent. In all cases, the desolvated mixtures were stirred for 3 hours after addition of non-solvent, and stored at 4 °C for particle size characterization and polymer coating.

Polymer Adsorption to NPs

Investigation of polymer adsorption to NPs were carried out by using NPs prepared from 10 mg/mL BSA in 10 mM phosphate buffer (pH 7.4) and with acetone:water ratio of 4. 300 μ L of NPs dispersion (with acetone) was added to equal volumes of 0, 10, 20, 50 and 100 μ g/mL PLL or PEI in 10 mM phosphate buffer solution (pH 7.4). The adsorption process was allowed for 1 h at room temperature and under constant shaking at 500 rpm. The coated NPs were then cleaned from the acetone and non-adsorbed polymer by extensive dialysis against 1 mM NaCl ($\times 3$). In some experiments, FITC-labeled polymers were used for NP coating in order to determine the exact amount of polymers adsorbed to the NPs (mg/g BSA). As above, the FITC-PLL or FITC-PEI coated NPs were dialyzed against 1 mM NaCl ($\times 3$) to remove the acetone and excess polymer. 200 μ L of the

samples in duplicate was then added to a black 96-well plate (NUNC, Rochester, NY, USA) and the fluorescence (λ_{ex} : 485 nm; λ_{em} : 527 nm) was determined with a multiwell plate reader (Thermo Labsystems, Franklin, MA, USA). The amounts of PLL-FITC or PEI-FITC adsorbed on the BSA NPs were calculated based on calibration curves generated by using known concentrations of PLL-FITC or PEI-FITC in 1 mM NaCl.

Hydrodynamic Size and Zeta Potential of NPs

The mean particle size and polydispersity index of polymer-coated and uncoated NPs were determined by photon correlation spectroscopy using a Malvern Zetasizer 3000HS (Malvern Instruments Ltd., UK). The measurements were carried out at 25 °C using a 633 nm He-Ne laser at a scattering angle of 90°. The NPs without coating were directly used for measurement in the coacervation system with ethanol or acetone. The polymer-coated NPs obtained after dialysis were diluted 1:5 with 1 mM NaCl before the measurement. The particle size values for each type of NPs were derived from at least three measurements in each batch, and the final values indicated were an average of three independent batches of NP preparations.

The surface charge of the polymer-coated BSA NPs was investigated by measuring the electrophoretic mobility of the particles using the Malvern

Zetasizer 3000HS at 25 °C. The conversion to zeta potentials was performed using Smoluchowsky relation $\zeta = u \cdot \eta / \epsilon_0 \epsilon_r$, where u is the electrophoretic mobility, ϵ_0 and ϵ_r are the permittivity of the vacuum and the relative permittivity of the medium respectively, η is the viscosity of the medium and ζ is the zeta potential. The coated samples for zeta potential measurement were prepared after dialysis and diluted 1:5 in 1 mM NaCl solution. The reported zeta potentials of the NPs were derived from three independent batches of NP preparations.

Atomic Force Microscopy (AFM)

The morphology of the uncoated and coated BSA NPs was examined by MFP-3D AFM (Asylum Research, Santa Barbara, CA, USA) using AC240TS cantilever throughout all measurements. The NP samples were appropriately diluted to visualize individual particles and 5 μ L of the diluted sample was dropped onto the surface of PELCO^R Mica Discs (TED PELLA, Inc.; Redding, CA, USA), and observed after drying under room temperature. Images were processed and analyzed by the Igor Pro imaging software (version 5.04B).

Encapsulation of BMP-2 in BSA NPs

A 10 mg/mL BSA solution (180 μ L) was mixed with equal volume of 10 mM phosphate buffer of pH 7.4 in a glass vessel. After stirring for 15 min, 90 μ L of 0.5 mg/mL BMP-2 was added to this solution. After incubation for 1 h, the

aqueous solution was desolvated with dropwise addition of acetone (acetone:water ratio: 4), and then stirred for 3 h at 800 rpm at room temperature. The BMP-2 loaded NPs were coated with PLL and PEI (50 $\mu\text{g}/\text{mL}$) as in previously described procedure. For comparison, BSA NPs without BMP-2 were used for coating under similar conditions. After the polymer adsorption, the coated NPs were dialyzed against PBS ($\times 2$), and then against low-glucose DMEM with 1% antibiotics (for hBMSC) or high-glucose DMEM with 100 $\mu\text{g}/\text{mL}$ streptomycin and 100 U/mL penicillin (for rBMSC). All solutions/apparatus used for BMP-2 encapsulation were sterilized before use, and procedures were performed in a biological safety cabinet to maintain sterility.

Biocompatibility of NP Formulations

Two types of cells, human and rat bone marrow stromal cells (hBMSC and rBMSC respectively) were used for assessment of NP biocompatibility. The preparation of hBMSC and rBMSC were described in [26] and [22], respectively. Both cells were cultured in an osteogenic medium, where the basal medium was supplemented with 50 $\mu\text{g}/\text{mL}$ ascorbic acid, 100 nM dexamethasone and 5 mM β -glycerolphosphate. In the case of hBMSC, the basal medium was low-glucose DMEM containing 10% FBS, 0.7% GM, 100 $\mu\text{g}/\text{mL}$ streptomycin, 100 U/mL penicillin, whereas in the case of rBMSC, the basal medium was high-glucose DMEM, 10% FBS, 100 $\mu\text{g}/\text{mL}$ streptomycin and 100 U/mL penicillin. The NPs

were prepared as described above and coated with PEI and PLL (10, 20, 50 and 100 $\mu\text{g}/\text{mL}$). The final dialysis of the NPs was performed against low-glucose DMEM (for hBMSC) containing 1% antibiotics or high-glucose DMEM (for rBMSC) containing 100 $\mu\text{g}/\text{mL}$ streptomycin and 100 U/mL penicillin. An aliquot of NP dispersion was then incubated with the cells (in triplicate) grown in 24-well tissue culture plates. After a 48 h incubation period in a humidified atmosphere with 95/5% air/ CO_2 , 200 μl of the MTT solution (5 mg/mL in HBSS) was added to the 1.0 mL culture medium in each well. The cells were incubated for a further 2 h, the supernatant was removed, and 1.0 mL of DMSO was added to the cells to dissolve the formazan crystals formed. The optical density of the solution was measured by a multi-well plate reader at 570 nm. Uncoated BSA particles and untreated cells served as controls.

BMP-2 Bioactivity by ALP assay

A kinetic ALP assay was used to determine the bioactivity of BMP-2 encapsulated in the PEI- and PLL-coated (50 $\mu\text{g}/\text{mL}$) and uncoated BSA particles. For comparison, the ALP assay was performed on similar NPs without BMP-2. Following NP fabrication, all particles were dialyzed in the same manner as described in the MTT procedure. hBMSC and rBMSC were incubated (in triplicate) with the NPs at the estimated concentration of 1 $\mu\text{g}/\text{mL}$ of BMP-2 per well in 24-well plates (1 mL medium/well). The cells were incubated with the

NPs for 3, 7 and 14 days. The medium was not changed in the case of 3 and 7 day incubation, but 1 mL of fresh medium was added to the cells after 7 days in the case of 14 day incubation. To perform the ALP assay, the cells were washed with an HBSS solution ($\times 2$) and lysed with 400 μL ALP buffer (0.5 M 2-amino-2-methylpropan-1-ol and 0.1% (v/v) Triton-X; pH = 10.5). After 1.5 h, 200 μL of 1.0 mg/mL ALP substrate (*p*-nitrophenol phosphate) was added to 200 μL of the cell lysate, and the rate of change in the optical density was determined with an ELISA plate reader by measuring the absorbance (405 nm) at intervals of 90 sec for 8 cycles. Untreated cells and cells treated with 1 $\mu\text{g}/\text{mL}$ of free BMP-2 served as negative and positive controls, respectively. A standard curve based on known concentration of *p*-nitrophenol in ALP buffer was used to convert the absorbance values obtained into concentration of *p*-nitrophenol formed per minute.

Calcification Assay

A calcification assay was used to measure the amount of calcium formed on the samples following the ALP assay. Only rBMSC was used in this study, since hBMSC did not provide calcification during the 14-day time period used in this study. After the removal of the lysed cells for ALP assay, 0.5 mL of 0.5 M HCl was added to each well for 48 h to dissolve the calcium/phosphate deposits formed. 20 μL of the dissolved calcium solution was added to 50 μL of a solution

containing 0.028 M 8-hydroxyquinoline and 0.5% (v/v) sulfuric acid, as well as 0.5 mL of solution containing 3.7×10^{-4} M o-cresolphthalein and 1.5% (v/v) AMP (2-amino-2-methyl-propan-1-ol). The absorbance was measured with an ELISA plate reader at 570 nm. A standard curve based on known concentration of calcium standards (SIGMA) was used to convert the absorbance values obtained into concentration of calcium.

Data Analysis

All data shown in figures are summarized as mean \pm SD, and where indicated, statistical differences ($p < 0.05$) between group means were analyzed by the two-sided Student's *t*-test or by analysis of variance (ANOVA).

3.3 RESULTS and DISCUSSION

Effect of Coacervation Process Parameters on NP Properties

In order to understand factors affecting the properties of NP prepared from the coacervation procedure, series of experiments were performed by controlling the BSA concentration (**Figure 3-1A and B**), the pH of coacervation medium (**Figure 3-1C and D**) and the non-solvent:water ratio during NP formation (**Figure 3-1E and F**). To explore the effect of protein concentration, BSA

solutions prepared at 10, 20, 30 and 50 mg/mL were mixed with 10 mM NaCl, and coacervated with ethanol:water ratios of 1, 2, 4 and 6. The BSA concentration significantly influenced the size of the resultant NPs. As shown in **Figure 3-1A**, a gradual reduction in NP size was observed as the BSA concentration was increased from 10 to 50 mg/mL. This was the case for all ethanol:water ratios investigated. A gradual increase in polydispersity, however, was also observed as the BSA concentration was increased from 10 to 50 mg/mL (**Figure 3-1B**). The results in this concentration range were consistent with the results from an earlier study by Rahimnejad et al. [15]. Increased BSA concentration during the coacervation process presumably led to increased nucleation of BSA particles upon ethanol exposure, leading to eventual formation of smaller NPs. The uncoated NP sizes obtained from our process were typically above 100 nm, and the smallest NPs (97 nm) were obtained with BSA concentration of 50 mg/mL and ethanol ratio of 2.

The effect of coacervation medium pH on NP sizes was then explored by changing the pH of the 10 mM phosphate buffer used to form coacervates. The BSA concentrations used in this study was 10, 20, 30 and 50 mg/mL, and the pH of the aqueous medium was varied from 4.3 to 9.3. As summarized in **Figure 3-1C**, NP size was inversely related to the pH of the medium, but the concentration of BSA also affected this behavior. As the pH of the phosphate

buffer was increased from 4.3 to 9.3, a decrease in size from 350 nm to 150 nm was noted for the 10 mg/mL BSA. The decrease in size was drastic when the pH was lower than 7.4, but not afterwards. A similar behavior was noted for 20 and 30 mg/mL BSA concentrations. For the 50 mg/mL BSA concentration, the effect of pH on NP size was not as significant as the lower concentrations, with typical NP size obtained ~160 nm irrespective of the pH. This observation was in good agreement with the earlier work of Lin et al. [14] and Langer et al. [2], who studied the preparation of HSA NPs by ethanol and acetone induced coacervation, respectively. The decrease of NP size with increasing pH value was considered to be due to increased ionization of the BSA whose isoelectric point (pI) is 4.7. At higher pH values, BSA has a net anionic charge, which acts as repulsive force against particle aggregation. This is unlike the neutral state of BSA at the lowest pH used in our study (4.3), which gave relatively neutral BSA molecules more amenable for protein-protein interactions and, possibly aggregation. When other proteins are used in this process, the pH value of the coacervation medium might need to be adjusted depending on the pI of the employed proteins.

The effect of ethanol:water ratio on NP properties is shown in **Figure 3-1E** (size) and **Figure 3-1F** (polydispersity). The NP size was significantly increased up to ethanol:water ratio of 2, whereas the polydispersity decreased, which was indicative of the incomplete coacervation process with a ratio less than

2. The NP size tended to decrease as the ethanol:water ratio was increased to 6, with a corresponding reduction in polydispersity. A similar observation was reported in a previous study by Weber et al. [13]. These observations can be explained by a basic mechanism underlying the coacervation process investigated by Kreuter [27], where gelatin was used for NP preparation. At low ethanol:water ratio (<2) before complete coacervation, the increased amount of solvated BSA in aggregates might have led to increasing particle size. At relatively higher ethanol:water ratio, where the coacervation process was completed, the decrease in particle size with increasing ethanol volume was the likely result of more solvent extraction or diffusion into the non-solvent phase, thus making the formed NPs more restrained.

Process Optimization by Taguchi Method

To optimize the NP preparation procedure, TM was applied to re-analyze the effects of the process parameters tested above. TM is a statistical method for analyzing experimental data for determining and optimizing the effects and levels of the various factors involved in a system [24,25]. As an integrated, statistical way of testing pair-wise interactions instead of varying one parameter at a time, it can create an efficient and concise test set with many fewer test cases than testing all combinations of all variables. Considering the system listed in **Table 1**, three factors (BSA concentration, ethanol:water ratio, and pH value) with four values

each and one factor (stirring rate) with three values were used for process optimization. The exhaustive test set would have required 192 ($4^3 \times 3$) test cases. The test set created by TM (using the orthogonal array in **Table 2**), however, had only 18 test cases with all of the pair-wise combinations.

After running the orthogonal array with a set of experiments, the analysis of the results was constructed by the level total (K_i), level average (k_i) and the maximum variance (R) from each factor with respect to particle size and polydispersity. Comparing the level average (k_i) and considering a ‘Smaller-Is-Better’ principle, the optimum condition with those levels that had the smallest level averages were decided as $A_4B_4C_3D_3$ for particle size and $A_1B_3C_1D_2$ for polydispersity. Based on the maximum variance (R) of particle size as shown in **Table 3-3** (R for BSA concentration, ethanol:water ratio, pH and stirring rate were 63.6, 63.2, 162.6 and 17.0 nm, respectively), TM results indicated the order of the importance of the parameters as: pH value > ethanol:water ratio ~ BSA concentration > stirring rate. As seen from **Figure 3-2**, the effects of BSA concentration, pH value and ethanol:water ratio on the particle size and size distribution were both consistent with the results from independent experiments shown in **Figure 3-1**.

Acetone as a Coacervation Agent

The size of the NPs obtained in previous studies, where ethanol was used as the non-solvent, was generally greater than 100 nm. This was in line with the most studies reported in the literature, where NP sizes between 100 and 600 nm were reported [2]. An exception to these observations was an early study reported by Lin et al. [14], where acetone was used for protein coacervation to obtain ~100 nm human serum albumin (HSA) particles. Ethanol had not been used by these investigators and it was not known if the smaller particle size was due to acetone or some other process parameter(s). To determine if acetone substitution for ethanol could indeed lead to smaller NPs, we used our established process to prepare NPs from BSA solution dissolved in NaCl (**Figure 3-3A**) or phosphate buffer (**Figure 3-3B**). The use of acetone consistently gave smaller particles as compared to ethanol for all BSA concentrations tested (10-50 mg/mL). The smallest NPs (~50 nm) were obtained with BSA dissolved in phosphate buffer (pH 7.4 or 9.3) and at acetone:water ratio of 4. As with ethanol, acetone:water ratio significantly affected the size of the final NP obtained (**Figure 3-3C**). The NP size increased from the ratio of 1 to 2, and decreased afterwards to ~50 nm at acetone:water ratios of 4-6. This trend was similar whether the pH of the medium was 7.4 or 9.3. The results from NP formation in pH of 4.3 and 5.5 were not shown since obvious precipitates were formed under such conditions, rather than

suspended NPs. The typical size distributions for the ethanol and acetone desolvated NPs was illustrated in **Figure 3-4** (10 mg/mL BSA in 10 mM phosphate buffer of pH 7.4 with non-solvent:water ratio of 4). The distribution was skewed to the right, with a small percentage of larger NPs present in both preparations. Whereas acetone desolvated NPs had a size range of 20-150 nm, the ethanol desolvated NPs had a size range of 100-300 nm.

Collectively, these studies led us to conclude that the use of acetone for BSA desolvation led to smaller NPs as compared to NPs formed by ethanol desolvation. The reason for the smaller NPs obtained from acetone desolvation might be related to acetone being a better non-solvent for BSA than ethanol, thus creating smaller particles with sizes similar to the primary particles (~50 nm in diameter) proposed by the phase inversion theory [28]. Though both ethanol and acetone are miscible with water, which is essential for the formation of particle nuclei and growth by solvent extraction, the better insolubility of BSA with the bulk non-solvent might be limiting smaller spatial expansion of the particles. Unfortunately, theoretical discussions on this issue are extremely rare at present, and thermodynamic and kinetic data are needed for further understanding of this process.

Coating of BSA NPs with PLL and PEI

BSA NPs prepared by coacervation are usually stabilized by GA crosslinking via the protein amines. However, as discussed above, besides potential toxicity of GA for *in vivo* use, GA cross-linking may affect the release rate and bioactivity of the encapsulated drugs. An alternative approach for NP stabilization is surface coating with a suitable molecule, for example, cationic polymers in the case of anionic BSA NPs. We previously reported the use of PEI for this purpose [21], where the surface charge of the particles shifted from negative to neutral or slightly positive. This change may reduce the plasma protein adsorption on particle surfaces and thus facilitate *in vivo* application of NPs [29,30]. We considered the well-known toxicity of PEI to be a potential shortcoming and, hence, explored another cationic polymer, PLL, for coating BSA NPs.

The BSA NPs were coated by different concentrations of PEI and PLL (10, 20, 50 and 100 $\mu\text{g}/\text{mL}$) and the amount of polymer adsorbed was quantitated by using FITC-labeled polymers. The results (mg polymer/g BSA) calculated from the calibration curves for individual polymers were summarized in **Figure 3-5A**. As the coating polymer concentration was increased, the amount of adsorbed polymer was increased as expected. There was no difference in the adsorbed polymer between PLL and PEI at 10 $\mu\text{g}/\text{mL}$, but a difference was noted at higher

concentrations (significantly different at 50 $\mu\text{g/mL}$, but not at 100 $\mu\text{g/mL}$ due to large SDs).

The size of the resultant NPs are summarized in **Figure 3-5B**. The mean particle size showed a dramatic change as a function of polymer concentration: a maximal size of >1000 nm was obtained at low polymer concentrations (10-20 $\mu\text{g/mL}$), after which the size of the NPs was reduced to 200-400 nm at presumably excess polymer concentration. Coating at polymer concentration of 10 $\mu\text{g/mL}$ and 20 $\mu\text{g/mL}$ also led to a significant variation in particle size (large SD in **Figure 3-5B**), presumably due to a bridging flocculation among the particles leading to aggregation [31]. For higher coating concentrations, the polymers presumably attained a better coating of the surfaces, with little bridging among the particles. Both PEI and PLL displayed the same behavior in this respect, given similar changes of NP size as a function of polymer concentration for both polymers.

The zeta potential of the polymer coated NPs increased gradually from -26 mV of uncoated NPs to ~ 16 mV as polymer concentration was increased to 100 $\mu\text{g/mL}$, as shown in **Figure 3-5C**. For NPs coated with 10 and 20 $\mu\text{g/mL}$ polymer concentrations, the surface charge of the coated particles was close to neutral, which was the likely reason for the dramatic increase in particle size in **Figure 3-5B**. The surface charge of particles coated with 50 and 100 $\mu\text{g/mL}$ polymer

became increasingly positive, which might have led to repulsive forces among the particles and prevented NP aggregation. It was interesting to note that there was no significant difference between PLL and PEI coated NPs with respect to zeta potential (and size), even though the amount adsorbed onto the NPs was higher for PEI as compared to PLL. This may suggest that the PEI penetrates deeper into the particles when it is conjugated to the surface or a denser combination was formed between the PEI and BSA NPs.

The BSA NPs were analyzed by AFM to confirm the size of the particles measured. As shown in **Figure 3-6A**, the NPs after the coacervation process were uniform in size, and generally spherical with smooth surface characteristics. No visible aggregates were evident. **Figure 3-6B** and **C** are typical AFM images for particles coated with 50 $\mu\text{g/mL}$ PLL and PEI, respectively. Larger particles after coating were evident, and the less uniform in particle size and rough surface were seen for the coated particles. The sizes obtained from these images were typically in the range of 100-200 nm, smaller than the measurement from dynamic light scattering results, which was possibly due to the shrinkage of the particles during the drying process for the AFM imaging.

Toxicity of PLL and PEI Coated BSA NPs

Previous studies with PEI coated BSA NPs indicated the PEI coating to be

the primary reason for the toxicity of the particles. We accordingly chose a relatively low concentration of polymers (<100 µg/mL), so as to minimize the previously observed toxicity of the NPs. Furthermore, the previous study used myogenic C2C12 cells for toxicity assessment; while they are particularly good for assessing BMP-2 activity, they are more robust than primary cells that may lead to underestimation of NP toxicity. Therefore, BMSC derived from both rats and humans were used in the present study for NP toxicity. BMSC were also chosen since the intended use of our NPs is to deliver BMP-2 and one of the primary targets of BMPs is stem cells at the bone marrow environment. The results of the toxicity assessment are summarized in **Figure 3-7**. Compared to untreated cells, the uncoated NPs did not provide any detectable toxicity, indicating complete removal of the desolvation agent (acetone) during the dialysis procedure. NPs coated with 10-100 µg/mL polymer (either PEI or PLL) also did not provide any significant toxicity in human BMSC (**Figure 3-7A**). There was a slight toxic effect of the particles on rat BMSC ($p \sim 0.02$; **Figure 3-7B**) compared to untreated cells, and a further slight toxic effect of the coatings (except PEI at 10 and 100 µg/mL) compared to the uncoated BSA particles ($p \sim 0.02$). Taken together, this indicated the rat BMSCs were more sensitive to the particles than the human BMSC, but the reduced concentration of PEI and PLL used for NP coating (as compared to Ref. 21) were still relatively well tolerated by the primary cell. Since we were able to get complete coating of the NPs at such low concentrations

(based on zeta-potential measurements), coating of NPs at higher concentrations, which might lead to toxicities, were not deemed necessary.

Bioactivity of BMP-2 Encapsulated in Polymer Coated NPs

The NP preparation process was adopted for BMP-2 encapsulation by adding BMP-2 to BSA solution before the coacervation process. The amount of BMP-2 added was only 2.5% of the BSA amount (per weight basis), so that no significant changes in the particle size was observed (as assessed by AFM; not shown), and based on our previous studies, the encapsulation efficiency is supposed to be achieved ~90%. Upregulation of ALP activity is a well-demonstrated feature of BMP-2 induced osteogenic activity on target cells. Several cell types, including myogenic C2C12 cells [21], osteoblastic hBMSC, as well as rBMSC in our hands [22], all display a stimulated ALP induction as a result of BMP-2 treatment. ALP activity is necessary for mineralization, since it is hypothesized to liberate free phosphate in the vicinity of the osteoblast-deposited extracellular matrix and facilitate its calcification. We previously conducted an extensive characterization of rat BMSC after BMP-2 and bFGF treatment, showing lasting effects of BMP-2 on ALP stimulation. We additionally used human BMSC in this study as a more realistic model for clinical application of BMP-2 in bone regeneration. The kinetics and mechanism of BMP-2 release was not addressed in this study due to the difficulties in separating the released BMP-2

and quantitative analysis of such small amount as well as the extensive additional testing that would have required.

Human BMSC were from third passage (P3) in our hands and displayed an ALP activity that was dependent on the passage (**Figure 3-8A, insert**). Cells from passage 4 and 5 displayed BMP-2 induced ALP activity with reduced robustness in the higher passage, and displayed no BMP-2 stimulated ALP activity in passage 6. Therefore, only cells from passage 4 were used for assessment of BMP-2 activity in BSA NPs. hBMSC in all study groups displayed ALP activity that gradually increased over a 14 days period (**Figure 3-8A**). No significant differences were evident among the cells on day 3 for all study groups. Free BMP-2 at 1 $\mu\text{g}/\text{mL}$ gave significantly higher ALP activity on day 7 as compared to untreated cells ($p=0.02$). None of the other groups had any significant ALP induction. On day 14, there was no significant ALP activity in cells treated with no BMP-2 (i.e., untreated cells and cells exposed uncoated and polymer-coated NPs in the absence of BMP-2). All BMP-2 containing NPs gave significantly higher ALP activity, and NPs coated with the polymers displayed an equivalent activity to that of free BMP-2. Uncoated NPs with BMP-2 displayed a relatively lower ALP induction. This was likely due to loss of BMP-2 during the processing of the particles since lack of a coating layer was expected to lead to unstable NPs and premature BMP-2 release, but there may also be difficulties in internalizing

non-coated particles due to its surface chemistry. Furthermore there was no calcium formation over the 2-week culture period in any of the samples (data not shown).

The ALP activity for the rat BMSC (**Figure 3-8B**) showed a significant increase after day 3 for all samples containing BMP-2 ($p \sim 0.01$). Over the entire culture period, the groups not exposed to BMP-2 showed no significant change in ALP activity, however all the groups containing BMP-2 showed a significant increase on day 7. NPs coated with PLL was an exception to this, since the change in ALP activity was not significant between day 3 and 7 due to large SD on day 7. The induced ALP was generally decreased by day 14, though only the uncoated BSA gave a significant decrease ($p \sim 0.003$). This decrease in ALP activity was indicative of the cells initiating the mineralization stage of bone formation, which was supported by the calcium assay. The calcium deposition by the rBMSCs was evident at day 14 (**Figure 3-9**) with a significant increase in calcification for all groups containing BMP-2 ($p \sim 0.01$). More importantly, the NP encapsulated BMP-2 gave a similar level of calcium deposition as the free BMP-2 at equivalent concentration.

Taken together, the bioactivity results obtained in this study indicated no adverse effect of encapsulation of BMP-2 in NPs. Given the relatively mild entrapment conditions, the use of non-solvent acetone was expected to be the only

impediment to retention of BMP-2 activity, and this did not seem to be a concern based on our results. The use of primary cells with direct relevance to osteogenesis provides encouraging data for *in vivo* testing of the proposed formulations. It must be noted that the exact concentration of BMP-2 in NPs were not determined in this study. Based on our previous studies (21), which indicated >90% encapsulation efficiency, we assumed full retention of BMP-2 amount in NPs and tested our formulations against an equivalent concentration of free BMP-2. More detailed studies on factors affecting BMP-2 encapsulation efficiency, BMP-2 release from the NPs, and their consequences on BMP-2 induced osteogenesis will be the subject of future studies.

Other Particulate Delivery Systems for BMP-2

A number of other particulate systems for delivery of BMP-2 have been investigated, including particles prepared from synthetic materials and natural polymers. Among them, hydrolytically degraded polylactic-co-glycolic acid (PLGA) are the most investigated delivery system for BMP-2. *In vitro* studies have shown the bioactivity of BMP-2 was maintained during encapsulation into such microparticles (250-430 μm), despite exposure to organic solvents [32]. The PLGA particles were effective in stimulating bone formation in several animal models, such as in rat femurs [33], calvarial defects in rabbits [34], and ovine vertebral bodies [35]. While some of these studies measured growth factor release,

subsequent studies focused on controlling the BMP-2 release from the PLGA particles by embedding them in a calcium phosphate cement [36] or by surface-grafting heparin to the particles for BMP-2 binding [37]. These studies utilized particles in the micron-scale, which are not suitable for systemic administration. Only one other system reported PLGA particles with size similar to our particles (~300 nm). This study focused on preventing the rapid diffusion of particles and growth factors away from the implant site by immobilizing PLGA NPs on the surface of a poly(*L*-lactide) scaffold [38]. In addition to synthetic PLGA-based particles, naturally-occurring polymers collagen [39] and dextran[40-42] were also used for BMP-2 entrapment. The particle sizes were again in the micron-scale for these systems (600-700 μm for collagen and 20-40 μm for dextran). Preclinical studies in a rabbit femur [39] and a canine periodontal defect model [40] demonstrated the bioactivity of the BMP-2 *in vivo*. All of the aforementioned delivery systems were designed for local delivery of BMP to a defect site. However, none would be suitable for systemic delivery, since particles <200 nm are ideal for systemic administration. To that extent our protein-based NPs, to the best of our knowledge, provide a unique systemic delivery system for BMP-2, with the ultimate goal of including a bone targeting mechanism. BSA will not be suitable for human clinical application, but this protein can be readily replaced with human serum albumin with little modification of process parameters for NP preparation [2].

3.4 CONCLUSIONS

This study demonstrated a reproducible coacervation procedure for preparation of BSA NPs with controllable particle size between 50 and 400 nm. The influences of several process parameters on the size and polydispersity of the NPs were investigated by independent experiments and a statistical methodology. The process variables found to most significantly influence the NP sizes were pH value of the coacervation medium, as well as the concentration of the polymers used for coating the particles. Although initial particle size could be tailored within sub-100 nm range, polymer coating of the particles resulted in an increase of size to ~200 nm range. Smaller particles are more desirable for *in vivo* administration, since they are less likely to get opsonized and more likely to get extravasated from the circulation. Polymers capable of forming brush-like structures on NP surfaces might be more desirable in this respect, since they might reduce van der Waals based interactions among the NPs, thereby stabilizing them. Nevertheless, the process described successfully entrapped the BMP-2 with significant retention of the bioactivity of the protein, based on *in vitro* bioassays using clinically relevant cell models. We conclude that the NPs described in this study has potential for novel means of BMP-2 delivery, that might further facilitate the clinical application of this protein in local and systemic regeneration of bone tissue.

Table 3-1 Experimental control factors and their levels for the statistical experiment testing.

Factors		Level 1	Level 2	Level 3	Level 4
A	BSA concentration (mg/mL)	10	20	30	50
B	Ethanol:water ratio	1	2	4	6
C	pH value	4.3	5.5	7.4	9.3
D	Stirring rate (rpm)	400	800	1200	

Table 3-2 Orthogonal array and results of the statistical experiment testing.

Experiment No.	A	B	C	D	Results			
	[BSA] (mg/mL)	Ethanol:water ratio	pH value	Stirring rate (rpm)	Size (nm)	SD (nm)	PDI	SD
1	10	1	4.3	400	334.2	11.5	0.286	0.236
2	10	2	5.5	800	241.8	9.6	0.235	0.056
3	10	4	7.4	1200	128.9	9.0	0.263	0.155
4	10	6	9.3	400	122.2	37.0	0.677	0.284
5	20	1	5.5	800	186.5	5.1	0.506	0.013
6	20	2	4.3	1200	296.8	4.2	0.161	0.027
7	20	4	9.3	400	158.0	1.9	0.117	0.043
8	20	6	7.4	800	97.6	0.6	0.097	0.015
9	30	1	7.4	1200	58.7	10.0	0.599	0.123
10	30	2	9.3	1200	102.9	4.6	0.636	0.054
11	30	4	4.3	800	260.6	0.8	0.256	0.058
12	30	6	5.5	400	163.7	2.3	0.161	0.019
13	50	1	9.3	800	93.0	2.6	0.509	0.015
14	50	2	7.4	400	149.0	5.7	0.454	0.069
15	50	4	5.5	1200	137.8	4.7	0.593	0.031
16	50	6	4.3	1200	193.1	1.7	0.285	0.01
17	30	4	9.3	800	150.4	0.8	0.188	0.065
18	20	6	7.4	400	92.8	3.2	0.377	0.098

Data were expressed as mean and SD (n = 3).

Table 3-3 Data analysis of the statistical experiment testing.

Analysis	Particle size (nm)				PDI			
	A	B	C	D	A	B	C	D
K_1	827.1	672.4	1084.7	1019.9	1.461	1.900	0.988	2.072
K_2	935.4	790.5	610.2	991.0	1.857	1.486	1.495	1.791
K_3	734.9	835.7	527.0	918.2	1.840	1.417	1.790	2.537
K_4	572.9	669.4	626.5		1.841	1.597	2.127	
k_1	206.8	168.1	271.2	170.0	0.365	0.475	0.247	0.345
k_2	187.1	197.6	152.6	165.2	0.371	0.372	0.374	0.299
k_3	147.0	167.1	105.4	153.0	0.368	0.283	0.358	0.423
k_4	143.2	133.9	125.3		0.460	0.319	0.425	
R	63.6	63.7	165.8	17.0	0.095	0.192	0.178	0.124

Level total K_i and level average k_i were the sum and average of the results of those experiments which had the i th level of a given factor. R was the maximum variance ($\max\{k_i\} - \min\{k_i\}$) of each factor. For example: $K_1(A) = 334.2+241.8+128.9+122.2=827.1$ (nm), $k_1(A)=K_1(A)/4=206.8$ (nm), $R(A)=206.8-143.2=63.6$ (nm).

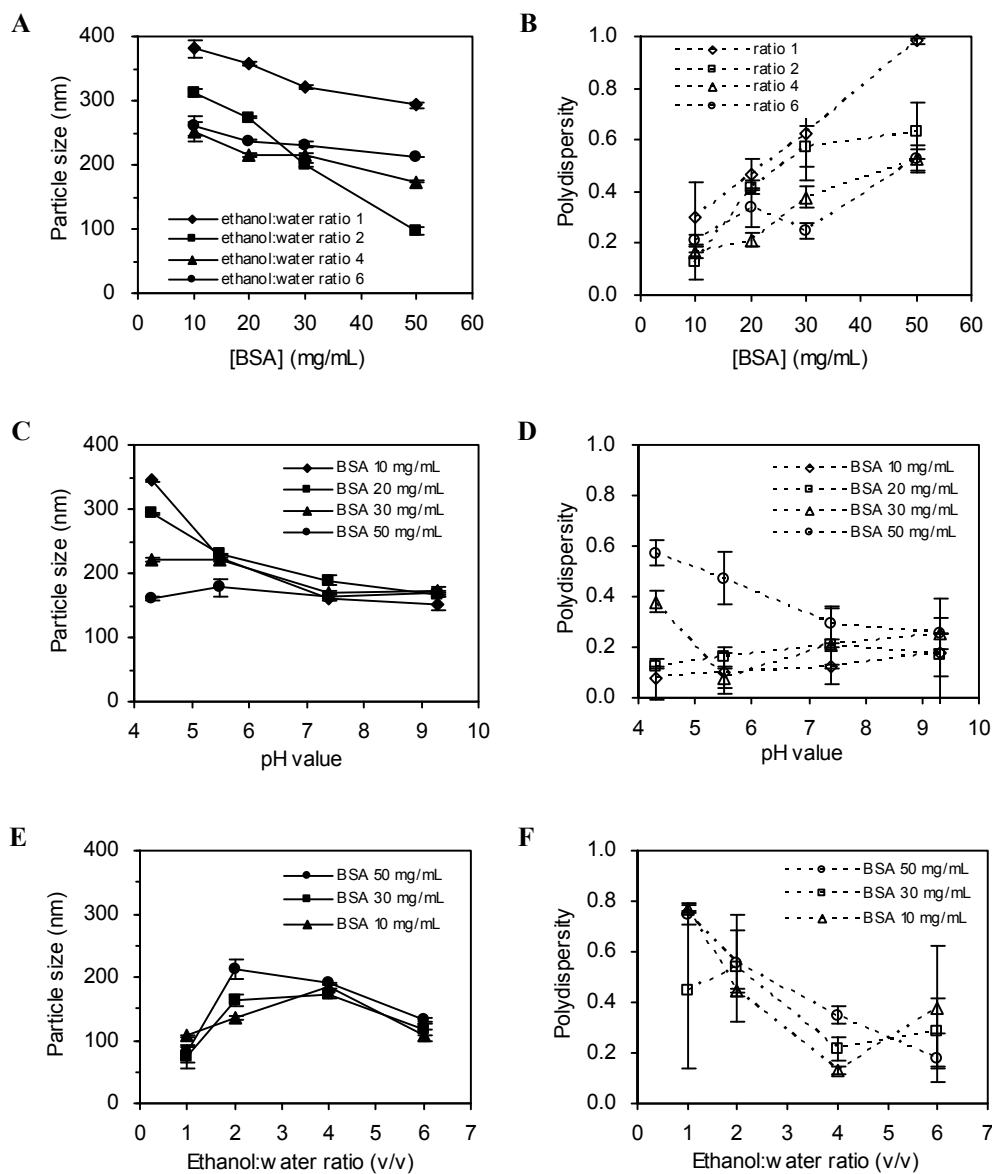


Figure 3-1 Influence of BSA concentration (**A**, **B**), pH value of coacervation solution (**C**, **D**) and ethanol:water ratio (**E**, **F**) on particle size and polydispersity of BSA NPs. BSA concentrations shown were the initial concentration mixed with equal volume of 10 mM NaCl in (**A**) and (**B**), 10 mM phosphate buffer (pH 4.3, 5.5, 7.4 and 9.3) in (**C**) and (**D**) with ethanol:water ratio of 4, and 10 mM phosphate buffer (pH 9.3) in (**E**) and (**F**) before coacervation. Data were expressed as mean \pm SD of three independent NP preparations ($n = 3$). The sizes of NPs prepared using ethanol as the non-solvent were mostly in the 100-400 nm range. Both the particle size and polydispersity were significantly dependent on these three process parameters investigated.

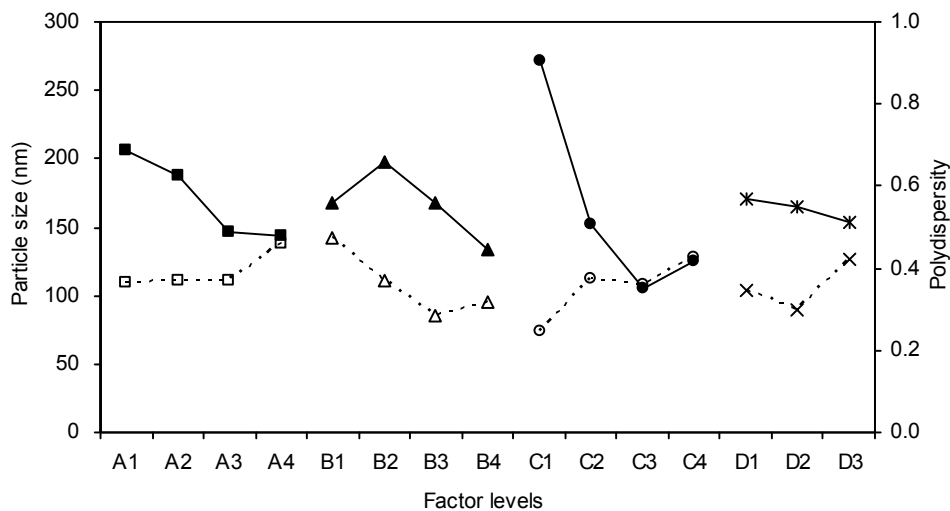


Figure 3-2 Dependence of particle size (solid symbol) and polydispersity (open symbol) on A: BSA concentration (square), B: ethanol:water ratio (triangle), C: pH value (circle) and D: stirring rate (cross). The factors and levels were from **Table 3.1**. Note that the effects of BSA concentration, pH of the coacervation medium, and ethanol:water ratio on NP size and polydispersity examined by the Taguchi method were consistent with the independent experiments shown in **Figure 3.1**.

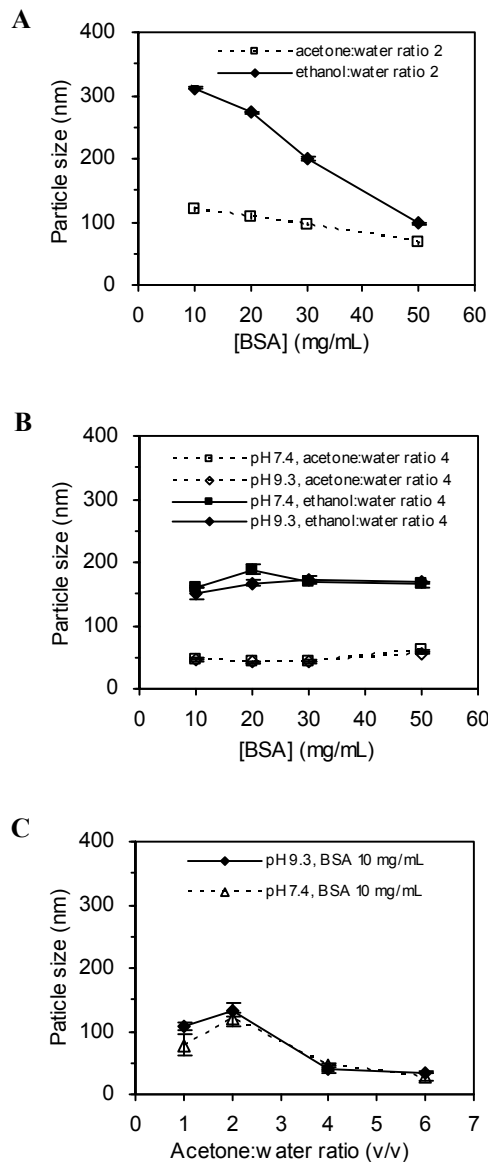


Figure 3-3 Comparison of the size of BSA NPs prepared by using ethanol and acetone as the non-solvent. BSA concentrations shown were the initial concentration mixed with either 10 mM NaCl (**A**), or 10 mM phosphate buffer (**B**) with pH 7.4 and 9.3 before coacervation. Note that acetone yielded NPs with smaller sizes than ethanol under all conditions tested. (**C**) Effect of acetone:water ratio on NP size when 10 mg/mL BSA was mixed with phosphate buffer at pH 7.4 and 9.3. As compared to ethanol (see **Figure 3-1C**), acetone also yielded smaller particles at the highest acetone:water ratio. Data in all graphs were expressed as mean \pm SD of three independent NP preparations ($n = 3$).

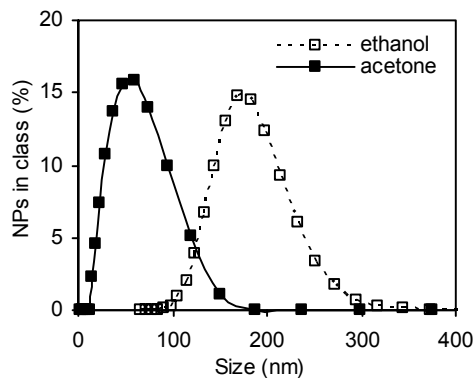


Figure 3-4 Size distribution of the NPs prepared by using acetone (solid) and ethanol (dashed) as non-solvent. NPs were prepared by using 10 mg/mL BSA mixed with equal volume of 10 mM phosphate buffer of pH 7.4, followed by dropwise addition of 4 volumes of acetone or ethanol. The distribution was based on intensity from dynamic light scattering measurement. Note that the size range of BSA NPs prepared by using acetone was lower.

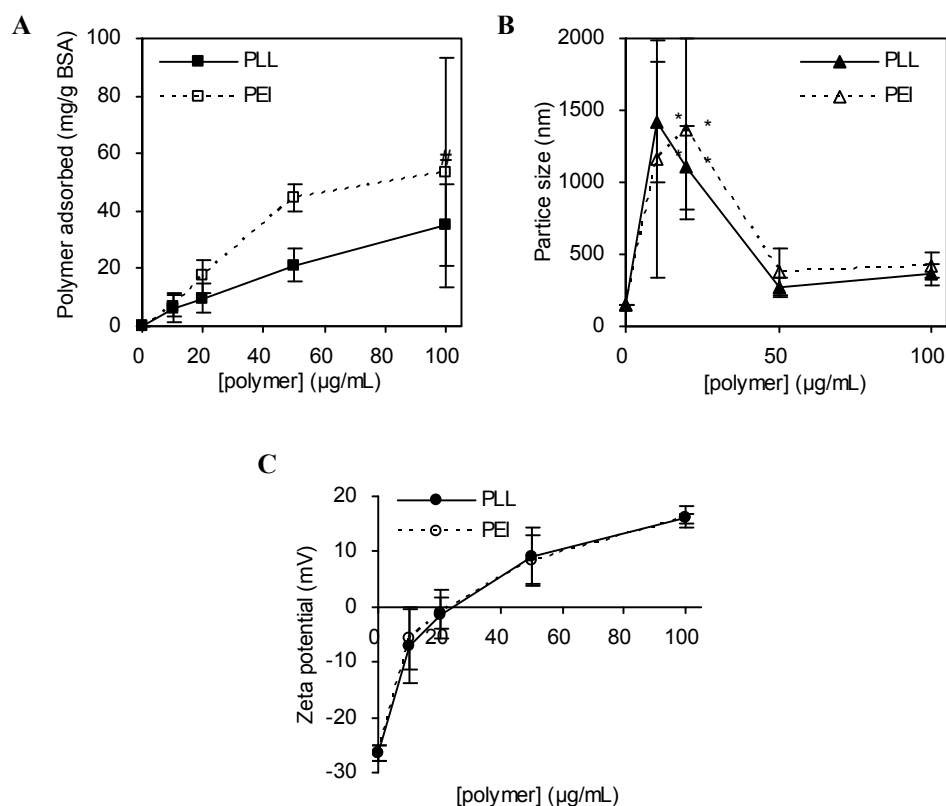


Figure 3-5 The amount of polymer adsorbed onto NPs (**A**), mean particle diameter (**B**) and zeta potential (**C**) of NPs coated with different concentrations of PLL and PEI. The amounts of PEI adsorbed onto the NPs were slightly more than the PLL at concentrations higher than 20 µg/mL. Note the drastic increase in particle size at low polymer concentrations for both polymers. The zeta potential of the PLL and PEI coated NPs increased gradually from -26 mV for uncoated NPs to ~16 mV at polymer concentration of 100 µg/mL. There was slight but not significant difference between PLL and PEI coated NPs with respect to particle size and zeta potential. Data in all graphs were expressed as mean ± SD of three independent NP preparations (n = 3). #: some precipitates were observed for one sample; *: Polydispersity greater than 0.7.

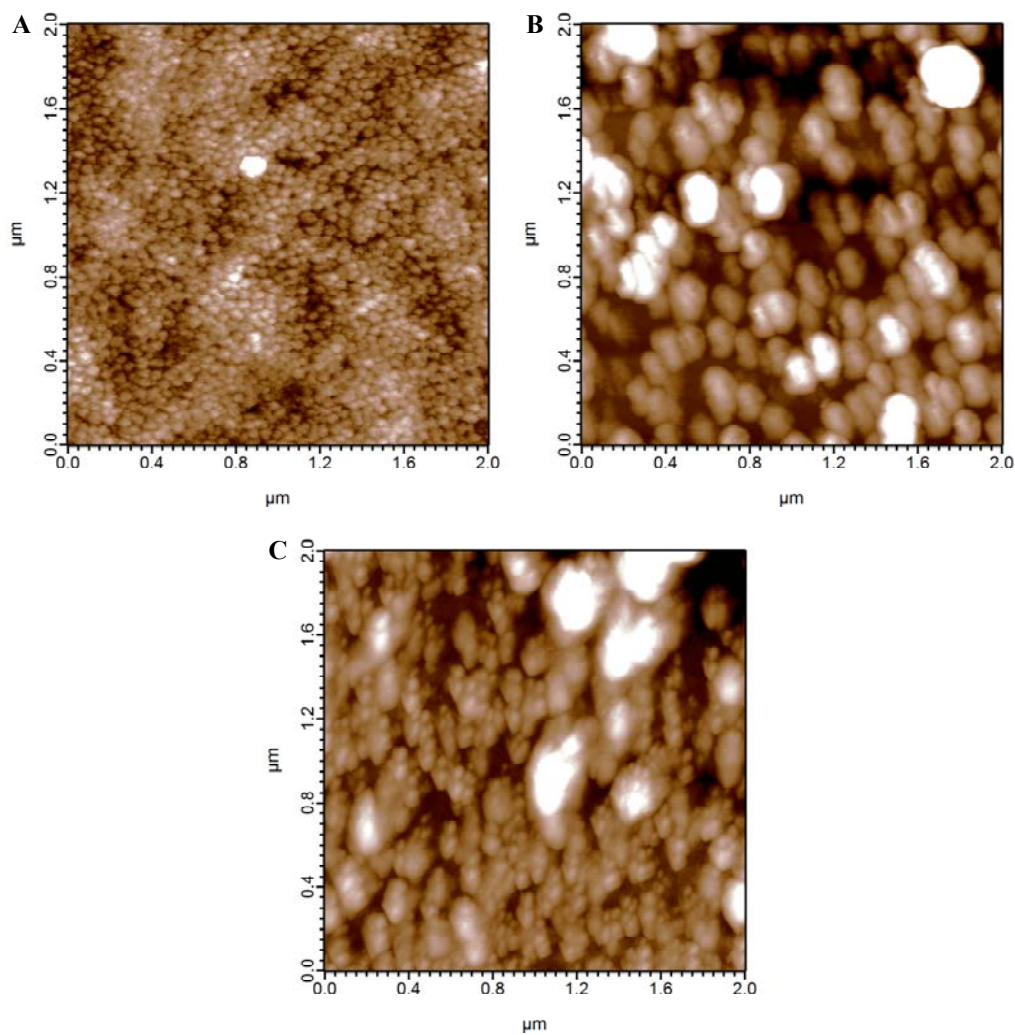


Figure 3-6 AFM of uncoated BSA NPs (**A**) obtained right after the coacervation process (i.e., without dialysis) and BSA NPs coated with 50 µg/mL PLL (**B**) and PEI (**C**). Note the uniformity in size and lack of aggregation from (**A**). Larger NPs (200~300 nm) were evident in the samples coated with PLL and PEI, with significant variations in particle sizes. All the images were 2 µm × 2 µm in scale and representative images were shown from a large series of images generated from the AFM.

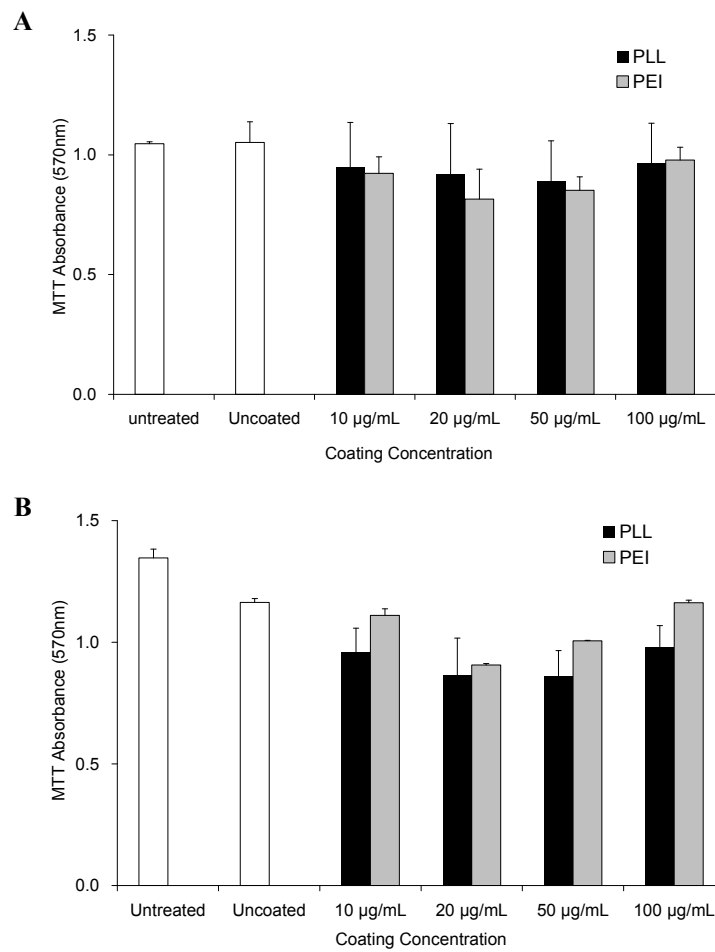


Figure 3-7 MTT assay of the PEI and PLL coated NPs in (A) human BMSCs and (B) rat BMSCs. No significant difference was seen in the toxicity coating concentrations, nor between the different polymer coatings. Data in all graphs were expressed as mean \pm SD (n = 3).

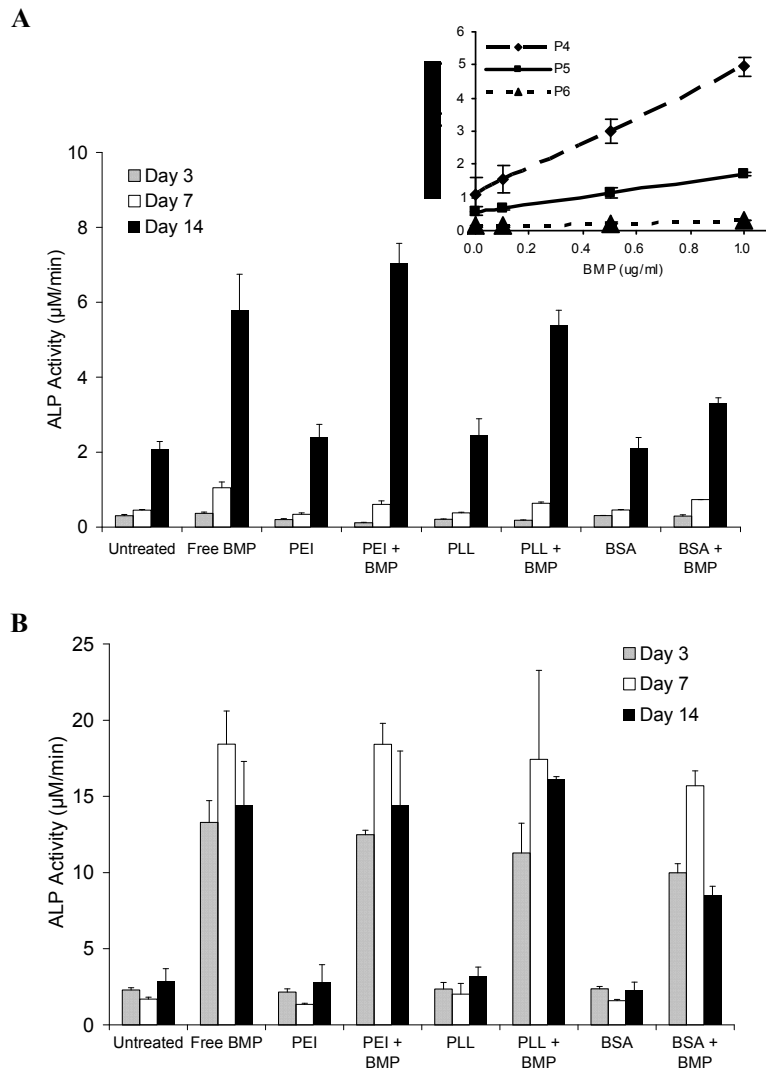


Figure 3-8 ALP activity of BMP-2 encapsulated in uncoated and coated NPs in (A) human BMSCs and (B) rat BMSCs. There was an increase of ALP activity for the NPs containing BMP-2 compared to those without BMP-2 ($p < 0.05$). Furthermore the ALP activity for the coated particles were higher than the uncoated ones ($p < 0.05$), which was similar to free BMP-2. ALP activity of human BMSCs (Inset A) was shown as a function of passage number with the addition of different concentrations of BMP-2. There was a dramatic decrease in ALP activity from passage 4 to passage 6. Data in all graphs were expressed as mean \pm SD ($n = 3$).

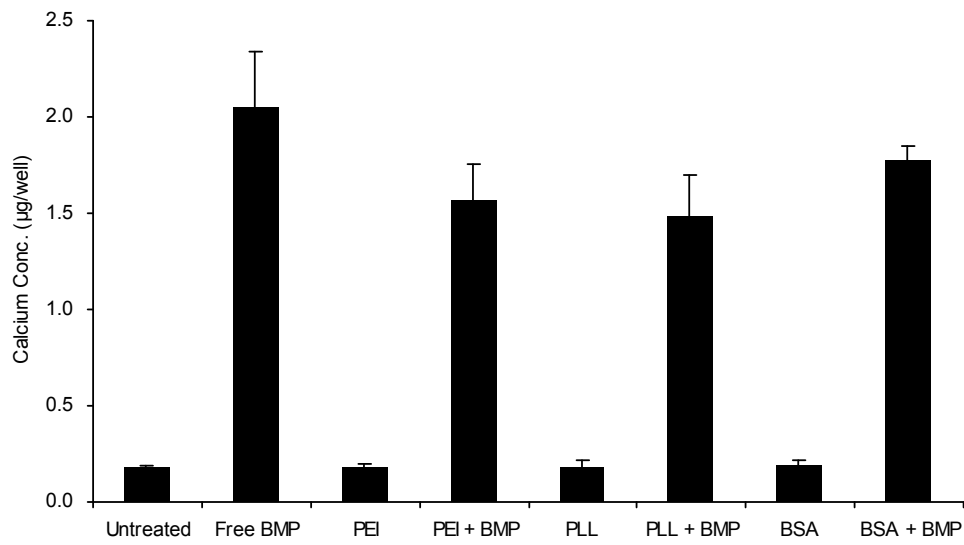


Figure 3-9 Calcification of rat BMSCs at day 14. All groups containing BMP-2 showed a significant increase in calcification compared to groups without BMP-2. Data in all graphs were expressed as mean \pm SD (n = 3).

REFERENCES

- [1]. Luginbuehl, V.; Meinel, L.; Merkle, H. P.; Gander, B. Localized delivery of growth factors for bone repair. *Euro J Pharm Biopharm* **2004**, *58*, 197-208.
- [2]. Langer, K.; Balthasar, S.; Vogel, V.; Dinauer, N.; von Briesen, H.; Schubert, D. Optimization of the preparation process for human serum albumin (HSA) nanoparticles. *Int J Pharm* **2003**, *257*, 169-180.
- [3]. Muller, B. G.; Leuenberger, H.; Kissel, T. Albumin nanospheres as carriers for passive drug targeting: an optimized manufacturing technique. *Pharm Res* **1996**, *13*, 32-37.
- [4]. Roser, M.; Fischer, D.; Kissel, T. Surface-modified biodegradable albumin nano- and microspheres. II: effect of surface charges on in vitro phagocytosis and biodistribution in rats. *Euro J Pharm Biopharm* **1998**, *46*, 255-263.
- [5]. Moghimi, S. M.; Hunter, A. C.; Murray, J. C. Long-circulating and target-specific nanoparticles: theory to practice. *Pharmacol Rev* **2001**, *53*, 283-318.
- [6]. Litzinger, D. C.; Buiting, A. M. J.; van Rooijen, N.; Huang, L. Effect of liposome size on the circulation time and intraorgan distribution of amphipathic poly(ethylene glycol)-containing liposomes. *Biochim Biophys Acta Biomembranes* **1994**, *1190*, 99-107.
- [7]. Harasym, T. O.; Bally, M. B.; Tardi, P. Clearance properties of liposomes involving conjugated proteins for targeting. *Adv Drug Deliv Rev* **1998**, *32*, 99-118.
- [8]. Devine, D. V.; Bradley, A. J. The complement system in liposome clearance: Can complement deposition be inhibited? *Adv Drug Deliv Rev* **1998**, *32*, 19-29.
- [9]. Thassu, D.; Deleers, M.; Pathak, Y. *Nanoparticulate drug delivery systems*; Informa Healthcare, New York, **2007**.
- [10]. Plank, C.; Mechtler, K.; Szoka, F. C.; Wagner, E. Activation of the complement system by synthetic DNA complexes: a potential barrier for intravenous gene delivery. *Hum Gene Ther* **1996**, *7*, 1437-1446.
- [11]. Rubino, O. P.; Kowalsky, R.; Swarbrick, J. Albumin microspheres as a drug

delivery system: relation among turbidity ratio, degree of cross-linking, and drug release. *Pharm Res* **1993**, *10*, 1059-1065.

- [12]. MacAdam, A. B.; Shafi, Z. B.; James, S. L.; Marriott, C.; Martin, G. P. Preparation of hydrophobic and hydrophilic albumin microspheres and determination of surface carboxylic acid and amino residues. *Int J Pharm* **1997**, *151*, 47-55.
- [13]. Weber, C.; Coester, C.; Kreuter, J.; Langer, K. Desolvation process and surface characterisation of protein nanoparticles. *Int J Pharm* **2000**, *194*, 91-102.
- [14]. Lin, W.; Coombes, A. G. A.; Davies, M. C.; Davis, S. S.; Illum, L. Preparation of sub-100 nm human serum albumin nanoparticles using a pH-coacervation method. *J Drug Target* **1993**, *1*, 237-243.
- [15]. Rahimnejad, M.; Jahanshahi, M.; Najafpour, G. D. Production of biological nanoparticles from bovine serum albumin for drug delivery. *Afr J Biotechnol* **2006**, *5*, 1918-1923.
- [16]. Van Miller, J. P.; Hermansky, S. J.; Losco, P. E.; Ballantyne, B. Chronic toxicity and oncogenicity study with glutaraldehyde dosed in the drinking water of Fischer 344 rats. *Toxicology* **2002**, *175*, 177-189.
- [17]. McGregor, D.; Bolt, H.; Cogliano, V.; Richter-Reichhelm, H. B. Formaldehyde and glutaraldehyde and nasal cytotoxicity: case study within the context of the **2006** IPCS human framework for the analysis of a cancer mode of action for humans. *Crit Rev Toxicology* **2006**, *36*, 821-835.
- [18]. Segura, S.; Gamazo, C.; Irache, J. M.; Espuelas, S. Gamma interferon loaded onto albumin nanoparticles: in vitro and in vivo activities against brucella abortus. *Antimicrob Agents Chemother* **2007**, *51*, 1310-1314.
- [19]. Segura, S.; Espuelas, S.; Renedo, M. a. J. s.; Irache, J. M. Potential of albumin nanoparticles as carriers for interferon gamma. *Drug Dev Ind Pharm* **2005**, *31*, 271-280.
- [20]. Leo, E.; ngela Vandelli, M.; Cameroni, R.; Forni, F. Doxorubicin-loaded gelatin nanoparticles stabilized by glutaraldehyde: involvement of the drug in the cross-linking process. *Int J Pharm* **1997**, *155*, 75-82.
- [21]. Zhang, S.; Wang Guilin; Lin, X.; Jennissen, H.; Chadzinikolaidou, M.; Uludag, H. Polyethylenimine-coated albumin nanoparticles for BMP-2

- delivery. *Biotechnol Prog* **2008**, *24*, 945-956.
- [22]. Varkey, M.; Kucharski, C.; Haque, T.; Sebald, W.; Uludag, H. In vitro osteogenic response of rat bone marrow cells to bFGF and BMP-2 treatments. *Clin Orthop Relat Res* **2006**, *443*, 113-123.
- [23]. Zhang, S.; Wright, J. E. I.; Uludag, H.; Ozber, N. The interaction of cationic polymers and their bisphosphonate derivatives with hydroxyapatite. *Macromol Biosci* **2007**, *7*, 656-670.
- [24]. Jeney, C.; Dobay, O.; Lengyel, A.; Adam, E.; Nasz, I. Taguchi optimisation of ELISA procedures. *J Immunol Methods* **1999**, *223*, 137-146.
- [25]. Hung, C. C.; Shih, H. C. Experimental design method applied to microwave plasma enhanced chemical vapor deposition diamond films. *J Crystal Growth* **2001**, *233*, 723-729.
- [26]. Jiang, H.; Secretan, C.; Gao, T.; Bagnall, K.; Korbitt, G.; Lakey, J.; Jomha, N. M. The development of osteoblasts from stem cells to supplement fusion of the spine during surgery for AIS. *Stud Health Technol Informat* **2006**, *123*, 467-472.
- [27]. Kreuter, J. Nanoparticles and nanocapsules---new dosage forms in the nanometer size range. *Pharm Acta Helv* **1978**, *53*, 33-39.
- [28]. Jacob, J. S.; Mathiowitz, E. A Novel Mechanism for spontaneous encapsulation of active agents: phase inversion nanoencapsulation. In *Carrier-Based Drug Delivery*, Svenson, S., Ed.; American Chemical Society: Washington, DC, USA, **2004**; pp 214-223.
- [29]. Merdan, T.; Callahan, J.; Petersen, H.; Kunath, K.; Bakowsky, U.; Kopeckova, P.; Kissel, T.; Kopecek, J. Pegylated polyethylenimine-Fab' antibody fragment conjugates for targeted gene delivery to human ovarian carcinoma cells. *Bioconjug Chem.* **2003**, *14*, 989-996.
- [30]. Faraasen, S.; Voros, J.; Csucs, G.; Textor, M.; Merkle, H. P.; Walter, E. Ligand-specific targeting of microspheres to phagocytes by surface modification with poly(L-lysine)-grafted poly(ethylene glycol) conjugate. *Pharm Res* **2003**, *20*, 237-246.
- [31]. Hiemenz, P. C.; Rajagopalan, R. *Principles of Colloid and Surface Chemistry*; 3 ed.; Marcel Dekker: New York, **1997**.
- [32]. Oldham, J. B.; Lu, L.; Porter, B. D.; Hefferan, T. E.; Larson, D. R.; Currier,

- B. L.; Mikos, A. G.; Yaszemski, M. J. Biological activity of rhBMP-2 released from PLGA microspheres. *J Biomech Eng* **2008**, *122*, 289-292.
- [33]. Lee, S. C.; Shea, M.; Battle, M. A.; Kozitza, K.; Ron, E.; Turek, T.; Schaub, R. G.; Hayes, W. C. Healing of large segmental defects in rat femurs is aided by RhBMP-2 in PLGA matrix. *J Biomed Mater Res* **1994**, *28*, 1149-1156.
- [34]. Schrier, J.; Fink, B.; Rodgers, J.; Vasconez, H.; DeLuca, P. Effect of a freeze-dried CMC/PLGA microsphere matrix of rhBMP-2 on bone healing. *AAPS PharmSciTech* **2001**, *2*, 73-80.
- [35]. Phillips, F. M.; Turner, A. S.; Seim III, H. B.; MacLeay, J.; Toth, C. A.; Pierce, A. R.; Wheeler, D. L. In vivo BMP-7 (OP-1) enhancement of osteoporotic vertebral bodies in an ovine model. *Spine J* **2006**, *6*, 500-506.
- [36]. Ruhe, P. Q.; Boerman, O. C.; Russel, F. G. M.; Spauwen, P. H. M.; Mikos, A. G.; Jansen, J. A. Controlled release of rhBMP-2 loaded poly(DL-lactic-co-glycolic acid)/calcium phosphate cement composites in vivo. *J Control Rel* **2005**, *106*, 162-171.
- [37]. Jeon, O.; Song, S. J.; Yang, H. S.; Bhang, S. H.; Kang, S. W.; Sung, M. A.; Lee, J. H.; Kim, B. S. Long-term delivery enhances in vivo osteogenic efficacy of bone morphogenetic protein-2 compared to short-term delivery. *Biochem Biophys Res Commun* **2008**, *369*, 774-780.
- [38]. Wei, G.; Jin, Q.; Giannobile, W. V.; Ma, P. X. The enhancement of osteogenesis by nano-fibrous scaffolds incorporating rhBMP-7 nanospheres. *Biomaterials* **2007**, *28*, 2087-2096.
- [39]. Wang, Y. J.; Lin, F. H.; Sun, J. S.; Huang, Y. C.; Chueh, S. C.; Hsu, F. Y. Collagen-hydroxyapatite microspheres as carriers for bone morphogenic protein-4. *Artif Organs* **2003**, *27*, 162-168.
- [40]. Chen, F.; Zhao, Y.; Zhang, R.; Jin, T.; Sun, H.; Wu, Z.; Jin, Y. Periodontal regeneration using novel glycidyl methacrylated dextran (Dex-GMA)/gelatin scaffolds containing microspheres loaded with bone morphogenetic proteins. *J Control Rel* **2007**, *121*, 81-90.
- [41]. Chen, F.; Wu, Z.; Wang, Q.; Wu, H.; Zhang, Y.; Nie, X.; Jin, Y. Preparation of recombinant human bone morphogenetic protein-2 loaded dextran-based microspheres and their characteristics1. *Acta Pharm Sin* **2005**, *26*, 1093-1103.

- [42]. Chen, F.; Wu, Z.; Sun, H.; Wu, H.; Xin, S.; Wang, Q.; Dong, G.; Ma, Z.; Huang, S.; Zhang, Y.; Jin, Y. Release of bioactive BMP from dextran-derived microspheres: A novel delivery concept. *Int J Pharm* **2006**, *307*, 23-32.

Chapter 4

Bisphosphonate-Coated BSA Nanoparticles Lack Bone Targeting after Systemic Administration¹

¹A version of this chapter has been published in: Wang G, Kucharski C, Lin X, Uludag H. *Journal of Drug Targeting* 2010;18: 611-626

4.1 INTRODUCTION

Nanoparticulate colloid systems have been employed in drug delivery and targeting systems, since they have the potential of selective targeting of drugs to specific tissues and cells [1-3]. Albumin is an endogenous protein suitable for preparation of particulate drug delivery systems due to its natural biodegradability, biocompatibility, non-toxicity in physiological systems [4-6]. Size and surface characteristics of nanoparticles (NPs), including surface charge and hydrophilicity, can significantly influence the distribution of administered formulations in the body [1]. The surface properties of albumin NPs may be mediated through adsorption or conjugation with other compounds, such as targeting ligands with antibodies and poly(ethylene glycol) (PEG) polymers. PEG is an amphiphilic polyether diol, which is non-toxic and has been approved by FDA for human intravenous, oral, and dermal application. PEG has also been widely used to improve the solubility [7] and biocompatibility of macromolecules [8,9], to prevent particulate aggregation and to reduce their interaction with blood components [10]. A large volume of research has shown that PEG modification on biomolecules can effectively reduce reticuloendothelial system (RES) clearance and prolong blood circulation time of the biomolecules [1,11,12]. PEGylated human serum albumin (HSA) NPs were studied by Mishra et al. [13] for brain targeting delivery of an antiviral drug, azidothymidine (AZT), and

enhancement of brain localization of AZT was observed for transferrin anchored PEGylated albumin NPs. Lin et al. [14-16] reported preparation of HSA NPs sterically stabilized with PEGylated copolymers. The existence of a hydrated steric barrier surrounding the NPs was verified and the surface modified particles were shown to reduce plasma protein adsorption compared with unmodified surfaces.

For development of a bone-targeting drug delivery system, another critical requirement is imparting the NPs with strong bone affinity. Bisphosphonates (BPs) have been proven to be a class of molecules with exceptional affinity to bone mineral hydroxyapatite (HA), and have been used as bone-targeting agents for several classes of drugs [2]. Successful targeting of BP conjugates were obtained with several proteins, including lysozyme, bovine serum albumin (BSA) and IgG[17-19]. Upon systemic injection, significantly increased bone deposition (as much as 7-fold) of the BP conjugated proteins was observed. However, the direct coupling of BPs to proteins might be problematic for sensitive proteins, since the covalent conjugation of BPs to proteins may result in loss of their native bioactivity. As an alternative, BPs can be conjugated to polymeric materials, such as polylactic-co-glycolic acid (PLGA) [20], poly[*N*-(2-hydroxypropyl) methacrylamide] (PHPMA) [21], polyethylenimine (PEI) and poly-*L*-lysine (PLL)[22], which might be a preferable platform for delivering sensitive

therapeutic agents to bone once the therapeutic agents are appropriately formulated with such polymers.

We recently optimized a coacervation procedure for preparation of BSA NPs [23], and proposed PEI-stabilized BSA NPs for delivery of growth factors (e.g., bone morphogenetic protein-2, BMP-2). This system was shown to reasonably control the release rate of encapsulated proteins with full retention of the bioactivity of the released protein [24]. However, the toxicity of PEI and its undesirable capacity to aggregate particles were two concerns when it was used to coat the albumin NP surfaces. PEG modification of PEI might be advantageous in this respect. PEG modified PEI has been studied for improved gene delivery[8-10], and showed that PEG modification of PEI reduced its toxicity and increased their solubility. In addition, PEG with dual functional groups at its terminal ends offer the possibility of further conjugating bioactive agents or targeting moieties to PEI.

In the present study, PEI was substituted with PEG (PEI-PEG), which was then conjugated with a thiolBP (2-(3-mercaptopropylsulfanyl)-ethyl-1,1-bisphosphonic acid; PEI-PEG-thiolBP) for bone targeting. The PEI-PEG and PEI-PEG-thiolBP were used for NP coating via simple electrostatic interaction between the negatively charged BSA surfaces and the cationic PEI backbone. The PEG chains were expected to coat and stabilize the BSA/PEI core, and present

thiolBP ligands on the surface. The physicochemical and biological properties, including particle size, surface charge, cytotoxicity and BMP-2 activity, were characterized *in vitro*, as well as bone mineral affinity in an implant and an intravenous injection model in rats.

4.2 MATERIALS and METHODS

Materials

ThiolBP was synthesized as previously described [19]. Branched PEI (MW ~25 kDa), BSA, ascorbic acid, 3-(4,5-dimethylthiazol-2-yl)-2,5-diphenyl-tetrazolium bromide (MTT), *p*-nitrophenol phosphate (*p*-NPP), and picrylsulfonic acid solution (TNBS, 5% w/v) were obtained from Sigma-Aldrich (St. Louis, MO, USA). The heterobifunctional PEG derivative, maleimide PEG N-succinimide ester (NHS-PEG-MAL, MW 3 500 Da) was obtained from JenKem Technology (Allen, TX, USA). Recombinant human bone morphogenetic protein-2 (BMP-2) was expressed in *E. coli* and purified as described before [25]. Na¹²⁵I (in 0.1 M NaOH) was purchased from GE Healthcare (Piscataway, NJ, USA). Synthetic HA was prepared according to the method described in [22]. Sterile saline (0.9% NaCl, non-pyrogenic) used for implantation and injection was obtained from Baxter Corporation (Toronto, ON, Canada). The Spectra/Por

dialysis tubing with molecular weight cut-off (MWCO) of 12–14 kDa was acquired from Spectrum Laboratories (Rancho Dominguez, CA, USA) and used in all dialysis procedures. Dulbecco's Modified Eagle Medium (DMEM), Hank's Balanced Salt Solution (HBSS), GlutaMax-1 (GM), penicillin (10,000 U/mL) and streptomycin (10 000 µg/mL) were from Invitrogen (Carlsbad, CA, USA). Fetal bovine serum (FBS) was from Atlanta Biologics (Atlanta, GA, USA). All tissue culture plasticware was from Corning (Corning, NY, USA). Distilled/de-ionized water (ddH₂O) used for buffer preparation and dialysis was derived from a Milli-Q purification system (Millipore, Billerica, MA). Skelite™ implants, a multiphase calcium phosphate matrix (67% Si-stabilized tricalcium phosphate and 33% HA), were obtained from Millenium Biologix Inc. (Mississauga, Ontario, Canada).

Synthesis of PEI-PEG-thiolBP

The thiolBP was conjugated to branched PEI by using heterobifunctional PEG derivative (NHS-PEG-MAL) as shown in Scheme 1. The NHS-PEG-MAL and thiolBP were separately dissolved in 0.1 M phosphate buffer (pH 7.2), and mixed at equal volumes under constant shaking at 400 rpm for 1 h to obtain the NHS-PEG-thiolBP. Various volumes of NHS-PEG-thiolBP were then added to a PEI solution at 2 mg/mL (the feed ratios shown in **Figure 4-2**) in 0.1 M phosphate buffer (pH 7.2), and incubated for 3 h at room temperature while stirring. For

comparison, PEI-PEG was synthesized by reacting NHS-PEG-MAL with PEI (both in 0.1 M phosphate buffer) with different molar ratios. The final products, PEI-PEG-thiolBP or PEI-PEG, were purified by dialyzing against excess 0.1 M carbonate buffer (pH 10.0, $\times 3$) and against distilled/de-ionized water (ddH₂O, $\times 2$).

Analysis of PEI-PEG-thiolBP

The PEG graft ratio on the PEI backbone was determined from ¹H-NMR spectra (analyzed after dissolving the polymer in D₂O). The BP conjugation efficiency (i.e., the average number of thiolBP per PEI) was calculated by dividing the thiolBP concentration by the PEI concentration in the samples. PEI concentrations were determined by a copper/PEI complex assay [26,27]. For this, 100 μ L of samples was added to 100 μ L of 20 mM CuSO₄ solution, and the mixture was diluted to 500 μ L with 0.1 M acetate buffer (pH 5.4). Known concentrations of native PEI served as the calibration standards, and the absorbance was read at 630 nm by a UV spectrophotometer (Ultrospec@2000, Pharmacia Biotech). A phosphate assay described by Ames [28] was used to determine the thiolBP content in the samples. 50 μ L of sample was mixed with 30 μ L of 10% Mg(NO₃)₂ in 95% ethanol in glass tubes and ashed over a flame. After boiling in 300 μ L of 0.5 N HCl for 15 min, 600 μ L of (NH₄)₆Mo₇O₂₄ (0.42% w/v in 1 N H₂SO₄) and 100 μ L of ascorbic acid (10% w/v) were added to the tubes

and the samples were incubated at 37 °C for 1 h. The absorbance was determined at 820 nm, and a calibration curve based on known concentrations of thiolBP was used to calculate the concentrations of conjugated BP.

***In Vitro* HA Affinity of Polymers**

The mineral affinity of the polymers was investigated by using a HA binding assay. 100 µL of polymer sample was diluted to 500 µL with phosphate buffer (pH 7.0) to give 0.1 M phosphate concentration. The diluted samples were then added to 1.5 mL microcentrifuge tubes containing 5 mg of HA in duplicate. As a control (i.e., 0% of binding), the samples were incubated in tubes without HA. The tubes were incubated at room temperature on an orbital shaker for 3 h, and centrifuged to separate the supernatant from the HA. A TNBS assay [29] was used for assessment of polymer concentrations in solution (based on amine groups). For this, 20 µL of the supernatant or control samples, or 20 µL of water as background, 130 µL of 0.1 M phosphate buffer (pH 7.0) and 850 µL of 1 mM TNBS in borate buffer (pH 9.4) were added to a cuvette, and the samples were incubated for 1 h at 37 °C. The absorbance of the solutions was read at 367 nm. The percentage of bound polymer to HA (% HA binding) was calculated by using the absorbance in supernatant and control as: $100\% \times (\text{Absorbance of control} - \text{Absorbance of supernatant}) / (\text{Absorbance of control} - \text{Absorbance of background})$.

Preparation of Polymer-Coated NPs

The BSA NPs were prepared by a coacervation method as described in our previous study [23]. Briefly, 10 mg/mL BSA solution was first mixed with equal volume of 10 mM phosphate buffer (pH 7.4) for 15 min under constant stirring at 600 rpm. Then, acetone was added dropwise to the BSA solution as a desolvating agent until an acetone:water volume ratio of 4:1 was reached, followed by further stirring over 2 h. The resulting BSA NP suspension was retained in the acetone/water system for polymer coating.

Two methods were utilized for preparation of polymer-coated NPs, namely a dialysis and an evaporation method. In the dialysis method, an appropriate amount of PEI, PEI-PEG or PEI-PEG-thiolBP was dissolved in 10 mM phosphate buffer solution (pH 7.4). An aliquot of BSA NP suspension was mixed with the same volume of polymer solution at various concentrations (1–12 μ M, see Figure legends for exact values). The final polymer concentrations in the NP suspension were 0.5–6 μ M. As a control, the uncoated BSA NPs were incubated with 10 mM phosphate at the same dilutions. The mixture was incubated at room temperature for 1 h, and then dialyzed against 1 mM NaCl (\times 3) to remove the acetone. For the evaporation method, an aliquot of BSA NP suspension was mixed with PEI-PEG or PEI-PEG-thiolBP as above, the polymer

was dispersed in a mixture of acetone/water (4:1) and the acetone was evaporated in a flowhood by constant stirring overnight.

Characterization of Polymer-Coated NPs

The zeta (ζ)-potential of the NPs was investigated by laser Doppler anemometry using the Malvern Zetasizer 3000HS (Malvern Instruments Ltd., UK) at 25 °C. Before the analysis, the polymer-coated NPs were diluted to a BSA concentration of 0.1 mg/mL with 1 mM NaCl. An electric field of 150 mV was applied to observe the electrophoretic velocity of the particles. The particle sizes and size distributions of the NPs were measured by photon correlation spectroscopy (PCS) using the same instrument. The measurements were carried out at 25 °C using a 633 nm He-Ne laser at a scattering angle of 90°. The reported sizes and ζ -potentials were derived from three independent batches of NP preparations.

Atomic force microscopy (AFM) was used to observe the size and morphology of the PEI-PEG-thiolBP coated BSA NPs (MFP-3D, Asylum Research, Santa Barbara, CA, USA). The NP sample was appropriately diluted to visualize individual particles and 5 μ L of the diluted sample was dropped onto the surface of PELCO Mica Discs (TED PELLA, Inc., Redding, CA, USA), and observed in a tapping mode by AC240TS cantilever after drying under room

temperature. Images were processed and analyzed by the Igor Pro imaging software (version 5.04 B).

Cytotoxicity of Polymers and NPs by MTT Assay

Two types of cells, human C2C12 myoblast cells and primary rat bone marrow stromal cells (BMSCs) were used for assessment of the cytotoxicity of the polymers and polymer-coated BSA NPs. Both cells were cultured in an osteogenic medium, where the basal medium (high-glucose DMEM, 10% FBS, 100 µg/mL streptomycin and 100 U/mL penicillin) was supplemented with 50 µg/mL ascorbic acid, 100 nM dexamethasone and 5 mM β-glycerolphosphate. The polymers and polymer-coated NPs (prepared as described above) were dialyzed once more against high-glucose DMEM containing 100 µg/mL streptomycin and 100 U/mL penicillin. An aliquot of polymer or NP dispersion (10% of the final volume) was then incubated with the cells grown in 24-well tissue culture plates (in triplicate). After 72 h incubation in a humidified atmosphere with 95/5% air/CO₂ at 37 °C, 100 µL of the MTT solution (5 mg/mL in HBSS) was added to the 500 µL culture medium in each well. The cells were incubated for further 2 h, the supernatant was removed carefully, and 500 µL of dimethyl sulfoxide (DMSO) was added to the cells to dissolve the formazan crystals formed. The optical density of the solution was measured by an *ELx800* plate reader (Bio-Tek Instruments Inc., Winooski, VT, US) at 570 nm. Untreated

cells served as reference and were taken as 100 % viability.

BMP-2 Bioactivity by Kinetic ALP Assay

A kinetic ALP assay was used to determine the bioactivity of BMP-2 encapsulated in the NPs. To prepare BMP-2 containing NPs, a certain amount of BMP-2 was first mixed with BSA solution, and then coacervated by acetone and coated with the polymers as described above. Following NP fabrication, all particles were dialyzed in the same manner as described in the MTT procedure. Human C2C12 cells and rat BMSCs were incubated (in triplicate) with the NPs at the estimated concentration of 1 $\mu\text{g}/\text{mL}$ of BMP-2 per well in 24-well plates (1 mL medium/well). The ALP assay was performed after incubation of C2C12 cells for 3 days, and rat BMSCs for 7 days, based on optimal procedures developed in Wang et al. [23]. To perform the ALP assay, the cells were washed with HBSS solution and lysed with 400 μL of ALP buffer (0.5 M 2-amino-2-methylpropan-1-ol and 0.1% (v/v) Triton-X, pH 10.5). After 2 h, 200 μL of 1.0 mg/mL ALP substrate (*p*-NPP) was added to 200 μL of the cell lysate, and the rate of change in the optical density was determined with a plate reader by measuring the absorbance (405 nm) at intervals of 90 sec for 8 cycles. Untreated cells and cells treated with 1 $\mu\text{g}/\text{mL}$ of free BMP-2 served as negative and positive controls, respectively. The kinetic ALP activity was expressed as the change of optical density of the wells per unit time (mAbs/min).

***In Vitro* HA Affinity of BMP-2 Containing NPs**

To determine the *in vitro* HA affinity of NPs, ¹²⁵I-labeled BMP-2 was encapsulated in the BSA NPs and the binding ability was assessed based on the ¹²⁵I counts. Labeling of BMP-2 with ¹²⁵I was performed as described previously[30], and it was confirmed that the radioiodinated BMP-2 contained <4% free ¹²⁵I at the time of encapsulation. To prepare BMP-2 encapsulating NPs, ¹²⁵I-labeled BMP-2 (diluted in ddH₂O) was first mixed with BSA solution, and then coacervated by acetone and coated with the polymers by the evaporation method as described above.

The mineral affinity of the NPs was investigated by using a HA binding assay as described previously for the polymers. In this case, counts in the supernatant and HA precipitate were separately determined by a γ -counter. The percentage of HA-bound NPs (% HA binding) was calculated as: $100\% \times (\text{count in HA precipitate}) / (\text{count in supernatant} + \text{count in HA precipitate})$.

***In Vivo* Retention of BMP-2 Encapsulated in NPs**

Six-to-eight week-old female Sprague-Dawley rats were purchased from Biosciences (Edmonton, AB, Canada). The rats were acclimated for one week under standard laboratory conditions (23 °C, 12 h of light/dark cycle) prior to the study. While maintained in pairs in sterilized cages, rats were allowed free access

to food and water for the duration of the study. All procedures involving the rats were approved by the Animal Welfare Committee at the University of Alberta.

The polymer-coated BSA NPs were prepared for implantation in 24 rats in four study groups. The study groups consisted of (1) BMP-2 in BSA solution, (2) BMP-2 in BSA NPs, (3) BMP-2 in PEI-PEG coated NPs and (4) BMP-2 in PEI-PEG-thiolBP coated NPs. The appropriate solution for each study group was soaked into Skelite™ implants for ~10 minutes (50 µL of ¹²⁵I-labeled BMP-2 formulation per implant). The exact counts in the added 50 µL solution was determined by a γ-counter and used as a measure of implanted BMP-2 dose. Once rats were anesthetized with inhalational Metofane™ (Janssen Pharmaceuticals Inc., Toronto, ON, Canada), two wet implants were implanted subcutaneously into bilateral ventral pouches in each rat. At indicated time points, two rats were euthanized with CO₂, the implants were recovered, and the counts associated with the excised implants were quantified by a γ-counter. The amount of BMP-2 retention, expressed as the percentage of implanted dose, was calculated as: $100\% \times (\text{recovered count in implant}) / (\text{initial count in implant})$. The results were summarized as mean ± SD (n = 4) of % BMP-2 retention in the implants at each time points.

Biodistribution of the BMP-2 Containing NPs

The BSA NPs containing ^{125}I -labeled BMP-2 were prepared as previously described and 30 rats were utilized for the five study groups: (1) free BMP-2 in saline (2) BMP-2 with BSA in saline solution, (3) BMP-2 in BSA NPs, (4) BMP-2 in PEI-PEG coated NPs and (5) BMP-2 in PEI-PEG-thiolBP coated NPs. A 300 μL of the sample were first counted by a γ -counter to determine the injected dose, and then administered intravenously (IV) to the rats via tail vein injection over ~ 30 seconds. The rats were sacrificed at designed time points, long bones (tibia and femur), both kidneys, a portion of the liver, spleen, thyroid and blood samples were collected, and counted with a γ -counter. The biodistribution was analyzed based on the percentage of injected dose corrected according to the weight of the collected organs. Results are expressed as mean \pm SD ($n = 6$ for femur, tibiae and kidney, $n = 3$ for other tissues).

Statistical Analysis

All experimental data were collected in triplicate at least, and expressed as mean \pm standard deviations (SD). Statistical analysis was performed using two-sided unpaired Student's t -test or one-way ANOVA test. Differences were considered statistically significant with a p -value < 0.05 .

4.3 RESULTS

Synthesis and Characterization of PEI-PEG-thiolBP Conjugate

The heterobifunctional NHS-PEG-MAL, which contains a thiol-reactive maleimide group and an amine-reactive NHS ester, was used for conjugating thiolBP onto PEI (Scheme 1). ThiolBP was first coupled onto PEG to form NHS-PEG-thiolBP via the reaction between thiol group of thiolBP and the maleimide on NHS-PEG-MAL. Then, NHS-PEG-thiolBP was grafted onto PEI by reacting with primary amines of PEI. Successful grafting of NHS-PEG-MAL or NHS-PEG-thiolBP onto PEI was confirmed by $^1\text{H-NMR}$ (**Figure 4-1**). The extent of PEG grafting was determined from the relative peak area of $-\text{CH}_2\text{CH}_2\text{O}-$ (δ : 3.64 ppm) of PEG to $-\text{CH}_2\text{CH}_2\text{N}-$ (2.5-3.1 ppm) of PEI. Using a variety of PEG/PEI ratios up to 150:1, the results indicated that the substitution of NHS-PEG-MAL or NHS-PEG-thiolBP on PEI was comparable to the PEG/PEI feed ratio (data not shown). The appearance of peak at 1.88 ppm ($-\text{CH}_2-$ of thiolBP) and the decrease or disappearance of maleimide signals at 5.85 and 6.25 ppm in $^1\text{H-NMR}$ spectrum (**Figure 4-1B** and **C**) indicated successful coupling of thiolBP to PEG-grafted PEI to some extent.

To obtain conjugates with different thiolBP substitutions, different concentrations of NHS-PEG-MAL was first reacted with excess thiolBP

(thiolBP/PEG ratio of 1.5:1 and 4:1), and then reacted with PEI at PEG/PEI mole ratios of 10 to 150. As shown in **Figure 4-2A**, the thiolBP substitution efficiency was increased linearly from 5 to 24 thiolBP/PEI for feed ratio of thiolBP/PEG 1.5:1, as the PEG/PEI molar ratio was increased from 25 to 150, and from 7 to 33 thiolBP/PEI for feed ratio of thiolBP/PEG 4:1, as the PEG/PEI molar ratio increased from 10 to 50. This indicated that only a fraction of (<20%) of the thiolBP was reacted with NHS-PEG-MAL and conjugated onto PEI branches. The obtained substitution pattern was similar to our previous study, where thiolBP was conjugated onto PEI using succinimidyl-4-(*N*-maleimidomethyl) cyclohexane-1-carboxylate (SMCC) as the linker [22].

In order to investigate the effects of PEG and thiolBP conjugation on the HA affinity of PEI, the HA affinity of PEI-PEG and PEI-PEG-thiolBP was examined in 0.1 M phosphate buffer (pH 7.4) and the results were summarized in **Figure 4-2B**. The unmodified PEI displayed significant HA affinity in phosphate buffer (>95% binding). The PEGylated PEI with low degree of substitution (<100 PEG/PEI) did not show significant loss in HA affinity, but at higher grafting ratio (>100 PEG/PEI), the ability to bind HA was reduced significantly ($p < 0.05$). However, the PEI-PEG-thiolBP conjugates recovered the mineral affinity (>97%) equivalent to unmodified PEI irrespective of the higher PEG substitution degree.

Particle Size and ζ -Potential

The uncoated BSA NPs had a ζ -potential of -12.1 ± 2.7 mV in 1 mM NaCl. The ζ -potential of polymer-coated NPs gradually increased as a function of polymer/BSA ratio. This was the case whether dialysis (**Figure 4-3A**) or evaporation method (not shown) was used for acetone removal. The ζ -potential of the PEI coated particles reached to a plateau (~ 20 mV) above a certain concentration, which was consistent with our previous study [23,24]. Reaching a plateau value was indicative of the excess polymer in solution that was not bound to the NPs. The ζ -potential of PEI-PEG (150 PEG/PEI) coated NPs decreased as compared with PEI coated NPs, having a maximum of ~ 14 mV. The PEI-PEG-thiolBP (24 thiolBP/PEI) reduced the ζ -potential more significantly and eventually maintained the NPs at neutral ζ -potential after $4 \mu\text{M}$ or higher coating concentration. Using a range of PEI-PEG-thiolBP conjugates with different extent of thiolBP conjugation, the ζ -potential was found to inversely depend on the thiolBP substitution (**Figure 4-3B**); at $4 \mu\text{M}$ coating concentration, the conjugates with higher thiolBP substitution led to lower ζ -potential.

Two methods used to prepare the polymer-coated BSA NPs were compared with respect to the obtained particle sizes and size distributions (**Figure 4-4**). The size of NPs suspended in acetone/water was 43.7 ± 4.6 nm, and narrowly distributed, with a polydispersity index (PDI) of 0.105 ± 0.059 in diameter. After

removing the acetone by dialysis, the zeta-average size and PDI of uncoated NPs were increased to 157.6 ± 21.8 nm and 0.463 ± 0.013 , respectively. The PEI-PEG-thiolBP coated NPs had a size of 130.6 ± 13.9 nm, and PDI of 0.365 ± 0.095 . Both the uncoated and coated NPs displayed two separate peaks for the size distribution, the left one (peak 1) being ~ 60 nm and the right one (peak 2) >200 nm (**Figure 4-4B** and **C**), indicating the presence of large aggregates in the samples. For the evaporation method, the average sizes of the uncoated and coated NPs were 117.5 ± 5.3 nm and 77.3 ± 2.0 nm, respectively, which were smaller than their counterparts from the dialysis method. For the coated NPs, although there was a decrease for zeta-average size from the dialysis method to evaporation method, the mean size of the single peak in **Figure 4-4E** was comparable to the first peak in **Figure 4-4C**. The peak in the larger size range disappeared for the evaporation method, which indicated no aggregates for the PEI-PEG-thiolBP coated BSA NPs.

The sizes of the NPs obtained as a function of coating concentration by dialysis method is summarized in **Figure 4-5**. Using a PEI-PEG with 150 PEG/PEI, the mean size showed a dramatic change as a function of polymer concentration, an increase up to ~ 380 nm for the lowest coating concentration (1 μM) and followed by a decrease to ~ 200 nm for 2 μM coating and a plateau of ~ 150 nm at > 4 μM . The sizes of PEI-PEG-thiolBP coated NPs (24 thiolBP/PEI)

increased slightly for the lowest concentration and then maintained at ~130 nm.

The NPs were analyzed by AFM to confirm the size of the particles measured by PCS. As shown in **Figure 4-6**, the BSA NPs in acetone/water were uniform with the size of ~50 nm, and generally spherical with smooth surface characteristics. The PEI-PEG-thiolBP coated NPs from the evaporation method showed a particle size of 50-70 nm, relatively rougher surfaces with no visible aggregates. The size of coated NPs obtained from these images was slightly smaller than that from PCS analysis, which was possibly due to the shrinkage of the particles during the drying process for the AFM sample preparation.

Cytotoxicity

Two types of cells, myogenic C2C12 cells and rat BMSCs, were used to assess the relative toxicity of the polymer conjugates (**Figure 4-7A** and **B**, respectively) and the polymer-coated NPs (**Figure 4-7C** and **D**, respectively). As shown in **Figure 4-7A**, the polymers did not show any toxicity on C2C12 cells at <4 μM . However, cell viability was significantly ($p < 0.05$) decreased at higher PEI concentrations (>8 μM) with >70% loss of cell viability. Conversely, PEI conjugates with PEG did not exhibit any cytotoxicity at a concentration of 8 μM , and it showed significantly improved cell viability as compared with PEI ($p < 0.05$) at the highest concentration tested. The incorporation of thiolBP did not impart

any additional toxicity on the PEI-PEG. The cytotoxicity of the polymers on rat BMSCs (**Figure 4-7B**) displayed a similar pattern to that of C2C12 cells, where PEI was found to be most toxic, and thiolBP conjugation to PEG did not cause any additional toxicity, except for a slight loss of viability at higher concentrations compared with the control.

The effects of polymer coating on NP toxicity were investigated after coating the NPs with PEI, PEI-PEG (150 PEG/PEI) and PEI-PEG-thiolBP (24 thiolBP/PEI-PEG). As shown in **Figure 4-7C**, only the PEI coated NPs at the highest concentration (12 μ M) displayed significant toxicity on C2C12 cells. There was no significant difference in cell viability for NPs coated with PEI-PEG and PEI-PEG-thiolBP. For rat BMSC, the highest concentration of PEI (12 μ M) showed significant toxicity again. Different from the C2C12 cells, the uncoated NPs showed some toxicity (~20% decrease in viability), and all polymer coated NPs showed a further 10-20% decrease in cell viability ($p < 0.05$, **Figure 4-7D**). Nevertheless, PEG substitution on PEI reduced PEI toxicity at high concentration and the toxicity of the PEI-PEG or PEI-PEG-thiolBP coated NPs were considered tolerable for *in vivo* studies.

Bioactivity of Encapsulated BMP-2

The change of ALP activity is a well-demonstrated hallmark of

osteogenesis phenomena in physiological tissues or cells. Myogenic C2C12 cells[24] and rat BMSCs [31] both display stimulated ALP induction as a result of BMP-2 treatment. In this study, we utilized both types of cells to evaluate the bioactivity of NP encapsulated BMP-2, and the results were summarized in **Figure 4-8**. The exact contents of BMP-2 in NPs were not determined in this study. We assumed full retention of BMP-2 amount in the NPs, based on our previous study [24], which indicated >90% encapsulation efficiency, and tested our NP encapsulated BMP-2 against an equivalent amount of free BMP-2. For the C2C12 cells (**Figure 4-8A**), no activity was noted for the untreated cells after 3 days incubation. All NP encapsulated BMP-2 showed significant ALP activity, and the numbers were equivalent to or higher than the cells treated with free BMP-2, except for the NPs coated with highest concentration of PEI, which might have induced some toxicity to the cells. Different from the C2C12 cells, the untreated rat BMSCs (**Figure 4-8B**) showed a strong background in ALP activity, whereas all NP encapsulated BMP-2 formulations showed significant increased ALP activity on day 7 ($p < 0.05$ compared to untreated control), which were equivalent to free BMP-2.

Bone Mineral Affinity of Polymer-Coated NPs

The mineral affinity of different NPs was investigated both *in vitro* and *in vivo*. For *in vitro* study, the extent of the polymer-coated NP binding to HA was

determined after encapsulating ^{125}I -labeled BMP-2 in the NPs. As shown in **Figure 4-9A**, the free BMP-2 could adsorb onto the HA by itself to some extent (~60%) either in water or in 0.1 M phosphate buffer (pH 7.4). All NP-encapsulated BMP-2 evaluated displayed a higher HA affinity (~90%) in both buffers. The binding assay did not indicate any significant difference in HA affinity among the NPs investigated.

The *in vivo* mineral affinity was also examined in a rat subcutaneous implant model (**Figure 4-9B** and **C**). Commercially available SkeliteTM, a microporous scaffold used in clinical osteoconductive bone repair, was used as an implant. ^{125}I -labeled BMP-2 was used to determine the retention of NPs in the implants. In one batch of NPs (**Figure 4-9B**), the retention of free BMP-2, BMP-2 encapsulated in BSA NPs, PEI-PEG coated NPs and PEI-PEG-thiolBP coated NPs after 2 days implantation were 51.2±3.4%, 66.3±6.7%, 73.8±7.9% and 83.3±4.5, respectively. The PEI-PEG-thiolBP coated NPs displayed enhanced BMP-2 retention compared to the free BMP-2 and uncoated BSA NPs ($p<0.05$). For another batch (**Figure 4-9C**), after 2 days, the retention of free BMP-2 (in BSA solution) was 37.4±3.4%, while the BMP-2 retention in uncoated, PEI-PEG coated and PEI-PEG-thiolBP coated BSA NPs were 55.4±4.9%, 64.8±4.0% and 72.2±3.0%, respectively. At day 10, the retention of BMP-2 for the latter three groups were 33.0±6.5%, 43.7±7.4% and 39.7±8.7%, while that of free BMP-2

was $20.0 \pm 3.5\%$. During the study period, the BMP-2 retention in the three NP formulations was significantly higher than free BMP-2 ($p < 0.05$), but only at day 2, the PEI-PEG-thiolBP coated NPs showed significantly improved BMP-2 retention than the uncoated ones ($p < 0.05$). The PEI-PEG-thiolBP coated BSA NPs had slightly higher BMP-2 retention than PEI-PEG coated ones till day 7, and lower at day 10, but the difference between the two groups was not significant ($p > 0.05$).

Biodistribution of the BMP-2 Containing NPs

To determine the feasibility of targeting NPs to bones, the NP formulations prepared with ^{125}I -labeled BMP-2 were intravenously injected in rats via tail vein, and analyzed for biodistribution at day 1 and day 4 after injection (**Figure 4-10A and B**). Thyroid had the highest uptake of radioactivity after 24 hours where 10-25% of the injected dose was localized. This was ~100 times higher than the deposition at other organs and reflected the presence of free iodine in circulation. Kidney, liver and spleen also showed obvious uptake except for the uncoated BSA NPs in spleen. The retention of the BMP-2 in blood after 1 day injection was drastically depressed ($< 0.02\%$). Although both the *in vitro* and *in vivo* binding results showed improved HA affinity for the NP encapsulated BMP-2 as compared with free BMP-2, the NPs did not indicate any superior bone-targeting ($< 0.03\%$ for all groups), and there was no significant difference in bone (femur and tibiae) deposition of the NPs. Instead, the PEI-PEG and PEI-PEG-thiolBP

coated BSA NPs had a significantly higher deposition in spleen compared with the uncoated ones.

Similar experiments were performed independently with NPs coated with thiolBP and alendronate (after thiolation) conjugated of PEI-PEG; however, the results were essentially the same as before (data not shown), and no beneficial effects were noted on bone deposition for any of the BP-coated NPs.

4.4 DISCUSSION

Coupling of thiol group to maleimide is a convenient method for PEG conjugation to thiolBP, as the reaction is site-specific, easy to control, and leads to a stable 3-thiosuccinimidyl ether linkage. Since branched PEI contains a combination of primary, secondary and tertiary amines, and 31% of the amino groups (~180 for 25 kDa PEI) are primary amines [27], ample PEG chains can be coupled to PEI via the amine-reactive NHS-ester. A stoichiometric reaction between the NHS-PEG-MAL and PEI at their predetermined molar ratios was reported previously [8]. In this study, we also observed 100% conjugation efficiency of NHS-PEG-MAL or NHS-PEG-thiolBP to PEI. Although the ¹H-NMR spectrum confirmed successful conjugating of thiolBP to PEG-grafted PEI, the relevant signals of thiolBP and maleimide were much weaker than the

broad H-signals of PEG and PEI residues, which made it difficult to accurately calculate the thiolBP content in the samples. Therefore, the conjugation efficiency of thiolBP was based on an organic phosphate assay and it was found to be relatively lower than expected, which was likely due to the formation of disulfides among thiolBPs, leading to reduction of available free thiols. Therefore, excess thiolBP was needed for saturation of the maleimide on the PEG.

We previously reported on PEI-coated BSA NPs, and observed cationic particles with size >200 nm [23,24]. The size and surface charge of the NPs were expected to be decreased by using PEG-substituted PEI as a result of surface shielding by PEG. As in our previous studies, physical adsorption was suitable for coating NPs with PEG-modified polymers given the cationic backbone in these polymers. The positively charged PEI backbone was expected to bind on NP surfaces, whereas the PEG and thiolBP chains to extend to the NP exterior. The hydrophilic PEG surface not only screened the highly positive charge of the adsorbed PEI, but also effectively stabilized the BSA NPs by reducing particle aggregation; even though PEI-coated cationic surfaces were expected to reduce NP aggregation, PEI-PEG-thiolBP coating resulted in smallest particles despite having almost neutral surfaces. The presence of the surface PEG chains might have prevented aggregation by a steric repulsion mechanism.

Since the particle sizes from PCS measurement were analyzed based on

the seventh moment of diameter [32], it might be extremely sensitive to presence of any larger aggregates, which was evident in some samples (**Figure 4-4**). For example, <10% of larger particles can increase the zeta-average size of uncoated NPs prepared by evaporation method from <60 nm to >100 nm. The appearance of two peaks in size distributions indicated obvious aggregates. For the dialysis method, the coating of PEI-PEG-thiolBP decreased the extent of aggregation (peak 2 area decreased from 32.5% to 14.1%), but could not completely prevent it. The evaporation method was advantageous for this purpose by displaying only a single peak at <60 nm. Compared with the BSA NPs in acetone/water, the uncoated BSA NPs after removing acetone was 15-20 nm larger (peak 1), which was likely due to the swelling of the particles. However, after adsorbing a layer of PEI-PEG-thiolBP, which has a coiled PEG chains less than 10 nm in length [33], their sizes were remained comparable to those in the acetone/water coacervation system. The unchanged sizes of NPs even after coating implied that ionic anchoring of the positively charged conjugate on the negatively charged surface might prevent NPs from swelling and aggregating after removing the coacervation agent acetone.

Significant toxicity is well established for PEI with high molecular weight[34], although the reasons for PEI toxicity are not completely clear. PEGylation of PEI effectively reduced the toxicity of PEI, and this was likely due

to the shielding effects on the net charge of the PEI backbone. Two types of cells were used in this study to test the toxicity of the polymer and particles. C2C12 cells are particularly suitable for assessing BMP-2 activity, whereas they are more robust than primary cells and their BMP-2 response is more predictable. BMSCs derived from rats were also used since the intended use of our formulations is to deliver BMP-2 and one of the primary targets of BMP-2 is stem cells at the bone marrow environment. Both the C2C12 cells and BMSCs indicated reduced PEI toxicity after PEG substitution. In our recent study, the potential of using BSA NPs for localized bone regeneration was affirmed, and the PEI coating on the BSA NPs displayed improved BMP-2 retention in implant. However, the surface coating of PEI at higher concentrations impaired the efficacy of BMP-2 to induce bone formation in a rat subcutaneous model [35]. The reduced toxicity of PEGylated PEI might be alternative for future study.

Maintenance of the native bioactivity of an osteogenic growth factor is essential for a NP formulation designed for local or systemic administration of growth factor. Our previous study [23] indicated that PEI and poly-*L*-lysine coated BSA NPs can fully retain the BMP-2 activity after encapsulation. PEI was shown to be a relatively toxic component of the NPs [35], but PEG-substitution on PEI was shown to reduce toxicity when this polymer was used for NP coating[36]. In this study, we further evaluated the effect of BP modification of

NPs on the activity of encapsulated BMP-2. The myogenic cells (C2C12 cells) showed a significant BMP-2 activity with the NPs decorated with thiolBP, which confirmed there was no adverse effect of the presence of BPs on BMP-2 induced osteogenesis response. The positive effects with the primary cells (rat BMSCs), which are directly relevant to physiological osteogenesis, also provide encouraging prospect for *in vivo* testing of the proposed NPs. Direct measurement of BMP-2 release from the NP formulations were not performed in this study. Based on previous results [23], we anticipate most BMP-2 (> 50%) to be released from the NPs in 1 week time under the cell culture conditions. Whether the NPs are internalized or whether the internalized BMP-2 exerts a significant bioactivity remain to be investigated.

The BPs are commonly used for inhibition of osteoclast activities, and known for their unique pharmacokinetic and biodistribution profiles favoring fast deposition and long residence in the skeleton tissues. Bone targeted delivery of NPs has been attempted by several groups based on BP molecules. Choi and Kim[20] conjugated alendronate to PLGA NPs via PEG-PLGA block copolymers and found that alendronate-modified NPs had a strong and specific adsorption to HA, and the potency of HA adsorption was dependent on the content of alendronate and the block length of PEG. PEI itself displays significant interaction with charged surfaces [37,38], and our previous study also indicated a

high affinity of PEI to bone mineral HA [22]. However, when conjugated with PEG, which has a negative effect on surface adsorption and HA affinity [2,21], the PEG modified PEI dramatically decreases its inherent ability of binding to HA as a function of PEG substitution degree. The loss of HA affinity caused by PEG substitution could be offset via the further conjugation with BP. This was confirmed by our results, which indicated that the HA binding ability of PEI-PEG was decreased gradually from 95% of pure PEI to 75% for PEI-PEG with 150 PEG per PEI, whereas the PEI-PEG-thiolBP remained >97% HA binding regardless the PEG substitution degree.

The excellent HA affinity of PEI-PEG-thiolBP makes this polymer potentially suitable to target therapeutic agents to the bone, besides the advantages discussed above with respect to non-aggregation, masked surface charge and reduced toxicity. However, such an affinity should be retained after the PEI conjugates are adsorbed onto the NPs. From the HA binding results, all NPs displayed higher percentage of NP binding to the HA as compared to free BMP-2, but the polymer-coated NPs did not show any improvement in the HA affinity compared with the uncoated ones. However, the *in vivo* BMP-2 retention study showed superiority of the NPs coated with PEI-PEG-thiolBP, which gave higher retention at specific time points. On one hand, these results suggest that *in vivo* HA affinity by BP conjugated NPs is better revealed. On the other hand, the

differences between PEI-PEG and PEI-PEG-thiolBP were not as strong as expected, and might indicate that mineral affinity of the formulations was likely dominated by the same factors. Nevertheless, the improved retention of BP-decorated NPs in mineral-rich scaffolds suggests that the prepared NPs might provide a potential candidate for localized delivery system of BMP-2 for bone repair and regeneration when administered locally with mineral-based scaffolds.

No beneficial effects of polymer coating was noted for NP targeting to bones after IV administration, despite strong evidence for NP binding to HA *in vitro*. The reasons for this observations remains to be elucidated. The organ accumulation of BMP-2 after 1 and 4 days of IV administration was estimated by assuming that the ^{125}I -labeling was stable on the protein *in vivo*. The distinct thyroid uptake (~100 times higher than other organs) of radioiodine indicated a significant de-iodination of the ^{125}I -labeled BMP-2 during the study. It was reported that free iodine formed by rapid deiodination of the radioiodinated proteins accumulated mainly in thyroid, stomach, lung or spleen [39]. However, this unavoidable artifact was not an impediment for the use of ^{125}I labeling in studying protein targeting to bones, and should not be the reason for the lack of bone targeting observed in this study.

In vivo deposition of particles to hard tissue is more complicated than retention in implants and requires a long blood circulation time and

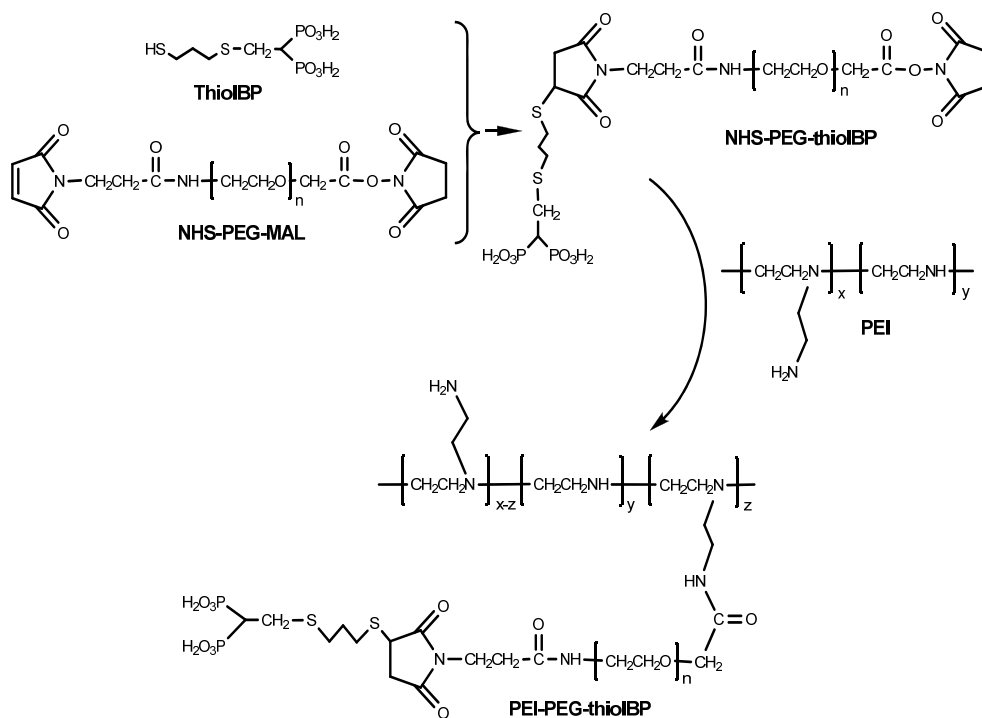
site-specificity. A hydrophilic surface and small particle size (<100 nm) are expected requirements to avoid the reticuloendothelial system [20]. The coating with PEI-PEG was designed for this purpose, and the size measurements indicated that the PEI-PEG-thiolBP coated BSA NPs (77 nm) exhibited hydrophilic surfaces. However, it is known that the fenestrated capillaries or sinusoids in the bone have pores of 80-100 nm [40]. In order to extravasate and deposit in bones, the hydrodynamic diameters of the NPs should be <80 nm. The sizes of the smallest BSA NPs investigated in this study was close to 80 nm, thus the extravasation of these particles into the bone fluid might have been hampered. Other factors affecting biodistribution of NPs include surface properties, which are directly correlated to the interactions between the particles and components in the physiological fluid. It is reported that negative charges influences the clearance of the particles from the blood circulation via kidney glomerular filtration and liver uptake [41]. The saturated calcium and iron ions in blood may bind to the BP-conjugated macromolecules to form chelate complex [42], which would presumably be removed faster by the clearance organs. The strength and stability of noncovalent binding of polymers to a NP surface might be another issue. In circulation, the surface adsorbed polymers might dissociate from the NP surface and/or displaced by plasma proteins, which may make the particles prone to phagocytosis. Even for the stably adsorbed polymers, the chemical breakdown processes of the polymeric texture, such as swelling, degradation and erosion,

may decrease the steric shielding effect and induce surface changes favorable for opsonization, leading to uptake by RES. Salts and proteins in the serum may induce disassociation of surface coating and/or *in vivo* aggregation, which might also affect the biodistribution of the NPs.

4.5 CONCLUSIONS

ThiolBP- and PEG-modified PEI was used to decorate BSA NPs to tune their particle size and surface charge, reduce the PEI toxicity, and improve their HA affinity. The polymer coating and BP decoration had no adverse effect on the bioactivity of the NP encapsulated BMP-2. All the NPs displayed significant *in vitro* HA affinity and *in vivo* retention for encapsulated BMP-2. The BP conjugated NPs, with enhanced *in vivo* retention in mineral implants, are potential candidate for localized delivery system of BMP-2 for bone repair and regeneration. However, when administered intravenously, no beneficial effects were observed for the thiolBP-coated BSA NPs on the bone-targeting. Although successful targeting of BP-conjugated copolymer to bone was reported [21], NPs prepared with BPs were only tested in *in vitro* HA binding [20,43-45], and none of these studies reported bone targeting *in vivo*. This includes several patents, which showed superior hydroxyapatite affinity of BP-derivatized NPs, but

provided no results on the feasibility of bone targeting by such NPs [46,47]. To the best of our knowledge, this study was the first to report the evaluation of *in vivo* bone targeting of BP-modified NPs, and the unsuccessful outcome calls for better understanding of the *in vitro* behavior of BP-decorated NPs with the hope of designing bone-seeking NPs.



Scheme 4-1 ThiolBP conjugation to PEI via NHS-PEG-MAL

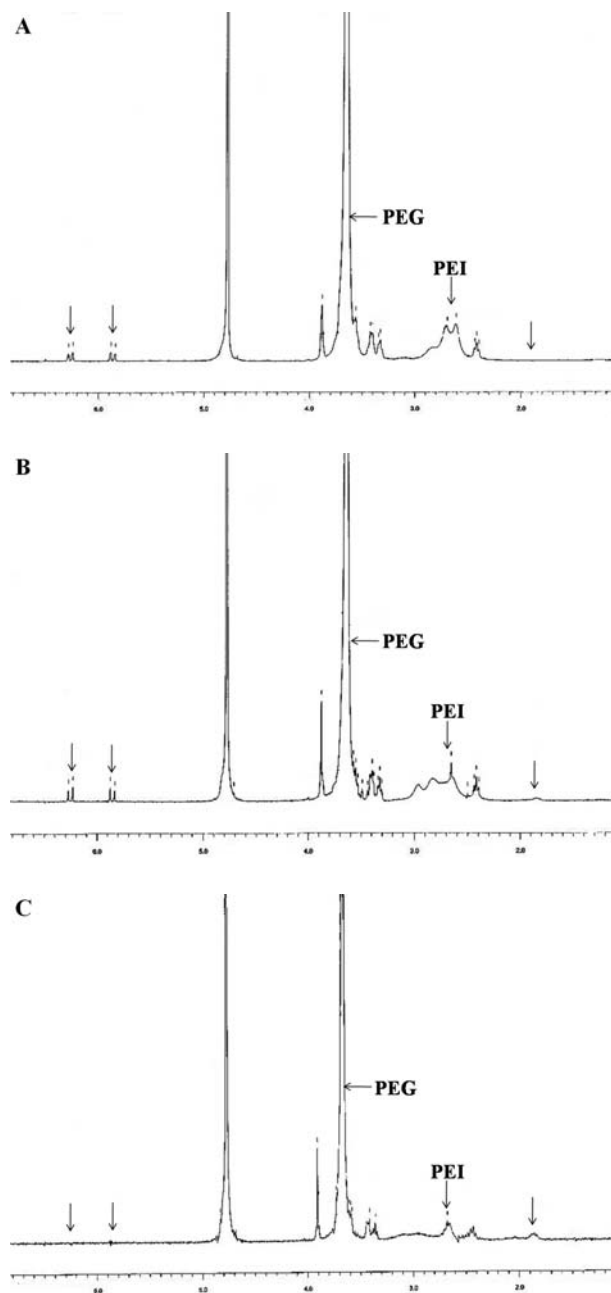


Figure 4-1 ^1H -NMR spectrum of PEI-PEG (**A**, 100 PEG per PEI) and PEI-PEG-thiolBP (**B**, 100 PEG and 18 thiolBP per PEI; **C**, 50 PEG and 33 thiolBP per PEI) in D_2O . The peak at 3.6 ppm was assigned to $-\text{CH}_2\text{CH}_2\text{O}-$ from PEG, and the peaks at 2.5-3.1 ppm to $-\text{CH}_2\text{CH}_2\text{N}-$ from PEI. Graft degree of PEG was determined from the relative peak area of PEG to PEI. Appearance of peak at 1.88 ppm (**B** and **C**) and disappearance of the maleimide peaks at 5.85 and 6.25 ppm (**C**) indicated that thiolBP was successfully conjugated to PEI.

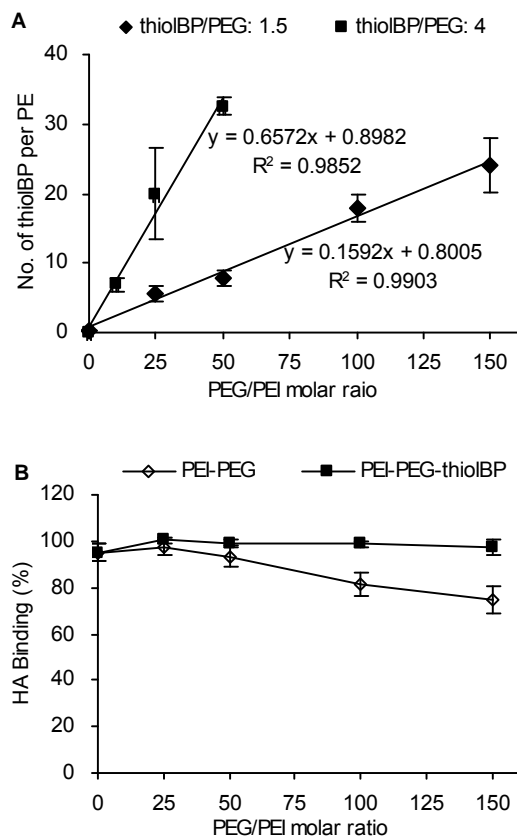


Figure 4-2 ThiolBP conjugation efficiency as a function of PEG/PEI molar ratio (A) and the influence of PEG substitution and thiolBP conjugation on HA affinity (B). The number of thiolBP per PEI was increased linearly from 6 to 24 as the PEG/PEI feed ratio increased from 25 to 150 for feed ratio of thiolBP/PEG 1.5:1 (diamond), and from 7 to 33 for feed ratio of thiolBP/PEG 4:1 as the PEG/PEI molar ratio increased from 10 to 50 (square). The PEG substitution on PEI led to reduced HA affinity at high PEG grafting, whereas the PEI-PEG-thiolBP conjugates displayed minimal affinity equivalent to unmodified PEI (0 PEG/PEI) at all PEG substitutions. Results are expressed as mean \pm SD from three independent batches of experiments.

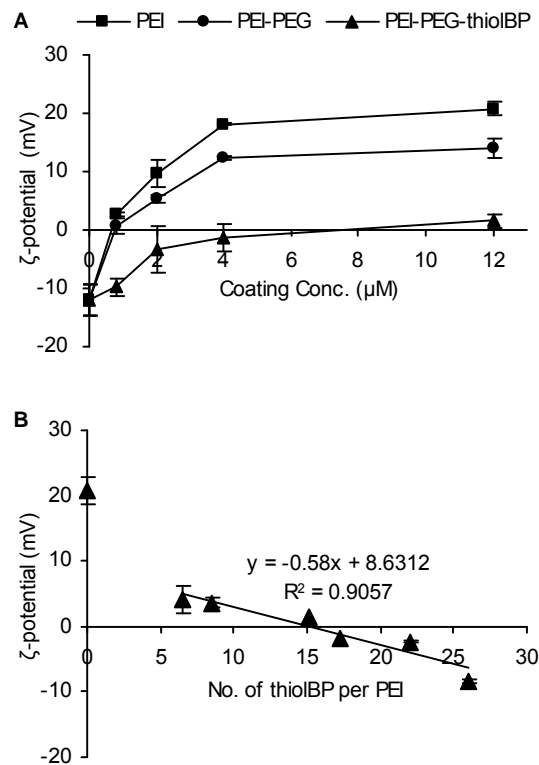


Figure 4-3 ζ -potential of BSA NPs coated by different concentrations of PEI, PEI-PEG and PEI-PEG-thiolBP (0-12 μM) (**A**) and the effect of thiolBP substitution on PEI-PEG-thiolBP on ζ -potential of the NPs (**B**). The NPs were coated by the dialysis method. Results in (**A**) are expressed as mean \pm SD from three independent binding experiment using PEI-PEG (150 PEG/PEI) and PEI-PEG-thiolBP (150 PEG and 24 thiolBP/PEI) for coating. Results in (**B**) are expressed as mean \pm SD from triplicate measurements for the NPs coated by 4 μM of PEI-PEG-thiolBP with indicated numbers of thiolBP per PEI.

A

NPs	Particle size ^a (nm)	PDI ^a	Peak 1 ^b		Peak 2 ^b	
			Area (%)	Mean (nm)	Area (%)	Mean (nm)
BSA NP in acetone/water	43.7±4.6	0.105±0.059	100	42.7		
<i>Dialysis method</i>						
Uncoated BSA NPs	157.6±21.8	0.463±0.013	67.5	64.0	32.5	290.7
PEI-PEG-thiolBP coated NPs	130.6±13.9	0.365±0.095	85.9	57.3	14.1	395.1
<i>Evaporation method</i>						
Uncoated BSA NPs	117.5±5.3	0.676±0.037	90.7	56.7	9.3	458.9
PEI-PEG-thiolBP coated NPs	77.3±2.0	0.376±0.025	100	57.9		

a: results are expressed as mean ± SD (zeta-average) from three independent batches of NPs. b: data are taken from a typical measurement for each formulation.

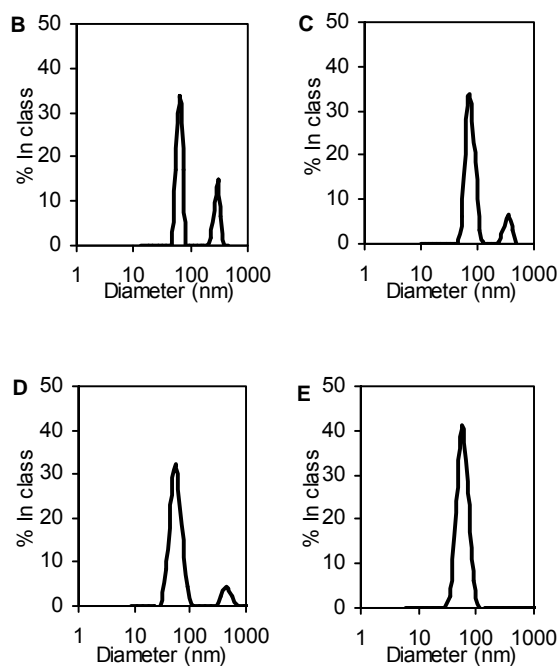


Figure 4-4 Particle size analysis (A) and size distributions of uncoated BSA NPs (B, dialysis method; D, evaporation method) and PEI-PEG-thiolBP coated NPs (C, dialysis method; E, evaporation method). Note that obvious aggregation existed for the uncoated BSA NPs in (B) and (D), and the PEI-PEG-thiolBP coated NPs by dialysis method (C), whereas the coated NPs by evaporation method (E) displayed a narrow single peak.

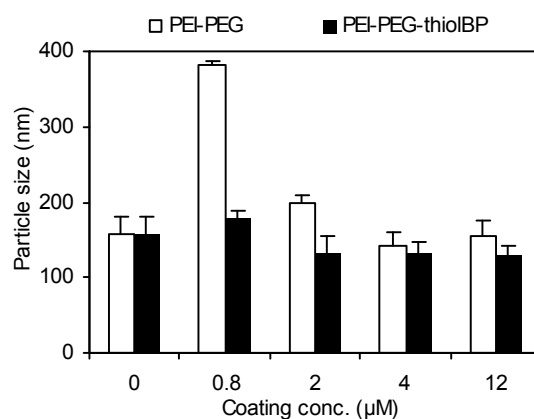


Figure 4-5 Effect of coating concentration on particle size of polymer-coated BSA NPs. The NPs were prepared by dialysis method with 0-12 μM of PEI-PEG (150 PEG/PEI) or PEI-PEG-thiolBP (150 PEG and 24 thiolBP/PEI). Results are expressed as mean \pm SD from three independent batches of NPs.

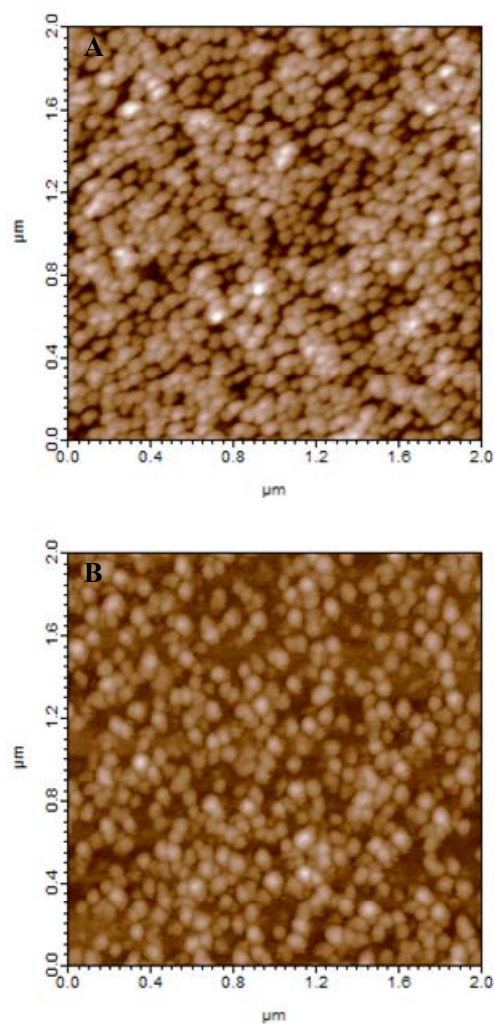


Figure 4-6 AFM images of BSA NPs in acetone/water (**A**) and PEI-PEG-thiolBP coated BSA NPs (**B**) prepared by using evaporation method for coating. The images are $2 \times 2 \mu\text{m}$ in scale and representatively selected from a large series of images generated from AFM.

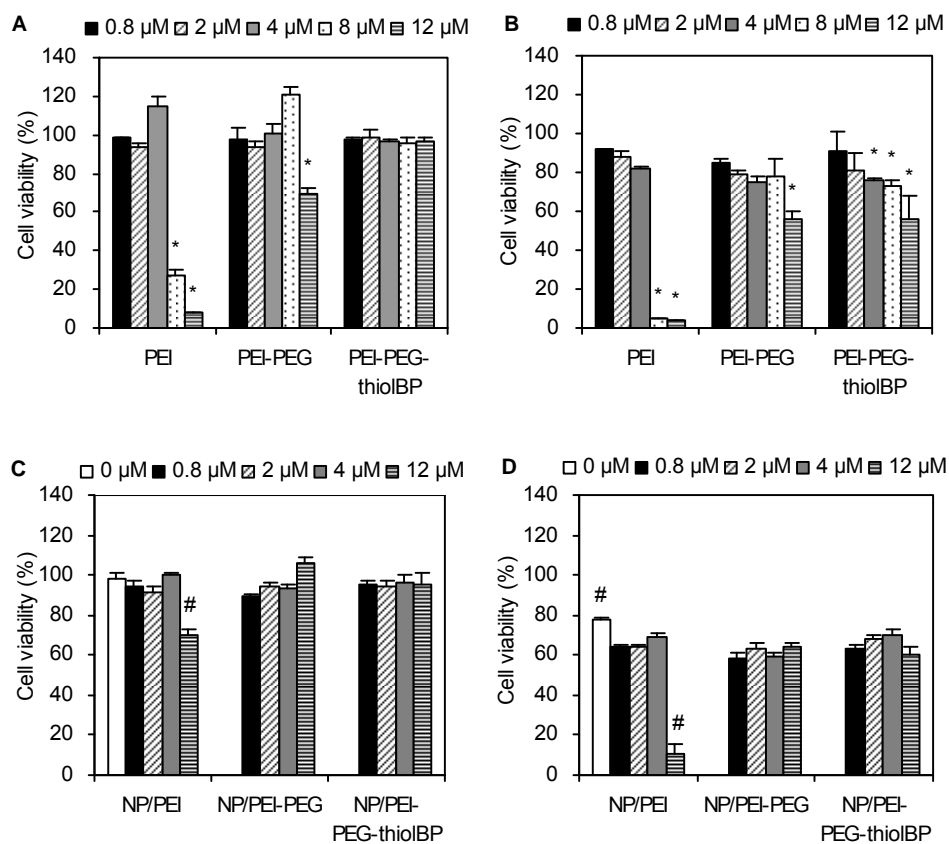


Figure 4-7 Cytotoxicity of polymer conjugates on (A) C2C12 cells, and (B) rat BMSCs, and polymer coated BSA NPs on (C) C2C12 cells, and (D) rat BMSCs. The conjugates used for coating were 150 PEG/PEI for PEI-PEG, 150 PEG and 24 thiolBP/PEI for PEI-PEG-thiolBP). The concentrations shown were equivalent to the polymer concentrations used for coating the BSA NPs. Untreated cells served as reference and were taken as 100% viability. Results are expressed as mean \pm SD from triplicate wells. Statistically significant ($p < 0.05$) groups compared to control (*) and other groups (#) are indicated.

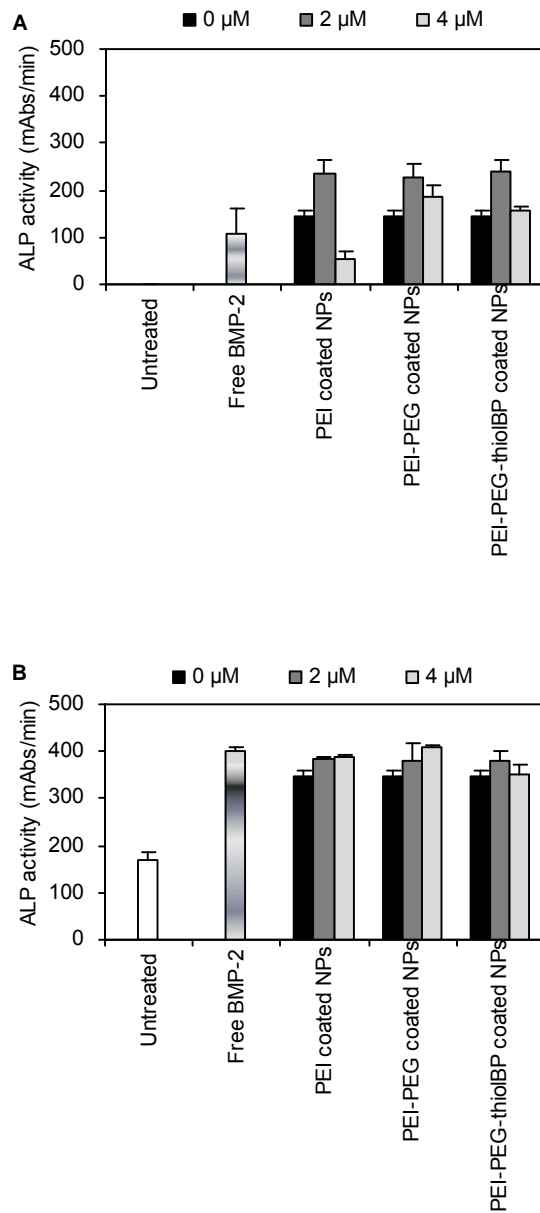


Figure 4-8 ALP activity of NP-encapsulated BMP-2 on (A) C2C12 cells and (B) rat BMSCs. Results are expressed as mean \pm SD from triplicate wells. The conjugates used for coating were 150 PEG/PEI for PEI-PEG, 150 PEG and 24 thiolBP for PEI-PEG-thiolBP. The concentrations shown were equivalent to the polymer concentrations used for coating the BSA NPs. All the NP-encapsulated BMP-2 showed equivalent or higher ALP activity compared to free BMP-2, except for the C2C12 cells treated with NPs coated with highest concentration of PEI.

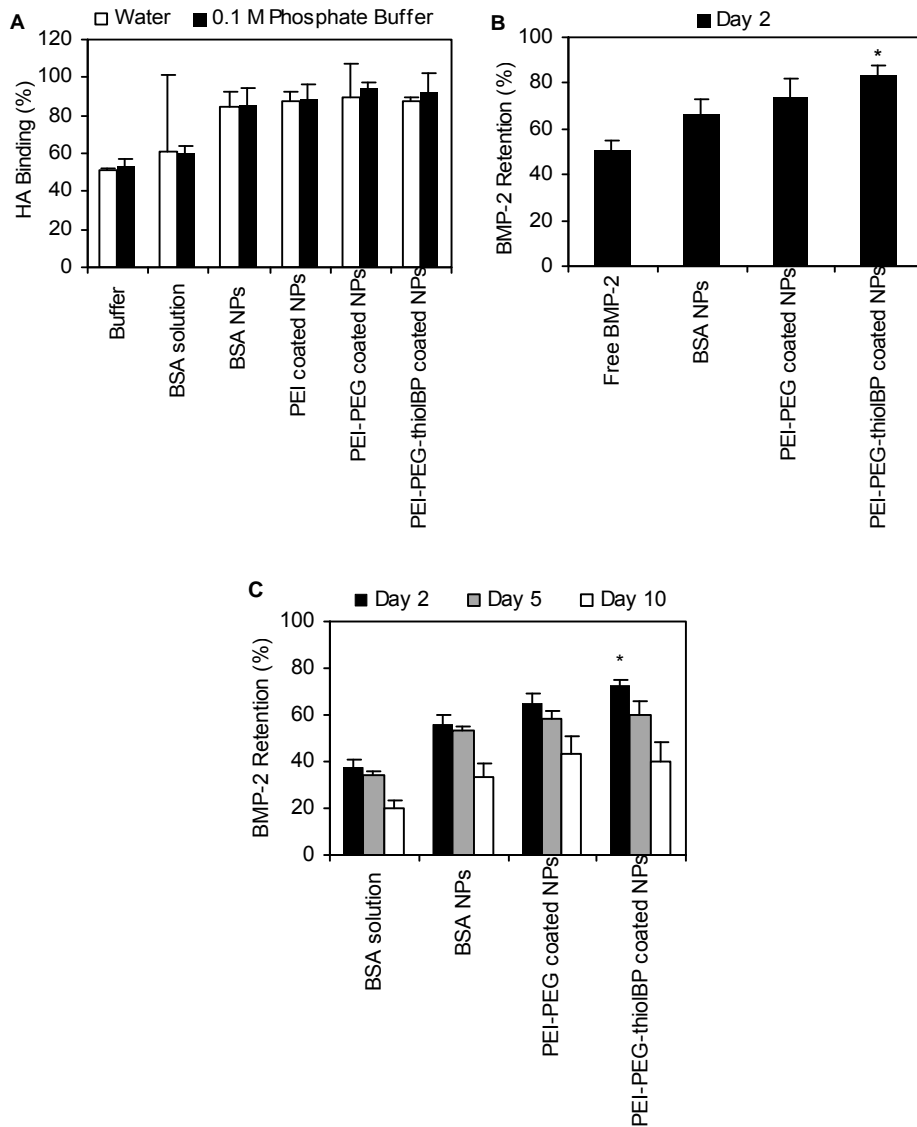


Figure 4-9 *In vitro* HA affinity (A) and *in vivo* implant retention (B, Day 2; C, Day 2-10) of ^{125}I -labeled BMP-2 in different NP formulations. The *in vitro* binding was performed in either ddH₂O or 0.1 M phosphate buffer (pH 7.4). All NPs displayed higher HA binding and *in vivo* retention of NP-encapsulated BMP-2 than the free BMP-2 and BMP-2 in BSA solutions ($p < 0.05$). However, no difference was seen among the HA affinity of various NPs *in vitro* (A). In the implant model (B and C), PEI-PEG-thiolBP coated NPs showed the highest retention among all NP formulations until day 5 post-implantation ($p < 0.05$ vs. free BMP-2 and uncoated NPs), though there was no significant difference from the PEI-PEG coated NPs ($p > 0.05$). At day 10, the BMP-2 retention was decreased for all groups, and the coated NPs retained the highest amount of BMP-2 (>40%) in implants ($n = 4$ implants at each time point).

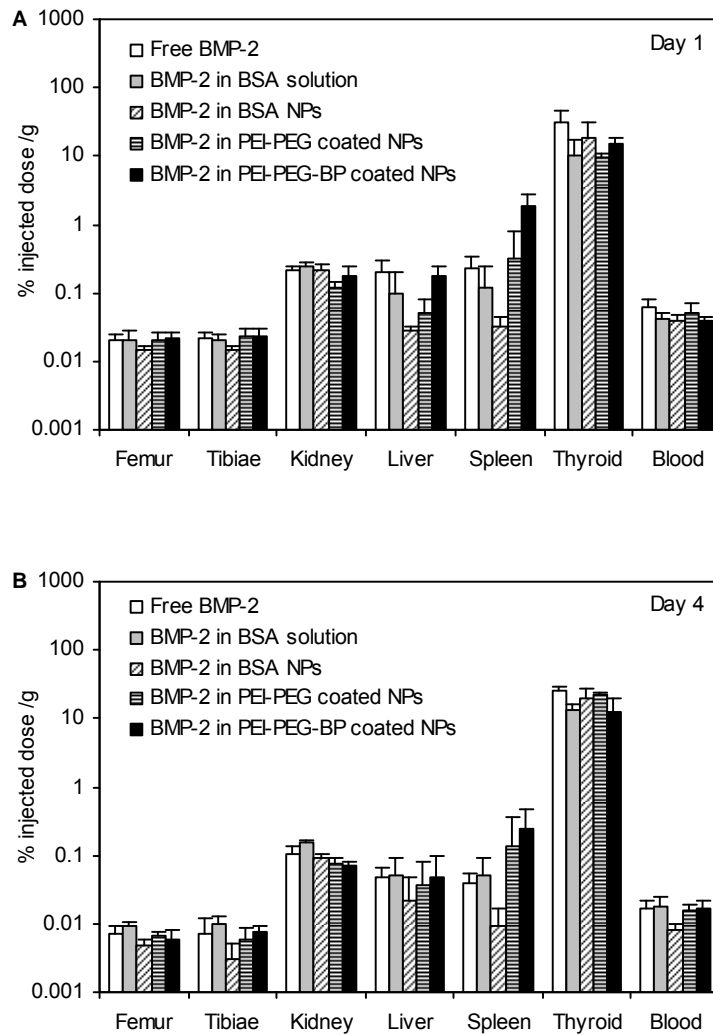


Figure 4-10 The biodistribution of ^{125}I -labeled BMP-2 encapsulated in different BSA NPs. The samples were administered intravenously to the rats by tail vein injection, and the biodistribution was analyzed at (A) day 1 and (B) day 4 after injection. Results (% injected dose) are expressed as mean \pm SD ($n = 6$ for femur, tibiae and kidney, $n = 3$ for other tissues) and normalized with the weight of the tissue (g).

REFERENCES

- [1]. Owens III, D. E.; Peppas, N. A. Opsonization, biodistribution, and pharmacokinetics of polymeric nanoparticles. *Int J Pharm* **2006**, *307*, 93-102.
- [2]. Wang, D.; Miller, S. C.; Kopeckova, P.; Kopecek, J. Bone-targeting macromolecular therapeutics. *Adv Drug Deliv Rev* **2005**, *57*, 1049-1076.
- [3]. Schafer, V.; von Briesen, H.; Andreesen, R.; Steffan, A. M.; Royer, C.; Troster, S.; Kreuter, J.; Rubsamen-Waigmann, H. Phagocytosis of nanoparticles by human immunodeficiency virus (HIV)-infected macrophages: a possibility for antiviral drug targeting. *Pharm Res* **1992**, *9*, 541-546.
- [4]. Merodio, M.; Arnedo, A.; Renedo, M. J.; Irache, J. M. Ganciclovir-loaded albumin nanoparticles: characterization and in vitro release properties. *Euro J Pharm Sci* **2001**, *12*, 251-259.
- [5]. Dreis, S.; Rothweiler, F.; Michaelis, M.; Cinatl, J.; Kreuter, J.; Langer, K. Preparation, characterisation and maintenance of drug efficacy of doxorubicin-loaded human serum albumin (HSA) nanoparticles. *Int J Pharm* **2007**, *341*, 207-214.
- [6]. Segura, S.; Espuelas, S.; Renedo, M. a. J. s.; Irache, J. M. Potential of albumin nanoparticles as carriers for interferon gamma. *Drug Dev Ind Pharm* **2005**, *31*, 271-280.
- [7]. Bronich, T. K.; Cherry, T.; Vinogradov, S. V.; Eisenberg, A.; Kabanov, V. A.; Kabanov, A. V. Self-assembly in mixtures of poly(ethylene oxide)-graft-poly(ethyleneimine) and alkyl sulfates. *Langmuir* **1998**, *14*, 6101-6106.
- [8]. Tang, G. P.; Zeng, J. M.; Gao, S. J.; Ma, Y. X.; Shi, L.; Li, Y.; Too, H.-P.; Wang, S. Polyethylene glycol modified polyethylenimine for improved CNS gene transfer: effects of PEGylation extent. *Biomaterials* **2003**, *24*, 2351-2362.
- [9]. Sung, S. J.; Min, S. H.; Cho, K. Y.; Lee, S.; Min, Y. J.; Yeom, Y. I.; Park, J. K. Effect of polyethylene glycol on gene delivery of polyethylenimine. *Biol pharm bull* **2003**, *26*, 492-500.
- [10]. Ogris, M.; Brunner, S.; Schuller, S.; Kircheis, R.; Wagner, E. PEGylated

DNA/transferrin-PEI complexes: reduced interaction with blood components, extended circulation in blood and potential for systemic gene delivery. *Gene Ther* **1999**, *6*, 595-605.

- [11]. Soppimath, K. S.; Aminabhavi, T. M.; Kulkarni, A. R.; Rudzinski, W. E. Biodegradable polymeric nanoparticles as drug delivery devices. *J Control Rel* **2001**, *70*, 1-20.
- [12]. Harris, J. M.; Chess, R. B. Effect of pegylation on pharmaceuticals. *Nat Rev Drug Discov* **2003**, *2*, 214-221.
- [13]. Mishra, V.; Mahor, S.; Rawat, A.; Gupta, P. N.; Dubey, P.; Khatri, K.; Vyas, S. P. Targeted brain delivery of AZT via transferrin anchored pegylated albumin nanoparticles. *J Drug Target* **2006**, *14*, 45-53.
- [14]. Lin, W.; Coombes, A. G. A.; Garnett, M. C.; Davies, M. C.; Schacht, E.; Davis, S. S.; Illum, L. Preparation of sterically stabilized human serum albumin nanospheres using a novel dextranox-mPEG crosslinking agent. *Pharm Res* **1994**, *11*, 1588-1592.
- [15]. Lin, W.; Garnett, M. C.; Schacht, E.; Davis, S. S.; Illum, L. Preparation and in vitro characterization of HSA-mPEG nanoparticles. *Int J Pharm* **1999**, *189*, 161-170.
- [16]. Lin, W.; Garnett, M. C.; Davies, M. C.; Bignotti, F.; Ferruti, P.; Davis, S. S.; Illum, L. Preparation of surface-modified albumin nanospheres. *Biomaterials* **1997**, *18*, 559-565.
- [17]. Uludag, H.; Yang, J. Targeting systemically administered proteins to bone by bisphosphonate conjugation. *Biotechnol Prog* **2002**, *18*, 604-611.
- [18]. Bansal, G.; Gittens, S. A.; Uludag, H. A di(bisphosphonic acid) for protein coupling and targeting to bone. *J Pharm Sci* **2004**, *93*, 2788-2799.
- [19]. Bansal, G.; Wright, J. E. I.; Zhang, S.; Zernicke, R. F.; Uludag, H. Imparting mineral affinity to proteins with thiol-labile disulfide linkages. *J Biomed Mater Res A* **2005**, *74A*, 618-628.
- [20]. Choi, S. W.; Kim, J. H. Design of surface-modified poly(D,L-lactide-co-glycolide) nanoparticles for targeted drug delivery to bone. *J Control Rel* **2007**, *122*, 24-30.
- [21]. Wang, D.; Miller, S.; Sima, M.; Kopeckova, P.; Kopecek, J. Synthesis and evaluation of water-soluble polymeric bone-targeted drug delivery systems.

Bioconjugate Chem **2003**, *14*, 853-859.

- [22]. Zhang, S.; Wright, J. E. I.; Uludag, H.; Ozber, N. The interaction of cationic polymers and their bisphosphonate derivatives with hydroxyapatite. *Macromol Biosci* **2007**, *7*, 656-670.
- [23]. Wang, G.; Siggers, K.; Zhang, S.; Jiang, H.; Xu, Z.; Zernicke, R.; Matyas, J.; Uludag, H. Preparation of BMP-2 containing bovine serum albumin (BSA) nanoparticles stabilized by polymer coating. *Pharm Res* **2008**, *25*, 2896-2909.
- [24]. Zhang, S.; Wang, G.; Lin, X.; Chatzinikolaidou, M.; Jennissen, H. P.; Laub, M.; Uludag, H. Polyethylenimine-coated albumin nanoparticles for BMP-2 delivery. *Biotechnol Prog* **2008**, *24* (4), 945-956.
- [25]. Nickel, J.; Dreyer, M. K.; Kirsch, T.; Sebald, W. The Crystal Structure of the BMP-2:BMPr-IA complex and the generation of BMP-2 antagonists. *J Bone Joint Surg Am* **2001**, *83* A (Suppl 1), S7-14.
- [26]. Perrine, T. D.; Landis, W. R. Analysis of polyethylenimine by spectrophotometry of its copper chelate. *J Polym Sci A* **1967**, *5*, 1993-2003.
- [27]. von Harpe, A.; Petersen, H.; Li, Y.; Kissel, T. Characterization of commercially available and synthesized polyethylenimines for gene delivery. *J Control Rel* **2000**, *69*, 309-322.
- [28]. Ames, B. N. Assay of inorganic phosphate, total phosphate and phosphatases. In *Methods in Enzymology*, Neufeld, E. F., Ginsburg, V., Eds.; Academic Press: New York, 1966; pp 115-117.
- [29]. Bullock, J.; Chowdhury, S.; Severdia, A.; Sweeney, J.; Johnston, D.; Pachla, L. Comparison of results of various methods used to determine the extent of modification of methoxy polyethylene glycol 5000-modified bovine Cupri-Zinc superoxide dismutase. *Anal Biochem* **1997**, *254*, 254-262.
- [30]. Gittens, S. A.; Bagnall, K.; Matyas, J. R.; Lobenberg, R.; Uludag, H. Imparting bone mineral affinity to osteogenic proteins through heparin-bisphosphonate conjugates. *J Control Rel* **2004**, *98*, 255-268.
- [31]. Varkey, M.; Kucharski, C.; Haque, T.; Sebald, W.; Uludag, H. In vitro osteogenic response of rat bone marrow cells to bFGF and BMP-2

treatments. *Clin Orthop Relat Res* **2006**, *443*, 113-123.

- [32]. Finsky, R.; De Jaeger, N. Particle sizing by photon correlation spectroscopy. Part II: average values. *Part Part Sys Char* **1991**, *8*, 187-193.
- [33]. Garbuzenko, O.; Barenholz, Y.; Priev, A. Effect of grafted PEG on liposome size and on compressibility and packing of lipid bilayer. *Chem Physics Lipids* **2005**, *135*, 117-129.
- [34]. Godbey, W. T.; Wu, K. K.; Mikos, A. G. Poly(ethylenimine)-mediated gene delivery affects endothelial cell function and viability. *Biomaterials* **2001**, *22*, 471-480.
- [35]. Zhang, S.; Doschak, M. R.; Uludag, H. Pharmacokinetics and bone formation by BMP-2 entrapped in polyethylenimine-coated albumin nanoparticles. *Biomaterials* **2009**, *30*, 5143-5155.
- [36]. Zhang, S.; Kucharski, C.; Doschak, M. R.; Sebald, W.; Uludag, H. Polyethylenimine-PEG coated albumin nanoparticles for BMP-2 delivery. *Biomaterials* **2010**, *31*, 952-963.
- [37]. Meszaros, R.; Thompson, L.; Bos, M.; de Groot, P. Adsorption and electrokinetic properties of polyethylenimine on silica surfaces. *Langmuir* **2002**, *18*, 6164-6169.
- [38]. Radeva, T.; Petkanchin, I. Electric properties and conformation of polyethylenimine at the hematite-aqueous solution interface. *J Colloid Interf Sci* **1997**, *196*, 87-91.
- [39]. Lin, R.; Liu, N.; Yang, Y.; Li, B.; Liao, J.; Jin, J. Radioiodination of protein using 2,3,5,6-tetrafluorophenyl 3-(nido-carboranyl) propionate (TCP) as a potential bi-functional linker: Synthesis and biodistribution in mice. *Appl Radiation Isotopes* **2009**, *67*, 83-87.
- [40]. Tye, C. E.; Rattray, K. R.; Warner, K. J.; Gordon, J. A. R.; Sodek, J.; Hunter, G. K.; Goldberg, H. A. Delineation of the hydroxyapatite-nucleating domains of bone sialoprotein. *J Biol Chem* **2003**, *278*, 7949-7955.
- [41]. Moghimi, S. M.; Hunter, A. C.; Murray, J. C. Long-circulating and target-specific nanoparticles: theory to practice. *Pharmacol Rev* **2001**, *53*, 283-318.
- [42]. Uludag, H. Bisphosphonates as a foundation of drug delivery to bone.

Curr Pharm Des **2002**, *8*, 1929-1944.

- [43]. Hengst, V.; Oussoren, C.; Kissel, T.; Storm, G. Bone targeting potential of bisphosphonate-targeted liposomes: preparation, characterization and hydroxyapatite binding in vitro. *Int J Pharm* **2007**, *331*, 224-227.
- [44]. Pignatello, R.; Cenni, E.; Micieli, D.; Fotia, C.; Salerno, M.; Granchi, D.; Avnet, S.; Sarpietro, M. G.; Castelli, F.; Baldini, N. A novel biomaterial for osteotropic drug nanocarriers: synthesis and biocompatibility evaluation of a PLGA-ALE conjugate. *Nanomedicine* **2009**, *4*, 161-175.
- [45]. Anada, T.; Takeda, Y.; Honda, Y.; Sakurai, K.; Suzuki, O. Synthesis of calcium phosphate-binding liposome for drug delivery. *Bioorg Med Chem Lett* **2009**, *19*, 4148-4150.
- [46]. Vail NK. Skeletally targeted nanoparticles. WO/2005/020965, **2005**.
- [47]. Vail NK. Targeted delivery of bioactive factors to the systemic skeleton. US 7 381 426 B2, **2008**.

Chapter 5

Bisphosphonate-Decorated Nanoparticles Designed as Drug Carriers for Bone Diseases¹

¹*A version of this chapter has been submitted for publication in: Wang G, Mostafa NAH, Kucharski C, Uludag H. Journal of Biomedical Materials Research part A.*

5.1 INTRODUCTION

Development of nanocarriers for delivering therapeutic agents specifically to bone is urgently needed for treatment of a wide-range of bone diseases. The carriers are expected to retain the therapeutic agents in an active form, enhance the efficacy of therapeutic agents by restricting their delivery to bone tissue (i.e., increase *in situ* concentration of therapeutic agents) and reduce the undesired side effects by minimizing non-specific distribution to other organs [1-3]. Micellar and liposomal systems have been employed for delivery of wide array of therapeutic agents, in particular anti-cancer therapeutics, but their utility in bone diseases have been limited due to lack of bone affinity. These versatile nanocarriers can be employed for bone-targeting of therapeutic agents as long as they can be further engineered for the desired bone affinity. This may be possible by incorporating a ligand with strong affinity to the unique component of bone tissue, namely the hydroxyapatite (HA), which does not exist at other sites under normal conditions.

Bone targeting of simple molecules by conjugation with bone-seeking ligands bisphosphonates (BPs) have been achieved *in vivo* for various pro-drug candidates such as estradiol [4], cisplatin [5], prostaglandin E₂ [6] and several model proteins [7-9]. Anada et al. [10] synthesized an amphipathic molecule containing a BP head group, 4-*N*-(3,5-ditetradecyloxybenzoyl)-aminobutane-1-hydroxy-1,1-bisphosphonic acid disodium salt, which was subsequently

formulated into liposomes along with distearoylphosphatidylcholine (DSPC) and cholesterol (CH). The liposomes having BP moieties showed high affinity for HA *in vitro*. Henst et al. [11] reported liposomes incorporating with cholesteryl-trisoxoethylene-bisphosphonic acid (CH-TOE-BP) designed for mineral affinity. However, the desired HA affinity of these liposomes has been limited to *in vitro* test on HA particles, and the feasibility of using the liposomes for encapsulation of therapeutic agents in a bioactive form remain to be demonstrated. Unlike larger liposomes, micellar nanocarriers could be also advantageous for certain applications, but no micellar delivery system for bone targeting was reported to-date.

This study explored the feasibility of creating of micellar and liposomal nanocarriers from building blocks that display bone mineral (HA) affinity. Towards this goal, we conjugated a thiol-containing BP, 2-(3-mercaptopropylsulfanyl)-ethyl-1,1-bisphosphonic acid (thiolBP), with distearoylphosphoethanolamine-polyethylene glycol-maleimide (DSPE-PEG-MAL) to form a DSPE-PEG-thiolBP conjugate. The preparation and *in vitro* characterization of bone-targeted micelles and liposomes derived from DSPE-PEG-thiolBP (**Figure 5-1**) was described in this report. The capacity of the prepared vehicles to encapsulate anti-cancer drug doxorubicin (DOX) and a model protein lysozyme (LYZ) was assessed. The mineral affinity of the vehicles

was investigated using HA particles as well as a biomimic bone model, HA-embedded collagen scaffold. We imparted an effective mineral affinity to the prepared drug delivery vehicles both *in vitro* and in an *in vivo* implant model, indicating that the described HA-binding nanocarriers will facilitate a novel approach for drug delivery in treatment of bone diseases.

5.2 MATERIALS AND METHODS

Materials

Cholesterol (CH), lysozyme (LYZ) from chicken egg white, 1,1'-dioctadecyl-3,3,3',3'-tetra-methylindocarbocyanine (DiI), and doxorubicin hydrochloride (DOX) were obtained from Sigma-Aldrich (St. Louis, MO, USA). Fluorescein isothiocyanate (FITC) was obtained from Pierce (Rockford, IL, USA) and used to label LYZ as described elsewhere [12]. 1,2-distearoylglycero-3-phosphatidylcholine (DSPC) and 1,2-distearoylglycero-3-phosphoethanolamine-*N*-[poly(ethyleneglycol) 2000] (DSPE-PEG) were provided by Lipoid GmbH (Ludwigshafen, Germany). DSPE-PEG₃₄₀₀-maleimide (DSPE-PEG-MAL) was purchased from Creative PEGWorks (Winston-Salem, NC, USA). ThiolBP was synthesized as previously described [13]. Recombinant human bone morphogenetic protein-2 (BMP-2) was expressed in *E. coli* and purified as

described elsewhere [14]. Synthetic HA was prepared according to the method described by Bernardi [15].

Conjugation of ThiolBP to DSPE-PEG

100 mg DSPE-PEG-MAL was slowly dissolved in 3 mL of 0.1 M phosphate buffer (pH 7.0), and mixed with 1 mL of thiolBP (molar ratio of DSPE-PEG-MAL:thiolBP = 1:4) dissolved in the same buffer. The mixture was incubated for 1 h and then transferred into dialysis tubing (MWCO 100 kDa) for dialysis against 50 mM sodium chloride (2×1 L; 3-5 h per period), followed by ddH₂O (3×1 L). The final solution was lyophilized to yield the DSPE-PEG-thiolBP as white solid.

Micelle Formation

DSPE-PEG or DSPE-PEG-thiolBP (2 μ mol) and trace amount of DOX (10 μ g) or LYZ (0.2 mg) (labeled with FITC) were dissolved in chloroform (1 mL). The organic solvent was removed by evaporator to form thin films integrated with DOX or LYZ. The lipid film was then hydrated with 1 mL of 10 mM HEPES-buffered saline (HBS; 10 mM HEPES with 150 mM NaCl, pH 7.4) at room temperature for 30 min to form the micelles spontaneously. The micelles were purified by dialysis (MWCO 14 kDa for DOX, 100 kDa for LYZ) against at least 300-fold excess of HBS ($\times 3$) for 24 h to remove the unloaded DOX or LYZ.

In one set of preparation, micelles with different ratios of DSPE-PEG and DSPE-PEG-thiolBP (0:100, 20:80, 50:50 and 100:0) were prepared.

Liposome Preparation

Two methods, lipid film hydration (LFH) method and reverse-phase evaporation vesicle (REV) method, were used to fabricate the liposomes. In the LFH method, DSPC (10 μmol) and CH (5 μmol) were dissolved in chloroform/methanol (85/15 v/v) and dried under reduced pressure. The resultant thin lipid film was hydrated with 2 mL of HBS buffer. For preparation of the PEG-liposomes and the BP-liposomes, 5% (molar percent of DSPC) DSPE-PEG or DSPE-PEG-thiolBP was added to the lipid solution before the formation of lipid film. To encapsulate the DOX or LYZ, the lipid film was hydrated with DOX (10 $\mu\text{g/mL}$) or LYZ (0.2 mg/mL) solution in 2 mL of HBS buffer at 60 °C. The preformed liposomes were extruded through a polycarbonate membrane (100 nm pore size) 11 times at 60 °C using a mini-extruder from Avanti Polar Lipids (Alabaster, AL, USA), and the un-encapsulated DOX or LYZ was removed by dialysis as described above.

For the REV method, DSPC (10 μmol), CH (5 μmol) and 5% (percent of DSPC) DSPE-PEG (for PEG-liposomes) or DSPE-PEG-thiolBP (for BP-liposomes) were dissolved in 6 mL of diethyl ether with the help of a small

amount of methanol. 2 mL of DOX (10 µg/mL) or LYZ (0.2 mg/mL) in HBS (buffer only for empty liposomes) was added to the organic phase, and the two-phase system was vigorously vortexed and sonicated in a bath-type sonicator for 3-5 min until a relatively stable emulsion was formed. The organic solvent was removed by a rotary evaporator under reduced pressure, and the mixture transformed into aqueous vesicle dispersion with the entrapped drug or protein. The preformed liposomes were extruded at 60 °C and purified by dialysis as described above. In one set of preparations, liposomes were prepared by using different fractions of DSPE-PEG-thiolBP (0, 1, 2.5 and 5% of DSPE-PEG-thiolBP (accordingly DSPE-PEG-thiolBP/DSPE-PEG ratio, 0:100, 20:80, 50:50 and 100:0).

Characterization of Micelles and Liposomes

The particle sizes (or hydrodynamic diameters) and polydispersity index of the empty micelles and liposomes were measured by photon correlation spectroscopy (PCS) using Zetasizer 3000HS (Malvern Instruments Inc., Southboro, MA). The measurements were carried out at 25 °C using 633 nm He-Ne laser at a scattering angle of 90°.

In order to determine the encapsulation efficiency (EE), the micellar and liposomal formulations with DOX or LYZ before and after dialysis were lysed in

1% Triton X-100. The fluorescent intensity ($\lambda_{\text{ex}} = 485 \text{ nm}$, $\lambda_{\text{em}} = 604 \text{ nm}$ for DOX; $\lambda_{\text{ex}} = 485 \text{ nm}$, $\lambda_{\text{em}} = 527 \text{ nm}$ for FITC-labeled LYZ) of the samples was measured by a spectrofluorometer (Thermo Labsystems, Franklin, MA) to obtain the EE: $\text{EE}\% = 100\% \times [(\text{fluorescence post-dialysis}) / (\text{fluorescence pre-dialysis})]$.

***In Vitro* Assessment of HA Binding Affinity**

For the purpose of quantification, the micelles and liposomes were labeled with a lipophilic fluorescent tracer, 1,1'-dioctadecyl-3,3,3',3'-tetramethylindocarbocyanine (DiI, 0.2% of total phospholipid) during the preparation. An aliquot solution of micelles or liposomes were incubated with 10 mg HA suspended in 0.5 mL of 1 × PBS (total lipid concentration 0.1 μmol/mL for micelles, 0.5 μmol/mL for liposomes) in a 1.5 mL microcentrifuge tube for 3 h at room temperature. For fluorescence imaging, the HA crystals were washed three times with 1 × PBS, resuspended in PBS and mounted on glass slides. The phase contrast and fluorescence images were acquired on an Olympus FSX100 epifluorescence microscope (Olympus America Inc., Center Valley, PA). The percentage of micelles or liposomes bound to HA was quantified by a spectrofluorometer for the fluorescent intensity of DiI ($\lambda_{\text{ex}} = 536 \text{ nm}$, $\lambda_{\text{em}} = 607 \text{ nm}$) in the supernatant after centrifugation of the suspension at 1000 rpm for 3 min. The initial amount of micelles or liposomes was determined by samples treated in the same way but without HA (control). The percent HA binding (%)

was assessed as: $100\% \times [(initial\ fluorescence - fluorescence\ in\ the\ supernatant)/(initial\ fluorescence)]$. Where indicated, the binding was also determined based on the fluorescence tag of the encapsulants (i.e., autofluorescence of DOX and FITC-tag of LYZ) rather than based on DiI labeling.

***In Vitro* Affinity of Liposomes to HA-impregnated Collagen Scaffold**

An HA-containing collagen scaffold composed of type-I collagen (isolated from rat tail tendons as described elsewhere [16]) and hydroxyapatite (Col/HA, 30/70 w/w) was prepared by freeze-drying method [17]. The DiI-labeled PEG-liposomes and BP-liposomes were suspended at a concentration of 0.5 $\mu\text{mol/mL}$ (equivalent phospholipid concentration) in $1\times$ PBS, and 1 mL of the sample was incubated with a piece of sponge (8 mm in diameter and 5 mm in thickness) in a 24-well tissue culture plate for 2 h. The percentage of bound liposomes to the scaffold was calculated by the fluorescence of DiI in the supernatant and in the control, which was equal volume of liposomal suspension without the sponge.

***In Vivo* Retention of Liposomes**

Six-to-eight week-old female Sprague-Dawley rats were purchased from Biosciences (Edmonton, Alberta). The rats were acclimated for one week under

standard laboratory conditions (23 °C, 12 h of light/dark cycle) prior to the study. While maintained in pairs in sterilized cages, rats were allowed free access to food and water for the duration of the study. All procedures involving the rats were approved by the Animal Welfare Committee at the University of Alberta (Edmonton, Alberta). The PEG-liposomes and BP-liposomes were prepared with DiI labeling and sterilized by filtration through a 0.45 µm Millipore filter before implantation in 18 rats in three study groups: (1) control, PEG-liposomes without DiI labeling, (2) DiI-labeled PEG-liposomes, and (3) DiI-labeled BP-liposomes. The appropriate solution for each study group was soaked into the Col/HA sponge for ~10 minutes (60 µL formulation per implant). Once rats were anesthetized with inhalational MetofaneTM (Janssen Pharmaceuticals Inc., Toronto, ON, Canada), two wet sponges were implanted subcutaneously into bilateral ventral pouches in each rat. At indicated time points (shown in **Figure 5-6B**), two rats from each group were euthanized with CO₂, the implants were recovered, and the explanted sponges were demineralized with 1 mL of 1 M HCl for 3 h and then the fluorescent intensity in the solution was measured. As the initial fluorescence in implant, 60 µL of solution was diluted to 1 mL by 1 M HCl, and the fluorescence intensity in the diluted solution was determined before the implantation. The liposome retention, expressed as the remaining percentage of implanted amount, was calculated as: $100\% \times [(\text{recovered fluorescence in implant}) / (\text{initial fluorescence in implant})]$.

Cytotoxicity

The MTT assay was performed to assess the cytotoxicity of the micelles and liposomes using human C2C12 myoblast cells. The cells were cultured as described previously [18]. After sterilization with an 0.45 μm Millipore filter, an aliquot of micellar or liposomal dispersion (50 μL) was added to the cells grown in 24-well plates (in triplicate) with 450 μL tissue culture medium (DMEM with 10% FBS, 100 $\mu\text{g}/\text{mL}$ Penicillin and 100 U/mL Streptomycin). After 48 h incubation for the micelles or 72 h for the liposomes in a humidified atmosphere with 95/5% air/ CO_2 at 37 $^\circ\text{C}$, 0.1 mL of the MTT solution (5 mg/mL in Hanks Balanced Salt Solution, HBSS) was added to the 0.5 mL culture medium in each well. The cells were incubated for 2 h, the supernatant was removed carefully, and 0.5 mL of dimethyl sulfoxide (DMSO) was added to the cells to dissolve the formazan crystals formed. The optical density of the solution was measured by an *ELx800* plate reader (Bio-Tek Instruments Inc., Winooski, VT, US) at 570 nm. Untreated cells served as reference and were taken as 100 % viability.

Bioactivity Assay for Liposome Encapsulated BMP-2

BMP-2 containing liposomes were prepared by the REV method and separated from free BMP-2 by dialysis as described above for LYZ. The formulations were sterilized with a 0.45 μm Millipore filter. Two cell lines,

human C2C12 cells and rat bone marrow stromal cells (BMSCs) were incubated (in triplicate) with the liposomes at estimated concentrations of 1, 0.5 and 0.25 $\mu\text{g}/\text{mL}$ BMP-2 (assuming an EE of 30% for BMP-2 similar to LYZ) in 24-well plates (0.6 mL medium/well) for 3 days, washed with HBSS solution and lysed with 0.4 mL of an ALP buffer (0.5 M 2-amino-2-methylpropan-1-ol and 0.1% (v/v) Triton-X; pH 10.5). After 2 h, 0.2 mL of 1.0 mg/mL ALP substrate (*p*-nitrophenol phosphate) was added to 0.2 mL of cell lysate, and the ALP activity was determined by a kinetic assay on a plate reader, where the rate of change in the optical density was measured at 405 nm with 90 sec intervals for 8 cycles. Untreated cells and cells treated with equivalent amount of free BMP-2 served as background and positive controls, respectively. The kinetic ALP activity was expressed as the change of optical density per unit time (mAbs/min), and the relative ALP activity was calculated by subtracting the absorbance of the untreated control from the absorbance of the samples.

Statistical Analysis

All experimental data were collected in triplicate at least, and expressed as mean \pm standard deviations (SD). Statistical analysis was performed using two-sided unpaired Student's *t*-test. Differences were considered statistically significant with $p < 0.05$.

5.3 RESULTS and DISCUSSION

The DSPE-PEG-thiolBP was synthesized by conjugating thiolBP with DSPE-PEG-MAL via a reaction between the sulfhydryl group of thiolBP and the maleimide group on the PEG terminal. The successful conjugation of thiolBP to DSPE-PEG-MAL was confirmed by ¹H-NMR spectroscopy (CDCl₃ as solvent, **Figure 5-2**), and the structures of DSPE-PEG-MAL and DSPE-PEG-thiolBP were shown in **Figure 5-1**. Micelles from DSPE-PEG (PEG-micelles) and DSPE-PEG-thiolBP (BP-micelles) alone or with loaded DOX or LYZ were prepared by organic solvent evaporation followed by lipid film hydration (LFH) method [19]. The DSPE-PEG or DSPE-PEG-thiolBP was able to spontaneously form micelles in aqueous solution. On the other hand, stable liposomes were obtained when DSPE-PEG and DSPE-PEG-thiolBP were mixed with DSPC and CH, and the fraction of DSPE-PEG was limited to less than 10% [20]. The liposomal formulation was extruded through a 100 nm polycarbonate membrane to control the liposomal size. DSPC and CH were used to prepare the liposomes because they have good stability *in vivo* [21], though the high gel-liquid crystalline phase transition temperature of DSPC required processing at a high temperature (>55°C).

The particle sizes and polydispersity index of the empty micelles and liposomes were summarized in **Table 5-1**. The obtained sizes for the

micelles (16-17 nm) and liposomes (98-105 nm) were in the expected size range, and thiolBP incorporation did not seem to affect the size of the respective carriers. The polydispersity index for all formulations was <0.3 , indicating a relative homogenous distribution of the nanocarriers.

DOX, a clinically used anti-cancer drug, and LYZ, due to its similarity to bone morphogenetic protein-2 (BMP-2) in molecular weight and net charge, were chosen as model drugs for encapsulation. DOX or FITC-labeled LYZ was entrapped in the micelles by simply adding them to the DSPE-PEG and DSPE-PEG-BP solution used for micellization, and the un-encapsulated molecules were removed by dialysis. As summarized in **Table 5-1**, the micelles could encapsulate DOX with a relatively high EE (~40%), whereas the EE for LYZ in micelles was quite low ($<5\%$), indicating the unsuitability of micelles for encapsulation of LYZ. It has been reported that drugs with small molecules such as DOX and docetaxel can be easily encapsulated into the core of micelles with high EE ($>80\%$) [19,22]. The EE for DOX in this study was lower than previously reports, possibly due to the leakage of loaded DOX from the micelles during dialysis. It is difficult to entrap macromolecules such as LYZ into the micelles because of the limited space of hydrophobic core, as well as the large size and partially hydrophilic characteristic of the protein. The inability of the micelles to entrap the protein led us to explore liposomes for bone delivery of hydrophilic

macromolecular drugs.

Two methods were used to fabricate the liposomes. LFH method is the simplest technique to prepare liposomes, and widely used to encapsulate various drugs. However, its poor capacity to entrap hydrophilic molecules limited its application in loading protein- or peptide-based bioactive therapeutics [23]. The REV method involves formation of aqueous/organic emulsions followed by solvent evaporation, and produced large trapped volumes in the liposomal aqueous core, thus leading to improved entrapment for water-soluble molecules[24]. The EEs for the two methods were summarized in **Table 5-1**; the LFH method had significantly higher EE for DOX (>60%) than the REV (~30%) method for both PEG-liposomes and BP-liposomes, but the EEs for LYZ were reversed (~30% for REV vs. ~10% for LFH). The results indicated that the LFH method was advantageous for loading DOX, whereas the REV method was preferable for loading proteins.

The desired mineral affinity was imparted by incorporating the HA-binding ligand thiolBP in the nanocarriers. A longer PEG spacer was used in the DSPE-PEG-thiolBP (PEG₃₄₀₀) conjugate than the DSPE-PEG (PEG₂₀₀₀) to facilitate the extension of the thiolBP further from the surface [25]. The mineral affinity of the micelles and liposomes was investigated based on an *in vitro* HA binding assay. For this purpose, the micelles and liposomes were labeled with DiI

during the preparation. Firstly, the HA binding of the BP-micelles and BP-liposomes was visualized by an epifluorescence microscope. As shown in **Figure 5-3**, the HA crystals treated with PEG-micelles and PEG-liposomes displayed no binding of red fluorescent dye, whereas the BP-micelles and BP-liposomes displayed strong affinity to HA, evident by the fluorescence retained on the HA crystals.

In order to identify an optimal thiolBP amount in nanoparticles, the effect of DSPE-PEG-thiolBP ratio on the HA binding of micelles and liposomes was examined. The micelles formed from DSPE-PEG alone showed very low HA binding (<5%), whereas micelles formed with 20% of DSPE-PEG-thiolBP had increased (~65%) HA binding (**Figure 5-4A**). Additional DSPE-PEG-thiolBP in the micelle formulation did not increase the HA affinity any further. The liposomes without thiolBP did not yield HA binding either (<5%), but DSPE-PEG-thiolBP incorporation (1 to 5%) imparted significant HA affinity to the liposomes (**Figure 5-4B**). The HA affinity with 1 to 5% of DSPE-PEG-thiolBP was similar, indicating that maximum binding was reached with as little as 1% of DSPE-PEG-thiolBP in the liposomes. The HA affinity of the liposomes was dependent on the liposome concentration under the experimental conditions (**Figure 5-5A**). Whereas complete HA binding was seen at low liposome concentration, a lower percentage of HA binding was obtained at

higher liposome concentration, possibly due to the saturation of the binding sites on HA. Since the formulations were intended for *in vivo* application, the existence of plasma protein or serum might affect their HA binding affinity. Therefore, the effect of serum on HA affinity was studied. As shown in **Figure 5-5B**, The HA binding by the BP-liposomes was gradually decreased when the serum content in binding medium was increased, which was likely to reflect protein adsorption onto HA surfaces, competing with the BP for surface binding. Despite of the interference effect of serum, the HA affinity of the BP-liposomes was retained significantly higher than PEG-liposomes, which indicated that the plasma protein would not affect the ultimate clinical implementation of the system.

The strongly HA binding nanocarriers are expected to deposit their cargo to HA surfaces by trapping them inside. To confirm whether the encapsulants can also display high mineral affinity, the HA binding was investigated based on the fluorescent encapsulants (rather than DiI labeling). As shown in **Figure 5-4C** and **D**, the results obtained by measuring the fluorescence of encapsulated DOX and LYZ also demonstrated significantly higher (2.4-5.9 fold, $p < 0.05$) HA binding ratio for the BP-micelles (**Figure 5-4C**) or BP-liposomes (**Figure 5-4D**) as compared to the PEG-micelles or PEG-liposomes. This was the case irrespective of the type of encapsulant (DOX or LYZ), the method of carrier fabrication (LFH vs. REV) or the extent of EE obtained. The difference between the

LYZ-containing BP-liposomes and PEG-liposomes did not seem to be as significant as that for the DiI-labeled liposomes. This may be partly due to the interaction between the protein and the liposome bilayer, which may result in unstabilizing a lipid membrane [26], and/or partly due to the fractional release of the encapsulated protein during the HA binding assay, leading to non-specific binding to HA [8].

Particulate HA has been routinely used to investigate *in vitro* mineral affinity of a compound or nanoparticles. However, particulate HA, with a propensity to disperse from an administration site, is not suitable for *in vivo* testing. Therefore, HA-impregnated collagen sponge (Col/HA) was employed in this study in order to test the mineral affinity of the nanocarriers *in vivo*. The Col/HA scaffold displays interconnected porous structure suitable for cellular migration and ingrowth, and has been widely studied as bone tissue engineering scaffold [27]. It is used as a bone model in this study, because its primary composition is similar to the human bone, and the presence of extensive collagen around the HA particles also provides a better mimic of native bone, where the endogenous HA is partly covered with extracellular matrix proteins. The affinity of the liposomes to Col/HA scaffold was first evaluated by using liposomes with different DSPE-PEG-thiolBP content (**Figure 5-6A**). DiI-labeled liposomes were used for this purpose. There was a gradual increase in liposome binding to

Col/HA scaffold when the DSPE-PEG-thiolBP content was increased from 0 to 5% in the lipid composition, which was consistent with the binding result obtained with pure HA (**Figure 5-4B**). Maximum mineral binding was obtained at 1% of DSPE-PEG-thiolBP for the HA alone, but at 5% of DSPE-PEG-thiolBP (**Figure 5-6A**) for the mineralized scaffold, suggesting that the surface density of targeting ligands need to be considered for maximum affinity *in vivo*. Taken together, these results confirmed that the designed nanocarriers displayed the expected affinity to a mineral-containing scaffold, which could be in turn used for *in vivo* assessment of mineral affinity.

In vivo mineral affinity of the BP-liposomes was assessed by implanting DiI-labeled liposomes in Col/HA scaffold subcutaneously in rats. Unlabeled PEG-liposomes soaked in Col/HA was used to assess the background from the implants; the results indicated no significance fluorescence in implants for this group (not shown), indicating no interference in DiI fluorescence measurements from the endogenous components at the subcutaneous site. The retention profiles for DiI-labeled PEG- and BP-liposomes were demonstrated in **Figure 5-6B**. ~60% of BP-liposomes were retained in the scaffolds until day 4, after which ~29% retention was seen at 7 days post-implantation. The retention of PEG-liposomes was less than 7% at all time points evaluated. Therefore, 9-20 fold higher ($p<0.005$) retention of liposomes was seen as a result of thiolBP

incorporation into the liposomes. The *in vivo* loss of liposomes was mainly due to rapid clearance by the physiological fluid around the implant site. The PEG-liposomes were merely passively loaded into the sponges, and thus removed fastly when exposed to the circulated body fluid, whereas the BP-liposomes could retain in the implantation site for a prolonged period because of the specific affinity to the HA-containing sponges. The results summarized in **Figure 5-6** confirmed the designed BP-liposomes did exhibit the expected *in vivo* affinity to a biomimic bone model, and the retention of BP-liposomes at mineral-bearing sites offers great promise for localization and sustainable release of drugs for bone treatment. Since the Col/HA scaffold has the potential for clinical application, the BP-liposomes reported in present study might be used as local delivery system for BMP-2, which can promote new bone formation in combination with the scaffold for bone repair.

Micellar or liposomal formulations are generally regarded as biocompatible systems from clinical perspective, since they are either accepted for use (liposomes [28]) or undergoing clinical trials (micelles [29]). To ensure that thiolBP addition did not alter the biocompatibility of the fabricated nanoparticles, MTT assay was used to determine the toxicity of the nanoparticles in an *in vitro* bioassay (using C2C12 cells as cell model). As expected, there was no or very low toxicity of the prepared micellar and liposomal formulations

(**Figure 5-7**). To determine the ability of the designed nanoparticles to deliver therapeutic drugs, BMP-2 was encapsulated in PEG-liposomes and BP-liposomes, and *in vitro* activities of the BMP-2 formulations were tested by alkaline phosphatase (ALP) induction assay. It was assumed that the EE for BMP-2 was 30% following the results obtained with the LYZ. The BMP-2 treated cells showed increasing ALP activity as a function of BMP-2 concentration in both human C2C12 cells and rat BMSCs (**Figure 5-8**). The BMP-2 encapsulated in PEG-liposomes and BP-liposomes displayed equivalent or higher ALP activity as compared to free BMP-2 in both C2C12 and BMSCs. The higher BMP-2 activity observed with liposomal formulations might be due to the higher EE than estimated during the fabrication or superior delivery of the protein by liposomal formulation (i.e., higher internalization [30]). The high activity of the liposome encapsulated BMP-2 indicated that the carrier fabrication procedures, including exposure to organic solvent, sonication, heating and shear force during the extrusion, did not impact the bioactivity of the BMP-2. Additionally, the liposomal vesicles could improve the delivery of bioactive proteins into specific cells by further modification of the liposome surface with cell-specific ligands via receptor-mediated endocytosis [31].

5.4 CONCLUSIONS

Conjugation of the thiolBP with DSPE-PEG enabled fabrication of nanoparticulate drug delivery vehicles with significant mineral affinity. Such micellar or liposomal nanocarriers were capable of effectively encapsulating small anti-cancer drugs and bioactive proteins, and efficient drug loading could be achieved by choosing the appropriate fabrication methods. Taking advantage of the strong mineral affinity of BPs, the BP-liposomes had sustained release and enhanced retention in mineralized collagen scaffolds. With their capacity to retain the bone-inducing protein BMP-2 in a bioactive form, the prepared liposomal formulations provide potential candidates for localized or bone-targeted drug delivery system for diseases affecting skeletal tissues, especially for curing bone defects via tissue engineering approach.

Table 5-1. Particle size and polydispersity index of micelles and liposomes and encapsulation efficiency (EE%) of DOX and LYZ in different formulations[#].

Formulations (Methods)	Size (nm)	Polydispersity index	DOX (EE%)		LYZ (EE%)	
			(LFH)	(REV)	(LFH)	(REV)
PEG-micelle	16.1 ± 0.9	0.288 ± 0.088	45.7 ± 0.5		4.5 ± 0.2	
BP-micelle	16.9 ± 0.1	0.288 ± 0.005	38.5 ± 0.3		3.3 ± 0.1	
PEG-liposome	97.9 ± 14.5	0.146 ± 0.053	85.4 ± 3.6	32.1 ± 2.8	11.6 ± 6.1	30.8 ± 2.9
BP-liposome	104.5 ± 17.3	0.124 ± 0.066	64.9 ± 2.7	34.3 ± 4.6	13.1 ± 5.9	29.9 ± 5.4

[#] The reported data were shown as mean ± SD derived from three independent batches.

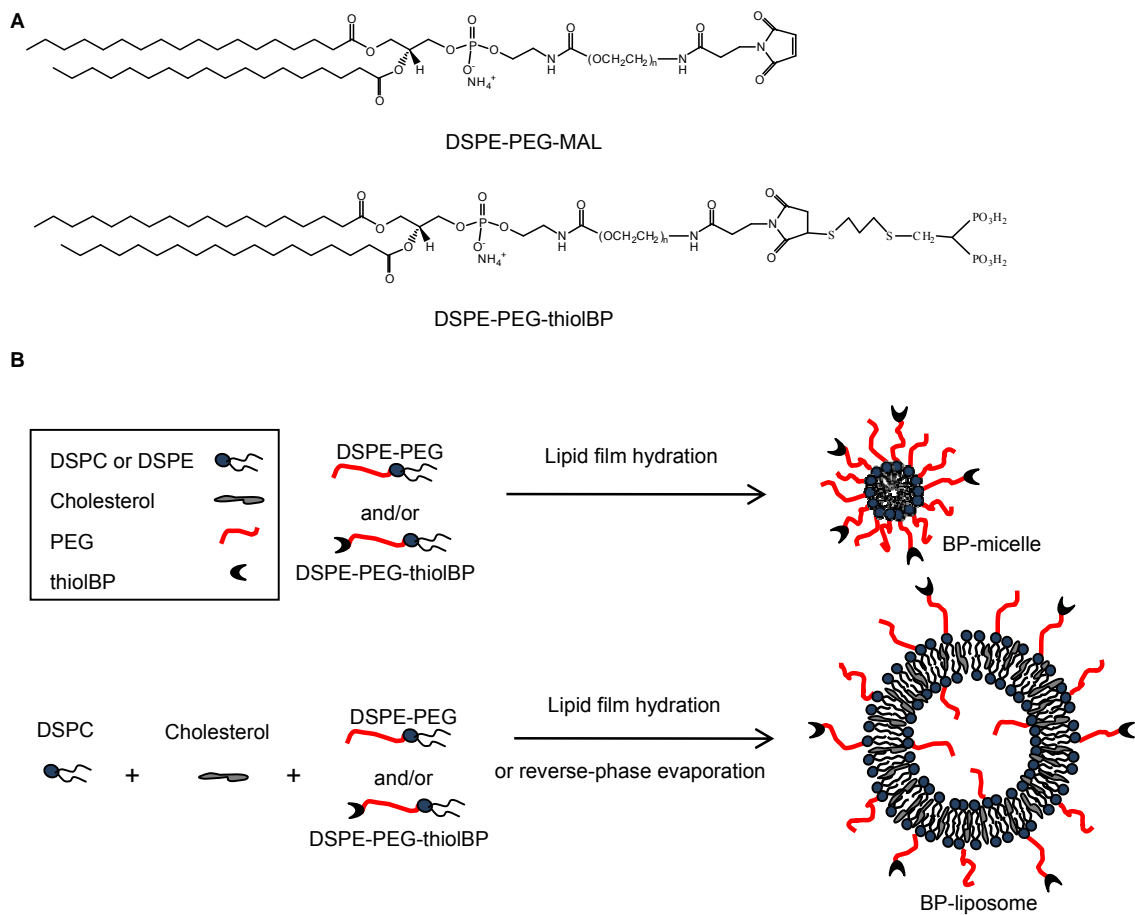


Figure 5-1. Chemical structure of DSPE-PEG-MAL and DSPE-PEG-thiolBP (A) and schematic for the preparation of the bisphosphonate-decorated micelles and liposomes (B)

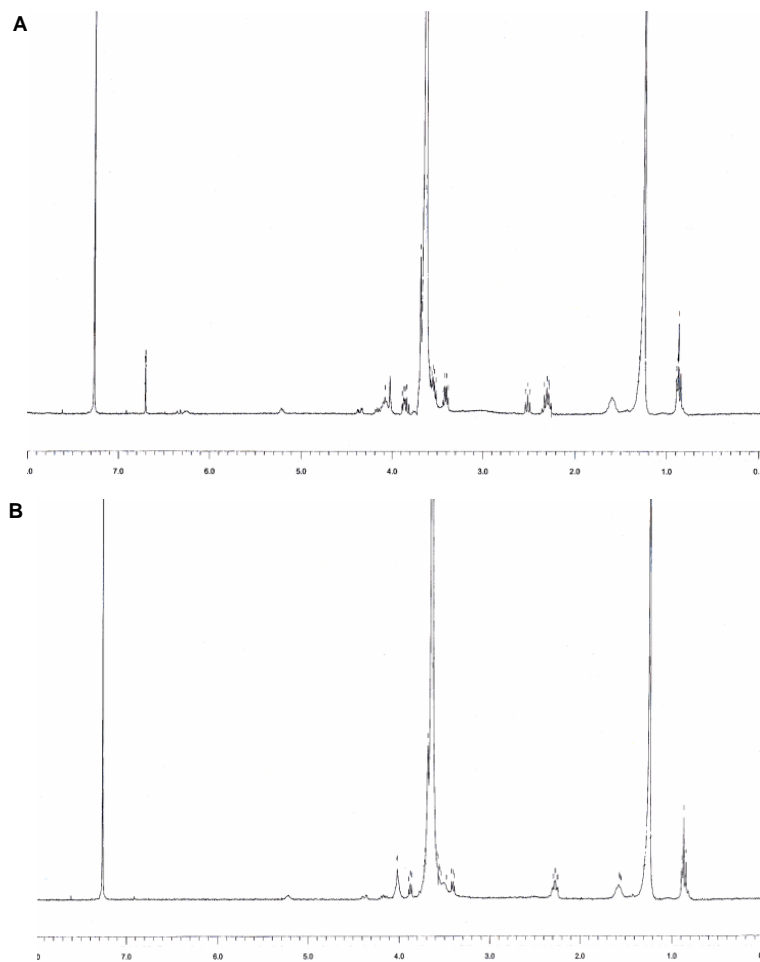


Figure 5-2. ¹H NMR spectra of DSPE-PEG-MAL (A) and DSPE-PEG-thiolBP (B). The peak at 1.26 ppm was assigned to $-\text{CH}_2-$ of the alkyl chain from DSPE, and the peak at 3.64 ppm was assigned to $-\text{CH}_2\text{CH}_2\text{O}-$ from PEG. The disappearance of peak at 6.70 ppm ($-\text{CH}=\text{CH}-$ of maleimide) in (B) indicated the successful conjugation of thiolBP to the DSPE-PEG-MAL.

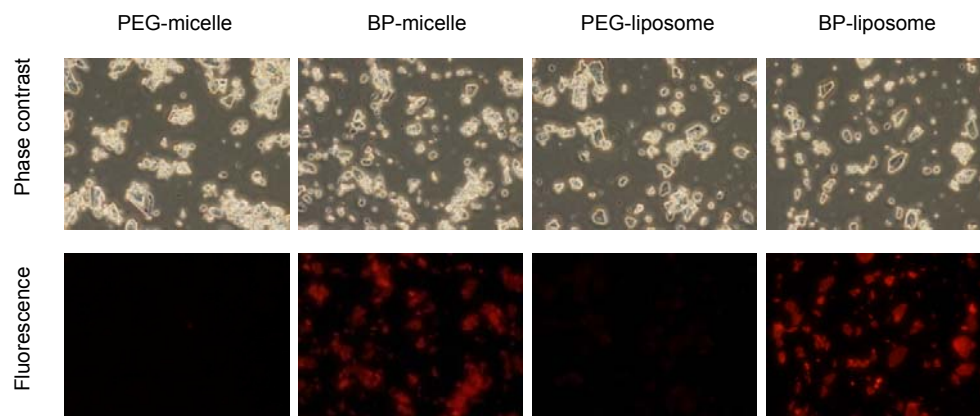


Figure 5-3. Visualization for HA binding of BP-micelles and liposomes. HA crystals were treated with micelles or liposomes (from left to right: PEG-micelle, BP-micelle, PEG-liposome and BP-liposome), and the phase contrast (top panels) and fluorescence images (bottom panels) were taken on an epifluorescence microscope.

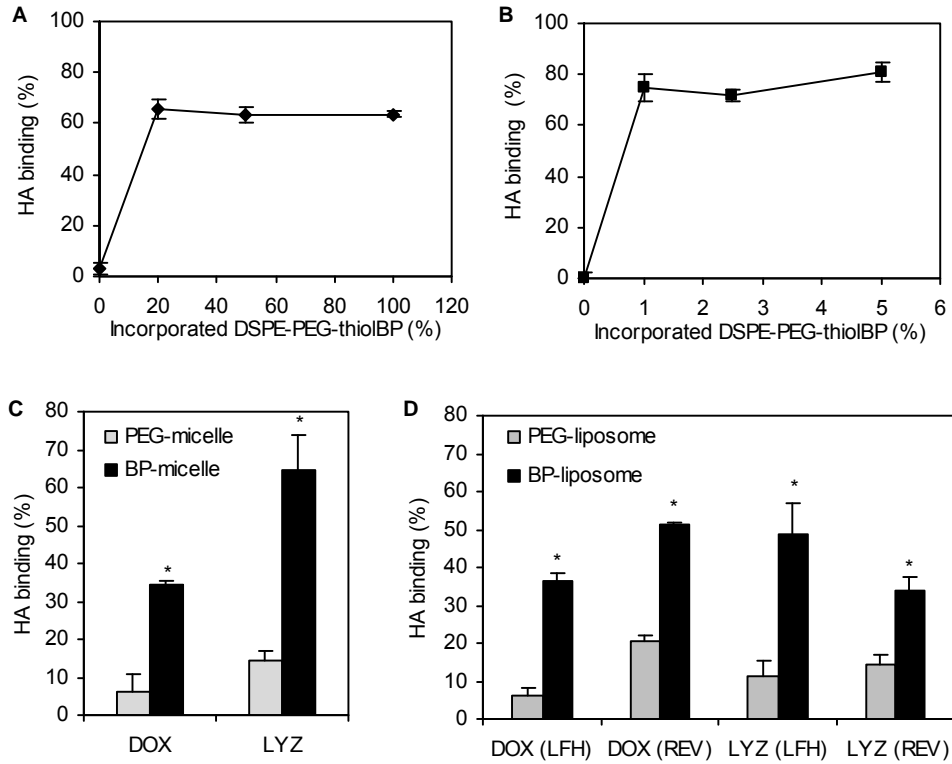


Figure 5-4 Effect of BP content on the HA binding of micelles (A) and liposomes (B) and the HA affinity of encapsulated DOX and LYZ in micelles (C) and liposomes (D). The HA binding assay of the liposomes was carried out parallelly with regards to the liposomes (DiI-labeled) and the encapsulants. The percentage of micelles or liposomes bound to HA was determined by measuring the fluorescence of DiI-labeling (A and B) or autofluorescence of DOX and FITC-tag of LYZ (C and D) in the supernatant.

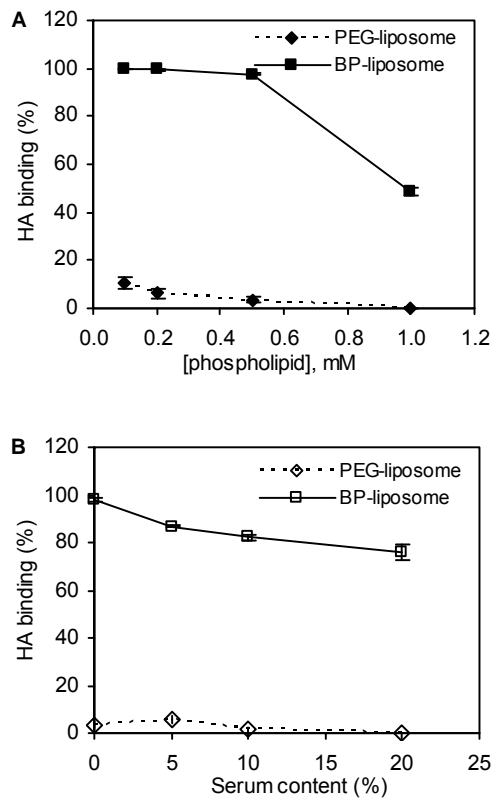


Figure 5-5. The binding of liposomes to HA in PBS (A) and serum-containing PBS (B). The HA affinity of the liposomes were investigated by changing the liposome concentration (A) or content of rat serum (B) in the binding medium. Results are expressed as mean \pm SD (n=3).

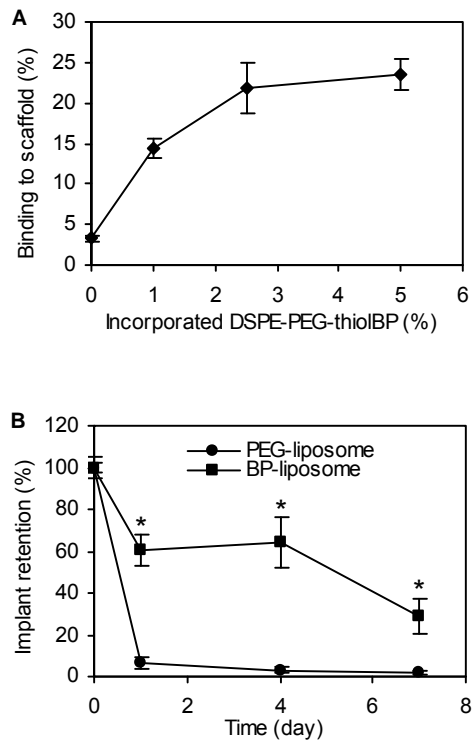


Figure 5-6. *In vitro* and *in vivo* affinity of liposomes to Col/HA scaffold. (A) *In vitro* affinity of liposomes to Col/HA scaffold, calculated based on fluorescence of DiI in the supernatant after incubation with scaffold and in the control without scaffold. (B) Liposome leakage from the Col/HA sponge, expressed as release of fluorescent dye from the scaffold after incubation of scaffold sequestered liposome in 1× PBS. (C) *In vivo* implant retention of liposomes within the scaffold by subcutaneous implant model in rats. Results are expressed as mean ± SD from triplicate measurements in A and B, and four implants in C.

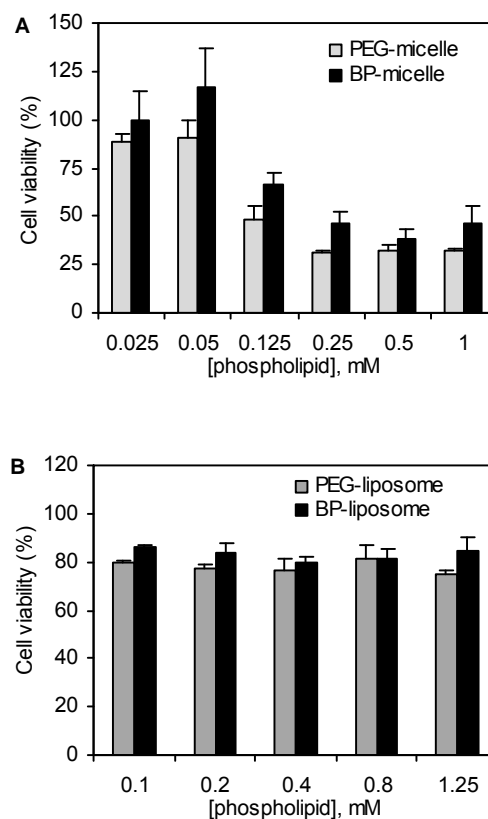


Figure 5-7. Cytotoxicity of micelles (A) and liposomes (B) on C2C12 cells. Cytotoxicity was determined by comparing the absorbance of MTT reduced by the cells treated with series of concentrations of micelles or liposomes to that reduced by untreated cells, assuming the absorbance at 570 nm of intact control cells to be 100%. The results are shown as mean \pm SD (n=3). The PEG-micelles displayed no obvious toxicity at \sim 0.05 mM, but when the concentration was increased over 0.125 mM, the cell viability was gradually decreased to \sim 30%. The BP-micelles had a similar trend as the PEG-micelles, with no adverse effect of thiolBP conjugation. All cells treated with liposome suspensions displayed \sim 80% viability irrespective of the liposome concentration. The 20% loss of cell viability was likely due to buffer of the liposomal formulation. There was no significant difference in the viability of cells treated with PEG-liposome and BP-liposome, again indicating no adverse effect of thiolBP in the formulations.

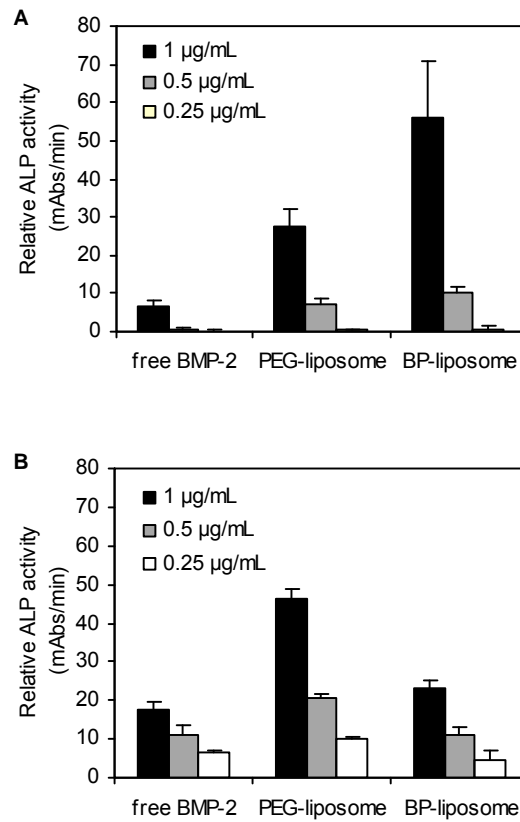


Figure 5-8. ALP activity of the BMP-2 encapsulated in the liposomes on human C2C12 cells (A) and rat BMSCs (B). The dosage shown was the concentration of BMP-2 in the wells for free BMP-2 and estimated concentration based on encapsulation efficiency of 30% for all liposomes. ALP kinetic assay was conducted after 3-days incubation of the liposomal formulations with the cells cultured in 24-well plate, and the relative ALP activity was calculated by subtracting the absorbance of the untreated control from the absorbance of the BMP-2 containing wells. Results are expressed as mean \pm SD from triplicate wells.

REFERENCES

- [1]. Wang, D.; Miller, S. C.; Kopeckova, P.; Kopecek, J. Bone-targeting macromolecular therapeutics. *Adv Drug Del Rev* **2005**, *57*, 1049-1076.
- [2]. Hirabayashi, H.; Fujisaki, J. Bone-specific drug delivery systems: approaches via chemical modification of bone-seeking agents. *Clin Pharm* **2003**, *42*, 1319-1330.
- [3]. Uludag, H. Bisphosphonates As a foundation of drug delivery to bone. *Curr Pharm Des* **2002**, *8*, 1929-1944.
- [4]. Bauss, F.; Esswein, A.; Reiff, K.; Sponer, G.; Muller-Beckmann, B. Effect of 17β -estradiol-bisphosphonate conjugates, potential bone-seeking estrogen pro-drugs, on 17β -estradiol serum kinetics and bone mass in rats. *Calcif Tissue Int* **1996**, *59*, 168-173.
- [5]. Klenner, T.; Valenzuela-Paz, P.; Keppler, B. K.; Angres, G.; Scherf, H. R.; Wingen, F.; Amelung, F.; Schmahl, D. Cisplatin-linked phosphonates in the treatment of the transplantable osteosarcoma in vitro and in vivo. *Cancer Treat Rev* **1990**, *17*, 253-259.
- [6]. Gil, L.; Han, Y.; Opas, E. E.; Rodan, G. A.; Ruel, R.; Seedor, J. G.; Tyler, P. C.; Young, R. N. Prostaglandin E₂-bisphosphonate conjugates: potential agents for treatment of osteoporosis. *Bioorg Med Chem* **1999**, *7*, 901-919.
- [7]. Uludag, H.; Kousinioris, N.; Gao, T.; Kantoci, D. Bisphosphonate conjugation to proteins as a means to impart bone affinity. *Biotechnol Prog* **2000**, *16*, 258-267.
- [8]. Uludag, H.; Yang, J. Targeting systemically administered proteins to bone by bisphosphonate conjugation. *Biotechnol Prog*. **2002**, *18*, 604-611.
- [9]. Gittens, S. A.; Bansal, G.; Zernicke, R. F.; Uludag, H. Designing proteins for bone targeting. *Adv Drug Del Rev* **2005**, *57*, 1011-1036.
- [10]. Anada, T.; Takeda, Y.; Honda, Y.; Sakurai, K.; Suzuki, O. Synthesis of calcium phosphate-binding liposome for drug delivery. *Bio Med Chem Lett* **2009**, *19*, 4148-4150.

- [11]. Hengst, V.; Oussoren, C.; Kissel, T.; Storm, G. Bone targeting potential of bisphosphonate-targeted liposomes: preparation, characterization and hydroxyapatite binding in vitro. *Int J Pharm* **2007**, *331*, 224-227.
- [12]. Bansal, G.; Wright, J. E. I.; Zhang, S.; Zernicke, R. F.; Uludag, H. Imparting mineral affinity to proteins with thiol-labile disulfide linkages. *J Biomed Mater Res A* **2005**, *74*, 618-628.
- [13]. Nickel, J.; Dreyer, M. K.; Kirsch, T.; Sebald, W. The crystal structure of the BMP-2:BMPr-IA complex and the generation of BMP-2 antagonists. *J Bone Joint Surg Am* **2001**, *83(Suppl 1)*, S7-14.
- [14]. Bernardi, G. Chromatography of nucleic acids on hydroxyapatite columns. *Methods Enzymol* **1971**, *21*, 95-139.
- [15]. Liu, X. D.; Skold, M.; Umino, T.; Zhu, Y. K.; Romberger, D. J.; Spurzem, J. R.; Rennard, S. I. Endothelial cell-mediated type I collagen gel contraction is regulated by hemin. *J Lab Clin Med* **2000**, *136*, 100-109.
- [16]. Cunniffe, G.; Dickson, G.; Partap, S.; Stanton, K.; O'Brien, F. Development and characterisation of a collagen nano-hydroxyapatite composite scaffold for bone tissue engineering. *J Mater Sci Mater Med* **2010**, *21*, 2293-2298.
- [17]. Wang, G.; Kucharski, C.; Lin, X.; Uludag, H. Bisphosphonate-coated BSA nanoparticles lack bone targeting after systemic administration. *J Drug Target* **2010**, *18*, 611-626.
- [18]. Gao, Y.; Chen, L.; Gu, W.; Xi, Y.; Lin, L.; Li, Y. Targeted nanoassembly loaded with docetaxel improves intracellular drug delivery and efficacy in murine breast cancer model. *Mol Pharm* **2008**, *5*, 1044-1054.
- [19]. Edwards, K.; Johnsson, M.; Karlsson, G.; Silvaner, M. Effect of polyethyleneglycol-phospholipids on aggregate structure in preparations of small unilamellar liposomes. *Biophys J* **1997**, *73*, 258-266.
- [20]. Garbuzenko, O.; Barenholz, Y.; Prie, A. Effect of grafted PEG on liposome size and on compressibility and packing of lipid bilayer. *Chem Phys Lipids* **2005**, *135*, 117-129.
- [21]. Hiramatsu, M.; Okabe, N.; Tomita, K. i. Preparation and properties of lysozyme modified by fluorescein-isothiocyanate. *J Biochem* **1973**, *73*, 971-978.

- [22]. Tang, N.; Du, G.; Wang, N.; Liu, C.; Hang, H.; Liang, W. Improving penetration in tumors with nanoassemblies of phospholipids and doxorubicin. *J Natl Cancer Inst* **2007**, *99*, 1004-1015.
- [23]. Kirby, C. J.; Gregoriadis, G. Preparation of liposomes containing factor VIII for oral treatment of haemophilia. *J Microencapsul* **2008**, *1*, 33-45.
- [24]. Szoka, F.; Papahadjopoulos, D. Procedure for preparation of liposomes with large internal aqueous space and high capture by reverse-phase evaporation. *Proc Natl Acad Sci USA* **1978**, *75*, 4194-4198.
- [25]. Yamada, A.; Taniguchi, Y.; Kawano, K.; Honda, T.; Hattori, Y.; Maitani, Y. Design of folate-linked liposomal doxorubicin to its antitumor effect in mice. *Clin Cancer Res* **2008**, *14*, 8161-8168.
- [26]. Jorgensen, L.; Martins, S.; van de Weert, M. Analysis of protein physical stability in lipid based delivery systems - the challenges of lipid drug delivery systems. *J Biomed Nanotechnol* **2009**, *5*, 401-408.
- [27]. Liu, L.; Zhang, L.; Ren, B.; Wang, F.; Zhang, Q. Preparation and characterization of collagen-hydroxyapatite composite used for bone tissue engineering scaffold. *Artif Cells Blood Substit Biotechnol* **2003**, *31*, 435-448.
- [28]. Immorfino, M. L.; Dosio, F.; Cattel, L. Stealth liposomes: review of the basic science, rationale, and clinical applications, existing and potential. *Int J Nanomed* **2006**, *1*, 297-315.
- [29]. Matsumura, Y.; Hamaguchi, T.; Ura, T.; Muro, K.; Yamada, Y.; Shimada, Y.; Shirao, K.; Okusaka, T.; Ueno, H.; Ikeda, M.; Watanabe, N. Phase I Clinical trial and pharmacokinetic evaluation of NK911, a micelle-encapsulated doxorubicin. *Br J Cancer* **2004**, *91*, 1775-1781.
- [30]. Diaz, C.; Vargas, E.; Gatjens-Boniche, O. Cytotoxic effect induced by retinoic acid loaded into galactosyl-sphingosine containing liposomes on human hepatoma cell lines. *Int J Pharm* **2006**, *325*, 108-115.
- [31]. Zhang, Y.; Wang, J.; Bian, D.; Zhang, X.; Zhang, Q. Targeted delivery of RGD-modified liposomes encapsulating both combretastatin A-4 and doxorubicin for tumor therapy: in vitro and in vivo studies. *Euro J Pharm Biopharm* **2010**, *74*, 467-473.

Chapter 6

Bisphosphonate-Derivatized Liposomes to Control Drug Release from Collagen/Hydroxyapatite Scaffolds¹

¹*A version of this chapter has been submitted for publication in: Wang G, Babadagli ME, Uludag H. Molecular Pharmaceutics.*

6.1 INTRODUCTION

Bone is susceptible to a range of pathological conditions, and the treatments for these diseases typically involve stimulation of bone regeneration to replace the original tissue. Especially for critical-sized bone defects where the bone tissue will not bridge the defect on its own, a bone substitute is needed to fill the defect and restore the lost tissue function. Many concerns regarding the autologous bone grafting, allografts and xenografts [1,2] have motivated development of tissue engineering bone constructs as well as synthetic bone scaffolds suitable for implantation. Bioactive molecule capable of modulating cellular events at the healing site is an integral part of these strategies, making it possible to accelerate or ensure healing within the defect site. However, it is difficult to deliver or retain bioactive molecules and drugs in a controlled manner within the scaffold in order to accelerate bone healing and to prevent the adverse pathology associated with delayed healing.

The phospholipid vesicles or liposomes have received widespread attention as drug carriers for controlled release and localization of various drugs at specific sites [3]. The liposomal lipid membrane formed around therapeutic agents creates a depot of bioactive molecules, whose local release is controlled by the membrane structure. The systemic application of liposomes is limited by their rapid clearance via the reticuloendothelial system and non-specific biodistribution

to other tissues [4,5]. It is possible to impart tissue specificity to liposomes by surface modification with targeting ligands [6], but the rapid systemic clearance still limits the application of liposomes for systemic bone diseases such as osteoporosis. Alternatively, liposomes can be used for local delivery of bioactive molecules after introduction of these carriers at an injection and/or implantation site [7]. Local delivery of liposomal drug formulations is a practical approach to maintain appropriate drug levels at a bone defect site, which would make it possible to use lower drug doses and reduce adverse side-effects associated with burst release of exuberant drug doses.

Liposomes have been loaded in biodegradable hydrogels prepared from collagen [8-10], gelatin [11], as well as other hydrophilic polymers [12-14]. Cross-linking liposomes to a hydrogel matrix via functional groups can further sustain the release rate of the entrapped drugs [9,15]. Although these liposomal gels can be injected or applied topically to facilitate liposomal drug absorption into the skin, the lack of mechanical rigidity in the liposomal gels limits their application in bone repair and regeneration. To obtain the desired mechanical strength, composite materials incorporating biodegradable polymers and bioceramics, including calcium phosphates, hydroxyapatite (HA) and silicate bioactive glasses, have been developed as bone scaffolds [1,16]. Collagen/HA (Col/HA) composite scaffold is one of the most promising scaffolds because of

the biocompatible and biodegradable properties of each component, the feasibility of precisely tailoring its mechanical properties, and its similarity to human bone in composition [2,17-21]. Collagen-based scaffolds have been used with human bone morphogenetic protein-2 (BMP-2) for bone regeneration in a clinical setting[22,23], but only a few attempts have been made to incorporate liposomes into collagen scaffolds [8-10]. Although growth factor containing liposomes were also reported [24,25], no attempts were made to incorporate these liposomes into a collagen scaffold for bone tissue engineering.

We recently described bisphosphonate-decorated liposomes (BP-liposomes) that displayed a strong affinity to HA [26]. The strong interactions between the HA and the BP component of BP-liposomes can be utilized to modulate the affinity of liposomes to a Col/HA scaffold, and possibly control the local retention of encapsulated bioactive molecules (e.g., osteogenic proteins to promote bone regeneration, anti-inflammatory drugs to suppress an undesirable host reaction, etc.) in the scaffold. This study explored the feasibility of creating a liposome-incorporating scaffold for controlled release of bioactive molecules. A Col/HA composite scaffold was created that was subsequently loaded with liposomes encapsulating different types of drugs. The binding affinity of the liposomes for Col/HA scaffold was characterized. The release behaviors of the liposomes from the Col/HA scaffolds as well as the model drugs,

carboxyfluorescein, doxorubicin and lysozyme, encapsulated in liposomes were investigated in detail. Our results showed that the combination of a Col/HA scaffold and BP-liposomes can localize a variety of drugs to the scaffold and control the release pattern of the drugs delivered in liposomes.

6.2 MATERIALS and METHODS

Materials

Cholesterol (CH), 5(6)-carboxyfluorescein (CF), doxorubicin hydrochloride (DOX), 1,1'-dioctadecyl-3,3,3',3'-tetra-methylindocarbocyanine (DiI), lysozyme (LYZ) from chicken egg white, and Triton X-100 were obtained from Sigma-Aldrich (St. Louis, MO, USA). 1,2-distearoylglycero-3-phosphatidylcholine (DSPC) and 1,2-distearoylglycero-3-phosphoethanolamine-N-[poly(ethyleneglycol) 2000] (DSPE-PEG) were kindly provided by Lipoid GmbH (Ludwigshafen, Germany). DSPE-PEG-thiolBP was synthesized as previously described [26]. Synthetic HA was prepared according to the method described by Bernardi [27]. Fluorescein isothiocyanate (FITC) was obtained from Pierce (Rockford, IL, USA) and it was used to label the LYZ according to previously described methodology [28]. The phosphate-buffered saline (PBS, pH 7.4) was diluted from the stock of 10× PBS (80 g/L NaCl, 2 g/L KCl, 14.4 g/L

Na₂HPO₄ and 2.4 g/L KH₂PO₄). Phosphate buffer were diluted from the stock prepared by mixing 0.5 M Na₂HPO₄ and 0.5 M NaH₂PO₄ solutions to obtain the appropriate pH. The dialysis tubing with molecular weight cut-off (MWCO) of 12–14 kDa and 100 kDa were acquired from Spectrum Laboratories (Rancho Dominguez, CA, USA). Distilled/de-ionized water (ddH₂O) used for buffer preparation and dialysis was derived from a Milli-Q purification system (Millipore, Billerica, MA).

Preparation of Col/HA Scaffold

Type-I collagen was isolated from rat tail tendons as described elsewhere[29] with modification. The tendons were excised from the tails of Sprague-Dawley rats, which were disinfected with 70% ethanol and stored at -20 °C. After removing other attached connective tissues, the tendons were washed with Tris-buffered saline (0.9% NaCl, 10 mM Tris), and dehydrated in serial concentrations of ethanol (50%, 75%, 95% and 100%). The dehydrated tendons were added into pre-cooled 0.5 M acetic acid (100 ml per 1 g wet tendon) and stirred at 4 °C for 48 h. After centrifugation at 2000 ×g for 1 h, the pellet was discarded, and the supernatant was precipitated with equal volume of pre-cooled 10% NaCl overnight at 4 °C. The collagen-rich insoluble material was collected by centrifuge for 1 h at 2000 ×g, and dissolved in 0.25 M acetic acid at 4 °C. The collagen was further purified by dialysis against 0.025 M acetic acid for 72 h

(MWCO: 12-14 kDa, buffer changed 3 times a day) and ddH₂O (x2). Collagen was obtained by freeze-drying the dialyzed sample for 48 h, and stored at 4 °C until use.

The Col/HA composite sponge was prepared by freeze-drying method as described in a previous publication [30]. The collagen was dissolved in 0.1 M acetic acid at 0.5 wt% by vigorous stirring at 4 °C. The synthesized HA particles was added to this solution (Collagen/HA: 30:70 w/w) and uniformly suspended in the collagen slurry. The mixture was degassed in vacuum desiccators for 1 h to remove the air bubbles, transferred into a BD Falcon™ 48-well plate as the mold and frozen to -20 °C overnight. Then, the sample in the mold was lyophilized by freeze-drying for 48 h. The Col/HA sponges were recovered from the wells and cross-linked by dehydrothermal treatment at 120 °C under vacuum for 24 h. The sponges were then exposed to UV radiation for 8 h in a biosafety cabinet. As a control, collagen scaffold without HA was prepared using the same method.

Characterization of Col/HA scaffold

Scanning Electron Microscopy (SEM) was used to examine the microstructure of the scaffolds. Scaffold samples were cut using a sharp blade and fixed to an adhesive carbon stub. After sputter coating with gold, imaging was carried out using a Philips/FEI LaB6 SEM (FEI Company, Hillsboro, OR, USA)

operated at an accelerating voltage of 20 kV. The porosity of the Col/HA scaffold was calculated using the following equation: $\text{Porosity} = 100 \times (1 - \rho_{\text{sample}}/\rho_{\text{material}})$, where ρ_{material} was the theoretical density of the composite material (2.12 g/cm^3), and ρ_{sample} was the density of the sample, calculated by dividing the measured weight by the volume of the scaffold.

Liposome Preparation

DSPC (10 μmol), CH (5 μmol) and 5% (molar percent of DSPC) DSPE-PEG (for PEG-liposomes) or DSPE-PEG-thiolBP (for BP-liposomes) were dissolved in chloroform and dried under reduced pressure. The resultant thin lipid film was hydrated with 2 mL of HEPES buffered saline (HBS: 10 mM HEPES, 140 mM NaCl, pH 7.4) at 60 °C, a temperature above the phase transition temperature of DSPC (55 °C), in a water bath. To encapsulate the CF, DOX and FITC-labeled LYZ, the lipid film was hydrated with CF (0.5 mg/mL), DOX (80 $\mu\text{g/mL}$) or FITC-labeled LYZ (1 mg/mL) solution in 2 mL of HBS buffer, respectively. The dispersions were then sonicated for 10 min in a bath-type sonicator at the same temperature as the incubation. The unencapsulated molecules were separated from the liposomal drugs by extensive dialysis against HBS (MWCO 100 kDa for FITC-labeled LYZ, 12-14 kDa for CF and DOX) for 24 h. The encapsulation efficiency (EE) was determined by measuring the fluorescent intensity of the samples (appropriately diluted with 1% Triton X-100

in PBS) before and after the dialysis (for CF and FITC-labeled LYZ, $\lambda_{\text{ex}} = 485 \text{ nm}$, $\lambda_{\text{em}} = 527 \text{ nm}$; for DOX, $\lambda_{\text{ex}} = 485 \text{ nm}$, $\lambda_{\text{em}} = 604 \text{ nm}$), $\text{EE} = 100\% \times [(\text{fluorescence post-dialysis}) / (\text{fluorescence pre-dialysis})]$.

Drug Release from Liposomes

The release of CF, DOX and FITC-labeled LYZ from the liposomes was assessed by a dialysis method [31]. Briefly, 0.8 mL of samples were added to the dialysis tubing (MWCO: 12-14 kDa for CF and DOX, 100 kDa for FITC-labeled LYZ), immersed in a 50 mL test tube containing 40 mL of PBS, and incubated on an orbital shaker (300 rpm) at 37 °C. At pre-determined time points, 200 μL of the external released medium was withdrawn and measured for fluorescence intensity. The same volume of fresh buffer was added to keep the total volume at 40 mL. The amount of released molecules was calculated based on a standard curve of free molecules in the same buffer, and used to determine the percentage of cumulative release.

Binding Affinity of Liposomes to Col/HA Scaffold

In order to evaluate the affinity of the liposomes to the scaffolds, DiI (0.2% of DSPC) was used to label the lipid bilayer in liposome for quantification purposes. The DiI-labeled PEG-liposomes and BP-liposomes were suspended at a concentration of 0.5 $\mu\text{mol/mL}$ (equivalent phospholipid concentration) in PBS,

and 1 mL of the sample was incubated with the Col/HA or collagen scaffold (cut into 9 mm in diameter and 5 mm in thickness) in a 24-well tissue culture plate for 3 h. The fluorescence intensity in the supernatant was measured by spectrofluorometer (200 μ L in 96-well black plates ($\lambda_{\text{ex}}=536$ nm, $\lambda_{\text{em}}=607$ nm). The percentage of bound liposomes to scaffolds was calculated based on the fluorescence intensity of DiI in the supernatant and in the control, which was equal volume of liposomal suspension without the sponge: %binding = $100 \times (\text{fluorescence in the control} - \text{fluorescence in the supernatant}) / \text{fluorescence in the control}$.

Release of Liposomes from Col/HA Scaffold

The liposome release from the scaffolds was investigated by an immersion method. The Col/HA and collagen control scaffolds were placed in a 24-well tissue culture plate, and 100 μ L of liposome samples (PEG-liposomes or BP-liposomes) was soaked into the scaffolds for 10 min. After incubation 37 $^{\circ}$ C in 1 ml PBS, or phosphate buffers of different concentrations, the supernatant was removed at predetermined time points and replaced with equal volume of fresh medium. The fluorescence intensity of DiI in the supernatant was measured by spectrofluorometer and used to calculate the cumulative release of liposome compared with the control (100 μ L sample diluted to 1 mL with PBS but without scaffold).

Drug Release from Liposome-Loaded Scaffolds

The liposomes with encapsulated CF, DOX or FITC-labeled LYZ were incubated with the scaffolds in 24-well plates (triplicate) as described above. At indicated time points, the medium was removed and replaced with fresh PBS. 200 μL of the collected medium was treated with 800 μL 1% Triton X-100 in PBS and used for analysis by fluorescence measurement. The cumulative release was calculated based on the fluorescence in the supernatant and the initial fluorescence in the control (100 μL sample diluted to 1 mL with PBS but without scaffold).

Statistical Analysis

All experimental data were collected in triplicate at least, and expressed as mean \pm standard deviations (SD). Statistical analysis was performed using two-sided unpaired Student's *t*-test. Differences were considered statistically significant with a *p*-value <0.05 .

6.3 RESULTS and DISCUSSION

Col/HA Composite Scaffold

Porous Col/HA composite scaffolds were successfully prepared by a

freeze-drying method. **Figure 6-1** shows the appearance of the scaffold and its pore structure as observed with SEM. The images show an open and interconnected porous structure with homogeneous pores in the range of 200-400 μm . HA particles were evenly distributed in the collagen matrix, and some of the particles were clearly exposed on the surface of the pore walls. The mean porosity of the Col/HA scaffolds was calculated to be $98.3 \pm 0.3\%$, and the value for the collagen scaffolds was $99.2 \pm 0.2\%$. As previously described by others [32,33], the wetted Col/HA scaffold displayed extensive flexibility and elasticity, and shape-recovery property against compression (not shown).

Porosity and pore size are important morphological properties of scaffolds intended for bone regeneration, and they can significantly influence the mechanical properties of the scaffold, cell adhesion and migration, *in vitro* and *in vivo* osteogenesis, and the delivery of cytokines. The minimum recommended pore size for bone tissue engineering scaffolds is 100 μm considering the size of cells that will penetrate the scaffold, but larger pores ($> 300 \mu\text{m}$) favor direct osteogenesis since they can allow vascularization and high oxygenation [34]. The pore size and porosity of Col/HA scaffold prepared in present study are expected to be suitable for bone regeneration, although they can be further optimized for mechanical strength, cellular adhesion and migration by changing the collagen/HA content and process parameters such as the freezing temperature and

rate. Collagen scaffolds are usually chemically or physically cross-linked in order to improve their mechanical properties and to reduce the degradation rate of the scaffolds. Chemical cross-linking has the risk for unacceptable *in vivo* toxicity due to residual molecules or compounds left from crosslinking reactions and, therefore, physical cross-linking by thermal dehydration at 120 °C under vacuum was utilized in this study. Exposure to ultraviolet light is another method to cross-link collagen, which might further sterilize the scaffolds as well.

Drug Encapsulation in Liposomes

To avoid self-quenching of the fluorophores at high concentrations due to intermolecular interactions, the liposome-encapsulated samples were diluted by Triton X-100 (1% in PBS) for measurement. Standard curves of fluorescence intensity vs. drug concentration confirmed that the drugs freed by the Triton X-100 showed no obvious self-quenching (**Figure 6-2**). Based on this approach, the encapsulation efficiency for CF, DOX and LYZ in the PEG-liposomes were $5.4 \pm 0.3\%$, $54.9 \pm 3.5\%$ and $10.9 \pm 0.9\%$, respectively. The values for the BP-liposomes were equivalent to the PEG-liposomes: $5.8 \pm 0.5\%$, $61.5 \pm 4.2\%$ and $12.1 \pm 2.6\%$. In a previous study [26], we investigated the encapsulation efficiency of DOX and LYZ in liposomes that were prepared by two different methods, namely lipid film hydration and reverse-phase evaporation method. However, only the lipid film hydration method was used in present study in order

to avoid any bilayer structure difference derived by different procedures. The encapsulation efficiencies for DOX and LYZ were consistent with our previous report [26]. The encapsulation efficiency for CF was relatively low, as expected. CF is a small hydrophilic molecule that is incorporated mainly in the aqueous phase in liposomes [35], whereas DOX and LYZ are lipophilic or partially lipophilic molecules that are mainly incorporated in the liposomal bilayers [36,37]. It has been reported that the encapsulation efficiency of CF was proportional to the liposome diameter or captured volume [35], and for multilamellar vesicles and small unilamellar vesicles, the CF encapsulation efficiency have been reported to be ~27% and ~1%, respectively. Considering that the encapsulation efficiency for CF in this study for either PEG-liposomes or BP-liposomes was ~6%, the vesicles prepared by the lipid film hydration method were expected to be multilamellar vesicles, possibly with a fraction of small or large unilamellar vesicles.

Drug Release from Liposomes

Several physicochemical properties of liposomes, such as lipid composition, surface charge, hydrophobicity, size and packing of lipid bilayers, are known to influence liposomal stability and release of the entrapped drugs[37-40]. In this study, we used DSPC and CH as the main component of the lipid bilayers, and DSPE-PEG to stabilize the liposomes. Liposomes obtained from cholesterol and DSPC, rather than phosphatidylcholines with unsaturated

fatty acyl chains, can minimize membrane defects, increasing packing of lipid bilayers and resisting leakage and degradation in the physiological environment[41-43].

To evaluate the release behaviors of the liposomal drugs, three model drugs with different molecular weights and hydrophobicities were used. The fluorescent CF dye is the most commonly used marker to assess the rates of leakage of water-soluble molecules from liposomes. DOX is a common chemotherapeutic drug and is widely employed in release studies due to the inherent fluorescence of the DOX molecule. Lysozyme is a bioactive enzyme with an anti-bacterial property, and it has similar physicochemical properties, in terms of size (~14.7 kDa) and net charge (pI ~ 11.4), to some of the osteogenic proteins, such as BMP-2 (~32 kDa, pI ~9.5). Since drug molecules can be entrapped in the inner aqueous phase and/or adsorbed to the inner and outer bilayer of liposomes, the style of entrapment would directly influence the release rate of drugs from the liposomes. Surface adsorbed or membrane incorporated molecules are expected to be released faster than the molecules entrapped in the core.

As shown in **Figure 6-3**, CF release was fast in the first 6 h (~30% released), which could be due to the release of the drug from the surface or near to the surface in bilayers [44]. After this initial period, the drug release was relatively slow in the next 48 h. The diffusion from the core of the liposomes,

where most of the CF was expected to be present, might be responsible for late slower release profile. The DOX release from the liposomes was faster in the first 24 h (~70% released). It was shown that the relatively hydrophobic drug DOX was mainly entrapped in the lipid bilayer region of the liposomes [36], which could account for this rapid release profile. Similar to DOX, ~70% of LYZ was released from the liposomes in the 48 h time period. The release of LYZ in the first 3 h was notably faster (~40% released), which was probably due to the release of protein molecules that were adsorbed on surfaces of liposomal bilayers[40]. Interestingly, for all three molecules, the release rates from the BP-liposomes were slightly faster than the PEG-liposomes, though the difference was statistically insignificant. It is likely due to that the thiolBP might have caused a minor destabilization of lipid bilayer for the BP-liposomes. In studies that employed RGD peptide [45] and Fab' antibody fragments [46], it was also reported that ligand attachment to liposome surface resulted in faster release of the entrapped drugs.

Liposome Affinity to Col/HA Scaffolds

In order to obtain prolonged retention of liposomes in scaffolds, liposomes have to be either chemically bound to the scaffolds or modified with strong affinity to scaffold components. The latter approach was taken in this study, and the affinity of the liposomes to scaffolds was summarized in **Figure 6-4**. Both

PEG-liposomes and BP-liposomes showed weak binding to the collagen scaffolds without HA (<10%). The liposomes without thiolBP also displayed low affinity to the Col/HA scaffolds (<10%), whereas the thiolBP modification imparted significant higher affinity to the liposomes (>90%) to the Col/HA scaffolds, demonstrating that the thiolBP plays a critical role in the binding process. The strong binding affinity between the Col/HA scaffold and the BP-liposomes was deemed to be due to specific interactions between the HA surface and the BP. To further confirm this mechanism, the liposome binding to scaffolds was tested in phosphate buffer with different concentrations of phosphate ions (**Figure 6-4b**). The results indicated that the Col/HA affinity of all liposomes was dependent on the phosphate concentrations but the affinity of the BP-liposomes to Col/HA scaffolds showed a larger decrease when phosphate concentration was increased from 0 to 200 mM. This was likely due to the competition between phosphate ions in the buffer and BP on the surface of BP-liposomes for binding to the HA. The suppressing of BP affinity to HA in phosphate buffers was also noted in previous studies, where aminoBP and thiolBP were conjugated with proteins[47,48]; the conjugates displayed reduced HA affinity in phosphate buffer compared that in water.

Liposome Release from Col/HA Scaffold

The release profiles of PEG-liposomes and BP-liposomes from the

scaffolds are shown in **Figure 6-5**. The PEG-liposomes were released from the scaffolds relatively faster, regardless of the presence of HA in the scaffold. The release of BP-liposomes from the Col/HA scaffolds (<10% until 7 days) was significantly slower than that from the collagen scaffolds (>90% after 24 h). Consistent with the binding result (**Figure 6-4b**), the release of liposomes from the scaffolds was accelerated with the phosphate ions, as shown in **Figure 6-5b**. At 24 h, the percentage of released PEG-liposomes in water was 76.7%, whereas the values in 50 and 200 mM phosphate buffer were 99.4% and 96.8%, respectively. For BP-liposomes, the percentages of released liposomes in 0, 50 and 200 mM phosphate buffer were 7.4%, 21.9% and 32.2%, respectively in the first 3 h, and those numbers were slightly increased to 8.4%, 33.1% and 39.8% at 7 days.

The binding of liposomes to Col/HA scaffolds can be attributed to non-specific as well as specific interactions [49]. The release of liposomes in water and phosphate buffer might have different mechanisms, the former mainly due to diffusion and the latter due to both diffusion and dissociation of liposomes from the scaffolds by phosphate ions. Since the size of the liposomes were much smaller than the pore size of the scaffolds, the PEG-liposomes, which had weak binding to both the collagen and Col/HA scaffolds, were capable of freely diffusing out of the sponges, leading to fast release immediately following

exposure to the release medium [49]. The BP-liposomes had strong affinity to the Col/HA scaffolds, and the dissociation of the HA-BP binding in the absence of phosphate ions was quite slow, which helped retain the liposomes in the scaffolds for a prolonged period. It is likely that the release of liposomes from the scaffolds might depend on other factors, such as lipid composition, liposomal size, scaffold porosity and pore size, the cross-link network and degradation rate of the scaffolds [11,12,50]. Since the focus of this study was to rely on the strong interaction between HA and BP for a sustained drug release, the effects of these factors on the release rate were not investigated. Additionally, since the binding of BP-liposomes to the Col/HA scaffolds was based on the HA content of scaffolds, the ionic dissolution of HA from the scaffold might also accelerate the release of bound BP-liposomes [50]. The effects of the HA dissolution on the liposome release remains to be studied in the future.

Release Behaviors of Drugs from Liposome-Loaded Scaffolds

Although the PEG-liposomes and BP-liposomes had similar release rates for each drug (**Figure 6-3**), the difference in the liposomal binding affinity to the scaffold (**Figure 6-5**) could modulate the release rate of the drugs from the scaffolds. The release profiles for CF, DOX, and LYZ from the liposome-loaded scaffolds are shown in **Figure 6-6**. For the collagen scaffolds (**Figure 6-6a, c and e**), almost all the free drugs (>90%) were released very fast in the first 12 h period.

This is indicative of a lack of affinity between the chosen drug molecules and the collagen scaffold. The complete release was also observed for the molecules encapsulated by PEG-liposomes after 12 h (>90% in all cases). The BP-liposomes lead to slower release compared to the free drugs and PEG-liposomes at all time points for CF (83.0% in 48 h period) and LYZ (83.4% in 48 h period), and for DOX (84.8% in 12 h period).

For the Col/HA scaffolds (**Figure 6-6b, d and f**), the free CF and PEG-liposome encapsulated CF displayed fast and complete release in 12 h (> 99%), similar to the results seen with collagen scaffolds alone. However, the CF encapsulated in BP-liposomes was released significantly slower (e.g., 54.5% after 48 h period). A similar release profile was observed for DOX and LYZ, where the order of the release rates for the three molecules was free DOX (or LYZ) > PEG-liposomes > BP-liposomes. Different from CF and DOX, the free LYZ was not completely released from the Col/HA scaffolds (73.3% till 48 h), which was likely due to the inherent affinity of the protein to the HA component of the scaffolds. This observation was noted in our previous study that LYZ bound strongly to HA [47], due to a combined effect of both electrostatic and hydrophobic interactions.

The drug release profile shown in **Figure 6-6** for each drug is a composite effect of (i) liposome affinity to scaffold (**Figure 6-5a**), and (ii) drug release from

liposomes (**Figure 6-3**). Since there was no difference in drug release between the PEG-liposomes and BP-liposomes (**Figure 6-3**), the slower release for BP-liposome encapsulated drugs and the difference between the release rates for PEG-liposomes and BP-liposomes in the Col/HA scaffolds are believed to result from the specific interaction between the BP and HA, rather than other components in the scaffolds and liposomes.

In a related study, liposomes with collagen-binding fibronectin was prepared and used for Growth Hormone (GH) delivery. Compared to liposomes without fibronectin, collagen-binding fibronectin liposomes significantly enhanced (30-50% more) *in vivo* retention of GH after intramuscular injection of liposome-containing collagen gels [8]. The gels did not contain HA and collagen was used as the binding template in this approach. Another related report investigated cross-linked gelatin gels for localized delivery of ciprofloxacin [11]; lack of liposomal affinity to the gelatin gel matrix was shown to significantly limit the quantity of liposomes that could be sequestered in a gel, promoting excessive liposome release. Regardless of the different factors investigated, the results obtained in the present study were functionally comparable to the cross-linked gel matrix sequestering the incorporated liposomes, but with the added advantage of obviating the need for chemical crosslinking in designing the sustained release formulation.

Implications for Bone Tissue Engineering

Liposome-containing collagen matrices could be suitable for a wide range of applications [8]. The current systems have been mostly prepared by passively loading the liposomes during the fabrication process. The sequestered liposomes can be chemically coupled to the gels; however, this technique requires that both the liposomes and the scaffold have chemically reactive groups [9,15], increases the risk of inactivation of bioactive molecules and may induce toxicity when utilized *in vivo*. The BP-liposomes and HA combination utilized here for specific interaction between the liposome and the scaffold did not involve any crosslinkers to impart an affinity between the liposome and the scaffold. The Col/HA scaffolds can be used as a substrate for cell attachment and proliferation^{7,20} as well as local implant for bone repair and regeneration [19,21]. Simply soaking the liposomes to the pre-fabricated scaffold for sequestering makes it convenient to entrap a variety of bioactive drugs just before therapeutic intervention. The range of drugs that can be encapsulated in the liposomes and used in bone diseases includes osteogenic growth factors (e.g., BMPs and TGF- β s, to accelerate extracellular matrix production and tissue integration) and anticancer, antimicrobial, anti-inflammatory and antiresorptive agents. The use of these drugs incorporated in three-dimensional scaffolds for bone tissue engineering was reviewed elsewhere[1,16,51]. Current delivery strategies have been mostly focused on

physical entrapment or chemical bonding of these drugs to the scaffolds. Drugs physically loaded by simply sequestering the drugs in a scaffold usually have a burst release that is undesired for their efficacy (as seen in this study as well). Covalent conjugation of these drugs directly to a scaffold is also problematic, especially for the protein-based agents, since it might affect their bioactivity. To avoid chemical modification and overcome burst release, affinity-based drug delivery strategies utilizing interactions between the therapeutic drug and the delivery system have been recommended to control drug loading and release [52]. If these drugs can be encapsulated in liposomes and then administered to a bone site with HA-containing scaffolds, a higher drug dose could be ensured at the site while reducing non-skeletal exposure to the drugs and their undesirable side-effects. Besides the liposome-scaffold interaction, drug release rate may also depend on the structure of the Col/HA scaffolds so that scaffold optimization for composition, pore size and degradation rate is worth investigating in the future. Although the main motivation of this study was to use the Col/HA scaffold and BP-liposomes for bone repair, the proposed system can be also utilized in topical applications for treatment of surgical wounds and burns or for regeneration of other tissues.

6.4 CONCLUSIONS

A drug delivery system that combined a Col/HA composite scaffold and BP-modified liposomes was designed for controlled release of therapeutic agents in bone tissue engineering. The Col/HA scaffold had an open and interconnected porous structure that is expected to be suitable for cell attachment and ingrowth at a bone site. BP-incorporating liposomes were designed that displayed similar drug release profiles to conventional liposomes without the BP moieties. The BP-liposomes loaded in the Col/HA scaffolds showed significant binding affinity to the scaffolds and prolonged the release of model drugs from the scaffolds. This was unlike the conventional liposomes that did not have a particular affinity to Col/HA implants. The reported BP-liposomes sequestered in Col/HA scaffolds are promising for application in bone tissue engineering and regenerative medicine. The versatility of the liposomes (i.e., their ability to encapsulate a variety of pharmacological agents) as well as their clinically accepted use should enable the use of the proposed scaffolds-liposome combination in a clinical setting.

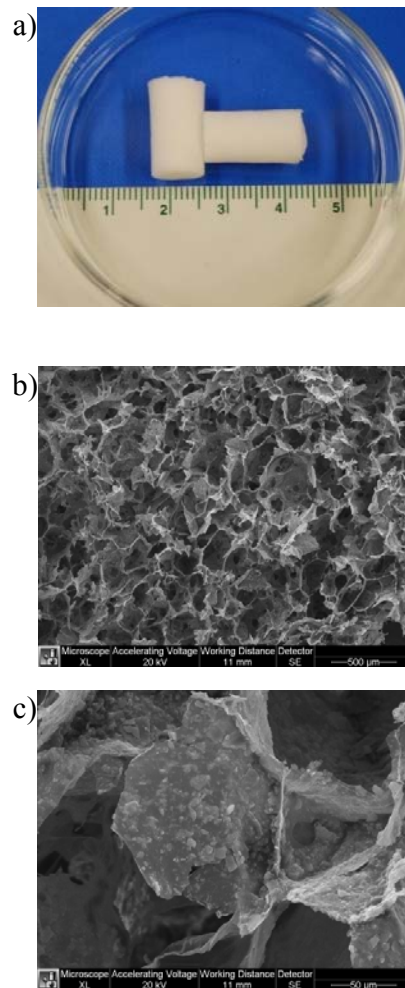


Figure 6-1. Appearance of the Col/HA scaffold (a) and its pore structure observed under SEM (b and c). The SEM images demonstrate the highly porous, interconnected structure of the scaffolds and HA particles exposed on the surface of the walls (scale bar: 500 μm in b, 50 μm in c).

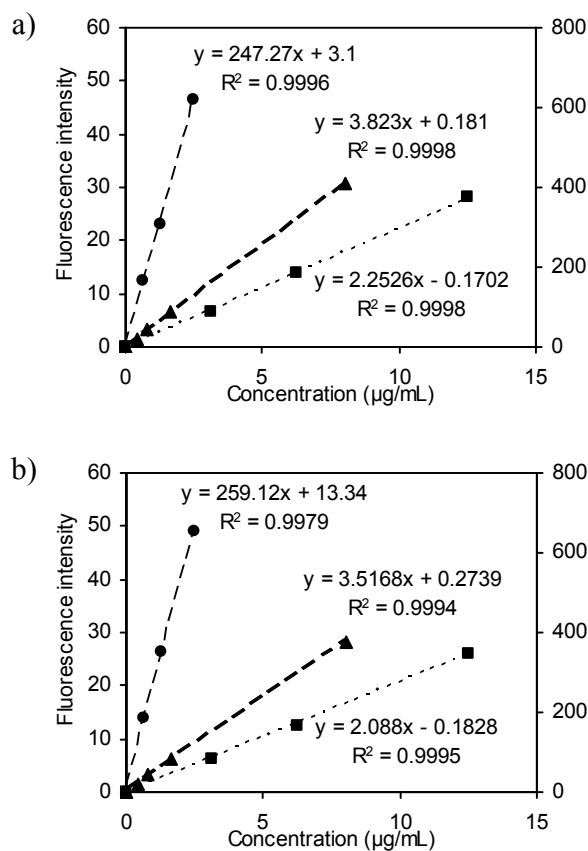


Figure 6-2. Standard curves for determination of CF, DOX and LYZ concentrations. The results shown are the correlations of fluorescence intensity (●: CF, ▲: DOX, and ■: FITC-labeled LYZ) vs. drug concentration for the PEG-liposomes (a) and BP-liposomes (b) diluted in PBS with 1% Triton X-100.

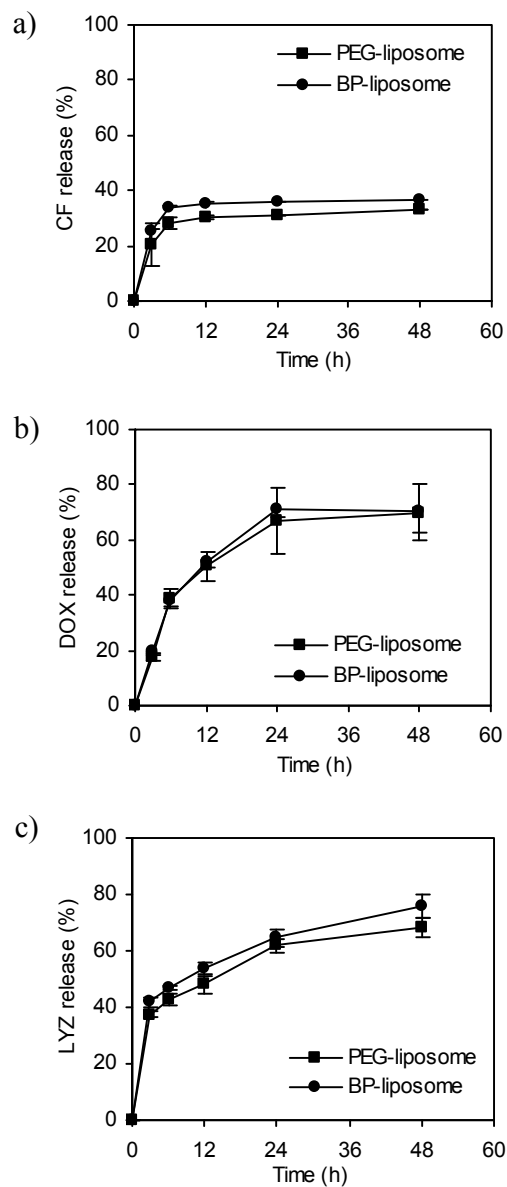


Figure 6-3. Release of CF (a), DOX (b) and FITC-labeled LYZ (c) from PEG- and BP-liposomes by dialysis method. Although the three molecules had distinctly different release rates, the BP-liposomes and PEG-liposomes displayed similar release profile for each molecule. Values are expressed as mean \pm SD (n = 3).

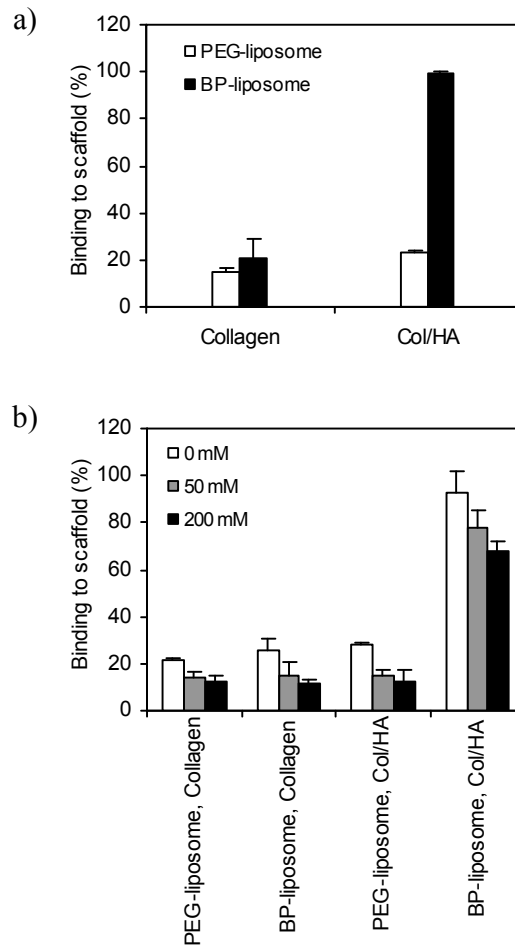


Figure 6-4. Binding affinity of the liposomes to collagen and Col/HA scaffolds in PBS (a) and different concentrations of phosphate buffer (b). The binding affinity of PEG-liposomes to either collagen or Col/HA scaffold was very low. The BP-liposomes displayed low affinity to collagen scaffold as well, but their affinity to Col/HA scaffold was significantly higher (almost complete). The binding affinity of the BP-liposomes to Col/HA scaffold was dependent on the concentrations of phosphate buffer in the binding medium, with higher phosphate concentration leading to decreased binding (b). Values are expressed as mean \pm SD (n = 3).

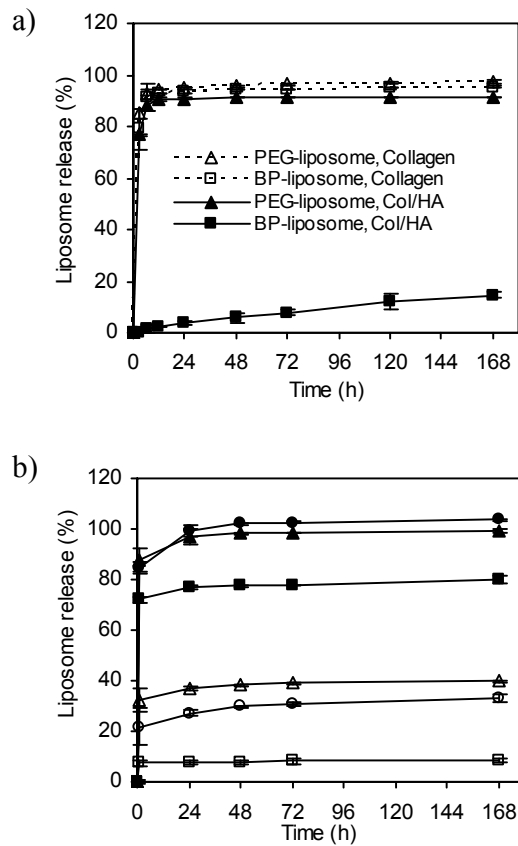


Figure 6-5. Release of liposomes from the Col/HA scaffolds in PBS (a) and the effect of phosphate concentration on the liposome release (b; for PEG-liposomes, ■: 0 mM, ●: 50 mM and ▲: 200 mM; for BP-liposomes, □: 0 mM, ○: 50 mM and △: 200 mM). The release of liposomes was determined by measuring the fluorescence of DiI-labeled liposomes at indicated time points. Values are expressed as mean ± SD (n = 3).

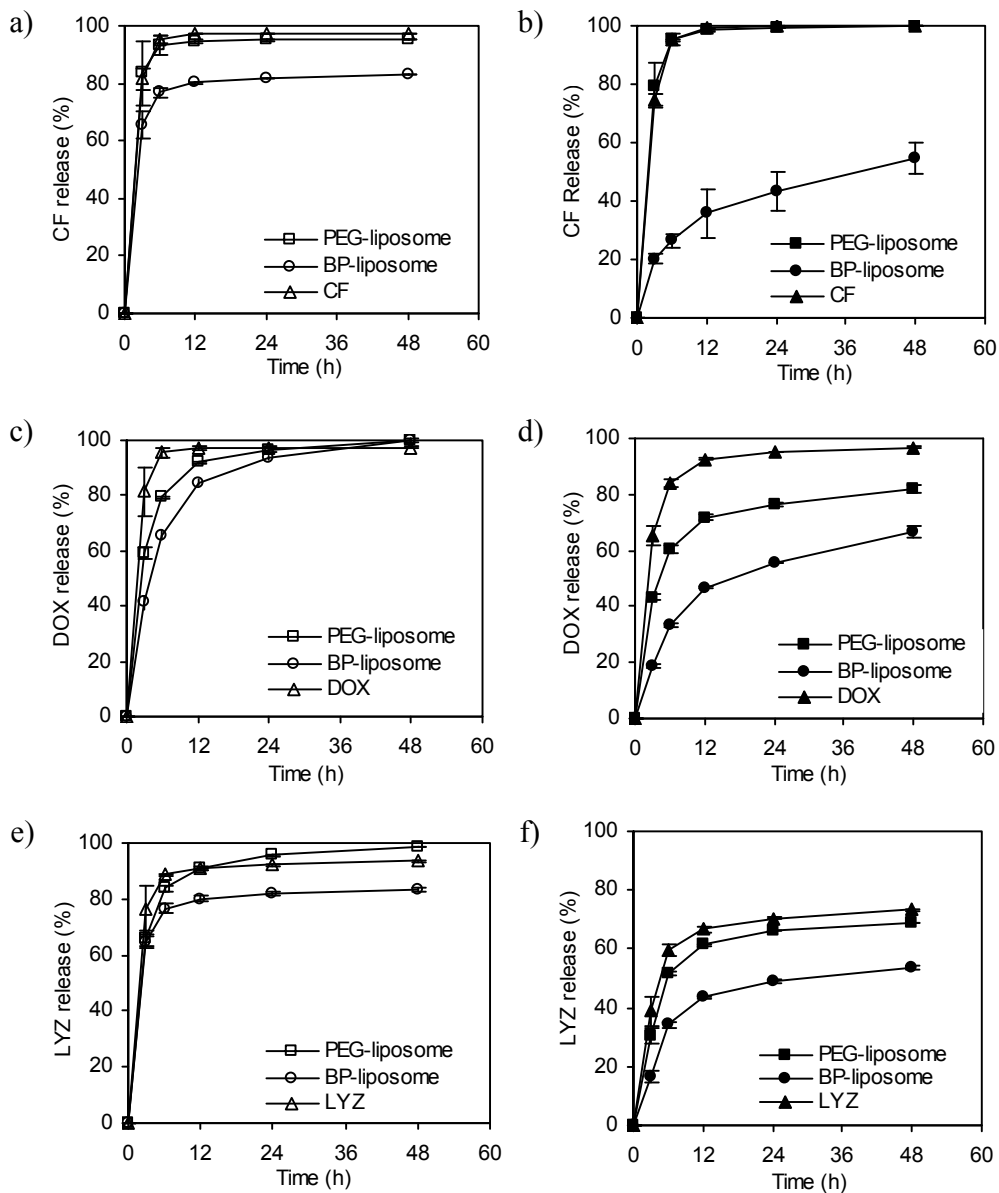


Figure 6-6. Release profiles of CF, DOX and LYZ from the liposome-loaded collagen (a, c and e) and Col/HA (b, d and f) scaffolds. The liposome-loaded scaffolds were incubated in PBS at 37°C, and the scaffolds sequestering free drugs (no liposomes) were employed as control. The analysis for released molecules was carried out at indicated time points. Values are expressed as mean \pm SD (n = 3).

REFERENCES

- [1]. Porter, J. R.; Ruckh, T. T.; Popat, K. C. Bone tissue engineering: A review in bone biomimetics and drug delivery strategies. *Biotechnol Prog* **2009**, 25 (6), 1539-1560.
- [2]. Wahl, D. A.; Czernuszka, J. T. Collagen-hydroxyapatite composites for hard tissue repair. *Euro Cells Mater* **2006**, 11, 43-56.
- [3]. Martins, S.; Sarmiento, B.; Ferreira, D. C.; Souto, E. B. Lipid-based colloidal carriers for peptide and protein delivery-liposomes versus lipid nanoparticles. *Int J Nanomed* **2007**, 2 (4), 595-607.
- [4]. Devine, D. V.; Bradley, A. J. The complement system in liposome clearance: Can complement deposition be inhibited? *Adv Drug Deliv Rev* **1998**, 32 (1-2), 19-29.
- [5]. Harasym, T. O.; Bally, M. B.; Tardi, P. Clearance properties of liposomes involving conjugated proteins for targeting. *Adv Drug Deliv Rev* **1998**, 32 (1-2), 99-118.
- [6]. Immorfino, M. L.; Dosio, F.; Cattel, L. Stealth liposomes: review of the basic science, rationale, and clinical applications, existing and potential. *Int J Nanomed* **2006**, 1 (3), 297-315.
- [7]. Alves, J. B.; Ferreira, C. L.; Martins, A. F.; Silva, G. A. B.; Alves, G. D.; Paulino, T. P.; Ciancaglioni, P.; Thedei Jr, G.; Napimoga, M. H. Local delivery of EGF-liposome mediated bone modeling in orthodontic tooth movement by increasing RANKL expression. *Life Sci.* **2009**, 85 (19-20), 693-699.
- [8]. Weiner, A. L.; Carpenter-Green, S. S.; Soehngen, E. C.; Lenk, R. P.; Popescu, M. C. Liposome-collagen gel matrix: a novel sustained drug delivery system. *J Pharm Sci* **1985**, 74 (9), 922-925.
- [9]. Rao, K. P.; Alamelu, S. Effect of crosslinking agent on the release of an aqueous marker from liposomes sequestered in collagen and chitosan gels. *J Membrane Sci* **1992**, 71 (1-2), 161-167.
- [10]. Pleyer, U.; Elkins, B.; Ruckert, D.; Lutz, S.; Grammer, J.; Chou, J.; Schmidt, K. H.; Mondino, B. J. Ocular absorption of cyclosporine A from

- liposomes incorporated into collagen shields. *Curr Eye Res* **1994**, *13* (3), 177-181.
- [11]. DiTizio, V.; Karlgard, C.; Lilge, L.; Khoury, A. E.; Mittelman, M. W.; DiCosmo, F. Localized drug delivery using crosslinked gelatin gels containing liposomes: Factors influencing liposome stability and drug release. *J Biomed Mater Res* **2000**, *51* (1), 96-106.
- [12]. Stenekes, R.; Loebis, A.; Fernandes, C.; Crommelin, D.; Hennink, W. Controlled release of liposomes from biodegradable dextran microspheres: a novel delivery concept. *Pharm Res* **2000**, *17* (6), 664-669.
- [13]. Takagi, I.; Shimizu, H.; Yotsuyanagi, T. Application of alginate gel as a vehicle for liposomes. I.factors affecting the loading of drug-containing liposomes and drug release. *Chem Pharm Bull* **1996**, *44* (10), 1941-1947.
- [14]. Gabrijelcic, V.; sentjurc, M. Influence of hydrogels on liposome stability and on the transport of liposome entrapped substances into the skin. *Int J Pharm* **1995**, *118* (2), 207-212.
- [15]. Alamelu, S.; Panduranga Rao, K. Liposomes sequestered in chitosan gel as a delivery device for dapsone. *Carbohydrate Polymers* **1994**, *24* (3), 215-221.
- [16]. Mourino, V.; Boccaccini, A. R. Bone tissue engineering therapeutics: controlled drug delivery in three-dimensional scaffolds. *J Royal Soc Interface* **2010**, *7* (43), 209-227.
- [17]. Liu, L.; Zhang, L.; Ren, B.; Wang, F.; Zhang, Q. Preparation and characterization of collagen-hydroxyapatite composite used for bone tissue engineering scaffold. *Artif Cells Blood Substit Biotechnol* **2003**, *31* (4), 435-448.
- [18]. Venugopal, J.; Low, S.; Choon, A.; Sampath Kumar, T.; Ramakrishna, S. Mineralization of osteoblasts with electrospun collagen/hydroxyapatite nanofibers. *J Mater Sci Mater Med* **2008**, *19* (5), 2039-2046.
- [19]. John, A.; Hong, L.; Ikada, Y.; Tabata, Y. A trial to prepare biodegradable collagenhydroxyapatite composites for bone repair. *J Biomater Sci Polym Ed* **2001**, *12*, 689-705.
- [20]. Cunniffe, G.; Dickson, G.; Partap, S.; Stanton, K.; O'Brien, F. Development and characterisation of a collagen nano-hydroxyapatite

- composite scaffold for bone tissue engineering. *J Mater Sci Mater Med* **2010**, *21* (8), 2293-2298.
- [21]. Gleeson, J. P.; Plunkett, N. A.; O'Brien, F. J. Addition of hydroxyapatite improves stiffness, interconnectivity and osteogenic potential of a highly porous collagen-based scaffold for bone tissue regeneration. *Euro Cells Mater* **2010**, *20*, 218-230.
- [22]. Howell, T. H.; Fiorellini, J.; Jones, A.; Alder, M.; Nummikoski, P.; Lazaro, M.; Lilly, L.; Cochran, D. A feasibility study evaluating rhBMP-2/absorbable collagen sponge device for local alveolar ridge preservation or augmentatio. *Int J Periodontics Restorative Dent* **1997**, *17* (2), 124-139.
- [23]. Dawson, E.; Bae, H. W.; Burkus, J. K.; Stambough, J. L.; Glassman, S. D. Recombinant human bone morphogenetic protein-2 on an absorbable collagen sponge with an osteoconductive bulking agent in posterolateral arthrodesis with instrumentation. a prospective randomized trial. *J Bone Joint Surg Am* **2009**, *91* (7), 1604-1613.
- [24]. Haidar, Z. S.; Azari, F.; Hamdy, R. C.; Tabrizian, M. Modulated release of OP-1 and enhanced preosteoblast differentiation using a core-shell nanoparticulate system. *J Biomed Mater Res A* **2009**, *91A* (3), 919-928.
- [25]. Matsuo, T.; Sugita, T.; Kubo, T.; Yasunaga, Y.; Ochi, M.; Murakami, T. Injectable magnetic liposomes as a novel carrier of recombinant human BMP-2 for bone formation in a rat bone-defect model. *J Biomed Mater Res A* **2002**, *66A* (4), 747-754.
- [26]. Wang, G.; Mostafa, N. A. H.; Kucharski, C.; Uludag, H. Bisphosphonate-decorated nanoparticles designed as drug carriers for bone diseases. *J Biomed Mater Res A* **2011**. (submitted)
- [27]. Bernardi, G. Chromatography of nucleic acids on hydroxyapatite columns. *Methods Enzymology* **1971**, *21*, 95-139.
- [28]. Hiramatsu, M.; Okabe, N.; Tomita, K. i. Preparation and properties of lysozyme modified by fluorescein-isothiocyanate. *J Biochem* **1973**, *73* (5), 971-978.
- [29]. Liu, X. D.; Skold, M.; Umino, T.; Zhu, Y. K.; Romberger, D. J.; Spurzem, J. R.; Rennard, S. I. Endothelial cell-mediated type I collagen gel contraction is regulated by hemin. *J Lab Clin Med* **2000**, *136* (2), 100-109.

- [30]. O'Brien, F. J.; Harley, B. A.; Yannas, I. V.; Gibson, L. Influence of freezing rate on pore structure in freeze-dried collagen-GAG scaffolds. *Biomaterials* **2004**, *25* (6), 1077-1086.
- [31]. D'Souza, S.; DeLuca, P. Development of a dialysis in vitro release method for biodegradable microspheres. *AAPS PharmSciTech* **2005**, *6* (2), E323-E328.
- [32]. Yoshida, T.; Kikuchi, M.; Koyama, Y.; Takakuda, K. Osteogenic activity of MG63 cells on bone-like hydroxyapatite/collagen nanocomposite sponges. *J Mater Sci Mater Med* **2010**, *21* (4), 1263-1272.
- [33]. Yunoki, S.; Ikoma, T.; Monkawa, A.; Ohta, K.; Kikuchi, M.; Sotome, S.; Shinomiya, K.; Tanaka, J. Control of pore structure and mechanical property in hydroxyapatite/collagen composite using unidirectional ice growth. *Mater Lett* **2006**, *60* (8), 999-1002.
- [34]. Karageorgiou, V.; Kaplan, D. Porosity of 3D biomaterial scaffolds and osteogenesis. *Biomaterials* **2005**, *26* (27), 5474-5491.
- [35]. Hernandez, J.; Estelrich, J.; Pouplana, R. Determination of the encapsulation efficiency in liposomes obtained by the 'extruder method'. *J Microencapsul* **1987**, *4* (4), 315-320.
- [36]. Goren, D.; Gabizon, A.; Barenholz, Y. The influence of physical characteristics of liposomes containing doxorubicin on their pharmacological behavior. *Biochim Biophys Acta* **1990**, *1029* (2), 285-294.
- [37]. Sessa, G.; Weissmann, G. Incorporation of lysozyme into liposomes. *J Biol Chem* **1970**, *245* (13), 3295-3301.
- [38]. Meyer, J.; Whitcomb, L.; Collins, D. Efficient encapsulation of proteins within liposomes for slow release in vivo. *Biochem Biophys Res Commun* **1994**, *199* (2), 433-438.
- [39]. Colletier, J. P.; Chaize, B.; Winterhalter, M.; Fournier, D. Protein encapsulation in liposomes: efficiency depends on interactions between protein and phospholipid bilayer. *BMC Biotechnol* **2002**, *2* (1), 9-16.
- [40]. Brgles, M.; Jurasin, D.; Sikiric, M. D.; Frkanec, R.; Tomasic, J. Entrapment of ovalbumin into liposomes-Factors affecting entrapment efficiency, liposome size, and zeta potential. *J Liposome Res* **2008**, *18* (3), 235-248.

- [41]. Huang, Y. Y.; Chung, T. W.; Wu, C. I. Effect of saturated/unsaturated phosphatidylcholine ratio on the stability of liposome-encapsulated hemoglobin. *Int J Pharm* **1998**, *172* (1-2), 161-167.
- [42]. Damen, J.; Regts, J.; Scherphof, G. Transfer and exchange of phospholipid between small unilamellar liposomes and rat plasma high density lipoproteins: dependence on cholesterol content and phospholipid composition. *Biochim Biophys Acta* **1981**, *665* (3), 538-545.
- [43]. Samuni, A. M.; Lipman, A.; Barenholz, Y. Damage to liposomal lipids: protection by antioxidants and cholesterol-mediated dehydration. *Chem Phys Lipids* **2000**, *105* (2), 121-134.
- [44]. Rudra, A.; Deepa, R. M.; Ghosh, M. K.; Ghosh, S.; Mukherjee, B. Doxorubicin-loaded phosphatidylethanolamineconjugated nanoliposomes: in vitro characterization and their accumulation in liver, kidneys, and lungs in rats. *Int J Nanomed* **2010**, *5*, 811-823.
- [45]. Nallamothe, R.; Wood, G.; Pattillo, C.; Scott, R.; Kiani, M.; Moore, B.; Thoma, L. A tumor vasculature targeted liposome delivery system for combretastatin A4: Design, characterization, and in vitro evaluation. *AAPS PharmSciTech* **2006**, *7* (2), E7-16.
- [46]. Bredehorst, R.; Ligler, F. S.; Kusterbeck, A. W.; Chang, E. L.; Gaber, B. P.; Vogel, C. W. Effect of covalent attachment of immunoglobulin fragments on liposomal integrity. *Biochemistry* **1986**, *25* (19), 5693-5698.
- [47]. Uludag, H.; Yang, J. Targeting systemically administered proteins to bone by bisphosphonate conjugation. *Biotechnol Prog* **2002**, *18* (3), 604-611.
- [48]. Zhang, S.; Gangal, G. 'Magic bullets' for bone diseases: progress in rational design of bone-seeking medicinal agents. *Chem Soc Rev* **2007**, *36*, 507-531.
- [49]. Wallace, D. G.; Rosenblatt, J. Collagen gel systems for sustained delivery and tissue engineering. *Adv Drug Deliv Rev* **2003**, *55* (12), 1631-1649.
- [50]. Kim, H. W.; Knowles, J. C.; Kim, H. E. Porous scaffolds of gelatin-hydroxyapatite nanocomposites obtained by biomimetic approach: Characterization and antibiotic drug release. *J Biomed Mater Res B* **2005**, *74B* (2), 686-698.

- [51]. Lee, K.; Silva, E. A.; Mooney, D. J. Growth factor delivery-based tissue engineering: general approaches and a review of recent developments. *J Royal Soc Interf* **2011**, *8*, 153-170.
- [52]. Wang, N. X.; von Recum, H. A. Affinity-based drug delivery. *Macromol Biosci* **2010**, (DOI: 10.1002/mabi.201000206).

Chapter 7

General Discussion, Conclusions and Future Directions

7.1 GENERAL DISCUSSION

Two categories of nanoparticulate drug delivery systems, (1) polymer coated BSA NPs and (2) lipid based NPs (liposomes and micelles), were investigated in this thesis. Both systems were designed as bone-targeted drug carriers by surface modification with BPs to obtain bone mineral affinity. This chapter provides a general discussion on the thesis work, summarizes the conclusions of this thesis, and suggests future avenues and additional studies that could be taken to continue and expand our knowledge of the relevant fields.

Polymer Coated BSA Nanoparticles with BP Modification

Particle size and surface properties are important parameters that influence the fate of the NPs when applied *in vivo*, and it is desirable that these properties can be modulated by the NP fabrication process. The preparation of the BSA NPs and optimization of the processing conditions were demonstrated in **Chapter 3**. The NPs were prepared by a coacervation method, and the effects of process parameters on NP size and polydispersity were examined. Albumin carries a certain net charge at different pHs and this enables strong electrostatic interactions among the charged segments of the protein and facilitates the albumin to form nanoparticles in the coacervation process. The properties of the final particles, especially the particle size, also depend on the balance between attractive and

repulsive forces existing among the particles during the fabrication and subsequent processes. Several parameters including BSA concentration, pH, the type and amount of non-aqueous phase, stirring rate and temperature, can influence the coacervation of BSA to some extent. To optimize the preparation procedure, we utilized Taguchi Method with an orthogonal array design to setup the experiments. Series of experiments were then conducted to investigate the effects of these parameters on the BSA coacervates with respect to particle size. We found that the most important factor that influences the NP size were the pH value of the solution and acetone-induced coacervation lead to smaller particles than ethanol-induced coacervation. A survey of literature confirms few systematic studies and theoretical discussions on simple coacervation systems, an exception being from an alcohol induced gelatin coacervation [1-4]. Although these studies provide fundamental aspects of coacervation process, for a better understanding of the albumin coacervation, theoretical discussions based on thermodynamic and kinetic data of the specific protein need to be explored, such as the charge density of albumin at a certain condition and the solute-solvent interactions in the system.

For stabilization and further modification, the BSA NPs were firstly coated with cationic polymers, PEI and PLL. After coating, the particle size of BSA NPs was significantly increased, and the ζ -potential was changed from negative to positive value and increased gradually with the increasing of polymer

coating concentration. To assess the toxicity of the BSA NPs after polymer coating and the bioactivity of BMP-2 encapsulated in such NPs, we carried out MTT assay and ALP assay on the NPs by using rat and human BMSC, respectively. The MTT assay indicated no toxicity of both the uncoated and coated NPs on BMSC. Based on ALP induction and calcification, full retention of BMP-2 bioactivity was retained in the polymer-coated NPs. These findings ensure our further modification with BP on the BSA NPs. Thus, a polymeric conjugate, PEI-PEG-thiolBP, was synthesized and used to coat the BSA NPs designed for bone-specific delivery of BMP-2 in **Chapter 4**. Besides the polymer concentration used for coating, the particle size and surface charge of the NPs could be further tuned by the PEG and thiolBP substitution ratios of the conjugate. The brush-like coat of PEG molecules to PEI build up a sterically repulsive shield and stabilized the particles with small size (< 80 nm). The PEG reduced the positive surface charge of PEI and the cytotoxicity, which was confirmed by our *in vitro* cell viability assessment of PEI and the coated NPs. BP modification further lowered the surface charge of BSA NPs, but did not affect the particle size, as well as the cytotoxicity of the NPs.

The Uludag group have previously studied a series of protein-BP conjugates [5,6], where the small targeting moiety BP is directly linked with large protein molecules. In this approach, multiple BP ligands can be conjugated to one

protein molecule in order to obtain maximum mineral affinity. However, multiple BP attachment on protein is not desirable since it increases the risk of protein deactivation. Considering this situation, BP modified NPs were intended as nanocarriers for proteins, which can isolate the payload from the covalent linking with BP. My colleague, Dr. Zhang, previously studied the release kinetics and osteogenic activity of BMP-2 encapsulated in PEI and/or PEI-PEG coated BSA NPs [7-9]. **Chapter 4** of this thesis examined the PEI-PEG-thiolBP for NP coating in order to determine the effects of PEG and BP on bone targeting of the NPs. By encapsulating ¹²⁵I-labeled BMP-2, the polymer-coated NPs were assessed for hydroxyapatite (HA) affinity both *in vitro* and *in vivo*. Our results indicated that all NP-encapsulated BMP-2 showed significant affinity to HA as compared with free BMP-2 *in vitro*, and the PEI-PEG-thiolBP coated NPs improved the *in vivo* retention of BMP-2 in HA implants compared with uncoated NPs by subcutaneous implantation in a rat model. However, after systemic administration via intravenous injection in rats, the biodistribution of NPs indicated no beneficial effects of thiolBP-coated NPs for bone targeting (**Chapter 4** and **Appendix**). This was disappointing but it may provide an opportunity for further studies.

Although successful *in vivo* bone deposition of protein and polymer conjugates with BP has been reported by Uludag [10,11] and Wang [12,13]

respectively, and bone affinity of NPs have been studied by *in vitro* HA binding model [14-16], this thesis is the first to report the tissue distribution of BP-conjugated NPs designed for bone targeting. Small size and near neutral surface charge have been the recommended requirements for an ideal drug carrier used for systemic application. We demonstrated the controllable size and ζ -potential for BSA NPs coated by BP-linked PEI, and obtained small particles (~80 nm) with neutral surface charge. Unfortunately, however, such NPs could not deposit specifically to the bone by systemic administration. Instead, the BP modified BSA NPs were actively taken by the spleen. We discussed several possible reasons for this in **Chapter 4**. The passage of drug delivery systems across the endothelium before reaching to the bone is sensitive to the size and surface properties of the system. Particle clearance by RES organs, such as spleen and liver, is a major problem for systemic administrated drugs, but the mechanisms involved in the RES clearance are still not fully understood. A better understanding of the effects of NP properties on their transportation and elimination in physiological environments is urgently needed but remains challenging.

BP-Modified Lipid Nanoparticles for Mineral Affinity

Considering the unsuccessful bone targeting with the BSA NPs, we turned to micelles and liposomes alternatively. The micelles and liposomes were first

used to encapsulate the small anti-cancer drug DOX and a model protein LYZ. The drug loading capability of the micelles and liposomes depends on the type of drugs, and this was discussed in **Chapter 5** based on the encapsulation efficiency obtained by using LFH and REV methods of liposome fabrication. Liposomes are thought to entrap both hydrophilic and hydrophobic drugs with relative high encapsulation efficiency, and this is advantageous over other types of NPs for a drug carrier. However, the comparison between LFH and REV methods used to encapsulate DOX and LYZ indicated that appropriate approaches need to be taken into consideration in order to obtain maximum loading efficiency for a specific drug.

Micelles and liposomes were designed so as to incorporate BP groups for bone targeting in **Chapter 5** and **6**. BP was conjugated with DSPE-PEG-MAL to obtain DSPE-PEG-thiolBP, and incorporated into micelles and liposomes to create mineral-binding affinity. The HA affinity of the micellar and liposomal formulations was assessed *in vitro*, and the results indicated that all the thiolBP incorporated nanocapsules had stronger HA affinity than the particles without thiolBP. Two parallel sets of experiments were carried out separately for this, one using DiI-labeled liposomes and one using the auto-fluorescence of the encapsulated DOX or LYZ (labeled with FITC). The results verified our hypothesis that if the NPs could bind to HA, it would deliver the cargos inside as

well when the integrity of the particles is maintained. This suggests that, besides therapeutic agents, those HA-binding liposomes have the potential application in carrying diagnostic agents locally to bone mineral for imaging of bone tissue[17,18].

For a better evaluation of bone affinity, we prepared a Col/HA composite scaffold, which is composed of the main components of human bone, collagen and HA, and utilized it as a biomimetic bone model to replace pure HA. Col/HA scaffold is commonly used as bone tissue engineering scaffold and more similar to bone in composition and structure than HA itself. Moreover, the scaffold is specially designed for *in vivo* test, since the particulate HA has a propensity to disperse from an implantation site, which will make it difficult to harvest the implant for analyzing. As expected, the BP-liposomes displayed significantly stronger binding affinity to the HA embedded collagen scaffold as compared with the collagen control scaffold. In a subcutaneous implant model in rats, the BP-liposomes also had prolonged retention in the Col/HA scaffold.

However, similar to BSA NPs, no beneficial effect was observed for the BP-modified micelles or liposomes based on the biodistribution after IV injection in rats (**Appendix**). Unlike uncoated albumin NPs, which are solid particles with a minimum size of 50 nm (coated BSA NPs are generally larger) [19], micelles are usually smaller (10-50 nm) and liposomal vesicles can also be fabricated to

small particles by extrusion technique. The particle sizes of the micelles and liposomes tested in **Appendix** were ~20 nm and ~100 nm respectively. The BP-conjugated proteins and polymers discussed in previous section are typically smaller than 10 nm, whereas most NPs are much larger than 10 nm, including the BSA NPs and lipid particles studied in this thesis. It is likely that there exists a threshold value for the size of a particle that can deposit to bone from systemic circulation. It has been cited that the fenestrated capillaries or sinusoids in the bone have pore size of 80-100 nm [12]. However, our findings indicated no difference between 20 nm micelles and 100 nm liposomes in their distribution to femur and tibia. To the best of our knowledge, no other *in vivo* biodistribution study has been reported for bone targeted NPs so far. How the particle size affects the bone deposition after systemic administration is still unclear, and it is complicated to draw a conclusion from our existing data since other NP properties are involved at the same time.

Instead of systemic administration, the HA binding liposomes can be utilized locally to enhance drug retention in the bone. Taking advantage of the high HA affinity of the BP-liposomes, we developed a drug delivery system, where sustainable drug release was expected from the liposomes loaded in an HA containing matrix. The release profiles of the liposomes and the liposomal drugs from liposome-loaded Col/HA composite scaffold was summarized in **Chapter 6**.

By comparing PEG- and BP-liposomes, Col/HA and collagen scaffolds, a sustained release profile were achieved via the specific interaction between BP-liposomes and HA in the Col/HA scaffolds. Three different model drugs were used in this study, and they all showed similar slowing effects of the BP-liposomes on the release of the encapsulated drugs from the liposome-loaded Col/HA scaffolds. Besides the BP-liposomes, we believe that the polymer coated BSA NPs studied in **Chapter 3** and **4** could also be loaded into the Col/HA scaffolds for controlled release of growth factors. This approach will offer a bioactive scaffold with potential application not only in bone tissue engineering but in other tissue (skin, cartilage) regeneration. The therapeutic aspects of this system for local bone regeneration are to be investigated.

7.2 CONCLUSIONS

Synthesis of BP-conjugated polymer, decoration of NPs using these BP-conjugates and *in vitro/in vivo* characterization of such NPs were presented in this thesis. Based on the data generated in this thesis, the following conclusions can be drawn:

- 1) The BSA NPs can be prepared with controllable physicochemical properties, such as particle size and surface charge. The designed

nanocarriers were non-toxic or with tolerable toxicity, and can encapsulate BMP-2 with full retention of its bioactivity.

- 2) By modification of the BSA NPs with BP, they were designed with strong mineral-binding affinity, and this was confirmed by both *in vitro* HA binding assay and *in vivo* NP retention test, but their systemic bone targeting was limited by physiological conditions.
- 3) BP-modified liposomes were also attempted for bone targeting, and they displayed strong affinity to HA and Col/HA scaffold. Different drugs, such as BMP-2 and DOX, can be efficiently encapsulated into the liposomes, and the BP-liposomes showed a sustained release profile for the drugs from the liposome-loaded scaffolds. The BP-decorated NPs are promising in local application of bioactive molecules in the bone, and as a controlled release system in tissue engineering scaffold.

Overall, this thesis expands the utilization of NP-based drug delivery systems specific for bone diseases, and provides a foundation for designing surface-functionalized NPs with controllable physicochemical properties and significant bone mineral affinity. It has contributed to the application of NPs in drug delivery and drug targeting for treatment of bone diseases.

7.3 FUTURE DIRECTIONS

A summary of the literature in **Chapter 1** covered the bone-seeking NPs published by Jan 2008. Since then, there have been a few reports published lately in this topic. An attempt was made to target paclitaxel (PTX), a potent anti-cancer agent, for bone metastases by conjugation PTX and a specific bone targeting agent alendronate with an N-(2-hydroxypropyl) methacrylamide (HPMA) copolymer[20]. This was not a NP system but rather a polymeric conjugate for systemic administration. A liposomal system composed of a 4-*N*-(3,5-ditetradecyloxybenzoyl)-aminobutane-1-hydroxy-1,1-bisphosphonic acid was synthesized and used to deliver DOX to HA [14]. Gold NPs functionalized with glutamic acid was reported as targeted X-ray contrast agent for damaged bone tissue [17]. All these studies successfully assessed the HA affinity of the designed systems *in vitro*, but none of them has reported *in vivo* evaluation. Clearly this is an area where this line of research will make an impact in the future.

Besides *in vitro* assessment that was employed in most literature studies, *in vivo* bone affinity (via implantation) was successfully achieved by the BP-modified NPs in the present work, but the systemic bone targeting studies (**Chapter 4** and **Appendix**) lead to a stage where more effort is needed. The work presented in this thesis provided valuable information on NP deposition to bone,

which has been rarely attempted before. Based on the present findings, numerous additional studies can be recommended as a complex network factors that will further expand our knowledge on bone-targeted drug delivery systems.

Systemically injected NPs did not efficiently deposit to bone. On one hand, a particle has to pass through various barriers from systemic circulation to bone (marrow), including fenestrated capillaries or sinusoids in the bone. Detailed information about the structure characteristics of those capillaries is needed. On the other hand, the particles have to escape from eliminating by other organs, especially the RES. The biodistribution study indicated that there were much more particles distributed in liver, spleen and kidneys than the bone, and interestingly it seemed that the BP-modified NPs were targeted to spleen. Detailed investigation of the mechanism of the elimination is required to take the appropriate preventative measures. When the elimination mechanism by different organs are all carefully investigated and better understood, they will provide valuable information that can guide the design of NPs with specific properties favorable to bone targeting.

To penetrate the capillaries and avoid RES elimination, attempt can be made to design nanoparticles smaller than 10-20 nm with immunosuppression properties. It has been suggested that particles should not exceed 200 nm for long-circulating carriers after systemic administration [21], but for a particle to

reach to the bone, its size has to be smaller than the fenestrated capillaries in the bone tissue, which is 80-100 nm as reported elsewhere [12]. We tested NPs with three different particle sizes in this work, 20 nm micelles, 80 nm BSA NPs, and 100 nm liposomes, but none of them showed any beneficial effects on bone targeting. We are led to conclude that size did not matter for bone targeting or the lack of it. Functionalized Gold NPs with 15 nm size was recently reported as a targeted X-ray contrast agent for bone damage imaging [17], but *in vivo* assessment was not provided in that study. It is worthwhile to assess the biodistribution of these tiny particles and determine whether they can be systemically targeted to bone. Since many other parameters are involved in the process of opsonization and elimination during the particle circulation, the size effects on bone targeting should be examined by controlling the NPs with similar surface characteristics, given that the NPs are capable of suppressing the opsonization and elimination, or at least, have the same rates in RES uptake. To prolong the NP circulation, we used PEG to modify the surface of the NPs with stealth properties [22]. The PEGylated surface was expected to have the ability to prevent opsonization and thus the RES elimination. However, the conjugated BP at the end of PEG might have diminished the function of PEG because of the undesired negative charge of BP. Optimization of PEG grafting on polymer and its surface density on NPs is needed to create a surface that can conceal the NPs from the opsonins in the circulation environments.

Using other bone-targeting moieties on the NP surface is possible direction to explore. This thesis was limited to thiolBP, which has a reactive thiol group that can be easily linked to other molecules. It has been recommended that BPs with OH and NH₂ substitutions have higher HA binding affinities than BPs with other substitutions [23,24], and this was probably due to that the former had tridentate binding site to calcium [20], whereas the latter had only bidentate binding site. To obtain a high density of BPs on the NP surface, dendritic molecules containing two or more BP moieties [11,25] are worthwhile to be attempted. One study has demonstrated that peptides conjugated with poly(aspartic acid) and poly(glutamic acid) oligopeptides exhibited greater or more rapid binding to HA than BP-incorporated molecules [26]. This could be a result of the larger region of negative charges to interact with calcium. Conjugate these more potent binding moieties to NP surface via synthesis chemistry might further improve the *in vivo* bone attraction of NPs.

Binding and distribution to bone and long-term skeletal retention are essential for a drug carrier to be used in bone regeneration. Since systemic administration is currently problematic as discussed above, local injection of the NP formulations to bone sites is another choice, since it can by-pass the systemic clearance mechanisms. Topical injection of liposomes incorporated BMP-2 was reported [27], and these liposomes were prepared with magnetic particles and

could be directed to bone defects with attached permanent magnet in a rat model. Our findings from the animal study indicated that the BP modification could help the NPs bind to bone mineral and retain longer within the HA based, or HA-embedded collagen-based implants in the implantation site. And from the therapeutic aspects, we believe that the BP-decorated NPs can deliver higher levels of bioactive agents to the bone site so that their efficacy can be enhanced. In combination of tissue engineering scaffold, such NPs can be loaded in the scaffold and served as sustained release system for growth factors such as BMP-2 to enhance cell growth and differentiation and/or anti-inflammatory drugs such as dexamethasone to prevent infection, while the scaffold will provide a substrate for cell attachment and proliferation.

REFERENCES

- [1]. Gupta, A.; Bohidar, H. B. Kinetics of phase separation in systems exhibiting simple coacervation. *Phys Rev E* **2005**, *72* (1), 011507.
- [2]. Gupta, A.; Reena; Bohidar, H. B. Free-energy landscape of alcohol driven coacervation transition in aqueous gelatin solutions. *J Chem Phys* **2006**, *125* (5), 054904-054907.
- [3]. Mohanty, B.; Bohidar, H. B. Systematic of alcohol-induced simple coacervation in aqueous gelatin solutions. *Biomacromolecules* **2003**, *4* (4), 1080-1086.
- [4]. Mohanty, B.; Gupta, A.; Bohidar, H. B.; Bandyopadhyay, S. Effect of gelatin molecular charge heterogeneity on formation of intermolecular complexes and coacervation transition. *J Polym Sci B Polym Phys* **2007**, *45* (13), 1511-1520.
- [5]. Uludag, H. Bisphosphonates as a foundation of drug delivery to bone, *Curr Pharm Design*, **2002**, *8*, 1929-1944.
- [6]. Zhang, S.; Gangal, G; Uludag, H. 'Magic bullets' for bone diseases: progress in rational design of bone-seeking medicinal agents. *Chem Soc Rev* **2007**, *36*, 507-531.
- [7]. Zhang, S.; Wang, G; Lin, X.; Chatzinikolaidou, M.; Jennissen, H. P.; Laub, M.; Uludag, H. Polyethylenimine-coated albumin nanoparticles for BMP-2 delivery. *Biotechnol Prog* **2008**, *24* (4), 945-956.
- [8]. Zhang, S.; Doschak, M. R.; Uludag, H. Pharmacokinetics and bone formation by BMP-2 entrapped in polyethylenimine-coated albumin nanoparticles. *Biomaterials* **2009**, *30*, 5143-5155.
- [9]. Zhang, S.; Kucharski, C.; Doschak, M. R.; Sebald, W.; Uludag, H. Polyethylenimine-PEG coated albumin nanoparticles for BMP-2 delivery. *Biomaterials* **2010**, *31* (5), 952-963.
- [10]. Uludag, H.; Yang, J. Targeting systemically administered proteins to bone by bisphosphonate conjugation. *Biotechnol Prog* **2002**, *18* (3), 604-611.
- [11]. Bansal, G.; Gittens, S. A.; Uludag, H. A di(bisphosphonic acid) for protein coupling and targeting to bone. *J Pharm Sci* **2004**, *93* (11), 2788-2799.

- [12]. Wang, D.; Miller, S.; Sima, M.; Kopeckova, P.; Kopecek, J. Synthesis and evaluation of water-soluble polymeric bone-targeted drug delivery systems. *Bioconjugate Chem.* **2003**, *14* (5), 853-859.
- [13]. Wang, D.; Sima, M.; Mosley, R. L.; Davda, J. P.; Tietze, N.; Miller, S. C.; Gwilt, P. R.; Kopeckova, P.; Kopecek, J. Pharmacokinetic and biodistribution studies of a bone-targeting drug delivery system based on N-(2-hydroxypropyl)methacrylamide copolymers. *Mol Pharmaceutics* **2006**, *3* (6), 717-725.
- [14]. Anada, T.; Takeda, Y.; Honda, Y.; Sakurai, K.; Suzuki, O. Synthesis of calcium phosphate-binding liposome for drug delivery. *Bioorg Med Chem Lett* **2009**, *19* (15), 4148-4150.
- [15]. Hengst, V.; Oussoren, C.; Kissel, T.; Storm, G. Bone targeting potential of bisphosphonate-targeted liposomes: preparation, characterization and hydroxyapatite binding in vitro. *Int J Pharm* **2007**, *331* (2), 224-227.
- [16]. Choi, S. W.; Kim, J. H. Design of Surface-modified poly(D,L-lactide-co-glycolide) nanoparticles for targeted drug delivery to bone. *J Control Rel* **2007**, *122*, 24-30.
- [17]. Zhang, Z.; Ross, R. D.; Roeder, R. K. Preparation of functionalized gold nanoparticles as a targeted X-ray contrast agent for damaged bone tissue. *Nanoscale* **2010**, *2* (4), 582-586.
- [18]. Zaheer, A.; Lenkinski, R. E.; Mahmood, A.; Jones, A. G.; Cantley, L. C.; Frangioni, J. V. In vivo near-infrared fluorescence imaging of osteoblastic activity. *Nat Biotech* **2001**, *19* (12), 1148-1154.
- [19]. Wang, G.; Uludag, H. Recent developments in nanoparticle-based drug delivery and targeting systems with emphasis on protein-based nanoparticles. *Expert Opin Drug Deliv* **2008**, *5* (5), 499-515.
- [20]. Miller, K.; Erez, R.; Segal, E.; Shabat, D.; Satchi-Fainaro, R. Targeting bone metastases with a bispecific anticancer and antiangiogenic polymer–alendronate–taxane conjugate. *Angew Chem Int Ed* **2009**, *48* (16), 2949-2954.
- [21]. Moghimi, S. M.; Hunter, A. C.; Murray, J. C. Long-circulating and target-specific nanoparticles: theory to practice. *Pharmacol Rev* **2001**, *53* (2), 283-318.

- [22]. Gref, R.; Luck, M.; Quellec, P.; Marchand, M.; Dellacherie, E.; Harnisch, S.; Blunk, T.; Muller, R. H. 'Stealth' corona-core nanoparticles surface modified by polyethylene glycol (PEG): influences of the corona (PEG chain length and surface density) and of the core composition on phagocytic uptake and plasma protein adsorption. *Colloids Surfaces B Biointerf* **2000**, *18* (3-4), 301-313.
- [23]. Papapoulos, S. E. Bisphosphonate actions: Physical chemistry revisited. *Bone* **2006**, *38* (5), 613-616.
- [24]. Vitha, T.; Kubicek, V.; Hermann, P.; Kolar, Z. I.; Wolterbeek, H. T.; Peters, J. A.; Lukes, I. Complexes of DOTA-bisphosphonate conjugates: probes for determination of adsorption capacity and affinity constants of hydroxyapatite. *Langmuir* **2008**, *24* (5), 1952-1958.
- [25]. Bansal, G.; Wright, J. E. I.; Kucharski, C.; Uludag, H. A dendritic tetra(bisphosphonic acid) for improved targeting of proteins to bone. *Angew Chem Int Ed* **2005**, *44* (24), 3710-3714.
- [26]. Murphy, M. B.; Hartgerink, J. D.; Goepferich, A.; Mikos, A. G. Synthesis and in vitro hydroxyapatite binding of peptides conjugated to calcium-binding moieties. *Biomacromolecules* **2007**, *8* (7), 2237-2243.
- [27]. Matsuo, T.; Sugita, T.; Kubo, T.; Yasunaga, Y.; Ochi, M.; Murakami, T. Injectable magnetic liposomes as a novel carrier of recombinant human BMP-2 for bone formation in a rat bone-defect model. *J Biomed Mater Res A* **2002**, *66A* (4), 747-754.

Appendix

Biodistribution of Micelles and Liposomes after Intravenous Injection

I) INTRODUCTION

The biodistribution of BSA NPs was investigated in **Chapter 4**, and the results showed that the BSA NPs lack bone targeting after systemic administration, even with BP functionalization. The micelles and liposomes were designed alternatively for bone targeting. As compared with solid BSA NPs, the liposomes are deformable and have more possibility for permeation through the endothelium, whereas the micelles have smaller particle size (~20 nm), which could be advantageous for long-circulation and passing through fenestrated capillaries. The BP-micelles and liposomes displayed significantly stronger mineral affinity than the unmodified ones based on an *in vitro* HA binding assay and *in vivo* retention test in rats (**Chapter 5**). This study was carried out to evaluate the bone targeting of the micelles and liposomes by systemic administration. The purpose for bone targeting as well as the methodology for assessing bone targeting have been well established in **Chapter 5**, so that it will not be repeated here.

II) METHODS

Six-to-eight week-old female Sprague-Dawley rats were purchased from Biosciences (Edmonton, Alberta). The rats were acclimated for one week under standard laboratory conditions (23 °C, 12 h of light/dark cycle) prior to the study. While maintained in pairs in sterilized cages, rats were allowed free access to food and water for the duration of the study. All procedures involving the rats were approved by the Animal Welfare Committee at the University of Alberta (Edmonton, Alberta).

Micelles and liposomes with DiI were prepared as described in **Chapter 5**. Two sets of experiments were carried out. Nine rats were used in the first set for three study groups: (1) saline, (2) PEG-micelles, and (3) BP-micelles, and in the second set, the same number of rats were used, but PEG- and BP-liposomes were tested instead of micelles. An aliquot of 300 μ L of the sample was administered intravenously to the rats via tail vein injection. The rats were euthanized by CO₂ after 24 h injection, and the organs including kidneys, liver (a portion), spleen, tibia, femur and blood were collected. The blood samples (1-1.5 mL from each rat) were centrifuged at 3000 \times g for 3 min, and 0.5 ml of the supernatant was mixed with 0.5 ml PBS, and measured for fluorescence intensity. The livers, spleens and kidneys were weighed, minced with scissors, homogenized with 3 ml PBS by a tissue grinder, centrifuged at 1000 \times g for 15 min, and the supernatant was

analyzed for fluorescence intensity. The tibia and femur were washed with PBS, weighed, decalcified with 3 ml of 1 M HCl overnight, and centrifuged at $1000 \times g$ for 15 min. The supernatant was measured for fluorescence intensity by a spectrofluorometer ($\lambda_{\text{ex}} = 536 \text{ nm}$, $\lambda_{\text{em}} = 607 \text{ nm}$) after centrifugation. The biodistribution was analyzed based on the fluorescence corrected according to the weight of collected tissues.

III) RESULTS and DISCUSSION

The PEG-micelles had equivalent DiI fluorescence to the BP-micelles (4452 au per 300 μL injection for both micelles). This was the case as well for PEG-liposomes and BP-liposomes (10445 au per 300 μL injection for both liposomes). The prepared formulations were intravenously injected into rats and analyzed for biodistribution at 24 h after injection. As can be seen in **Figure A-1**, both the PEG-micelles and PEG-liposomes had higher retention in the blood than the BP-micelles and BP-liposomes (2.9 ($p < 0.05$) and 13.7-fold ($p < 0.05$) higher), respectively, indicating that (i) PEG modification improved systemic retention of micelles and liposomes (as expected), and (ii) the BP-modification resulted in increased clearance of particles from the blood stream. The differences in particle size might account for this as well, indicated by the fact that the BP-micelles ($\sim 20 \text{ nm}$) had higher retention in blood than the BP-liposomes ($\sim 100 \text{ nm}$) (the %retention was calculated to be 0.15% per mL plasma for BP-liposomes and

1.6% for BP-micelles). Different from the micelles and liposomes, the BSA NPs were present relatively less amount in blood at 24 h post-injection, but more in the kidney, liver and spleen (**Figure 4-10**).

All the formulations had similar distribution in the kidneys, which was comparable to the saline control. This was indicative of non-detectable levels of PEG and BP derivatized liposomes/micelles in kidneys. The strong interference from tissue autofluorescence is also problematic since it limits the sensitivity of *in vivo* DiI fluorescence measurements. However, both liposomes ($p < 0.05$) and micelles ($p < 0.05$) had evident uptake in the livers, significantly higher than the saline control. The BP-micelles displayed higher uptake in the spleen than the saline control, and so also did the PEG-and BP-liposomes, but because of the large error bars for the data, the difference was not significant in the case of spleen delivery. This was also the case for the BP-modified BSA NPs, which had higher uptake in liver and spleen than PEGylated BSA NPs at 24 h after injection (**Figure 4-10**). These findings provided evidence for opsonisation of the particles, which accounted for the particle clearance from the blood, and thus limited the distribution of the NPs to the bone. The presence of BP seems to be adversely affecting the biodistribution of the NPs in this regard.

Although the BP-micelles and liposomes showed stronger *in vitro* bone mineral affinity (**Chapter 5**), their *in vivo* deposition in the femur and tibia were

not evidently higher than the saline control, which displayed some autofluorescence, and either than the PEG-micelles or liposomes. This indicates that either (i) the level of uptake is very low, or (ii) the assay used for detecting the liposomes and micelles (DiI fluorescence) are not very sensitive.

It should be noted that the *in vivo* disintegration of liposomes or micelles would also affect their biodistribution. The liposomes and micelles used in this study were expected to be stable *in vivo*. For this purpose, the liposomes were prepared with selected components that are considered to be suitable for systemic administration, as discussed in **Chapter 5**. The micelles were prepared at a concentration of 5 mM, and it would be diluted after entering the blood stream of the rats (by ~50 times). The *in vivo* diluted concentration of the micelles was expected to be well above the critical micelle concentration (defined as the concentration of surfactants above which micelles are spontaneously formed) of DSPE-PEG, which is around 1 μ M. However, there exist some inherent lipid components in the blood, and the influence of these molecules on the integrity of the micelles and the liposomes was not investigated in this work.

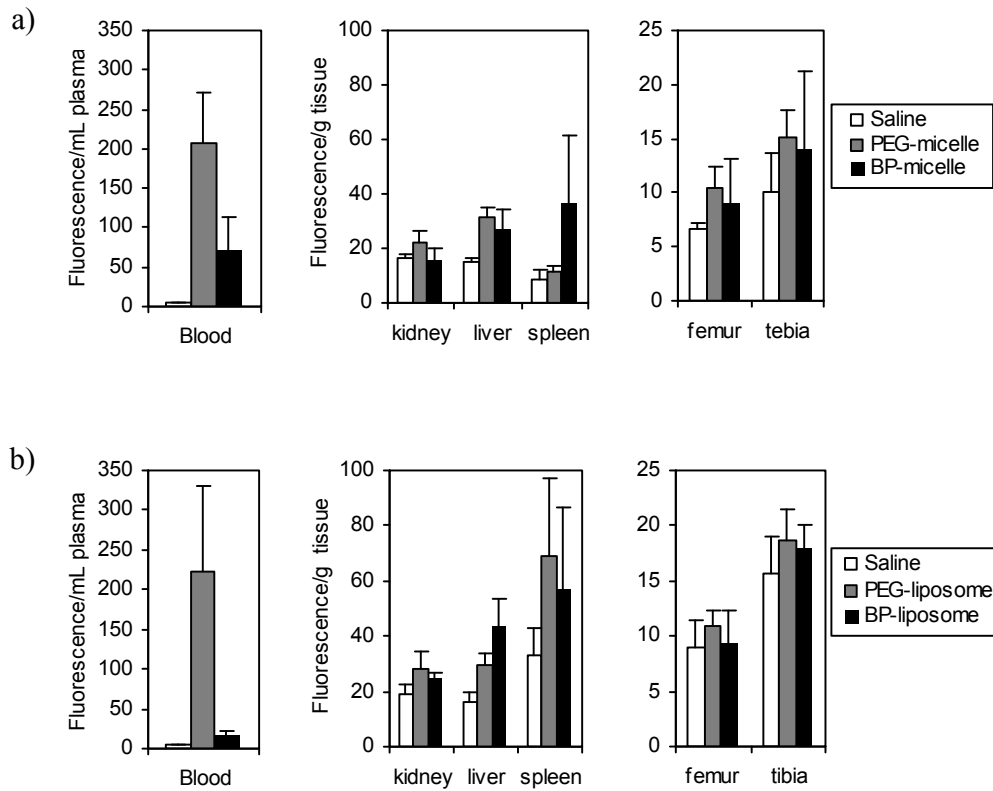


Figure A-1. The biodistribution of DiI-labeled micelles (a) and liposomes (b) in rats after IV injection. The samples were administered intravenously via tail vein injection, and the biodistribution was analyzed at 24 h after injection. Results are expressed as mean \pm SD (n = 3), and normalized by the weight of the tissues.